From single cell to single molecule: Elucidation of the intracellular dynamics of the Hypoxia Inducible Factor (HIF)

Thesis submitted in accordance with the requirements of the University of Liverpool for the degree of Doctor in Philosophy

By

Sarah Taylor

September 2015

Abstract

Hypoxia signalling pathway acts in all mammalian cells to try and avert damage occurring during periods of limited oxygen availability (hypoxia). The cellular response to a low oxygen environment is mediated by the transcription factor hypoxia-inducible factor (HIF), which activates the transcription of genes that aid cell survival and act to restore oxygen homeostasis. The heterodimeric transcription factor consists of a constitutively expressed beta subunit (HIF-1β) & an alpha subunit (HIF-1α / HIF-2α). The alpha subunits are regulated in an oxygen-dependent manner.

The main aim of this thesis was to elucidate if the spatial localisation and/or the temporal fluctuations of HIF-1α and HIF-2α are altered in response to hypoxia and participate to the regulation of HIF activity. The experimental strategy focused on studying HIF at several scales ranging from single cell to single molecule level. I first investigated the temporal and spatial dynamics of the HIF-α subunits in living cells using time-lapse imaging. This was part of a larger study, which was initiated before the start of this thesis. It was published in January 2014 in the *Journal of Biological Chemistry*. We demonstrated that HIF-α accumulates transiently in the nucleus in response to hypoxia and this was necessary to ensure cell survival. We further demonstrated using a combination of mathematical modelling and knock-down experiments that the negative feedback loop involving PHD2 has an essential role in these dynamics. Secondly, we observed that HIF-2α exhibits a non-homogenous sub-nuclear localisation, whereas HIF-1α is distributed homogenously within the nucleus. Since protein localisation is commonly linked to function we sought to elucidate the purpose of this heterogeneous distribution using a combination of live cell imaging, co-localisation and photo-bleaching experiments. Lastly, to avoid molecule averaging errors, we planned to employ single molecule tracking to elucidate sub-cellular dynamics of HIF-2α and gain further insight into the movement of HIF-2α between the speckles and the rest of the nucleus. Our aim was to image and monitor gold nanoparticles (GNPs) conjugated to HIF-2α in real time in living cells, using photo-thermal microscopy. In collaboration with Prof. D. G. Fernig and Dr. R. Levy's research groups, we developed a protocol using the Halotag (an engineered enzyme that reacts with a substrate (Halo-ligand) to form a covalent bond) to label a protein of interest with gold nanoparticles. This was achieved by: immobilising the Halotag ligand on the surface of GNPs and producing purified recombinant Halotag-fusion protein. We have obtained positive results by using

the fibroblast growth factor 2 as proof of principle. Due to difficulties in expression and purification of recombinant Halotag-HIF-2α single molecule tracking of HIF-2α has not been achieved yet, but this work is still on-going.

Overall my results show that: (1) the temporal dynamics of HIF-1α elicited by hypoxia have a critical role in HIF activity and function, (2) the non-homogenous speckle localisation of HIF-2α is associated with a slow diffusion time within the nucleus, 7-10X (depending on condition) slower than the homogeneous HIF-1α. Finally, using single molecule measurements, we did not observe any significant difference in speckle organisation or HIF-2α mobility, so single molecular tracking will be required to provide a non-average quantitative measurement of HIF-2α movement between the speckles and inter-speckle space.

Contents

List of Figures

Figure 5.13 Plan for conjugation of mammalian expressed Halotag-HIF-2α
Figure 5.14 Halotag-HIF-2α-IRES-dTomato
Figure 5.15 Halotag-HIF-2α expressed in HEK293T cells

List of Tables

List of Supplemental Data

Available on the attached CD

Movies

M1 HIF-1α-GFP BAC nuclear accumulation in hypoxia
M2 HIF-2α speckles
M3 Speckle trajectory 1
M4 Speckle trajectory 2
M5 FRAP - Tracking HIF-2α speckles in bleached region
M6 FRAP - Tracking individual HIF-2α speckle in bleached region 1
M7 FRAP - Tracking individual HIF-2α speckle in bleached region 2

List of Abbreviations

aa	Amino acid
ADP	Adenosine diphosphate
aka	Also known as
APS	Ammonium persulphate
ARNT	Aryl receptor nuclear transporter
ATP	Adenosine triphosphate
BAC	Bacterial artificial chromosome
bHLH	Beta helix loop helix
bp	nucleotide basepairs
BSA	Bovine serum albumin
CBP	CREB binding protein
CCI	Centre for cell imaging
CM	Carboxymethyl
CMV	Cytomegalovirus
CREB	cAMP response element-binding protein
Da	Daltons
DAEA	Diethylaminoethanol
ddH2O	Ultrapure water / double distilleds water
DM	Double mutant
DMEM	Dulbecco's modified medium
DMOG	Dimethyloxaloylglycine
DMSO	Dimethyl sulphoxide
DNA	Deoxyribonucleic acid
dTOM	dTomato fluorescent protein
DTT	Dithiothreitol

e-	Electron
EDTA	Ethylenediaminetetraacetic acid
EGFP	Enhanced green fluorescent protein
EPAS	Endothelial PAS domain protein 1
EPO	Erythropoietin
FADH	Flavin adenine dinucleotide
FBS	Fetal Bovine serum (cell culture)
FCS	Fluorescence correlation spectroscopy
FGF	Fibroblast growth factor
FIH	Factor inhibiting HIF
FLIP	Fluorescence loss in photobleaching
FRAP	Fluorescence recovery after photobleaching
FRET	Förter / fluorescence resonance transfer
GFP	Green fluorescent protein
GLUT	Glucose transporter
GNP	Gold nanoparticles
h	Hours
HAF	Hypoxia associated factor
HDAC5	Histone de-acetylase 5
HIF	Hypoxia-inducible factor
His	Histadine
HisTag	Poly-Histadine tag
HIV	Human immunodeficiency virus
HL	Halotag ligand
HRE	Hypoxia response element
HT	Halotag
IF	Immunofluorescence

IPTG	Isopropyl β-D-1-thiogalactopyranoside
IRES	internal ribosome entry site
Lab	Laboratory
LB	Lysogeny broth aka Luria-Bertani medium
LSM	Laser scanning microscope
MEM	Modified eagle medium
min	Minute
mRNA	Messenger RNA
MSD	Mean squared displacement
MW	Molecular weight
NADH	Nicotinamide adenine dinucleotide
NiNTA	Nickel nitrilotriacetic acid
NLS	Nuclear localisation signal
OD600	Optical density measured at a wavelength of 600
ODD	Oxygen dependent degradation
PAS	PER-ARNT-SIM domain
PBS	Phosphate buffered saline
PCR	Polymerase chain reaction
PEG	Polyethylene glycol
PEI	Poly(ethylenimine)
PER	Period circadian protein
PFA	Paraformaldehyde
PHD	Prolyl hydroxylase domain protein
pI	Isoelectric point
PML	Promyelocytic leukemia protein
POI	Protein of interest
PTM	Post-translational modification

RNA	Ribonucleic acid
RNAPII	RNA polymerase II
ROI	Region of interest
RPM	Revolutions per minute
RT-qPCR	Real time quantitative polymerase chain reaction
SD	Standard deviation
SDS PAGE	Sodium dodecyl sulfate polyacrylamide gel electrophoresis
sec	Seconds
SFC	Splicing factor compartments
sh	Short hairpin RNA
SIM	Single minded protein
SMSS	Slope of the moment scaling factor
SMT	Single molecule tracking
SR	Super-resolution
SUMO	Small ubiquitin-like protein
TAD	Trans-activation domain
TEMED	Tetramethylethylenediamine
TEV	Tobacco etch virus
TF	Transcription factor
TMR	Tetramethylrhodamine
Tris	Tris(hydroxymethyl)aminomethane
UV	Ultraviolet light
VEGF	Vascular endothelial growth factor
VHL	von Hippel Lindau protein
vs	Versus
WT	Wild type
YFP	Yellow fluorescent protein

Chapter 1: Introduction

1.1 Cell signalling

Cell to cell communication is vital in multi-cellular organisms for coordination of cellular events such as metabolism and growth. Cell signalling is orchestrated by several factors such as signalling molecules (e.g. hormones and cytokines), that are detected via receptors that trigger a chain of events whereby proteins are sequentially activated / deactivated leading to the up / down regulation of genes and a change in protein expression.

As well as signalling molecules, cells can sense changes in their environment. They relentlessly monitor and respond to environmental cues causing the activation / deactivation of signalling pathways. For example extreme temperatures, changes in pH and exposure to toxins trigger stress response pathways that orchestrate a change in gene expression facilitating cellular protection.

In addition to this, cells monitor the levels of oxygen, a vital component for life, and it is the signalling pathway that facilitates cells to sense and adapt to low oxygen (hypoxia) that is the focus of this study.

1.2 Oxygen and metabolism

As obligate aerobes, humans cannot survive without oxygen. Homo sapiens (and many other living organisms) require oxygen to generate chemical energy in the form of Adenosine triphosphate (ATP) to fuel energetically unfavourable processes and biochemical reactions at the cellular level. It is generated via a number of mechanisms in eukaryotic cells, but the greatest yield of ATP comes from aerobic respiration, a process involving the oxidation of organic compounds such as sugars (Figure 1.1).

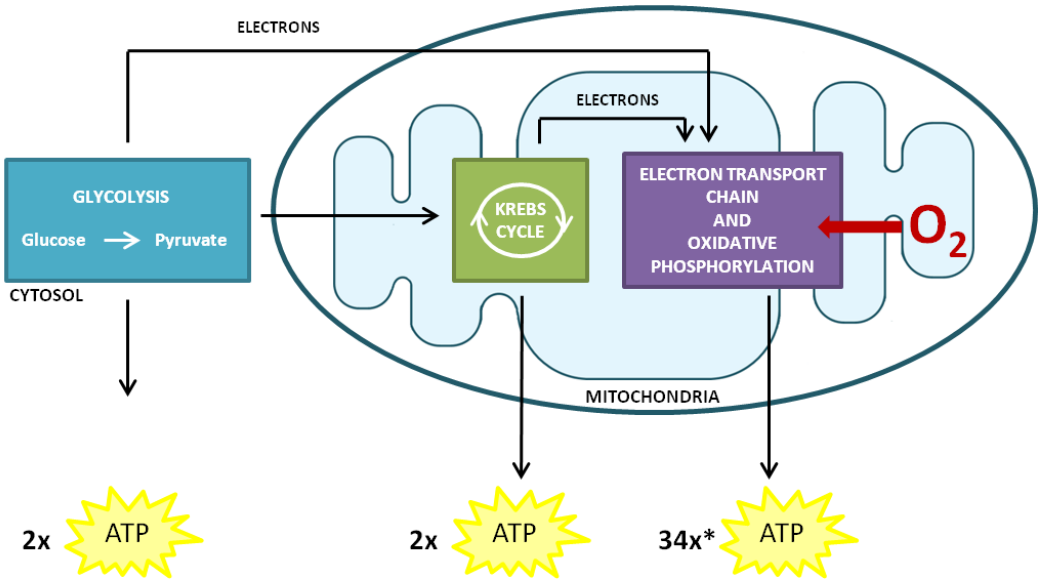

Figure 1.1 | Cellular metabolism. *A simplified schematic of the three stages of cellular metabolism. Glucose is broken down into pyruvic acid in the cytosol. This product is transported into the mitochondria where it is converted into acetyl CoA. Acetyl CoA enters the Krebs cycle (aka citric acid cycle) which produces high energy electrons that are passed onto the electron transport chain (ETC), situated in the inner membrane. As the electrons travel down the ETC, it creates a proton gradient which drives ATP synthase to create ATP from ADP and Pi. Oxygen acts as the electron acceptor at the end of ETC and is split to create two molecules of water. *Net gain is 32 or 34 ATP molecules depending on which electron shuttle transports the electrons from the cytosol into the mitochondria.*

Glycolysis literally means “lysis of sugar”. One molecule of glucose is converted to two pyruvate molecules in a ten step process to yield a net gain of two ATP molecules. It is a primitive form of ATP production and is present in nearly all organisms including anaerobes as it does not require molecular oxygen.

The pyruvate molecules produced are transported in the mitochondrial matrix where they are converted to acetyl CoA, the substrate of the Krebs cycle (citric acid cycle). Although the Krebs cycle is part of “aerobic metabolism”, this process does not itself require molecular oxygen. It does however produce high energy electrons, transported in the form of NADH and FADH, which are required for the subsequent oxygen-dependent step in aerobic respiration. These electrons pass down the electron transport chain and eventually combine with oxygen. The proton gradient created during this process drives ATP synthase which produces a net value of 32 (or 34) molecules of ATP. Meaning that in presence of sufficient oxygen, a cell can produce 36 (or 38) molecules of ATP per one molecules of glucose in total.

1.3 Hypoxia

Hypoxia occurs when oxygen levels fall below the threshold of a particular tissue. Figure 1.2 highlights the partial pressures of a selection of organs and tissues. In simple terms, organs, tissues and cells require delivery of sufficient oxygen to meet their particular metabolic needs and when the demand for oxygen becomes greater than the supply, they become hypoxic.

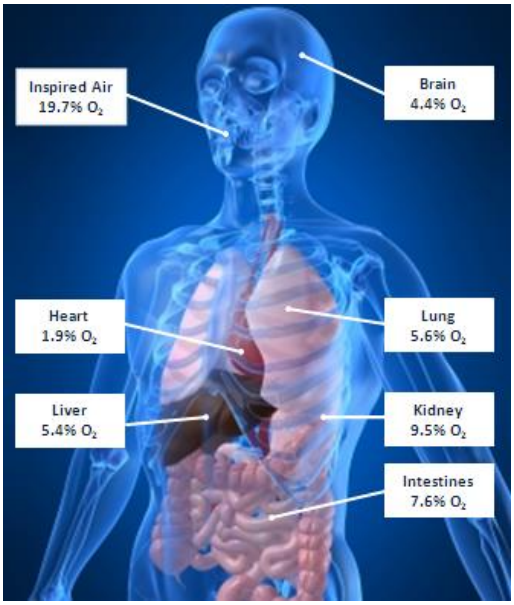

Figure 1.2 | Examples of the partial pressure of oxygen in different organs and tissues. *Values taken from Wiener et al. (1976) and Carreau et al. (2011). Image source http://media.tumblr.com/tumblr_m5z390bppP1qmovzi.jpg*

Hypoxia results from pathological conditions where the oxygen supply is reduced or impeded such as anaemia, sleep apnoea and ischemic events. Hypoxia has been shown to play a role in physiological and developmental processes, such as wound healing (Brahimi-Horn & Pouyssegur, 2009), embryogenesis (Dunwoodie, 2009) and maintenance of pluripotent stem cells (Forristal *et al.*, 2010).

1.3.1 Maintaining oxygen homeostasis

Hypoxic events trigger a highly conserved canonical signalling pathway that results in the up-regulation of genes that aid cell survival by restoring oxygen levels, improving tissue oxygenation and/or increasing anaerobic respiration (Table 1.1).

For example, hypoxia triggers an increase in the levels of the hormone erythropoietin (EPO) that controls the maturation of red blood cells. This results in an increase in the number of red blood cells and therefore increases the oxygen carrying capacity of the blood. There is also an increase in vascular endothelial growth factor (VEGF). This protein stimulates angiogenesis (development of new blood vessels), which restores or increases blood supply to tissues. Together, these responses contribute towards re-establishing sufficient tissue oxygenation.

Table 1.1 | Examples of cellular processes that are up-regulated during hypoxia.

Process	HIF target gene(s)	Reference
Erythropoiesis	EPO	Wang & Semenza (1993)
Angiogenesis	VEGF	Forsythe *et al*. (1996)
Switching cellular metabolism to glycolysis	GLUT1 GLUT3 GAPDH	Wolfe and Voelkel (1983), Chen *et al.* (2001)
Iron metabolism	Transferrin Transferrin receptor Ferroxidase	Rolfs et al. (1997), Tecchini *et al.* (1999), Lok & Ponka (1999), Mukhopadhyay *et al.* (2000)

1.4 Hypoxia-inducible factor (HIF)

In 1995 it was determined that the protein responsible for the hypoxic induction of erythropoietin (EPO) was hypoxia-inducible factor (HIF) (Wang *et al.*, 1995). Subsequent studies found that HIF is a heterodimeric transcription factor that is composed of an alpha subunit, which is tightly regulated in an oxygen-dependent manner, and a constitutively expressed beta subunit (HIF-1β) (Wang & Semenza, 1995;Reyes *et al.*, 1992;Huang *et al.*, 1996).

1.4.1.1 HIF-α

There are three isoforms of the alpha subunit (HIF-1α, -2α and -3α). HIF-1α was discovered by Gregg Semenza in 1992 (Semenza & Wang, 1992). It was determined that this basic helix-loop-helix (bHLH) protein was made up of the following domains: PER/ARNT/SIM (PAS) domains, the oxygen-dependent degradation (ODD) domain and two transactivation domain (TAD) (Figure 1.3) (Depping *et al.*, 2008;Jiang *et al.*, 1996;Wang *et al.*, 1995;Lee *et al.*, 2004).

Five year after the discovery of HIF-1α, several laboratories published reports on an HIF-1α isoform, HIF-2α. The simultaneous discovery led to its publication under several names: endothelial PAS domain protein-1 (EPAS1), HIF-1α-like factor (HLF) or members of PAS superfamily 2 (MOP2) (Wenger & Gassmann, 1997;Tian *et al.*, 1997;Ema *et al.*, 1997;Hogenesch *et al.*, 1997). This, like HIF-1α, is a beta-helix-loop-helix protein that heterodimerises with HIF-1β, recognises the HRE DNA consensus sequence and activates transcription of hypoxia inducible genes (Tian *et al.*, 1997).

The third isoform, HIF-3α, has numerous splice variants. The resulting proteins range from 667 to 7 amino acids, with some splice variants having an ODD and an N-terminal TAD like HIF-1α and HIF-2α (Maynard *et al.*, 2003;Gu *et al.*, 1998). Although the role of HIF-1α and -2α in the cellular adaptation to low oxygen is well established, the function of this third isoform is complex, with some splice variants have been shown to act as negative or positive regulators in the hypoxia response (Hara *et al.*, 2001;Maynard *et al.*, 2005;Maynard *et al.*, 2003;Gu *et al.*, 1998).

1.4.1.2 HIF-β

Otherwise known as aryl hydrocarbon nuclear translocator (ARNT), this member of the bHLH-PAS superfamily was first described in 1991 as the binding partner of the aryl hydrocarbon receptor (AhR / dioxin receptor) (Hoffman *et al.*, 1991;Reyes *et al.*, 1992). When hetero-dimerised, this transcription factor is responsible for regulating xenobiotic (chemicals foreign to the body) metabolism. It was later discovered that ARNT also forms heterodimers with HIF-1α and HIF-2α, thus acquiring the name HIF-β (Wang *et al.*, 1995;Wang & Semenza, 1995). There are two isoforms: HIF-1β and HIF-2β (HIF-1β2 / ARNT2). Both isoforms can mediate the hypoxic response, but HIF-2β has a more limited

tissue expression compared to the ubiquitous HIF-1β (Hirose *et al.*, 1996;Drutel *et al.*, 1996;Maltepe *et al.*, 2000).

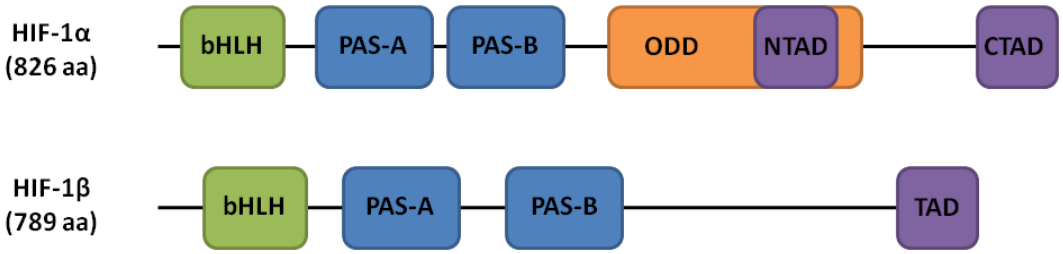

Figure 1.3 | Domain structure of HIF-1α and HIF-1β. *PAS = PER/ARNT/SIM domains, ODD = oxygen-dependent degradation domain, TAD = transactivation domains.*

1.4.2 Oxygen-Dependent regulation of HIF

The availability of oxygen regulates both the stability and transcriptional activity of HIF, via two independent processes. HIF-α subunits are continually synthesised but they are rapidly degraded in normoxia (Figure 1.4A). This is regulated by members of the Fe (II) and 2-oxoglutarate-dependent dioxygenase superfamily: the prolyl-4 hydroxylase domain (PHD1, 2 and 3) proteins (Bruick & McKnight, 2001;Kallio *et al.*, 1999). These proteins use oxygen as a co-substrate, thus the availability of oxygen regulates their enzymatic activity and enables them to sense local or general hypoxia (Steinhoff *et al.*, 2009;K *et al.*, 2004;Epstein *et al.*, 2001). Under normoxic conditions, the PHD proteins catalyse the hydroxylation of specific prolyl residues located within the oxygen dependent degradation (ODD) domain of the alpha subunit (Figure 1.4B) (Bruick & McKnight, 2001;Epstein *et al.*, 2001). Hydroxylation initiates the association of von Hippel-Lindau (VHL) tumour suppressor protein (an E3 ubiquitin ligase) with the alpha subunit and targets it for proteasomal degradation (Maxwell *et al.*, 1999;Kallio *et al.*, 1999;Ivan *et al.*, 2001). During periods of hypoxia, the lack of oxygen leads to a marked reduction in the activity of the PHD proteins, resulting in fewer prolyl residues being hydroxylated and the stabilisation of the alpha subunit (Epstein *et al.*, 2001).

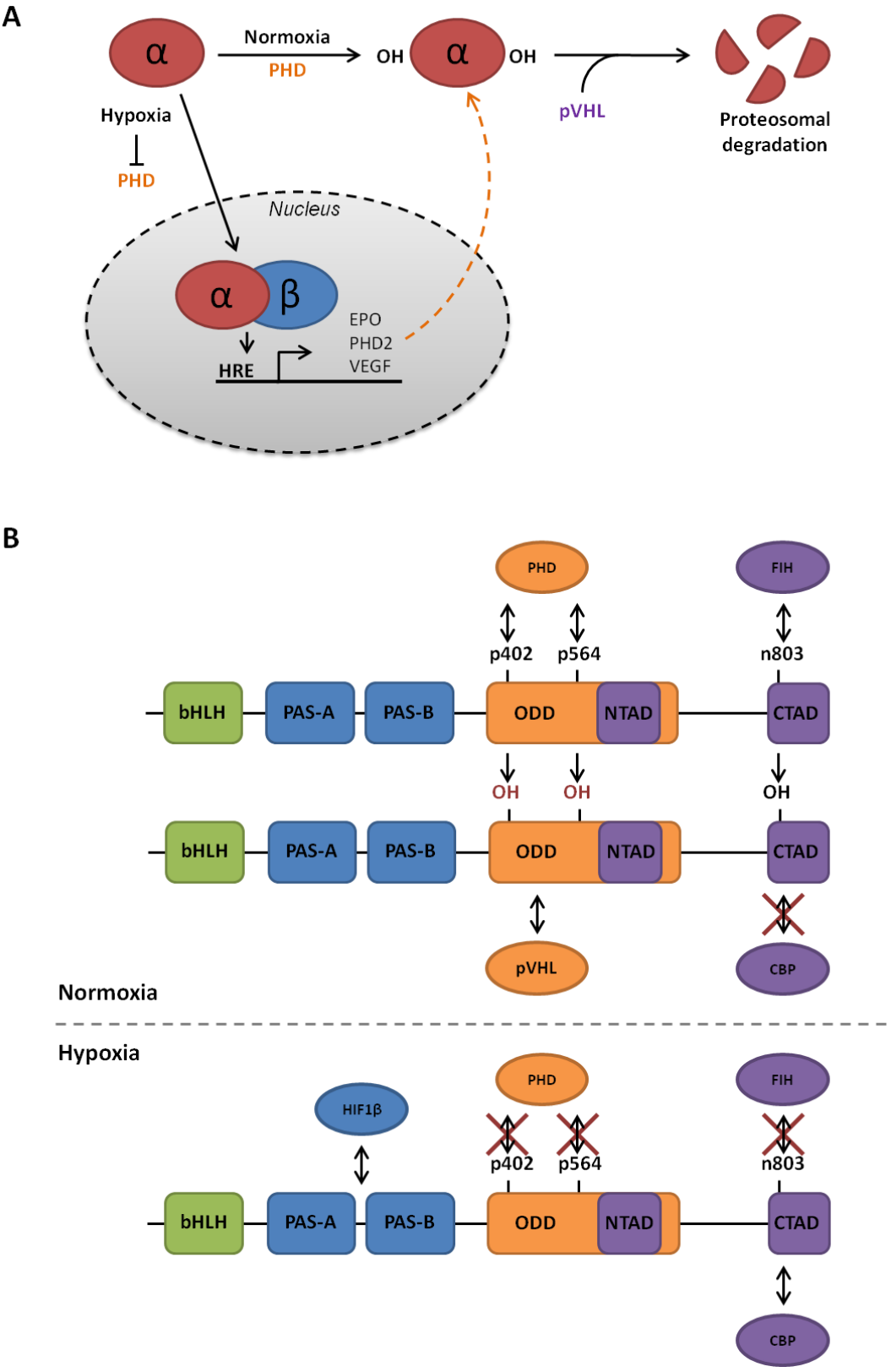
A
α
Normoxia
PHD
OH
α
OH
pVHL
Proteosomal degradation
Hypoxia
PHD
Nucleus
α
β
EPO
PHD2
VEGF
HRE
B
PHD
FIH
p402
p564
n803
bHLH
PAS-A
PAS-B
ODD
NTAD
CTAD
OH
OH
OH
pVHL
CBP
Normoxia
Hypoxia
HIF1β

Figure 1.4 | Oxygen dependent regulation of HIF-α subunit. *A) During periods of sufficient oxygen (normoxia) the HIF alpha subunits are degraded. Reduced oxygen (hypoxia) causes a decrease in PHD activity, allowing HIF-α subunits to accumulate and dimerise with HIF-1β to form active HIF in the nucleus. There it binds to a highly conserved consensus sequence, (A)CGTG, located within the enhancer domain. This sequence is termed the hypoxic response element (HRE) and leads to transcription of hypoxia-inducible genes (Luo & Shibuya, 2001). pVHL = Von Hippel-Lindau tumour suppressor protein. Negative feedback highlighted in orange. B) Schematic representation of the domain structures of HIF-1α highlighting the key protein interactions in normoxia and hypoxia. PER/ARNT/SIM (PAS-A & PAS-B) domains, oxygen-dependent degradation domain (ODD) and N-terminal / C-terminal transactivation domain (NTAD / CTAD) are shown. The proline residues highlighted in the oxygen degradation dependent domain are hydroxylated by Prolyl Hydroxylase Domain (PHD) enzymes and the asparagine residues at the C-terminus is hydroxylated by factor-inhibiting HIF (FIH). Adapted from Lee et al.(2004). Illustration of the key interactions that take place between the alpha subunit and other proteins, highlighting the domain through which they occur. HIF-1β = Hypoxia Inducible Factor Beta, PHD = Prolyl Hydroxylase Domain, FIH = Factor Inhibiting HIF, CBP = CREB Binding Protein, pVHL = Von Hippel-Lindau tumour suppressor protein.*

Factor Inhibiting HIF (FIH) is an asparaginyl hydroxylase and regulates the transcriptional activity of HIF. During normoxia, factor inhibiting HIF (FIH) catalyses the hydroxylation of an asparagine residue which blocks the interaction of HIF with its co-activators CREB-binding protein (CBP)/p300 through the transactivation domain (TAD, Figure 1.4B) (Kallio *et al.*, 1998;Zhang *et al.*, 2010). In hypoxia, the asparagyl residues are not hydroxylated, allowing the interaction of HIF with CBP/p300 and therefore the transcription of HIF target genes. Therefore in hypoxia, the impaired activity of the PHD and FIH enzymes leads to the alpha subunit evading degradation allowing it to form transcriptionally active heterodimers with HIF-1β via the PAS domains in the nucleus.

1.4.3 Oxygen-independent regulation of HIF

HIF is not only activated in response to low oxygen. For example, HIF-1α levels increase in proliferating cells, because the resulting daughter cells require more oxygen than the single parent cell. It is likely that growth factors increase synthesis of HIF-1α in a pre-emptive move to maintain oxygen-homeostasis. This increase in HIF switches ATP production to glycolysis and increased VEGF expression to ensure the oxygen needs for the cells are met (Brand & Hermfisse, 1997;Seagroves *et al.*, 2001;Jiang *et al.*, 1997). It has been shown that HIF can be regulated by the PI3K/AKT/mTOR pathway, a regulator of the cell cycle. The activation of this signalling pathway leads to an increase in translation of a subset of mRNAs including HIF-1α and HIF-2α (Laughner *et al.*, 2001;Hudson *et al.*, 2002;Toschi *et al.*, 2008;Hay & Sonenberg, 2004).

Non-hypoxic stimulation of HIF has also been observed in cells responsible for the immune response such as macrophages (Blouin *et al.*, 2004). For example cells exposed to the endotoxin lipopolysaccharide (LPS) have been shown to have increased levels of active HIF-1 and this regulation is believed to be at the transcriptional level as HIF-1α mRNA increase significantly in the presence of LPS (Blouin *et al.*, 2004).

Several other components regulate the stability of the alpha subunit in an oxygen-independent manner. For example all of the following lead to the alpha subunits evading proteasomal degradation in normoxia: inhibition of PHD proteins by intermediaries of the Kreb's cycle, sequestration of pVHL in nucleoli due to increased acidity and overexpression of a deubiquitase (DUB) called pVHL protein-interacting deubiquitinating enzyme 2(VDU2 aka USP20) (Fong & Takeda, 2008;Mekhail *et al.*, 2004;Li *et al.*, 2005). Stability of HIF-1α is also regulated by protein-protein interaction. For example, HSP90 and RACK1 actively compete to bind to HIF-1α and have antagonistic effects on protein stability (Hogenesch *et al.*, 1997;Liu *et al.*, 2007;Isaacs *et al.*, 2002).

1.5 HIF-1α versus HIF-2α

This study focuses on the spatial and temporal dynamics of HIF-1α and -2α. Even though these two isoforms have been implicated in activating and regulating the hypoxic response, it has become clear that they do not have redundant roles and do have many differences. Here I discuss some of the key differences that have been described so far.

Firstly, HIF-1α and HIF-2α are encoded by different genes, HIF1A and EPAS1, which are located on chromosome 14 (14q23.2) and chromosome 2 (2p21-p16), respectively. The translated proteins differ slightly in length (826 and 870 amino acids, respectively) with an overall sequence similarity of 48%. They have a similar domain structure (Figure 1.5) with the greatest amount of similarity within the bHLH, PAS-A and PAS-B domains (Table 1.2). Both isoforms have an ODD domain where residues 549-572 and 517-534 are vital for the VHL-dependent degradation of HIF-1α and HIF-2α, respectively (Huang *et al.*, 1998;O'Rourke *et al.*, 1999;Ema *et al.*, 1999;Ohh *et al.*, 2000;Cockman *et al.*, 2000;Tanimoto *et al.*, 2000;Kamura *et al.*, 2000). Additionally, both alpha subunits have nuclear localisation signals. Lys737, Arg738 and the surrounding amino acid sequence, function as the nuclear localisation for HIF-2α and residues 718-721 for HIF-1α (Hara *et al.*, 1999).

A

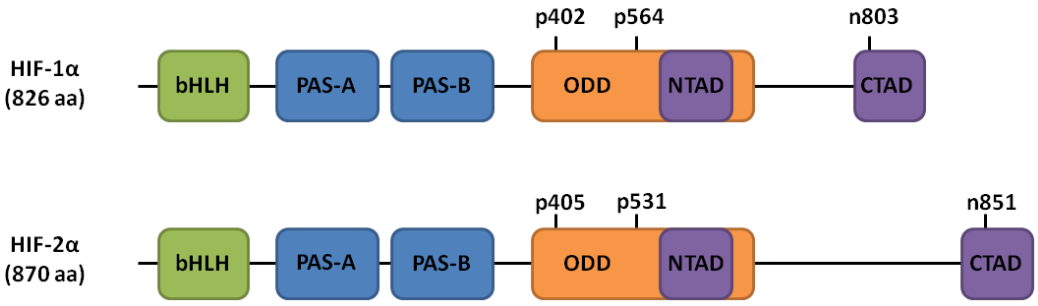

B

Domain	HIF-1α		HIF-2α		Sequence similarity
	Length (aa)	Position (aa)	Length (aa)	Position (aa)	
bHLH	54§	17-70§	54§	14-67§	94%
PAS-A	74§	85-158§	71§	84-154§	89%
PAS-B	71§	228-298§	71§	230-300§	94%
ODD	203§	401-603§	166#	517-682#	See below
NTAD	45§	531-575§	47§	496-542§	78%
CTAD	41§	786-826§	41§	830-870§	70%

C

>ODD_HIF1a
APAAGDTIISLDFGSNDTETDDQQLEEVPLYNDVMLPSPNEKLQNINLAMSPLPTAETPKPLRSSADPALNQEVALK
LEPNPESLELSFTMPQIQDQTPSPSDGSTRQSSPEPNSPSEYCFYVDSDMVNEFKLELVEKLFAEDTEAKNPFSTQD
TDLDLEMLAPYIPMDDDFQLRSFDQLSPLESSSASPESASPQSTVTVFQ

>ODD_HIF2a
TQTDFNELDLETLAPYIPMDGEDFQLSPICPEERLLAENPQSTPQHCFSAMTNIFQPLAPVAPHSPFLLDKFQQQLE
SKKTEPEHRPMSSIFFDAGSKASLPPCCGQASTPLSSMGGRSNTQWPPDPPLHFGPTKWAVGDQRTEFLGAAPLG
PPVSPPHVSTFKTR

Figure 1.5 | Comparison of HIF-1α and HIF-2α domains. *A) Schematic representation of the domain structures of HIF-1α and HIF-2α. A) Highlighted are the key residues and their position that are hydroxylated in hypoxia. (p = proline, n = asparagine). B) The size and location of domains, regions and motifs found within the protein sequence of HIF-1α and HIF-2α. Sequence similarities were calculated by performing sequence alignment using BlastP. §Data obtained from Uniprot, #Fedele et al. (2002). C) Alignment of the ODD sequences using BlastP Three regions are similar. The highlighted amino acids are those that are identical.*

1.5.1 Differential regulation of the HIF-α isoforms

The two alpha subunits are regulated at all levels: transcription of the *HIF1A* and *EPAS1* genes, mRNA translation, protein stability and transcriptional activity of the isoforms

themselves. Here are some examples of regulation that is unique to one isoform or an event that targets both isoforms but has a different effect.

TRANSCRIPTION – As previously discussed LPS has been shown to upregulate transcription of HIF-1α in an oxygen-independent manner. But **c**ytokines have been shown to differentially regulate HIF-1α and HIF-2α mRNA expression. Takeda *et al.* (2010) demonstrated that interferon gamma (IFNγ) increases HIF-1α but significantly decreases HIF-2α mRNA expression. Conversely, interleukin-4 (IL-4) initiates prolonged increase in HIF-2α mRNA expression, but has no effect on HIF-1α (Takeda *et al.*, 2010).

TRANSLATION – As mentioned previously, HIF-α can be regulated independently of oxygen levels by the PI3K/AKT/mTOR pathway (see chapter 1.3.2) however there is discrimination between the two HIF-α isoforms. Toschi *et al.* (2008) demonstrated that in renal cell carcinoma cell lines *HIF1A* translation is regulated by mTORC1 and mTORC2 but *EPAS1* translation is regulated by mTORC2 only (Toschi *et al.*, 2008). They also looked at Akt, a substrate of mTORC2, and found that the expression of HIF-1α and HIF-2α was dependent on different Akt isoforms (Toschi *et al.*, 2008).

In addition to this, HIF-2α is regulated at the post-transcriptional level by iron-response element binding protein 1 (IREBP1). This protein specifically inhibits the translation of HIF-2α when bound to the iron response element within the *EPAS1* transcript (Sanchez *et al.*, 2007).

It has also been suggested that HIF-1α protein synthesis is regulated by antisense HIF-1α (αHIF1, a transcript that is complementary to the 3' untranslated region (3'-UTR)). Upon hypoxic stimulation, in addition to an increase in *HIF1A* mRNA expression, there is an increase in the αHIF1 which associates with and destabilises the *HIF1A* mRNA transcript, thus preventing further translation (Uchida *et al.*, 2004). It is unknown whether a similar mechanism exists for HIF-2α.

PROTEIN STABILITY – It is well established that the protein stability of both alpha subunits is regulated via the hydroxylation of specific prolyl residues (Ivan *et al.*, 2001;Lando *et al.*, 2002) and that this leads to degradation following VHL-dependent poly-ubiquitination (Maxwell *et al.*, 1999;Kallio *et al.*, 1999;Ivan *et al.*, 2001). However, it has been shown that there are differences in the specificity of the PHD enzymes, for instance PHD3 preferentially hydroxylates HIF-2α (Appelhoff *et al.*, 2004). Furthermore, it appears that there are

differences in the stabilisation of HIF-1α and HIF-2α in hypoxia. Firstly, it has been shown that, in HeLa and other cell lines, HIF-2α stabilises at oxygen levels of 2-5% but levels need to be lower for HIF-1α stabilisation (0-2% O_2) (Nilsson *et al.*, 2005;Holmquist-Mengelbier *et al.*, 2006;Li *et al.*, 2009). Secondly, a difference in the duration of protein stabilisation has been observed. Holmquist-Mengelbier *et al.* (2006) found that in prolonged hypoxia, high levels of HIF-2α levels were maintained whereas levels of HIF-1α decline after several hours in neuroblastoma cells (Holmquist-Mengelbier *et al.*, 2006;Uchida *et al.*, 2004). This will be discussed further in chapter 3.

There are a number of mechanisms that specifically regulate HIF-1α stability. For example, Heat shock protein 70 (HSP70) and carboxyl terminus of HSP70-interaction protein (CHIP) have been shown to bind HIF-1α in prolonged hypoxia and target the subunit for proteasomal degradation (Luo *et al.*, 2010). Secondly, arrest defective 1 (ARD1) has been shown to specifically acetylate HIF-1α, which results in the destabilisation of the protein (Jeong *et al.*, 2002;Yoo *et al.*, 2006). And finally heat shock protein 90 (HSP90) and receptor for active kinase 1 (RACK1), previously mentioned in section 1.4.3 (Hogenesch *et al.*, 1997;Liu *et al.*, 2007;Isaacs *et al.*, 2002).

TRANSCRIPTIONAL ACTIVITY – FIH regulates both HIF-1α and HIF-2α in an oxygen-dependent manner, however Bracken *et al.* (2006) demonstrated that FIH preferentially hydroxylates HIF-1α (Bracken *et al.*, 2006). In addition to this, several kinases (CK1, MAPK, ATM) have been identified to phosphorylate HIF-1α and increase its activity (Kalousi *et al.*, 2010;Mylonis *et al.*, 2006;Cam *et al.*, 2010). However, it is yet to be determined whether these kinases also modify HIF-2α. Sirtuin1 (SIRT1) has been shown to de-acetylate both HIF isoforms, but with differential effects. The removal of the acetyl group results in the transcriptional repression of HIF-1α and the transcriptional activation of HIF-2α (Dioum *et al.*, 2009;Lim *et al.*, 2010).

More interestingly, HIF associated factor (HAF aka SART1), fits into several categories. HAF promotes VHL-independent degradation of HIF-1α in acute hypoxia but upregulates HIF-2α transcriptional activation in chronic hypoxia, which has led to this molecule being put forward as a differential regulator that switches cells from HIF-1α to HIF-2α dependent signalling in prolonged hypoxia (Koh *et al.*, 2008).

Table 1.2 | Examples of protein-protein interactions that regulate transcription and translation of HIF-1α and HIF-2α mRNA in an O_2-independent manner.

	Protein	Isoform		Outcome	Reference
Transcription	IFNγ	HIF-1α	✓	↑	Takeda *et al.* (2010)
		HIF-2α	✓	↓	
	IL-4	HIF-1α	×	-	
		HIF-2α	✓	↑	
Translation	Antisense HIF1A	HIF-1α	✓	↓	Uchida *et al.* (2004)
		HIF-2α	×	-	
	IREBP1	HIF-1α	×	-	Sanchez *et al.* (2007)
		HIF-2α	✓	↓	

Table 1.3 | Examples of post-translation modifications and protein-protein interactions that regulate protein stability and transcriptional activity of HIF-1α and HIF-2α in an O2-independent manner.

	Protein	PTM / interaction	Isoform		Outcome	Reference
Protein stability	ARD1	PTM	HIF-1α	✓	↓	Jeong *et al.* (2002), Yoo *et al.* (2006)
			HIF-2α	×	-	
	HSP70	PTM	HIF-1α	✓	↓	Luo *et al.* (2010)
			HIF-2α	×	-	
	HAF	PTM	HIF-1α	✓	↓	Koh *et al.* (2011), Koh *et al.* (2008)
			HIF-2α	×	-	
	HSP90	Interaction	HIF-1α	✓	↑	Liu *et al.* (2007), Hogenesch *et al.* (1997), Isaacs *et al.* (2002)
			HIF-2α	×	-	
	Rack1	Interaction	HIF-1α	✓	↓	Liu *et al.* (2007)
			HIF-2α	×	-	
Transcriptional activity	HAF	Interaction	HIF-1α	×	-	Koh *et al.* (2011), Koh *et al.* (2008)
			HIF-2α	✓	↑	
	SUMO-1/2/3	PTM	HIF-1α	✓	↓	van Hagen *et al.* (2010), Berta *et al.* (2007)
			HIF-2α	✓		
	SIRT1	PTM	HIF-1α	✓	↓	Dioum *et al.* (2009), Lim *et al.* (2010)
			HIF-2α	✓	↑	
	CHFs	Interaction	HIF-1α	×	-	Chin *et al.* (2000)
			HIF-2α	✓	↓	

It should be noted that there is far less known about mechanisms that specifically regulate HIF-2α largely due to HIF-1α being the more popular focus of research in the field of hypoxia. But it is clear that the two isoforms are differentially regulated at all levels.

1.5.2 Differential roles of HIF-1α and HIF-2α in physiological processes

HIF-1α and HIF-2α exhibit some redundancy in function. However, there are some processes that are either differentially regulated or uniquely regulated by one of the two isoforms.

HYPOXIA INDUCIBLE GENES – Hundreds of HIF target genes have been identified so far (Mole *et al.*, 2009) and there is increasing evidence that some genes are specifically regulated by either HIF-1α or HIF-2α (Table 1.4). Genomic studies have found that generally, but not exclusively, HIF-1α regulates genes involved in the metabolic response and HIF-2α target genes control the respiratory response to oxygen deprivation (Mole *et al.*, 2009;Hu *et al.*, 2003). There is substantial evidence that HIF-2α is solely responsible for regulating erythropoiesis (reviewed in Haase, 2013), iron homeostasis (Haase, 2013) and lipid metabolism (Schoenenberger *et al.*, 2015).

Table 1.4 | Examples of target genes unique to HIF-1α or HIF-2α. *Adapted from Keith et al. (2012).*

	Gene	Process	Reference
HIF-1α target genes	BNIP3 (BNIP3)	Autophagy and apoptosis	Raval (2005)
	HK1 (hexokinase 1)	Glycolysis	Iyer (1998), Ryan *et al.* (1998)
	HK2 (hexokinase 2)		Hu *et al.* (2003), Iyer (1998), Ryan *et al.* (1998)
	PFK (phosphofructokinase)		Hu *et al.* (2003), Iyer (1998), Ryan *et al.* (1998)
	ALDOA (ALDA)		Hu *et al.* (2003), Iyer (1998), Ryan *et al.* (1998)
	PGK1 (PGK1)		Hu *et al.* (2003), Ryan *et al.* (1998)
	LDHA (LDHA)		Hu *et al.* (2003), Ryan *et al.* (1998)
HIF-2α target genes	EPO (erythropoietin)	Erythropoiesis	Scortegagna *et al.* (2003), Gruber (2007), Rankin *et al.* (2007), Kapitsinou (2010)
	ANGPT2 (angiopoietin 2)	Blood vessel remodelling	Skuli (2009)
	POU5F1 (OCT4)	Stem cell identity	Covello *et al.* (2006)
	SCGB3A1 (secretoglobin 3A1)	Growth-inhibitory cytokine	Mazumdar (2010)
	TGFA (TGFα)	Growth factor	Raval (2005), Gunaratnam (2003)
	CCND1 (cyclin D1)	Cell cycle progression	Raval (2005)

ACUTE VS CHRONIC HYPOXIA – It has also been hypothesised that the response to different types of hypoxia is differentially controlled by the two isoforms i.e. HIF-1α is the mediator of the response to acute hypoxia, but during periods of prolonged hypoxia control switches to HIF-2α (Holmquist-Mengelbier *et al.*, 2006;Koh *et al.*, 2011).

CELL CYCLE – The HIF-α isoforms regulate components of other signalling pathways. For example, HIF-1α has been shown to up-regulate p53 and down-regulate c-Myc, mTOR and β-catenin, whereas induction of HIF-2α has the converse effect on these signalling molecules, suggesting that HIF-1α suppresses cell proliferation and HIF-2α promotes cell cycle progression (Koshiji *et al.*, 2004;Koshiji *et al.*, 2005;Gordan *et al.*, 2007;Florczyk *et al.*, 2011)

NO PRODUCTION – The two alpha subunits are regulated by the levels of interferon gamma (IFNγ) resulting opposing effects on nitrous oxide (NO) production. Low levels of IFNγ result in high levels of HIF-2α and reduced NO production due to an increase in arginase, the enzyme that catalyses the conversion of aginine (the substrate required for NO production) to ornithine and urea (Figure 1.6). Whereas high levels of IFNγ leads to HIF-1α domination and increased NO productions (Figure 1.6)(Takeda *et al.*, 2010).

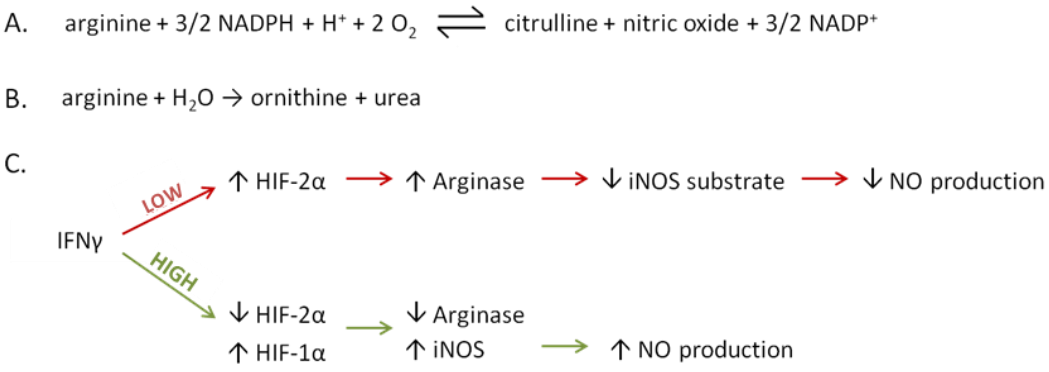

Figure 1.6 | Differential effect of HIF-α levels on nitrous oxide production. *A) Reaction catalysed by nitrous oxide synthase (iNOS). B) Reaction catalysed by arginase. C) The antagonistic effect of interferon gamma (IFNγ) levels on NO production.*

EMBRYONIC DEVELOPMENT – Knockout mice experiments have shown that the loss of the HIF-1α or HIF-2α gene is embryonic lethal. However, lethality is due to defects in the heart and impaired lung formation, respectively (Loboda *et al.*, 2010). Thus, indicating that both play vital yet different roles in embryonic development (Peng *et al.*, 2000;Tian *et al.*, 1998;Iyer *et al.*, 1998;Ryan *et al.*, 1998).

1.5.3 Differential role of HIF-1α and HIF-2α in disease

The involvement of HIF in a range of disease makes it an interesting and promising therapeutic target. However, depending on the disease, HIF can have a protective role or can contribute to the pathogenesis (Figure 1.7).

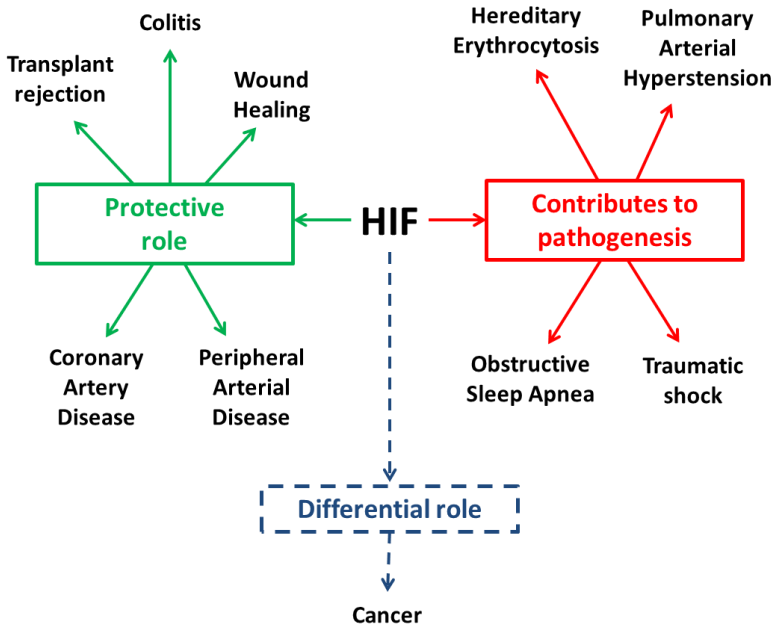

Figure 1.7 | Differential role of HIF in disease.

There is particular focus on the relationship between HIF and cancer, as many HIF target genes are related to tumour progression and metastasis (Gilkes & Semenza, 2013). Furthermore, it has been shown that a hypoxic tumour microenvironment is associated with aggressiveness and resistance to treatment (Liu *et al.*, 2008;Nardinocchi *et al.*, 2009). However, the role of HIF in cancer is complex. Both HIF-1α and HIF-2α can be over-expressed in many different cancers with HIF-2α being generally seen as a tumour promoter and HIF-1α a tumour suppressor; a classic example being clear cell renal cell carcinoma (ccRCC). However, this characterisation is not always true and in some cancers HIF-2α has a tumour suppressive role. For example, Mazumdar *et al*. (2010) demonstrated that knocking out HIF-2α in the KRAS mouse model led to increased tumour growth due to the down regulation of the tumour suppressor gene Scgb3al (Mazumdar *et al.*, 2010).

To complicate matters further, not only does the prognostic role of HIF-1α and HIF-2α vary between cancers, they even vary within the same types of cancer e.g. hepatocellular cancer (Table 1.5).

Table 1.5 | Differential roles of HIF-1α and HIF-2α in cancer.

Cancer / Model	HIF isoform	Up/down regulated	Prognosis	Reference
Breast Cancer	HIF-1α	↑	Poor	Gilkes and Semenza (2013)
Neuroblastoma	HIF-1α	↑	Good	Keith *et al.* (2012)
		↑	Poor	Dungwas *et al.* (2012)
Renal Cell Carcinoma	HIF-1α	↑	Good	Qing and Simon (2009)
Soft Tissue Sarcoma	HIF-1α	↑	Poor	Eisinger-Mathason *et al.* (2013)
	HIF-2α	↓	Good	
Gastric cancer	HIF-2α	↑	Poor	Wang *et al.* (2010), Yoon (2014)
Hepatocellular cancer (HCC)	HIF-2α	↑	Poor	Talks *et al.* (2000), Bangoura *et al*. (2007), Yang *et al.* (2014), Zhao *et al.* (2014)
		↓	Poor	Sun *et al.* (2013)
		↑	Good	Menrad *et al.* (2010)
Pancreatic cancer	HIF-2α	↑	Poor	Talks *et al.* (2000), Criscimanna *et al.* (2013)
Colorectal cancer	HIF-2α	↑	Poor	Talks *et al.* (2000), Hui *et al.* (2002), Franovic *et al.* (2009), Cleven *et al.* (2008), Koukourakis *et al.* (2006)
		↓	Poor	Imamura *et al.* (2009)

Although HIF is of great interest as a potential therapeutic target and it is evident that there is a link between deregulation of HIF and therapeutic outcome, there is not a clear cut relationship.

1.5.4 Tissue distribution

As with cancer, the expression of the alpha subunits differs in tissues. HIF-1α is ubiquitously expressed throughout the body in all cell types; however HIF-2α is limited to distinct populations on cells in certain tissues or organs (Wiesener *et al.*, 2003). For example: in the liver, HIF-2α accumulates in the nuclei of hepatocytes, i.e. parenchymal distribution; in the kidneys, pancreas and brain, HIF-2α nuclear accumulation is predominantly in non-parenchymal cells; and, in myocardial tissue equal distribution is observed (Wiesener *et al.*, 2003).

1.5.5 Cellular localisation

Within our research group, single cell imaging of HIF-1α and HIF-2α has revealed that the two proteins exhibit different nuclear localisation patterns. HIF-1α is only observed in cells that have been subjected to hypoxia or treated with an inhibitor of the PHD enzymes, Dimethyloxalylglycine (DMOG). Approximately 2-4 hours after oxygen levels fall, homogenous extra-nucleolar accumulation of HIF-1α is observed in the nucleus. Whereas, in cells expressing EGFP-HIF-2α, punctate foci are observed (see Figure 1.8). Moreover, some HIF-2α stabilisation is observed without subjecting cells to hypoxia or DMOG treatment, therefore hinting that HIF-2α may evade oxygen-dependent degradation.

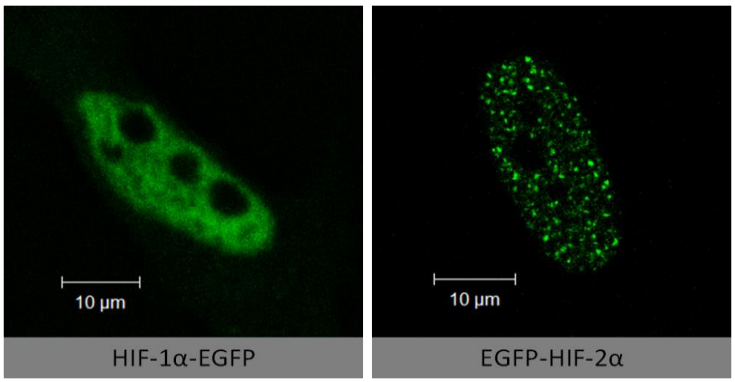

Figure 1.8 | Nuclear localisation of HIF-1α and HIF-2α in HeLa cells. *HeLa cells transiently transfected with HIF-1α-EGFP (right) and HIF-2α-EGFP (left) showing different nuclear sub-localisation patterns. HIF-1α shows a homogenous nuclear localisation during hypoxia, whereas HIF-2α localises in sub-nuclear foci or "speckles".*

These observations strongly correlate with previous findings:

1) Hypoxic accumulation of HIF-1α in the nucleus was first described by Huang *et al* (1996). They also observed the translocation of HIF-1α from the cytoplasm into the nucleus when in hypoxia. However, they too observed that HIF-2α tagged with GFP was stabilised in the nucleus regardless of oxygen levels (Hara *et al.*, 1999).

2) Takahashi *et al* also noticed that in Bovine aortic endothelial cells HIF-2α localised in the nucleus (excluded from the nucleoli) in "dots" and they too found that hypoxia or treatment with a hypoxia mimic ($CoCl_2$) did not affect the nuclear localisation of HIF-2α (Takahashi *et al.*, 2004).

1.6 The Cell Nucleus

The nucleus was first described by Franz Bauer in 1802. It holds the majority of the cells genetic material and controls the activities of the cell by regulating gene expression. As with the cytoplasm, spatial organisation plays an important role within the nucleus to contain, regulate and streamline processes. However, unlike the cytoplasm, where processes are contained within organelles, nuclear functions are compartmentalised into domains. The different nuclear bodies can be distinguished by their size, shape, number and presence of particular proteins. Some examples follow.

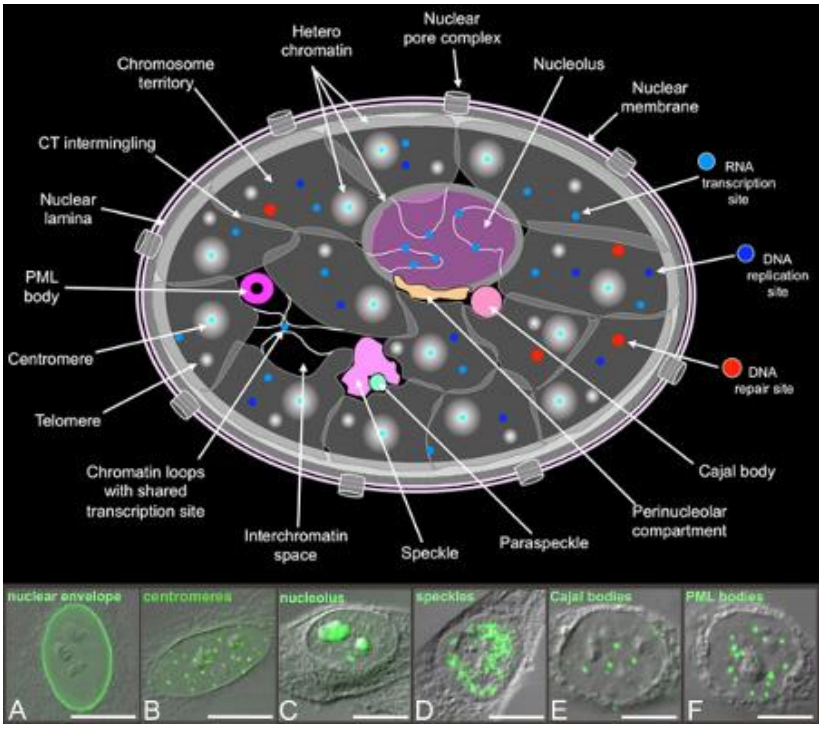

Figure 1.9 | Structure of the nucleus. *Schematic diagram of the nucleus, highlighting key domains and sub-compartments. (Taken from http://www.fli-leibniz.de/www_imaging/structure_en.php)*

NUCLEOLUS – The nucleolus is the largest and most well studied substructure in the nucleus. Many processes relating to ribosome biosynthesis takes place here such as transcription of ribosomal DNA and assembly of the ribosomes (Cmarko *et al.*, 2008;Busch & Smetana, 1970). Although it is mainly seen as a "ribosome factory" it has recently come to light that it may also have a role in the regulation of cell cycle, proliferation and lifespan of a cell (Pederson, 1998;Carmo-Fonseca *et al.*, 2000;Visintin & Amon, 2000;Takemura *et al.*, 2002;Chestukhin *et al.*, 2002).

CAJAL BODIES – Also known as coiled bodies (CBs) due to being composed of tangled fibrillar strands (Almeida *et al.*, 1998;Pombo *et al.*, 1999;Iborra *et al.*, 2001), there are between 1-5 of these spherical compartments per nucleus but this can change depending on cell cycle stage and disease state (Brasch & Ochs, 1992;Boudonck *et al.*, 1999;Gall, 2000). They are highly mobile and dynamic and have been observed: moving throughout the nucleoplasm; merging with and travelling through the nucleolus; and, going through joining and separation events, to make larger or smaller CBs (Platani *et al.*, 2000;Lyon *et al.*, 1997). Although reasonably well studies, the function of CBs has not been clearly defined as

yet, but there is some evidence to suggest that they are involved in the storage of small nuclear ribonucleic proteins (snRNPs) and may deliver these to the nucleolus (Lamond & Earnshaw, 1998;Matera, 1999;Spector, 2001;Zhou *et al.*, 2002). It has also been suggested that the transcription machinery assembles within CBs before relocating to transcription factories (Platani *et al.*, 2002).

PML BODIES – PML bodies get their name from the distinguishing presence of promyelocytic leukemia (PML) protein. They are donut shaped nuclear bodies, typically 0.25-0.5 μm in diameter and number around 10-30 per nucleus (Ascoli & Maul, 1991;Stuurman *et al.*, 1992). As well as PML, many other proteins such as CBP, SP100, p53, NRF2 and eIF-4E have been shown to localise at these nuclear bodies (LaMorte *et al.*, 1998;Lai & Borden, 2000;Sternsdorf *et al.*, 1999;Fogal *et al.*, 2000;Ben-Dor *et al.*, 2005). The function of the PML bodies is not clearly defined but based on the additional occupants it has been suggested that they may play a role in transcriptional regulation or translational regulation. They have also been linked to viral replication (Maul, 1998).

TRANSCRIPTION FACTORIES – It was previously thought that RNA polymerase II (RNAPII) is recruited to the promoters of genes that are to be transcribed, however it is now believed that active loci migrate to domains where the transcriptional machinery is located (Iborra *et al.*, 1996;Jackson *et al.*, 1998). Different genes, even genes that are separated by great distances, in the genome have been shown to concurrently occupy the same transcription factories (Osborne *et al.*, 2004;Jackson *et al.*, 1993;Jackson *et al.*, 1998).

SPLICING FACTOR COMPARTMENTS – Pre-mRNA splicing occurs co-transcriptionally. Splicing factors continuously exchange between splicing factor compartments (SFCs) and sites of transcription. SFCs are irregular in shape but following inhibition of transcription these nuclear speckles increase in size and change shape, indicating further these are storage sites of inactive splicing factors (Sinclair and Brasch, 1978).

There is little known about how nuclear bodies are formed as they are not delineated by a lipid bilayer (like the nucleus itself). The lack of intra-nuclear membranes has led to suggestions that they form via “self-organisation”, whereby the architecture and function of the structure is determined via the physical interaction of its components (Misteli, 2001).

There is some evidence that there is a sub-nuclear framework, similar to the cytoskeleton, which is composed of a mixture of proteins such as lamin B (Stuurman *et al.*, 1990;Berezney

& Coffey, 1977). It has been suggested that this nuclear matrix may play a role in the orchestrating nuclear processes and is likely to act as a "substratum" for nuclear bodies (Mitchell & Fraser, 2008;Ascoli & Maul, 1991;Stuurman *et al.*, 1992).

The discovery and study of the heterogeneous localisation of nuclear proteins and nuclear domains has been facilitated by the advancements in microscopy and protein labelling techniques made over the last century.

1.7 Microscopy

1.7.1 A brief history of fluorescent confocal microscopy

1595 saw the invention of the first instrument that facilitated the visualisation of objects that could not be seen by the naked eye but it wasn't until 1911 that the first successful fluorescent microscope was constructed by the physicist, Oskar Heimstädt (Heimstadt, 1911). This design was reconfigured by Ellinger and Hirt (1929) so that the light source was on the same side of the specimen as the objective, resulting in both the emission and excitation light passing through the objective (Figure 1.10), creating the epi-fluorescence microscope (Ellinger & Hirt, 1929).

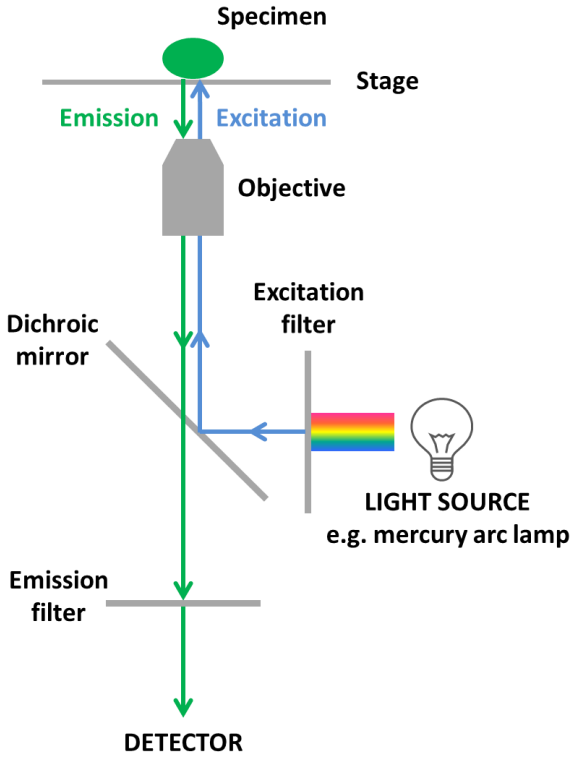

Figure 1.10 | Lightpath of an epi-fluorescence microscope. *Schematic representation of the basic setup of an inverted epifluorescence microscope.*

The problem of "out of focus light" associated with epi-fluorescence microscopes was circumvented by Minsky's confocal microscope, which incorporated pinhole apertures to block this non-specific fluorescence from reaching the detector (Minsky, 1961). He also introduced "raster scanning", whereby an image is created by systematically illuminating

the field of interest line by line, to reduce the amount of the specimen that is illuminated at any one time. Minksy's design was further improved by the addition of dichroic mirrors (Ploem, 1967) and upgrading the light source to a laser beam (White *et al.*, 1987;Van Meer *et al.*, 1987) resulting in the basis of the modern laser scanning confocal microscope.

Table 1.6 | Timeline of key events in the history of light microscopy.

1595	Invention of microscope
1911	First fluorescent microscope
1929	First epi-fluorescence microscope
1942	First example of immunofluorescence
1961	Minsky's patent of confocal microscope accepted
1972	Development of Fluorescence correlation spectroscopy (FCS)
1976	Development of Fluorescence recovery after photobleaching (FRAP) Försters / fluorescence resonance transfer (FRET) experimentally proven
1987	Laser scanning confocal microscope
1993	Light sheet microscopy Single molecule microscopy
1992-1996	Cloning and development of GFP
1999	Cloning of red fluorescent proteins
2000	Development of super-resolution method - STED & SIM
2002	Photoactivatable fluorescent proteins
2006	Development of Super-resolution methods - PALM / fPALM / STORM
2008	Nobel prize for chemistry awarded to researchers involved in the cloning and development of GFP
2014	Nobel prize for chemistry awarded to developers of super-resolution imaging

1.7.1.1 Fluorescence microscopy and labelling methods

Fluorescence refers to the ability of a substance to absorb light at a certain wavelength and emit light at a higher wavelength (Figure 1.11) and was first described in 1852 by Sir George Stokes. However, the earliest recorded use of fluorescence in biological investigations wasn't until almost a century later. However, when the fluorescent microscope was first invented, scientists relied upon autofluorescence (the natural emission of light from a specimen) until Ellinger and Hirt pioneered the use of "secondary fluorescence", whereby they introduced an exogenous fluorescent substance (fluorescein) to improve contrast of the sample (Ellinger & Hirt, 1929).

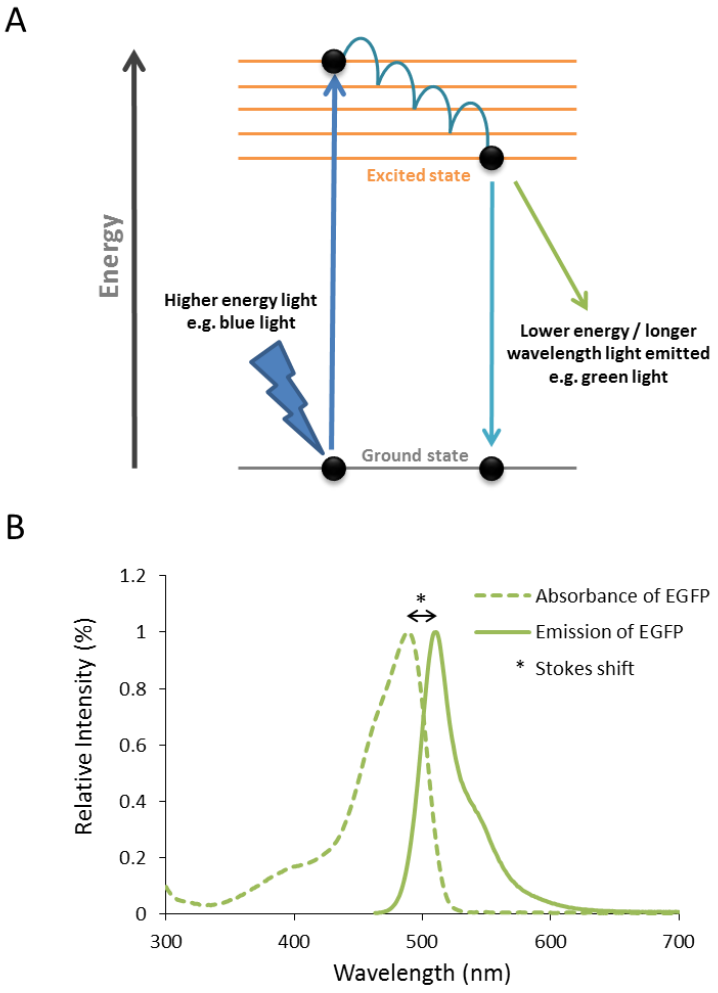

Figure 1.11 | Overview of fluorescence. *A) Schematic representation of the principle of how fluorescence occurs. Briefly, an orbital electron of a molecule or atom is electronically excited by absorbing photons from higher energy light (e.g. blue). As the electron relaxes through energy levels (orange lines) to its ground state, photons of a lower energy wavelength (e.g. green) are emitted. B) Example excitation - emission spectra of enhanced green fluorescent protein (EGFP).*

It was only in the 1940's that immunofluorescence, a technique that permits specific labelling of cells, structures and proteins with fluorescent probe, emerged. Coons *et al* took antibodies raised against strains of pneumococcus and attached a fluorescent molecule (Coons *et al.*, 1941). They labelled tissue from patients positive and negative for this bacteria and observed a clear difference in the signal between the two samples (Coons *et al.*, 1942). However, the biggest breakthrough for fluorescence microscopy came in 1994 when Chalfie *et al*. demonstrated how the green fluorescent protein (GFP), from the jellyfish *Aequorea victoria*, could be used to visualise proteins in living organisms (Chalfie *et al.*, 1994). The cloning of GFP opened the door for the creation of genetically labelled proteins of interest facilitating the study of intracellular localisation and dynamic behaviour of proteins of interest in real time *in vivo*.

Further developments were made when Roger Tsien and colleagues conducted exploratory mutagenesis of GFP creating enhanced GFP (EGFP), a derivative that is 30x brighter than the wildtype, and derivatives with a shift in the excitation / emission spectra: BFP (blue), CFP (cyan) and YFP (yellow) (Heim & Tsien, 1996). To add to these tools, the orange-red fluorescent protein, dsRED, that emits at 583 nm following excitation at 558 nm, was cloned from a reef coral *Discosoma sp* in 1999 (Matz *et al.*, 1999). The availability of these different fluorescent proteins (only a subset mentioned here) has meant that genetically-encoded spectrally-discrete reporters can be created, thus facilitating the simultaneous study of several proteins of interest *in situ*. Furthermore, it has permitted the non-invasive study of protein kinetics and interactions in living cells. The invaluableness of GFP (and its variants) and the genetic tagging of biomolecules to scientific research was recognised by the award of the Nobel Prize in chemistry in 2008.

1.7.2 Probing the dynamics of proteins further

In the 1970s, it was proposed that fluorescence microscopes could be utilised for more than just imaging, but could also be used to study reaction kinetics, diffusion and intermolecular interactions. Some examples include: fluorescence correlation spectroscopy (FCS), Förster / fluorescence resonance electron transfer (FRET) and fluorescence recovery after photobleaching (FRAP).

1.7.2.1 FCS

This technique measures fluctuations in fluorescent signal coming from labelled molecules moving in and out of a defined region. These measurements can be used to determine the concentration and diffusion rate of the molecule being studied. Advancements in detection methods led to the quantification of the dynamics of single molecules, with Rigler and Widengren being the first to demonstrate this in 1990.

In principle, FCS can be used to measure intermolecular interactions of a fluorescently labelled protein as the diffusion rate would slow upon binding to a larger molecule. However, the development of two-colour FCS (fluorescence cross-correlation spectroscopy / FCCS) has meant the interaction of any two molecules, regardless of size, can be studied (Schwille *et al.*, 1997).

1.7.2.2 FRET

This technique is based on the principle, proposed by Theodor Förster in the 1940s (Förster, 1946) and confirmed experimentally in 1967 (Stryer & Haugland, 1967), that the energy generated from electronic excitation can be passed from one fluorophore (donor) to another (acceptor) when the two chormophores are within close enough proximity (10 nm). However, it wasn't until the development of GFP variants CFP and YFP, that FRET was utilised to study protein-protein interactions *in vivo* (Bacskai *et al.*, 1993). Shortly after, FRET-sensors were developed that act as biological indicators. Examples include calcium (Miyawaki *et al.*, 1997;Romoser *et al.*, 1997;Emmanouilidou *et al.*, 1999), cyclic AMP (Zaccolo *et al.*, 2000), apotosis (Xu *et al.*, 1998) and synaptic activity (Vanderklish *et al.*, 2000).

Table 1.7 | Key landmarks of FRET

Year	Event	Reference
1993	First application of FRET to study molecular interactions *in situ*.	Bacskai *et al.* (1993)
1995	Development and application of fluorescence lifetime imaging (FLIM)-FRET to study the dimerization of cell surface receptors in single cells.	Gadella and Jovin (1995)
1998	Confirmation of the existence of 'lipid rafts'.	Kenworthy and Edidin (1998), Varma and Mayor (1998)
1997>	Development of FRET-sensors	See text

1.7.2.3 FRAP

This fluorescence perturbation technique involves irreversible bleaching of fluorescently labelled proteins. The redistribution of non-bleached molecules (or "recovery") into the bleached region is monitored (Figure 1.12) and subsequent analysis of the recovery of fluorescent molecules provides information on mobility.

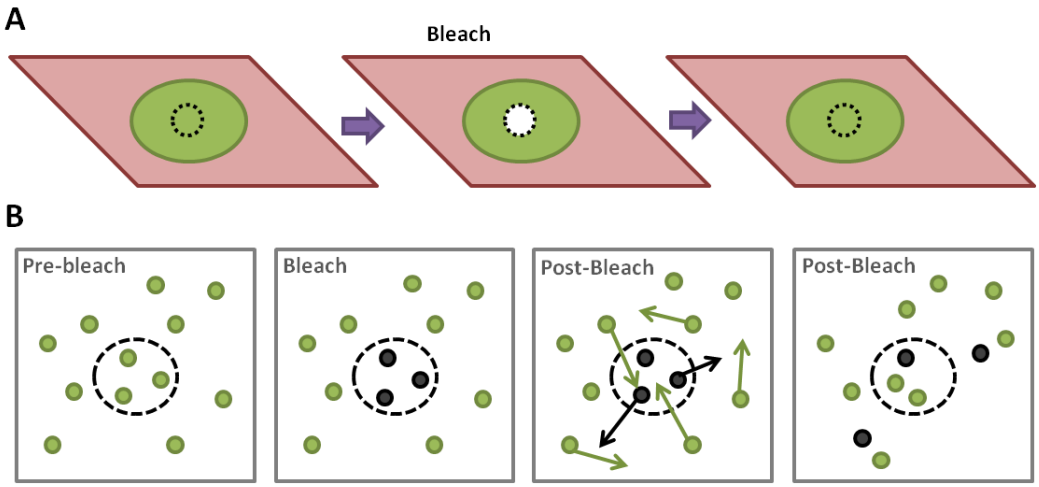

Figure 1.12 | Fluorescent recovery after photobleaching. *A) Schematic of time-lapse imaging to capture recovery of fluorescence. B) Schematic of molecular redistribution following photobleaching. Black broken circle = bleached region, black circles = bleached molecules, green circles = non-bleach molecules.*

Although FCS can be used to measure diffusion of single molecules, for answering certain biological questions FRAP is more advantageous as the whole cell can be monitored and it can detect the presence of immobile populations of molecules.

Due to ease of labelling, FRAP was first utilised to study the movement of protein within the cell membrane (Peters *et al.*, 1974) as these could be easily labelled. However, today, genetic labelling enables the study of protein trafficking anywhere within the cell.

It may seem surprising that these aforementioned techniques were all invented before the realisation of the laser scanning confocal microscope and the cloning of GFP (Table 1.7). However, these later developments only broadened the applications of these techniques by facilitating the non-invasive study of real-time diffusion and interactions of fluorescently labelled protein in living cells.

1.7.3 Super-resolution microscopy

The diffraction limit theory was conceived in 1873 and states that the smallest resolvable distance between two points is half the wavelength of the light used for illumination (Abbe, 1873), which essentially means that objects less than 150-200 nm apart cannot be resolved with conventional light microscopy. Now, over 100 years later, with the arrival of super-resolution we are able to see beyond the diffraction limit, with distances down to tens of nanometres being resolved. Up until recently, to resolve structures that were closer than 200 nm, either electron microscopy (Ruska, 1987) or total internal reflection (TIRF) microscopy (Axelrod, 1981) were used. Although modern electron microscopes are capable of achieving more than 1 nm resolution (Erni *et al.*, 2009), they cannot be used to image living cells and there is an intensive sample preparation protocol. TIRF is also limited to certain applications as only structures that are no more than 100 nm away from the coverslip can be studied. However, the last twenty years has seen the emergence of new super-resolution (SR) imaging techniques which can be divided into two categories: illumination-based such as stimulation emission depletion (STED) (Hell & Wichmann, 1994) or structured illumination (SIM) microscopy (Gustafsson, 2000); and, single-molecule / probe-based e.g. photo-activated localisation (PALM) (Betzig *et al.*, 2006;Hess *et al.*, 2006) or stochastic optical reconstruction (STORM) microscopy (Rust *et al.*, 2006). These methodologies mean that structures can be visualised in living cell at the molecular level and have already been utilised in discerning the three-dimensional organisation of molecules in the nuclear pore complex (Schermelleh *et al.*, 2008) and the distribution of proteins in structures such as microtubules (Huang *et al.*, 2008) and lysosomes (Betzig *et al.*, 2006). SR has also been utilised to study dynamic processes such as the formation of

macromolecular complexes e.g. focal adhesions (Shroff *et al.*, 2008). The recent ground-breaking developments to surpass the diffraction limit of conventional fluorescence microscopy resulted in E. Betzig, S. Hell and W. Moerner being awarded the Nobel Prize in chemistry in 2014.

1.7.4 Single molecule tracking (SMT)

Although perturbation (e.g. FRAP) and correlation (e.g. FCS) techniques can provide information on diffusion, this information is based on the average behaviour of the protein of interest meaning that, as with any population technique, any heterogeneity within the population will be masked (Brameshuber & Schuetz, 2008). Single molecule tracking (SMT) is a technique that allows the elucidation of the spatial and temporal dynamics of individual molecules by direct monitoring of said molecules in real time.

Several techniques have been developed for SMT of fluorescently labelled proteins (reviewed in Meuller *et al.,* 2013) and have been implemented in tracking RNA polymerase II in three dimensions (Abrahamsson *et al.*, 2013) and deciphering how transcription factors search target binding sites (Chen *et al.*, 2014).

One alternative to fluorescence microscopy, which can be utilised for SMT in living cells, is photothermal imaging of protein labelled with gold nanoparticles, which is discussed in Chapter 5.

1.8 Project aims

The aim of my project is to study the spatial and temporal regulation of the main intracellular effectors of the hypoxia signalling pathway.

The specific aims of my project were:

- Improving molecular and cellular tools for imaging HIF-1/2α.
- Investigating the temporal dynamics of HIF-1/2α at the single cell level
- Investigating the sub-nuclear spatial localisation of HIF-2α at the single cell and single molecule levels

I have employed live cell imaging techniques to elucidate the spatial and temporal dynamics of the key mediators of the hypoxia signalling pathway at the cellular level. I have also utilised confocal microscopy to study sub-cellular localisation and perturbation techniques to elucidate molecular dynamics. All of this was done with a view to contributing to the understanding of the mechanisms of cellular responses and adaptation to environmental stress but also toFR potentially provide insight into improving therapeutic strategies developed to either inhibit (e.g. cancer) or enhance (e.g. stroke) the hypoxic response.

Chapter 2: Materials and Methods

In this chapter, the general materials and methods used during this project are described. For some areas, such as recombinant protein expression and purification, specific details can be found in the respective chapters.

2.1 Chemicals and reagents

All chemicals and reagents were from Sigma Aldrich (MO, USA) unless stated otherwise. With the exception of cell culture regents which were from Life Technologies (CA, USA) and all plastic ware was Corning® (Corning Inc., NY, USA), unless stated otherwise.

2.2 Molecular Biology

2.2.1 Plasmids

Plasmids encoding fluorescent HIF-1α and HIF-2α fusion proteins were as described in Bagnall *et al.* (2014). pLNT-Ubc-HIF-2α-Venus was created by replacing the region encoding HIF-1α in pLNT-Ubc-HIF-1α-Venus (a generous gift from J. Bagnall, University of Manchester, UK) with a fragment encoding HIF-2α using Infusion HD cloning protocol (see Plasmid Cloning). pCMX-PL1-YFP-mHDAC5 was a generous gift from R. M. Evans Laboratory, (The Salk Institute, CA, USA). CMV-Halotag-HIF-2α (pFN21AB4384) was purchased from Kazusa DNA Research Institute, Japan. pET-M11-His-Halotag-HIF-2α was created by inserting the Halotag-HIF-2α coding region (from CMV-Halotag-HIF-2α) and inserting this into the pETM-11-His plasmid (obtained from G. Stier, EMBL. See Plasmid Cloning).

2.2.2 Propagation of Expression Plasmid DNA

2.2.2.1 Transformation

50 µL commercial competent DH5α *E. coli* cells (Invitrogen, CA, USA) were thawed on ice and transferred to pre-chilled 14 mL BD Falcon 17x100 mm round-bottom polypropylene tube (Becton Dickinson, NJ, USA). 5 ng of plasmid DNA was added to the competent cells and were incubated on ice for 30 min. The cells were then heat-shocked at 42 °C for 45 sec in a water bath, followed by a second incubation on ice for 2 min. 950 µL pre-warmed SOC medium (Invitrogen, CA, USA) was added and the culture was incubated for 1 hour at 37 °C in an orbital shaker (225 rpm). The cells were diluted 1:10-1:100 in pre-warmed SOC

medium and 100 µL spread onto LB agar (Merck KGaA, Germany; prepared according to manufacturer's instructions) plates containing the appropriate antibiotic (at a final concentration as stated in Table 2.1) and incubated overnight at 37 °C.

Table 2.1 | Antibiotic concentrations used

Antibiotic	Final Concentration (µg mL^{-1})
Ampicillin	100
Kanamycin	50
Chloramphenicol	34

2.2.2.2 Small scale Plasmid DNA purification (Mini-prep)

A single colony was selected from the agar plate for mini-culture using aseptic techniques and added to 5 mL LB broth (Merck KGaA, Germany; prepared according to manufacturer's instructions) containing the appropriate antibiotics. Following incubation for 6 h-8 h at 37 °C in an orbital shaker (225 rpm), 2 mL of the bacterial culture was processed and the plasmid DNA extracted using the GeneJET Plasmid Miniprep Kit (Thermo Scientific, Ma, USA) following the manufacturers guidelines.

2.2.2.3 Large Scale Plasmid DNA purification (Maxi-Prep)

Using aseptic technique, 2 mL of bacterial mini-culture was transferred to a 1 L flask containing 200 mL LB broth & selective antibiotic(s). This was then incubated overnight at 37 °C in the orbital shaker (225 rpm). Cells were harvested using a Sorvall centrifuge, they were spun at 4 °C, 6800 × g for 15 min. DNA was isolated from bacterial cells using Purelink TM HiPure Plasmid Filter Purification Kit (Invitrogen, CA, USA), following the protocol provided by manufacturer. The purified DNA was diluted to 1 µg $µL^{-1}$.

2.2.3 Polymerase Chain Reaction (PCR)

PCR was used to amplify gene inserts for In-Fusion cloning (see below). KOD Hot Start DNA polymerase (Novagen, Germany) was used according to Table 2.2. PCR was carried out in a Px2 Thermal Cycler (Thermo Scientific, MA, USA). The standard PCR conditions used are stated in Table 2.3.

Table 2.2 | Standard set up for PCR reaction

Component	Volume / amount
MgSO4	3 µl
2mM dNTPs	5 µl
10x PCR buffer	5 µl
10 µM Forward-primer	1.5 µl
10 µM Reverse-primer	1.5 µl
Template DNA	20 ng
KOD hot start polymerase	1 µl
ddH2O	Up to final volume of 50 µl

Table 2.3 | Standard conditions used for PCR reaction

Stage	Temperature (°C)	Time	Cycles
1	94	5 min	1
2	94	20 seconds	30
	50-70	1 min / 1kb T_{hyb}	
	72	3 min	
3	72	10 min	1
Hold	4	-	-

2.2.4 Restriction Digests

Digests were set up according to Table 2.4. The 10x buffer used was dependent on the restriction enzyme used and chosen based upon manufacturers guidelines. Total reaction volume made up to 20 µL with ddH_2O and incubated at 37 °C (or the temperature recommended by the manufacturer) for a minimum of 2 h followed by enzymes inactivation (if required) by heating to 65 °C for 15 min. Digests were validated via gel electrophoresis.

Table 2.4 | Standard set up for restriction digest

	Component	Volume / amount
Single digest	Enzyme 1	1 µl
	10x Buffer	2 µl
	DNA	1µg
Double digest	Enzyme 1	1 µl
	Enzyme 2	1 µl
	10x Buffer	2 µl
	DNA	1 µg

2.2.5 Plasmid Cloning

The constructs listed in Table2.5 were created using the Clontech In-Fusion® HD cloning protocol. Inserts were amplified using specifically designed primers that have 20 bp insert specific regions and 15 bp that are homologous to the destination vector (Table 2.6). The destination vectors were linearised using the protocol in Table 2.4 using the enzymes listed in Table 2.5 Both the PCR product and linearised vector were run on a 1% agarose gel at 100 V for 1 h and excised. These DNA fragments were purified using E.Z.N.A. gel extraction kit (Omega Biotek, GA, USA) according to manufacturer's instruction.

The In-Fusion® (Clontech, Canada) reaction was carried out according to the manufacturer's instructions. The volume of linearised vector and insert were calculated based on the mass

of each required, as determined by the In-Fusion® Molar Ratio Calculator (http://bioinfo.clontech.com/infusion/molarRatio.do; insert:vector ratio = 2). Briefly, 2 µL of 5X In-Fusion HD Enzyme was added to make a total reaction volume of 10 µL. The reaction was incubated in a heat block at 50 °C for 15 min. In order to reduce toxicity and improve the number of transformants the In-fusion enzyme was digested via incubation with 1 µL Proteinase K (Invitrogen, CA, USA) for 10 min at 37 °C prior to transformation into Stellar™ competent cells (Clontech, Canada). 50 µL of cells were thawed on ice and transferred to pre-chilled 14 mL BD Falcon 17x100 mm round-bottom polypropylene tube (Becton Dickinson, NJ, USA). Approximately 5 ng of DNA was added. The cells were incubated on ice for 30 min, heat shocked at 42 °C for 45 sec and returned to ice for 2 min. 450 µL pre-warmed SOC medium was added and the culture was incubated in an orbital shaker for 1 h at 37 °C (225 rpm). 200 µL was then spread onto selective LB agar plates and incubated for 16 h at 37 °C. DNA from isolated colonies was purified (see mini-prep) and screened using restriction digest and imaging of transiently transfected cells. The best candidate was sent away for sequencing (GATC, Germany) before large scale DNA purification (maxi-prep).

Table 2.5 | Components used to create plasmids via Infusion HD cloning method

Plasmid	Destination Vector	Restriction Enzymes	Insert	Insert amplified from
pETM-11-HIS-HaloTag- HIF-2α	pETM-11-HIS*	NcoI & EcoRI (Roche, UK)	Halotag-HIF-2α	CMV-Halotag-HIF-2α
CMV-HaloTag-HIF-2α-IRES-dTomato	CMV-Halotag-HIF-2α	NotI & XbaI (Roche,Uk)	IRES-dTomato	pHIV-EGFP-HIF-2α-IRES-dTOM
pLNT-Ubc-HIF-2α-Venus	pLNT-Ubc-HIF-1a-Venus#	XbaI & BamHI (New England Biolabs, MA, USA)	HIF-2α	pG-EGFP-HIF-2α

*[*G. Stier, EMBL; #J. Bagnall, University of Manchester]*

Table 2.6 | Primers used for infusion cloning. *20 bp are specific for the insert and 15 bp (red) are specific to the destination vector, this creates overhangs allows the amplified insert to be directionally ligated into the linearised destination vector.*

Plasmid	Primer	Sequence (5' to 3')
pETM-11-HIS-HaloTag- HIF-2α	Forward	GACGGAGCTCGAATTCAACGGTGGCCTGGTCCAGG
	Reverse	TTTCAGGGCGCCATGGGCAGAAATCGGTACTGGC
CMV-HaloTag-HIF-2α-IRES-dTomato	Forward	TACCCGGGGATCCTCTAGAAGTACCCGGGCTAGGATC
	Reverse	TCATGTCTGCTCGAAGCGGCCGCCGATTTACTTGTACAGCTCGT
pLNT-Ubc-HIF-2α-Venus	Forward	GGGCTGCAGGTCGACTCTAGAATGACAGCTGACAAGGAG
	Reverse	GGTGGCGACCGGTGGATCCGCGGTGGCCTGGTCCAGGGCTC

Table 2.7 | Sequencing primers

Plasmid	Primer Sequence (5' to 3')	Details
pETM-11-HaloTag-HIF-2α	TCAAGACCCGTTTAGAGG; ATACATGGACTGGCTGCAC; CATCAGCAAGTTCATGGGAC; TCATCTCTCTGGATTTCGG; CTCTCCAACAAGCTGAAGC	Covered full Halotag- HIF-2α insert
CMV-HaloTag-HIF-2α-IRES-dTomato	Same as those used for cloning (Table 2.6)	Covered IRES and dTOM insert
pLNT-Ubc-HIF-2α-Venus	CATGAAGTTCACCTACTG	Binds in the middle of *EPAS1* and sequences towards 3' end

2.3 Cell Culture

2.3.1 Cell line propagation

All cell lines were maintained in humidified air at 37 °C in a Sanyo CO_2 (CO_2 set at 5%) incubator (SANYO Electric Biomedical Co., Japan).

Table 2.8 | Cell lines and culturing conditions

Cell Line		Growth Conditions		Comments
Name	Details	Medium	Supplements	
HeLa	Human cervix epitheloid carcinoma	MEM	10% v/v FCS, 1% v/v NEAA	ECACC no: 93021013
shPHD2 HeLa	Stable cell line knocked down for PHD2 via small hairpin RNA (shRNA)	MEM	10% v/v FCS, 1% v/v NEAA, 10 µg mL^{-1} Puromycin (Invitrogen, CA, USA).	generous gift from D Hoogewijs, D Stiehl and R Wenger, University of Zürich, Switzerland
shPHD3 HeLa	Stable cell line knocked down for PHD3 via small hairpin RNA (shRNA)	MEM	10% v/v FCS, 1% v/v NEAA, 10 µg mL^{-1} Puromycin (Invitrogen, CA, USA).	HeLa cells transduced with shPHD3 lenti virus. shPHD3 plasmid from D Stiehl and R Wenger, University of Zürich, Switzerland
PML-YFP HeLa	cell line that stably express PML-YFP construct	MEM	10% v/v FCS, 1% v/v NEAA, 1 µg mL^{-1} Blasticidin, 1% v/v Penicillin/Streptomycin	generous gift from E. G. Jaffrey, University of Dundee
HEK 293TN	Human embryonic kidney	DMEM	10% v/v FCS.	#LV900A-1; System Biosciences, Inc., CA, USA
HIF-1α-GFP BAC HeLa	HeLa cells stably expressing HIF-1α-GFP	MEM	10% v/v FCS, 1% v/v NEAA, 400 µg mL^{-1} geneticin	Stably cell line created by transfection of HIF-1α-GFP BAC (generous gift from Prof R van de Water, Leiden University)
C2C12	Mouse myoblasts	–	–	Provided by Dr J Ankers, University of Liverpool, UK

2.3.2 Cell treatments

Hypoxic incubation was carried out either directly on the microscope stage or incubated in a H35 Hypoxysation (Don Whitley, UK). DMOG was used as a hypoxia mimic at a final concentration of 0.5 mM used (Enzo Life Sciences; NY, USA).

Table 2.9 | Definitions of different cell treatments

Treatment Name	Description
Normoxia	19% O_2, 5% CO_2, 37 °C
Hypoxia	1% O_2, 5% CO_2, 37 °C
Dimethyloxalylglycine (DMOG)	2OG-hydroxylase (PHD) inhibitor

2.3.3 Transient Transfection

The transfection reagent, FuGene®6 (Roche, Switzerland) was used for delivery of plasmids into cells. Transfection of cell was carried out 24 h before imaging or other analysis, following the manufacturer's protocol and using a ratio of 2:1 (transfection reagent: plasmid DNA mass).

Table 2.10 | Volumes of reagents used for different vessels for transient transfection of HeLa cells.

Vessel	Volume of Serum Free Medium (µL)	Volume of Fugene (µL)	Total Mass of DNA (µg)
12 well plate	50	1.5	0.75
35 mm glass bottom dish	100	2	1
60 mm culture dish	200	6	3
10 cm culture dish	1700	34	17

2.4 Stable cell line production

2.4.1 Lentivirus

The shPHD3 and ODD-EGFP stable cell lines were made via lenti-viral transduction. The pLKO.1.shPHD3 construct was obtained from D Hoogewijs and R Wenger (University of Zürich). The pHIV-ODD-EGFP-IRES-dTomato lentiviral construct was cloned by Amelie Schober (Erasmus Masters student). This was done by amplifying the ODD-EGFP coding region from pG-ODD-EGFP (Bagnall, 2011) and ligating this into a pHIV-IRES-dTomato plasmid (plasmid 21374; Addgene, MA, USA).

2.4.1.1 Viral particle production

HEK 293TN cells were plated in 10 cm at a density of 1.5×10^6. The lentiviral construct was transfected into HEK 293TN cells using FuGene®6 (Roche Applied Science, UK) along with packaging plasmids psPAX2 (plasmid 12259; Addgene, MA, USA) and pMD2.G (plasmid 12260; Addgene, MA, USA). The three plasmids were mixed in the ratio of 4:2:1 respectively and transfected using a ratio of 2:1 (Fugene®6 volume: total DNA mass). 16 h post transfection, the media was aspirated and replaced with fresh media. The media was then collected 72 h after transfection and the viral particles concentrated by ultracentrifugation, following the protocol in Kutner *et al.* (2009). In brief, the 20 ml of viral-particle containing medium was placed in sterilized Ultra-clear SW28 centrifuge tubes with a 4 mL 20% sucrose solution (20 g of ultrapure sucrose dissolved in 100 mM NaCl, 20 mM Hepes pH 7.5 and 1 mM EDTA) at the bottom. Ultracentrifugation was carried out as stated in protocol. Viral particles were resuspended in 100 µL PBS and were combined to make a total of 200 µL.

2.4.1.2 Transduction of HeLa cells

Wt HeLa cells were seeded in a 24 well plate and grown to approximately 60% confluency. The concentrated virus was added to the cells along with polybrene (8 $\mu g\ mL^{-1}$; Sigma, MO, USA). The media was changed after 16 h. When confluent, the transduced cells were transferred to a 25 cm^3 flask and eventually maintained in 75 cm^3 flask. The ODD-EGFP and

shPHD3 HeLa cell lines were grown in MEM (10% FCS, 1% NEAA). The shPHD3 medium was supplemented with 10 μg mL^{-1} puromycin (Invitrogen, CA, USA).

2.4.2 Bacterial artificial Chromosome (BAC)

Bacteria containing the HIF-1α-GFP BAC (generous gift from Dr S Le Dévédec, Leiden University; RP11-867-L15, http://www.mitocheck.org/cgi-bin/BACfinder) were streaked onto an LB agar plate (containing 31.25 μg mL^{-1} Kanamycin and 12.5 μg mL^{-1} Chloramphenicol) and incubated at 37 °C overnight. Isolated colonies were picked and grown in 4 mL of LB broth (containing 31.25 μg mL^{-1} Kanamycin and 12.5 μg mL^{-1} Chloramphenicol) at 37 °C in an orbital shaker (225 rpm) for 8 h. Five hundred microlitres of this culture was transferred to 500 mL LB broth (containing 31.25 μg mL^{-1} Kanamycin and 12.5 μg mL^{-1} Chloramphenicol) and incubated at 37 °C in an orbital shaker (225 rpm) for 16 h. The bacteria were harvested via centrifugation (Sorvall RC-5B Refrigerated Superspeed Centrifuge; GSA rotor) at 6000 rpm, 4 °C for 10 min. The supernatant was discarded and the BAC was extracted and purified from the pellet using a NucleoBond Bac 100 kit (Macherey-Nagel GmbH, Germany) following the manufacturers protocol (BAC 100 Maxi).

One million HeLa cells were seeded in 10 cm dishes 24 h hours before transfection. HIF-1a-GFP BAC was transfected into HeLa cells using polyethylenimine (PEI) ‘‘Max’’ (Polysciences Inc., PA, USA) in a ratio of 2:1 (PEI:BAC) following the same protocol as used for Fugene6® (see section 2.3.3). A second plate was left non-transfected as a selection control. After 72 h, the medium was replaced with medium containing 400 μg mL^{-1} geneticin (Sigma Aldrich, MO, USA). The medium was changed every 48 h until all cells on control plate had died and colonies had started to form on the transfected plate.

Isolated colonies were picked and transferred to a 96 well plate (one colony per well). Cells were kept under selection until confluent enough to be transferred into a larger vessel. This process was repeated until there were enough cells to create frozen stocks. Expression of HIF-1α-GFP was verified by western blot and microscope experiments.

2.5 Microscopy

2.5.1 Overview of Microscopes used

Table 2.11 | Microscopes used and the application used for

Microscope	Application
Zeiss, LSM 510	EGFP-HIF-2α FRAP
	HIF-1α-EGFP FRAP
Zeiss, LSM 710	Co-localisation of HIF-2α
	TMR-Halotag-FGF2
Zeiss, LSM 780	EGFP-HIF-2α FLIP
	HIF-1α-EGFP BAC imaging
Epifluorescence	Speckle characterisation
	Microinjection

Table 2.12 | Details of settings used for different fluorophores on each microscope

	Fluorophore	Laser	Filter set up	Objective	Image capture software
LSM 510	EGFP	488 nm laser 5% power output	Emitted light reflected by a 540 nm dichroic mirror through a 505-550 nm bandpass filter and detected through a 530 nm longpass filter.	Plan-apochromat 63× 1.4 oil	LSM510 version 3 software
	dTomato	543 nm laser	Emitted light was detected through a 560 nm longpass filter		
LSM 710	AlexaFluor488 / YFP	488 nm laser 5% power output	MBS 488/561/633	Plan-Fluar 100× / 1.40 oil	Zen 2010 software
	AlexaFluor555	561 nm laser 2.4% power output	MBS 458/561		
	Topro-3-Iodide	633 nm laser 2% power output	MBS 488/561/633		
	TMR	561 nm laser 2.6% power output	MBS 561 / 633	C-apochromat 63x/1.20 Oil	
LSM 780	EGFP	Argon ion laser at 488 nm 2% power output	488 MBS, detection range 493-598 nm.	Plan-apochromat 63× 1.4 oil DIC	Zen 2012 software

MBS = main beam splitter

2.5.2 Immunofluorescence (IF)

Cells were seeded at a density of 1×10^5 / glass cover slip, 24 h before treatment. Following treatment, cells were rinsed three times with PBS and subsequently fixed for 15 min with 4% paraformaldehyde at room temperature, followed by three 10 min PBS washes. To reduce auto-fluorescence, 50 mM NH_4CL was added for 20 min, removed and the cells were blocked for 20 min (blocking buffer: 1% w/v BSA, 0.1% v/v Triton X-100, and 0.4% v/v Tween 20 in PBS). Cells were then incubated for 1 h with primary antibody (see table). Cells were washed three times in blocking buffer and then incubated for 30 min with the secondary antibody. All steps were carried out at room temperature and antibodies were diluted in blocking buffer according to table. Cover slips were mounted onto glass microscope slides with Dako Fluorescent Mounting Medium (Dako UK Ltd., UK). Precautions were taken throughout to ensure minimal exposure of samples to light.

Table 2.13 | Antibodies used for immunocytochemistry

	Reactive against	Species	Source	Reference	Dilution
Primary	Anti-HIF-2α	Rabbit	Abcam, UK	ab20654	1:500
	Anti-HIF-2α	Rabbit	Abcam, UK	ab179825	1:100
	Anti-HIF-1α	Mouse	BD Biosciences, NJ, USA	610959	1:1000
	Anti-HIF-1β	Mouse	Novus Biologicals, CO, USA	NB100-124	1:100
	Anti-RNAPII (phospho ser5)	Mouse	Abcam, UK	ab24759	1:50
	Anti-SC35	Mouse	Abcam, UK	ab11826	1:1000
	Anti-Sart1	Mouse	Abcam, UK	ab88583	10 µg / mL
Secondary	Anti-rabbit-AlexaFluor555	Goat	Invitrogen, CA, USA	A-21428	1:500-1:1000
	Anti-mouse-AlexaFluor488	Goat	Invitrogen, CA, USA	A-11008	1:500-1:1000
Nanobodies	Anti-GFP-Atto594	Alpaca	ChromoTek GmbH, Germany	gba594	1:200

2.5.3 Imaging Fixed samples

Fixed samples were imaged with a Plan-Fluar 100× / 1.30 oil immersion objective on a LSM 710 confocal microscope (Zeiss, Germany). Z-stacks were taken through the nucleus of single cells, with a distance of 0.5 µm between each slice. 1024x1024 pixel images were acquired using a 100x oil-immersion objective with a numerical aperture >1.40, zoom x2 and the pinhole set at 70 µm. Images were captured using the Zen 2010 software (Zeiss, Germany).

2.5.4 Live cell imaging

2.5.4.1 LSM 510

Twenty four hours before each experiment, 1.5×10^5 cells were seeded in a 35 mm glass bottom dish (Greiner Bio One, UK). Cells were transiently transfected at the time of seeding. Imaging dishes were placed in a PeCon O_2 controller incubator (PeCon GmbH, Germany) mounted on the confocal microscope stage. Conditions were as described in Table 2.9.

2.5.4.2 Epifluorescent microscope

Imaging dishes were prepared as described above and mounted on the stage of an Axio Observer Z.1 Epifluorescent microscope (Zeiss, Germany) fitted with an incubation system. Conditions were as described in Table 2.9. Cells expressing EGFP-HIF-2α were imaged for 1000 frames with an Andor iXon 879 (16 µm pixels 512×512) camera (Andor, UK). To achieve high magnification a 63× objective and 2.5× optovar lens were used.

2.5.5 Analysis

2.5.5.1 Co-localisation analysis

Post-acquisition processing and co-localisation analysis was carried out using ImageJ (Schneider *et al.*, 2012). The middle slice from each z-stack was analysed. The background was subtracted for both the red and green channel (pixel size of 5 for HIF-2α, 5 for RNAPII,

10 for HDAC5-YFP). Analysis was performed with an ImageJ plugin for co-localisation analysis (http://fiji.sc/Colocalization_Threshold).

2.5.5.2 Cell Tracker

For each time lapse the fluorescence intensities, for a number of cells, was determined using Cell Tracker version 0.6 software (software website: www.dbkgroup.org/celltracker/) (Shen *et al.*, 2006). Using this software, EGFP positive cells were manually tracked by drawing a circle in the cell and adjusting it accordingly to ensure it remained within the cell boundaries through each frame. Cells were tracked from the start of imaging up to point of cell death or until the end of the experiment. For any cell division, the parent cell was tracked up to point of division and after division tracking continued following one of the daughter cells. Any cells that started outside of the frame or moved out of the frame during the time course were not tracked. All data was exported as the mean intensity of fluorescence.

2.5.5.3 Characterisation of EGFP-HIF-2α Speckles

Analysis was performed in Fiji (Schindelin *et al.*, 2012) on calibrated image stacks (1000 frames). The image stack was duplicated: one was processed as follows. Background was subtracted using a 5 pixel filter and a mask applied (threshold type Li, dark background). To separate touching objects a watershed was applied and any holes were filled (using Fill Holes option). The masked images was analysed (size of pixel = 10-infinity) and measurements were redirected to the original (unprocessed) image. The results output gave the number, size, total area etc.

2.5.5.4 Analysis of EGFP-HIF-2α Speckle Dynamics

Image stacks (1000 frames) were analysed with the plugin Particle Tracker 2D/3D (Sbalzarini & Koumoutsakos, 2005; parameters using radius = 5, cut-off = 1, percent = 5, link = 1, displacement = 5) in ImageJ. The trajectory coordinates were exported to Excel (Microsoft Corporation, WA, USA). Analysis of trajectories of individual speckles was performed using a macro written by Dr D Mason (Image Analyst, Centre for Cell Imaging, University of Liverpool, UK). The velocity and slope of the moment scaling spectrum

(corresponds to diffusion mode) were calculated based on formulas in Ewers *et al.* (2005), Sbalzarini & Koumoutsakos (2005) and Scheweizer (2007).

2.5.6 Advanced Microscopy Techniques

2.5.6.1 Fluorescence Recovery After Photobleaching (FRAP)

FRAP was performed on an Axiovert 200M LSM510 (Zeiss, Germany) confocal microscope. Ten pre-bleach and 290 post-bleach images were acquired every 300 ms, using a 63× oil immersion objective. Bleaching of a region of interest (ROI) was performed with an Argon ion laser (488 nm) at 100% output power for 50 iterations for EGFP-HIF-2α. The pinhole was set at ~3 airy units. Data was captured by LSM510 version 3 software (Zeiss, Germany).

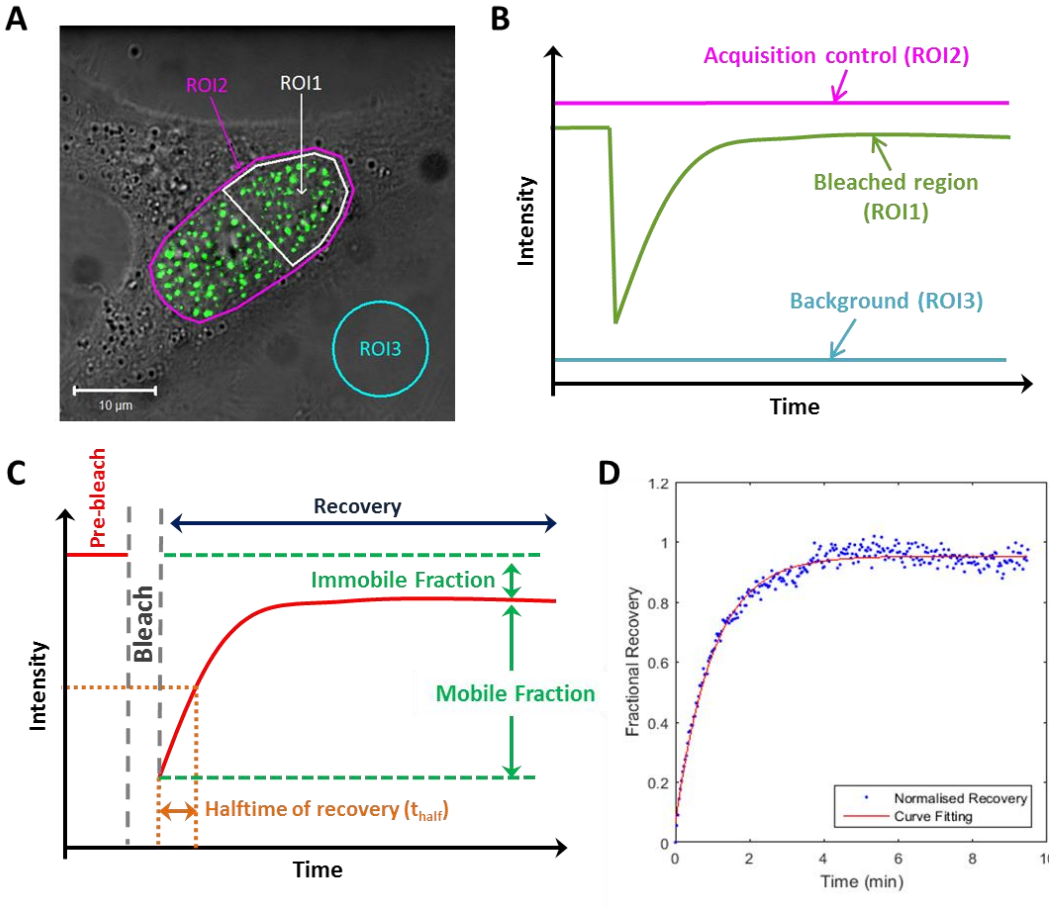

Figure 2.1 | Overview of FRAP EGFP-HIF-2α analysis. *A) Example of the three regions acquired for analysis Region of interest (ROI) 1 = bleached region, ROI2 = whole fluorescent region / acquisition bleach control, ROI3 = background fluorescence. B) Schematic of the quantitative data obtained from the three regions in B plotted against time. C) Schematic of a normalised recovery curve and the different information that can be extrapolated. D) Example of final recovery curve after background subtraction and normalisation from a single bleached cell. Half time and mobile fraction calculated from the fitted curve. All performed in Matlab (see methods).*

For each FRAP experiment, fluorescent intensities for the bleached region (ROI1), non-bleached region (acquisition control; ROI2) and background (ROI3) were extracted using the LSM510 software (Figure 2.1). ROI1 and ROI2 were background subtracted (average) and normalised to their respective pre-bleach values (average). The resulting ROI1 values were normalised to the ROI2 values (ROI1 / ROI2). This ratio was then corrected for any non-specific bleaching during acquisition using the following equation:

$$\frac{(Rt - Rp)}{(1 - Rp)}$$

Where *Rt* is the bleach value at a given time point and *Rp* is the first post-bleach value. These values were plotted against time and the curves were fitted using the following equation:

$$(a - b) \times e^{-cx} + b$$

Where a= Value of Y intercept, b= Value of Y at infinity, c= rate constant for graph.

Both the normalisation and curve fitting was performed in Matlab (Mathworks, UK) using a code written by SiSeet Chan (Honours project student, Violaine See Group, University of Liverpool, UK). Using the curves the mobile fraction and half time for each FRAP experiment was calculated.

Due to the rapid recovery exhibited by HIF-1α-EGFP, the experimental set-up was altered slightly whereby a strip across the nucleus was bleached and was performed at 100% output power for 50 iterations.

2.5.6.2 Fluorescence Loss in Photobleaching (FLIP)

FLIP was performed on a LSM780 (Zeiss, Germany) confocal microscope. Following the acquisition of 10 images, cells expressing EGFP-HIF-2α were bleached within a region of interest with an Argon ion laser (488 nm) for 100 iterations at 100% output power. Twenty post-bleach images were captured before bleaching was repeated. Cycles of imaging and bleaching were carried out until fluorescence in the non-bleached region was lost. For acquisition of images, Images were captured by Zen 2012 software (Zeiss, Germany).

For each FLIP experiment, the fluorescent intensities for the bleached region (ROI1), non-bleached region (ROI2) and background (ROI3) were extracted using Fiji. The average of the background fluorescence over the course of the time-lapse was subtracted from each ROI2 value. These background corrected values were then normalised to average of the pre-bleach fluorescence values. This data was plotted against time. The half time for each experiment was calculated by fitting each FLIP curves with a one component exponential decay curve in Matlab.

2.6 Bulk cell analysis

2.6.1 Western Blot

Cells were plated at a density of 4 x 10^5 – 5 x 10^5 per 60 mm culture dish (Corning, NY, USA) 24 h before the experiment. Following the respective treatment, samples were washed with PBS and 350 µL lysis buffer (50 mM Tris-HCl pH 7.5, EDTA 1 mM, EGTA 1mM, Na_3VO_4 1 mM, 1% v/v Triton X-100, 50 mM Sodium Fluoride, 5 mM Sodium pyrophosphate, 19 mM sodium B-glycerophosphate, 0.1 mM phenylmethylsulfonyl fluoride (PMSF), 10 µl / mL Phosphatase Inhibitor Cocktail) added. Cells were detached with a cell scraper and collected in 1.5 mL eppendorf tubes. Samples were rotated for 45 min at 4 °C and then centrifuged at 14000 g (≈10,000 rpm) for 15 min at 4 °C and the supernatant was collected. The protein concentration of the supernatant was measured using the BCA Protein Assay Kit (Thermo Scientific Pierce) according to manufacturer's instruction. Protein samples were mixed in a 1:1 ratio with Laemmli (2×) buffer (25% v/v 0.5 M Tris base pH 6.8, 20% v/v glycerol, 10% w/v SDS, 5% v/v β-mercaptoethanol and 0.1% w/v bromophenol blue) and boiled for 5 min prior to loading. Samples were resolved on 10% SDS-PAGE resolving gel (0.4 M Tris base pH 8.8, 0.1% w/v SDS, 10% acrylamide, 0.25 ng/µl APS and 0.125% v/v Temed) and 4% stacking gels (0.4 M Tris base pH 6.8, 4% acrylamide, 0.65 ng/µl APS and 0.325% v/v Temed). 30 µg of protein was loaded per well and 8 µL of protein ladder (Precision Plus Protein All Blue Standards; Biorad, CA, USA) was loaded in one well. Gels were run at 130 V in running buffer 1× (25 mM Tris, 192 mM glycine and 3.4 mM SDS) until adequate separation achieved. Protein was transferred for 1.5 h (4 °C, 300 mA) onto a nitrocellulose membrane (Biorad, CA, USA) in transfer buffer (20% v/v ethanol, 25 mM Tris, 192 mM glycine). Membranes were blocked with 5 % w/v milk (in TBST; 0.2 M Tris pH 7.6, 0.14 M NaCl, 0.1% v/v Tween 20) for 1 h and incubated with primary antibody (prepared in

5 % w/v BSA in TBST) for 16 h at 4 °C. Following three TBST washes, membranes were incubated with the secondary antibody (prepared in 5% w/v skimmed milk powder in TBST) for 1 h. Protein bands were visualised with Amersham ECL western blotting detection reagent (GE Healthcare, UK) and membranes imaged on the Syngene G-box (Geneflow, UK).

Table 2.14 | Antibodies used for immunoblotting.

	Antibody	Species	Source	Reference	Dilution
Primary	HIF-1α	Mouse	BD Biosciences, NJ, USA	610959	1:1000
	HIF-2α	Rabbit	Abcam, UK	ab20654	1:1000
	PHD3	Rabbit	Novus Biologicals, CO, USA	NB100-139	1:1000
	GFP	Rabbit	Abcam, UK	ab290	1:1000
	Beta-Actin	Mouse	Abcam, UK	ab8226	1:1000
	Cyclophillin A	Rabbit	Abcam, UK	ab3563	1:1000
Secondary	Anti-mouse HRP conjugated	Horse	Cell Signalling, MA, USA	7073S	1:5000
	Anti-rabbit HRP conjugated	Goat	Cell Signalling, MA, USA	7074S	1:3000

2.6.2 Real-time qPCR (RT-qPCR)

Cells were plated 24 hours before treatment at a density of 4-5 x 10^6 cells in 60 mm culture dishes. Following treatment cells were rinsed with PBS and lysed with 350 µL of RLT buffer (provided in the RNeasy kit; QIAGEN, Netherlands) with 1% v/v β-mercaptoethanol, cells were scraped and collected in eppendorf tubes and stored at -80 °C. When all samples were collected, the lysates were homogenised using QIAshredder mini spin columns (QIAGEN, Netherlands). RNA extraction was carried out according to manufacturer's instruction. RNA was eluted in 30 µL RNase free water and concentration was measured using a spectrophotometer (Nanodrop 2000; Thermo Scientific, MA, USA).1 µg of extracted RNA was converted to cDNA using SuperScript® VILO cDNA Synthesis Kit (Invitrogen, CA, USA) according to manufacturer's instruction. RT-qPCR reactions were ran in triplicates and carried out in a 96 well plate. Each reaction consisted of 18 µL master mix (10 µL 1x SYBR Green PCR master mix, 1 µL 5 µM forward primer, 1 µL 5 µM reverse primer, 6 µL RNase

free H_2O) and 2 µL cDNA sample. Temperature cycling was performed using a LightCycler® 480 (Roche, UK) using the parameters stated in Table 2.15. Results were analysed using the LightCycler® 480 software (version 1.5.0.39; Roche, UK). Target genes were normalised to the house-keeping gene cyclophillin A, with control sample used as the calibrator.

Table 2.15 | Cycle parameters for RT-qPCR

Stage	Temperature	Time	Ramp Rate (°C/s)	No. Of Cycles
Pre-Incubation	95 °C	5 min	4.4	1
Amplification	95 °C	10 s	4.4	45
	60 °C	30 s	2.2	
Melt Curve	95 °C	5 s	4.4	1
	65 °C	61 s	2.2	
	97 °C	Continuous	0.11	
Cooling	40 °C	10 s	1.5	1

Table 2.16 | Primers used for RT-qPCR

Gene	Sequence
Cyclophillin A (forward)	gctttgggtccaggaatgg
Cyclophillin A (reverse)	gttgtccacagtcagcaatggt
PHD2 (forward)	tgcagatgagagagcacg
PHD2 (reverse)	ttagcgaccgaatctgaagg
PHD3 (forward)	agatcgtaggaacccacacg
PHD3 (reverse)	ttctgccctttcttcagcat
VEGF (forward)	gggcagaatcatcacgaagt
VEGF (reverse)	cacacaggatggcttgaaga

2.7 Recombinant protein and nanoparticle work

2.7.1 Bacterial transformation for recombinant protein expression

Fifty microlitres of C41 (DE3) *E. coli*, were thawed on ice and 5 ng of Halotag-FGF2 were added. The cells were incubated on ice for 20 min, heat shocked at 42 °C for 1 min and returned to ice for 2 min. 950 µL pre-warmed SOC medium was added and the cells incubated for 1 h at 37 °C in an orbital shaker (225 rpm). Following this, the cells were centrifuged at 8000 g for 1 min, the supernatant removed and the pellet re-suspended in 200 µL of pre-warmed SOC medium. 20-50 µL transformed cells were spread on selective LB agar plates (for antibiotics used see Table 2.1, note: BL21.pLysS also required 50 µg mL^{-1} Chloramphenicol) and incubated at 37 °C overnight. See Table 2.17 for the variations in the transformation protocol for each strain of *E. coli* used.

Table 2.17 | Details of the variations in protocols for transforming pET-M11-Halotag-HIF-2α into different strains of competent cells

Strain of E. coli	Mass of DNA	Time on ice	Heat shock	Return to ice
BL21(DE3)	5 ng	30 min	10 sec at 42 °C	2 min
C41 (DE3)	5 ng	30 min	45 sec at 42 °C	2 min
BL21(DE3).pLysS	10 ng	10 min	45 sec at 42 °C	2 min
Rosetta(DE3)	5 ng	5 min	30 sec at 42 °C	2 min
Lemo21	5 ng	30 min	10 sec at 42 °C	5 min
SoluBL21	5 ng	15 min	45 sec at 42 °C	-

Table 2.18 | Antibiotics used for recombinant protein expression

Plasmid	Antibiotic	Final Concentration
pET-14b-Halotag-FGF2	Ampicillin	As in Table 2.1
pETM-11-Halotag-HIF-2α	Kanamycin	

2.7.2 Assessing recombinant protein expression

Single colonies of transformed bacteria were picked using aseptic techniques and added to 10 mL LB broth (Merck KGaA, Germany; prepared according to manufacturer's instructions) containing respective antibiotic. The 10 mL cultures were incubated at 37 °C in an orbital shaker (240 rpm). When the OD_{600} (optical density / absorbance measured at a wavelength of 600 nm) reached 0.6-0.8 protein expression was induced by the addition of 1 mM Isopropyl β-D-1-thiogalactopyranoside (IPTG; Bioline, MA, USA). Cultures were then incubated at different temperatures for varying times in an orbital shaker (240 rpm). From this point all samples were kept on ice. Cells were pelleted via centrifugation at 4 °C, 8000 x g for 30 min and the supernatant discarded. The pellet was re-suspended in PBS and the centrifugation step repeated. The supernatant was discarded and samples were taken for analysis via SDS PAGE.

2.7.3 Assessing recombinant protein solubility

10 mL culture was inoculated with a single colony and incubated overnight at 37 °C, 225 rpm. 5 mL of the overnight culture was transferred to 200 mL LB broth (100 μg mL^{-1} Ampicillin) and incubated at 37 °C, 225 rpm. When the OD_{600} reached 0.6-0.8, 1 mM IPTG added and incubated for a further 4 h. Bacteria was pelleted via centrifugation at 8000 rpm, 16 min, 4 °C (RC6+ Centrifuge). Pellets re-suspended in 20 mL PBS and centrifuged again.

Cells were lysed via sonication. Each pellet was thawed on ice, resuspended in 30 mL resuspension buffer (30 mM Tris, 0.6 mM EDTA, 0.5 M NaCl, 3 mM $MgCl_2$, 6% v/v Glycerol) and transferred to a pre-chilled 50 mL beaker. The cells were sonicated for 30 s (DAWE Ultrasonic Generator 7533A, pulsed sonication, 40-50% duty of cycles, output 10) followed by 60 s on ice. This was repeated five times. The sample was transferred to a 50 mL tube and centrifuged at 18000 rev / min for 30 min at 4 °C. The supernatant (soluble fraction) was transferred to a new tube and samples from the pellet and supernatant were analysed via SDS-PAGE and coomassie staining.

2.7.4 Purification of Recombinant protein

Preliminary purification described in Chapter 5. Final purification protocol as described in Sun *et al.* (2015).

2.7.5 Labelling bacterial cell lysates with Fluorescent Halotag Ligand for SDS PAGE

Purified protein: 10 µL of protein was incubated with 2 µL 50 µM Oregon Green Halotag Fluorescent Ligand for 15 min at room temperature. 4 x loading buffer was added and samples heated to 80 °C for 2 min. 15 µL of sample was analysed via SDS PAGE.

Bacterial lysate: Bacterial cell pellets were re-suspended in 1 mL 50 mM Hepes buffer (Life Technologies, CA, USA) and 1 mL lysis buffer (1x Fast Break Cell lysis reagent (Promega, WI, USA) diluted in PBS, 2 mg mL^{-1} Lysozyme (Sigma Aldrich, MO, USA), 0.02 units RQ1 RNase Free DNase (Promega, WI, USA)). Samples were rotated for 30 mins at 4 °C, followed by centrifugation for 30 min. 100 µL of supernatant, 45 µL 50 mM Hepes buffer and 5 µL Oregon Green Halotag ligand (50 µM) were incubated for 20 min at room temperature in a 1.5 mL Eppendorf tube. Appropriate volumes of each sample were mixed with 5x loading buffer (250 mM TrisHCl pH6.8, 10% SDS, 30% Glycerol, 5% β-mercaptoethanol, 0.02% bromophenol blue) and heated at 80 °C for 2 min prior to analysis via SDS-PAGE with coomassie staining and by western blot.

Mammalian cell lysate: 20 µL of protein (whole cell lysate) was incubated with 4 µL Oregon Green Halotag ligand (50 µM) for 20 min at room temperature. 6 µL 5x loading buffer was added, and each sample heated to 80 °C for 2 min. Samples were analysed by SDS PAGE and western blot.

2.7.6 Fluorescent labelling of Halotag-Fusion protein for microscopy

Purified protein: Two microlitres of recombinant protein (30 µM) was mixed with 3 µL TMR Halotag Ligand (50 µM, diluted in DMSO) and made up to a total reaction volume of 20 µL with PBS. The reaction was allowed to proceed at room temperature for 30 minutes. The labelled protein was passed through a Heparin column. To remove any unbound ligand the column was washed with PBS and the TMR-Halotag-FGF2 was eluted with 2x 30 µL 1.5 M NaCl. The eluted fraction was diluted to 0.8 µM. Rama-27 cells seeded and fixed in 35 mm glass bottom microscope dishes (Greiner Bio-One, UK) were provided by Daniel Nieves (Prof. D. G. Fernig's group, University of Liverpool). The cells were incubated for 10 minutes

with Ringer BSA (10 mg / mL) buffer (stock Ringer solution: 10 mM Hepes pH 7.4, 140 mM NaCl, 5 mM KCl, 2 mM CaCl2, 2 mM MgCl2, 11 mM Glucose. Diluted 1:1 with 20 mg / mL BSA prepared in PBS). The cells were incubated for 1 hour in 200 µL incubation buffer (TMR-Halotag-FGF2 diluted in Ringer and added in ratio of 9:1 to PBS supplemented with 10 mg / mL BSA to give final protein concentration of 2 nM). This was followed by 3x 1 mL Ringer BSA (10 mg / mL) washes.

Cells ectopically expressing Halotag-Fusion: HeLa cells were seeded in 35 mm glass bottom imaging dishes (Greiner Bio One, UK) and transiently transfected with the CMV-Halotag-HIF-2α construct as described earlier. Cells were labelled with the Oregon Green or TMR Fluorescent Halotag ligand following Promega's guidelines for live cell imaging (rapid protocol). The cells were directly observed on a LSM 710 confocal microscope (For details see microscopy).

2.7.7 *in vitro* Protein Expression

Protein synthesis was carried out using the PURExpress® In Vitro Protein Synthesis kit (NEB, MA, USA) following the manufacturers guidelines. 250 ng of pET-M11-Halotag-HIF-2α was used per 25 µL reaction. 5 µL of protein was labelled with various concentrations (as stated in Figure x) of Oregon Green Halotag ligand for 30 minutes at room temperature. Samples were analysed via SDS PAGE and western blot.

2.7.8 Expression of recombinant protein in Mammalian Cells

HeLa cells: 5×10^5 HeLa cells were seeded in 6 cm dishes in a total of 4 mL medium and were transiently transfected with CMV-Halotag-HIF-2α using FuGene®6 (as described in section X). 24 h post transfection, cells were incubated in normoxia or hypoxia or treated with 0.5 mM DMOG for 8 h. Cells were lysed with 150 µL western blot lysis buffer (see Western Blot). Samples were labelled with Halotag Oregon Green ligand (Promega, WI, USA) following the manufacturer's guidelines.

HEK 293TN: cells were seeded in 10 cm dishes at a density of 1×10^7 (total) in 10 mL medium. The CMV-Halotag-HIF-2α construct was transiently transfected following the protocol in section xx. 48 h post transfection the cells were harvested. The medium was carefully aspirated away and cells washed gently with PBS. 500 µL lysis buffer (50 mM Tris

HCl pH 7.4, 150 mM NaCl, 1% NP-40, 1x Protease Inhibitor Cocktail (G6521; Promega, WI, USA)) was used per 10 cm dish. A sterile cell scraper was used to detach the cells, which were collected in pre-chilled 1.5 mL Eppendorf tubes. All following procedures were done on ice or at 4 °C. The samples were incubator on a rotator for 1 h to aid cell lysis and then centrifuged for 1 h, 13000 rpm (Eppendorf MiniSpin). The supernatant was transferred to pre-chilled Eppendorf tubes. Total protein concentration was determined using a BCA assay (as described in Section 2.6.1)

2.7.9 Gold Nanoparticles

2.7.9.1 Synthesis and Functionalisation of Gold Nanoparticles

Gold nanoparticle synthesis and functionalisation was carried out in collaboration with Dr U Shaheen (Dr R Levy's group, University of Liverpool). Nanoparticles with a gold core 10 nm in diameter and a ligand shell comprised of polyethylene glycol (PEG) only or PEG and a custom made Halotag ligand (Promega, WI, USA) were synthesised. Briefly, capped nanoparticles were made by mixing colloidal gold (Sigma Aldrich, MO, USA) with the ligand(s) in a ratio of 9:1, respectively (Duchesne *et al.*, 2012). To make 1 mL of 1% Halotag ligand (HL) GNPs 2 µL of Halotag Ligand (1 mM) and 98 µL PEG (2 mM) was used. The ligands were added sequentially, the HL ligand first followed by the PEG. In between each step the nanoparticles were vortexed gently for 1 min. The nanoparticles were incubated at room temperature for 16 h on a rotator. Excess ligands were removed by washing with (PBS with 0.2% v/v Tween20), nanoparticles were centrifuged (13200 rpm for 1.5 h) and resuspended in PBST four times.

2.7.9.2 Gold nanoparticle conjugation

Nanoparticle (70 nM; PEG-GNPs or 1% HL-GNPs) were incubated with 750 µg protein (HaloTag-HIF2α or control HEK-293TN lysate) made up to a final volume of 100 µL with PBST. Protein degradation was prevented by inclusion of 1x EDTA-free protease inhibitor (Promega, WI, USA). Additional control reactions were set up with nanoparticles or lysate only. The nanoparticles were mixed with lysates (Halotag-HIF-2α) and for 18 h at 4 °C with mixing to allow conjugation to occur. To remove unbound protein, the nanoparticles were pelleted via centrifugation (13200 rpm at 4°C for 1 h) and the supernatant removed. The nanoparticles were then resuspended in 500 µL PBST. This was repeated four times and after each wash a small volume was taken for analysis by western blot or dot blot.

2.7.9.3 UV-visible spectroscopy

To monitor loss of nanoparticles following each step (of functionalisation or conjugation), samples were taken so the absorption spectrum could be measured. Measurements were made at room temperature using a Spectra Max Plus spectrophotometer (Molecular Devices, Wokingham, UK) between 450–700 nm.

2.7.9.4 Stripping Gold Nanoparticles

After washing, nanoparticles (PEG-GNPs or 1 % HL-GNPs) incubated with the various lysates were incubated in stripping buffer (60 mM TrisHCl, 10 % Glycerol, 50 mM DTT, 2 % SDS, 0.01 % Bromophenol Blue) with mixing for 36 h and then centrifuged (13200 rpm at 4 °C for 1 h) to remove the stripped gold nanoparticle cores. The supernatant was then boiled for 5 min prior to analysis via western blot.

2.7.9.5 Dot Blot

Four microlitres of nanoparticles was added to nitrocellulose membrane and allowed to dry. The dot blots were blocked for 1 h in 5 % milk (in TBST) and incubated overnight with primary antibody (prepared in 5 % BSA in TBST) at 4 °C. Following three TBST washes, membranes were incubated with the secondary antibody (prepared in 5 % milk powder) for 1 h. Protein was visualised with Amersham ECL Select western blotting detection reagent (GE Healthcare UK, UK) and membranes developed on a Syngene G-Box (Geneflow, UK).

2.7.9.6 Microinjection

Cells were plated sparsely (1.5×10^5 / mL, 2 mL total) in 35 mm gridded dishes (Grid500; Ibidi GmbH, Germany) 24 h prior to injection. Were required, transfection was carried out concurrently.

Microinjection was performed on a Zeiss Epifluorescent Axio Observer Z.1 (Zeiss, Germany) fitted with an incubation system that maintains humidity and allows control of temperature, CO_2 and O_2 levels. The microinjection system was set up in a manner that allows injection to occur whilst the imaging dish is mounted on the microscope stage. Microinjection was performed by Dr J Wnetrzak (Technician, Centre for Cell Imaging, University of Liverpool). Cells were injected into nucleus via microcapillaries (Eppendorf, Germany) with the injection time of 1 s, injection pressure of 150 KPa and compensation pressure of 30 kPa using the Eppendorf FemtoJet® Microinjector (Eppendorf, Germany).

Chapter 3: Investigating the temporal dynamics of HIF-α at the single cell level

This chapter starts with a brief introduction to single cell imaging and its advantages over bulk-cell analysis techniques. It is followed by the presentation of a paper published in January 2014 and then additional work that I conducted relating to this study.

3.1 Investigating Protein Dynamics

Live cell imaging of fluorescently labelled proteins allows the quantification of protein abundance over time as well as allowing the visualisation of intracellular localisation. Studies using live cell imaging have revealed that temporal and spatial dynamics play a role in regulating the activity of key signalling molecules. For example, Lahav *et al.*(2004) were the first to observe the pulsatile nuclear accumulation of p53 and showed that the frequency of pulses positively correlated with the amount of DNA damage. Continually, NFκB has been shown to transiently translocate from the cytoplasm into the nucleus upon stimulation with TNFα (Nelson *et al.*, 2004). This group also determined that the timing of the nuclear-cytoplasmic shuttling directly affected gene expression, highlighting that temporal and spatial dynamics of transcription factors has a role in regulating their activity (Ashall *et al.*, 2009).

The aforementioned discoveries were made by utilising live cell imaging, which has numerous advantages over other methods used for protein analysis. For example, with western blot analysis any spatial information such as sub-cellular localisation is lost and so spatial kinetics such as nuclear-cytoplasmic oscillations (such as those observed for NFκB) are missed. Also, heterogeneity within cell populations can be obscured when using bulk cell techniques such as western blot and quantitative PCR, due to “averaging effects” (Spiller *et al.*, 2010). Observations at the single cell level have highlighted that the timing of cellular responses are not always synchronised (Nelson *et al.*, 2004;Bagnall *et al.*, 2014) and this cell to cell variation can only be detected by observing single cells in real-time.

Our hypothesis was that HIF-1/2α might have complex/oscillatory dynamics due to their regulation by negative feedback loops (Epstein *et al.*, 2001;Stiehl *et al.*, 2006). Our aim was to utilised single cell imaging techniques to capture the intracellular dynamics of the HIF-α subunits to determine which components are involved in this auto-regulatory mechanism.

3.2 Tight Control of HIF-α Transient Dynamics Is Essential for Cell Survival in Hypoxia

As previously mentioned, live cell imaging has revealed that temporal and spatial dynamics play a key role in the regulation of the activity of transcription factors such as p53 and NFκB (Lahav *et al.*, 2004;Nelson *et al.*, 2004). At the start of my PhD project, I had the opportunity to participate towards an on-going project (initiated by Dr James Bagnall, former PhD student in the laboratory) utilising live cell imaging to study the dynamics of HIF-1α/-2α at the single cell level. Our findings were published in an article entitled "Tight Control of Hypoxia-inducible Factor-α Transient Dynamics Is Essential for Cell Survival in Hypoxia" in the Journal of Biological Chemistry (Bagnall *et al.*, 2014).

We found that in hypoxia HIF-1α accumulates transiently in the nucleus after approximately 4 hours with a peak in protein levels lasting 2-4 hours. In order to validate these data obtained from HeLa cells ectopically expressing HIF-1α-EGFP, a stable cell line was created. The ODD-EGFP HeLa were produced via lenti-viral transduction of a construct containing a fragment that spans 529aa to 652aa of the HIF-1α protein, i.e. part of the oxygen-dependent degradation (ODD) domain containing the second hydroxylation site (p564), fused with EGFP. Live cell imaging of this cell line revealed a similar transient accumulation of the fusion protein in hypoxia, suggesting that the transient accumulation of HIF-1α is not an artefact of ectopic expression.

The oscillatory behaviour observed is indicative of a negative feedback loop and led to the hypothesis that there is an auto-regulatory mechanism controlling the levels of HIF-1α in hypoxia. Mathematical modelling (performed by Joseph Leedale; Mathematics Department, University of Liverpool) based on gene expression data from qPCR and live cell imaging of PHD2 and PHD3 led to the proposal that PHD2 was the principal component of the negative feedback loop. Simulations based on these mathematical models suggested that the transient increase of HIF-1α protein levels would be lost if PHD2 was knocked out and knocking out PHD3 would have little effect. Live cell imaging of shPHD2 and shPHD3 HeLa cell lines ectopically expressing HIF-1α-EGFP confirmed these predictions.

Moreover, in the shPHD2 cells, we observed that levels of HIF-1α continued to accumulate and eventually lead to the cells undergoing apoptosis, suggesting that prolonged HIF activity in hypoxia triggers cell death. To complement this, it was demonstrated that gene

expression relating to apoptosis (PUMA and NOXA) was induced in these cells in hypoxia. This led to the proposal that the PHD2-negative feedback mechanism is in place to protect cells by tightly controlling levels of HIF in hypoxia.

My specific contributions to this paper:

- Single cell imaging and analysis of ODD-EGFP HeLa cells (Figure 1I)
- Analysis of PHD2 and PHD3 gene expression in the ODD-EGFP via qPCR (Figure 1J)
- Creating the shPHD3 HeLa cell line via lenti-transduction of shRNA (Figure 6H)
- Single cell imaging and analysis of shPHD2 and shPHD3 HeLa cell lines transiently expressing HIF-1α-EGFP (Figure 6E and 6I, respectively)
- qPCR experiments looking at the upregulation of VEGF mRNA and genes relating to apoptosis (PUMA and NOXA) (Figure 6E, F and G, respectively)

Author contributions:

James Bagnall

- Conceived and designed the experiments
- Performed the experiments
- Analysed the data
- Wrote the paper
- Prepared figures / tables
- Reviewed drafts of the paper

Joseph Leedale

- Performed mathematical modelling
- Analysed data
- Wrote the paper
- Prepared figures / tables
- Reviewed drafts of the paper

Sarah E. Taylor

- Performed the experiments (Details above)
- Analysed the data
- Reviewed drafts of the paper

David G. Spiller

- Reviewed drafts of the paper

Michael R. H. White

- Reviewed drafts of the paper

Kieran J. Sharkey

- Reviewed drafts of the paper

Rachel N. Bearon

- Wrote the paper
- Prepared figures / tables
- Reviewed drafts of the paper

Violaine Sée

- Conceived and designed the experiments
- Wrote the paper
- Prepared figures / tables
- Reviewed drafts of the paper

(Manuscript)

⌘ *Author's Choice*

THE JOURNAL OF BIOLOGICAL CHEMISTRY VOL. 289, NO. 9, pp. 5549–5564, February 28, 2014

Tight Control of Hypoxia-inducible Factor-α Transient Dynamics Is Essential for Cell Survival in Hypoxia

Received for publication, July 9, 2013, and in revised form, December 3, 2013 Published, JBC Papers in Press, January 6, 2014, DOI 10.1074/jbc.M113.500405

James Bagnall[‡1,2,5], **Joseph Leedale**[§1,3], **Sarah E. Taylor**[‡4], **David G. Spiller**[‡5], **Michael R. H. White**[‡5], **Kieran J. Sharkey**[§], **Rachel N. Bearon**[§6], **and Violaine Sée**[‡7]

From the [‡]*Centre for Cell Imaging, Institute of Integrative Biology, and the* [§]*Department of Mathematical Sciences, University of Liverpool, Liverpool L69 7ZL, United Kingdom*

Background: Hypoxia inducible factor-α (HIF-α) is the main transcription factor activated in low oxygen conditions.
Results: Single cell imaging reveals pulses in nuclear levels of HIF-α.
Conclusion: The transient nature of the HIF-α nuclear accumulation is required to avoid cell death.
Significance: The duration of HIF-α response depends on cellular oxygenation, and can encode information and dictate cell fate.

Intracellular signaling involving hypoxia-inducible factor (HIF) controls the adaptive responses to hypoxia. There is a growing body of evidence demonstrating that intracellular signals encode temporal information. Thus, the dynamics of protein levels, as well as protein quantity and/or localization, impacts on cell fate. We hypothesized that such temporal encoding has a role in HIF signaling and cell fate decisions triggered by hypoxic conditions. Using live cell imaging in a controlled oxygen environment, we observed transient 3-h pulses of HIF-1α and -2α expression under continuous hypoxia. We postulated that the well described prolyl hydroxylase (PHD) oxygen sensors and HIF negative feedback regulators could be the origin of the pulsatile HIF dynamics. We used iterative mathematical modeling and experimental analysis to scrutinize which parameter of the PHD feedback could control HIF timing and we probed for the functional redundancy between the three main PHD proteins. We identified PHD2 as the main PHD responsible for HIF peak duration. We then demonstrated that this has important consequences, because the transient nature of the HIF pulse prevents cell death by avoiding transcription of p53-dependent pro-apoptotic genes. We have further shown the importance of considering HIF dynamics for coupling mathematical models by using a described HIF-p53 mathematical model. Our results indicate that the tight control of HIF transient dynamics has important functional consequences on the cross-talk with key signaling pathways controlling cell survival, which is likely to impact on HIF targeting strategies for hypoxia-associated diseases such as tumor progression and ischemia.

In physiological and/or pathological situations where oxygen homeostasis is lost, the oxygen concentration drops and cells experience hypoxia. The cellular adaptation to hypoxia is mediated at the molecular level by the evolutionary conserved transcription factor hypoxia inducible factor (HIF).[8] HIF is a heterodimer composed of α and β subunits. The β subunit is constitutively expressed, whereas the main α subunits of HIF, HIF1α and HIF2α, are regulated in an oxygen-dependent manner. Under normoxic conditions, HIFα is hydroxylated, which promotes its binding to the ubiquitin ligase von Hippel-Lindau protein, thereby targeting it for proteasomal destruction (1). However, under hypoxic conditions, HIF-1 and -2α hydroxylation decreases, leading to their rapid accumulation. They then activate the transcription of hundreds of genes encoding proteins involved in cell survival and energy metabolism, but paradoxically also ones involved in apoptosis and autophagy (2). This double-edged sword function of HIF in promoting different cell fates has previously been described and depends on the physiopathological context and differential binding to key partners such as p53 (3). However, the switch from a pro-survival to a pro-apoptotic signal is not well understood. This is an important problem with implications beyond basic biology, because it has direct impact on the management of treatments for solid hypoxic tumors.

We postulated that the temporal regulation of HIF might explain its ability to determine two opposite cell fates. The HIF-VHL and p53-mdm2 signaling systems have previously been shown to share similar network structures in terms of degradation/transactivation loops (4). Furthermore, it has previously been demonstrated, using single cell imaging, that the dynamic behavior of p53 varies, depending on the stimulus, which can

[S] This article contains supplemental Fig. S1 and Movies S1 and S2.
⌘ *Author's Choice*—Final version full access.
[1] Both authors contributed equally to this work.
[2] Recipient of a Biotechnology and Biological Sciences Research Council doctoral training studentship.
[3] Holds University of Liverpool studentship.
[4] Recipient of a Medical Research Council capacity building studentship.
[5] Present address: Faculty of Life Sciences, University of Manchester, Manchester M13 9PT, United Kingdom.
[6] To whom correspondence may be addressed: Peach Street, University of Liverpool, Liverpool L69 7ZL, UK. Tel.: 44-0-151-794-4022; Fax: 44-0-151-794-4061; E-mail: rbearon@liverpool.ac.uk.
[7] Recipient of Biotechnology and Biological Sciences Research Council David Phillips Fellowship BB/C520471/1. To whom correspondence may be addressed: Dept. of Biochemistry, Institute of Integrative Biology, Biosciences Building, University of Liverpool, L69 7ZB, UK. Tel.: 44-0-151-7954598; Fax: 44-0-151-7954404; E-mail: violaine@liverpool.ac.uk.

[8] The abbreviations used are: HIF, hypoxia inducible factor; PHD, prolyl hydroxylase; PI, propidium iodide; EGFP, enhanced green fluorescent protein; HRE, hypoxia response element; ODD, oxygen-dependent domain; qPCR, quantitative PCR.

influence cell fate decision (5, 6). One important component that can lead to pulsatile or oscillatory behavior is the presence of a negative feedback motif. In the HIF system, prolyl hydroxylase (PHD) -2 and -3 have been proposed as potential delayed negative feedback proteins (7–9). Indeed, PHD1–3 are responsible for HIF hydroxylation, leading to its subsequent degradation (10). Their activity decreases in hypoxia, resulting in HIF accumulation that can in turn activate the transcription of PHD2 and -3. The subsequent PHD increase can compensate for the decrease of activity in prolonged hypoxia and could potentially bring HIF back to low and undetectable levels (7).

We therefore hypothesized that the potential HIF pulse/oscillatory dynamics due to PHD negative feedback could underlie the different cell fate outcomes that have been observed to result from hypoxia. To test this, we have applied a combination of single cell imaging and mathematical modeling. We measured HIF levels in single cells with a high temporal resolution over 20 h. We observed discrete single and repetitive transient pulses of HIF-1α and -2α accumulation when cells were exposed to a hypoxic environment (1% O_2). We developed a new mathematical model of the HIF-PHD negative feedback loop, which was able to accurately reproduce the single-cell dynamic data, both during a switch from normoxia to hypoxia and during re-oxygenation. We then used the model and experimentation to address the role of the individual PHDs in the generation of HIF dynamics. This demonstrated an essential role for PHD2 in the control of the transient dynamics of HIF and in the prevention of cell death triggered by long lasting HIF-1α levels. Changes in HIF dynamics and levels will likely affect directly HIF transcriptional activity, as well as the activity of its binding partners, for example, mdm2 (11). Indeed the effects of PhD2 silencing on cell death were correlated with a strong transcription of p53-dependent pro-apoptotic genes in hypoxia. Moreover, coupling of HIF and p53 mathematical models (12) predicted significant effects of the variations of HIF dynamics on the oscillations and levels of the p53 protein, indicating that HIF dynamics not only affects HIF signaling but also its cross-talk with other essentials signaling systems involved in the control of cell fate.

EXPERIMENTAL PROCEDURES

Reagents and Antibodies

Tissue culture medium was from Invitrogen; fetal calf serum (FCS) from Harlan Seralab (UK); and pharmacological inhibitor dimethyloxaloylglycine from Alexis Biochemicals (Enzolife Sciences, New York). Cycloheximide was from Calbiochem (Merck, Darmstadt, Germany). The antibody against HIF-1 was from BD Biosciences (catalog number 61-0959) and the antibody against HIF-2 was from Santa Cruz Biotechnology (catalog number Sc 13 596). EGFP antibody was from Abcam (catalog number ab290).

Cell Culture and Hypoxia

HeLa cells were grown in Dulbecco's modified Eagle's medium (DMEM) supplemented with 10% FCS (v/v) and 1% nonessential amino acids (v/v), at 37 °C, 5% CO_2. Cells (between passages 8 and 20) were plated at 1×10^5 cells/ml. shPHD2 HeLa cells (generous gift from D. Hoogewijs, D. Stiehl, and R. Wenger, University of Zürich, Switzerland) were grown in the same medium as WT HeLa supplemented with 10 μg/ml of puromycin for maintaining the hairpin expression. The C51 colon adenocarcinoma cells pH3SVL (generous gift from S. Lehmann and R. Wenger, University of Zürich, Switzerland) have a stably integrated plasmid containing a minimal SV40 promoter regulated by 3 HREs from the human transferrin promoter. There were grown in DMEM high glucose, 10% FCS (v/v), and 400 μg/ml of G418. The ODD-EGFP HeLa cell line was generated by transduction of a HIV-ODD-EGFP-ires dTomato lentivirus. For imaging experiments, cells were plated in 35-mm glass bottom dishes (Iwaki, Bibby Sterilin, UK). Hypoxic incubation was performed either directly onto the microscope stage equipped with a PeCon incubator with an O_2 controller unit or in a hypoxic work station (Don Whitley Scientific, England) for bulk cell experiments (1% O_2, 5% CO_2, 94% N_2).

Immunoblotting

Total protein was extracted with a lysis buffer (50 mM Tris-HCl, pH 7.5, 1 mM EDTA, 1 mM EGTA, 1% (v/v) Triton X-100, 50 mM NaF 50, 5 mM sodium pyrophosphate, 10 mM sodium β-glycerophosphate, 0.1 mM PMSF, 1/100 protease inhibitor mixture, and 1/100 phosphatase inhibitor mixture). After 1 h at 4 °C on a rotating wheel shaker, the lysates were centrifuged at 10,000 × *g* for 15 min at 4 °C and total protein concentration was measured with BCA assay in the supernatant. 40 μg of proteins were resolved by SDS-PAGE (10% gels) and transferred onto nitrocellulose membrane. The membranes were blocked with 5% nonfat dry milk in TBS-T (10 mM Tris-HCl, pH 8, 100 mM NaCl, 1% (v/v) Tween 20) and incubated with appropriate primary antibody (overnight, 4 °C), followed by incubation with horseradish peroxidase-conjugated secondary antibody (1 h at RT). SuperSignal West Dura Extended Duration Chemiluminescent Substrate was used for the ECL reaction and the signal was detected and quantified using the G:box gel doc system (Syngene, UK).

Quantitative RT-PCR (qPCR) and Primers

Cellular RNA was purified using Qiagen RNeasy mini kit according to the manufacturer's instructions. cDNA was synthesized with a QuantiTect Reverse Transcription Kit and qPCR was performed using ABI Power SYBR Green PCR master mix according to the manufacturer's instructions. We used an ABI 7500 Fast Real-time PCR System. Cyclophilin A was used as a calibrator for the relative amplification of genes of interest calculations. Primer sequences used were: cyclophilin A forward, GCTTTGGGTCCAGGAATGG, reverse, GTTGTCCACAGTCAGCAATGGT; PHD2 forward, GGAAGATGGAGAACCTGCTG, reverse, GCTTGTGCTTCTTCCAGTCC; PHD3 forward, AGATCGTAGGAACCCACACG, reverse, TTCTGCCCTTTCTTCAGCAT; PHD1 forward, ACTGGGACGTTAAGGTGCAT, reverse, AAATGAGCAACCGGTCAAAG; VEGF forward, TCTTCAAGCCATCCTGTGTG, reverse, ATCTGCATGGTGATGTTGGA; Puma forward, CTTGGAGGGTCCTGTACAAT, reverse, CACCTAATTGGGCTCATCT; and Noxa forward, CGAAGATTACCGCTGGCCTA, reverse, ATGTGCTGAGTTGGCACTGA.

Gene Transfer

Plasmids—Fluorescent HIF-1 and -2α fusion constructs were cloned in the Gateway system (Invitrogen). HIF sequences were amplified by PCR using a plasmid template and cloned into a Gateway Entry vector by recombination. The final EGFP fusion was obtained by recombination of the HIF-entry vector with a EGFP destination vector. PHD1-EGFP and PHD3-EGFP were obtained from the Addgene non-profit making plasmid repository (catalog number plasmids 21400 and 21402), both plasmids were described in Ref. 13. PHD2-EGFP was a generous gift of Dr. R. Depping (University of Lübeck, Germany). pPHD2-PHD2-EGFP was constructed by replacing the CMV promoter of the PHD2-EGFP plasmid by 1 kb of the PHD2 promoter (amplified from a Bacterial Artificial Chromosome template from Invitrogen).

Transfection—Cells were transfected 24 to 48 h before imaging using FuGENE 6 (Roche Applied Sciences, UK) according to the manufacturer's instructions with a FuGENE/DNA ratio of 2/1.

Lentivirus—ODD-EGFP lentiviral transfer vectors were produced by insertion of the fusion of human HIF-1α ODD (amino acids 529–652)-EGFP, amplified from previously made gateway plasmid pG-ODD-EGFP into the lentivector pHIV-ires-Tomato (Addgene plasmid 21374). The shPHD3 lentivirus was obtained from D. Hoogewijs and R. Wenger (University of Zurich). pMD2.G (Addgene plasmids 12259 and Addgene plasmid 12260) was used for packaging.

Viral Transduction—Lentiviral particles were produced by transfection of the 293TN cell line using calcium chloride. The medium was replaced 16 h post-transfection and collected 24 h later, cleared by low speed centrifugation, and filtered through a 0.45-μm pore filter. After ultracentrifugation on 20% sucrose, the virus pellet was re-suspended in 200 μl of PBS. A serial dilution of concentrated virus was used to transduce HeLa cells in the presence of Polybrene (8 μg/ml).

Time Lapse Confocal Microscopy

Cells were incubated on the microscope stage at 37 °C, 5% CO_2, 1 or 20% O_2 and observed by confocal microscopy using a Zeiss LSM510 with a Plan-apochromat ×63 1.3 NA oil immersion objective. Excitation of EGFP was performed using an argon ion laser at 488 nm. Emitted light was detected through a 505–550 nm bandpass filter from a 545-nm dichroic mirror. Excitation of the empty dsRed used as a control was performed using a green helium-neon laser (543 nm) and detected through both a 545-nm dichroic mirror and a 560-nm long pass filter. Data capture was carried out with LSM510 version 3 software (Zeiss, Germany) using the Auto-time series macro (14). For time lapse experiments mean fluorescence intensity was extracted and the fluorescence intensity was determined for each cell using CellTracker version 0.6 software (15). These experiments were performed three times and ~100 cells were analyzed for each HIF-1α and -2α construct. For promPHD2-PHD2-EGFP, the experiment was performed three times and ~50 cells were analyzed.

Imaging Analysis

For analysis, cells were always co-transfected with an empty dsRed plasmid to monitor transfection in normoxia as well as normalize fluorescence levels over time. Only cells visibly transfected with a dsRed-expressed control plasmid were analyzed. A region of the nucleus was followed by CellTracker and the data exported as mean intensity of fluorescence. Cells that were clearly transfected with the empty red plasmid and which showed a change in green fluorescence, but not in red fluorescence, were scored as responsive. The fluorescence intensity data were then averaged by calculating the mean of 10 consecutive time points. A threshold technique was used for characterization of the response time and response duration. This threshold was calculated for each cell, and was defined as the 50% value between maximum and minimum fluorescence intensity. Cells that died or migrated out of the recorded field within the first 4 h of the experiment were not analyzed. Cells that died less than 3 h after a HIF-EGFP increase were also removed from the analysis. Cell death was monitored on bright field images. For classification between transient, prolonged, and multiple peak response, an automatic peak detection was implemented. The threshold, calculated as described previously, was additionally scaled to the maximal amplitude and standard deviation. Cells with a response shorter than 280 min were considered as transient. Cells with multiple threshold crossing were classified as multiple responders.

Annexin V/PI Labeling

Apoptosis was assessed by addition in culture medium of propidium iodide (PI) to 0.5 μg/ml and annexin V-FITC (Sigma) to 1.0 μg/ml. Images were taken every 15 min through a ×20 objective. Excitation was at 488 nm for PI and fluorescein. PI fluorescence was collected through a 560-nm long-pass filter and FITC from a 505–530 nm bandpass filter.

Statistical Analysis

Statistical significance was determined by one-way analysis of variance followed by a Bonferroni multiple comparison test. Difference was considered as significant at $p < 0.01$. All the experiments were performed at least 3 times.

Luminescence Microscopy

Luciferin was added (0.5 mM, Biosynth AG, Switzerland) to 3 ml of medium containing cells in 35-mm glass coverslip culture dishes (Iwaki), and incubated on the microscope stage at 37 °C, 5% CO_2, and 20 or 1% O_2. Imaging was carried out using a Zeiss Axiovert 100 microscope with a Fluor 10 × 0.5 NA objective. The photons emitted by individual cells were collected using a Hamamatsu ORCAII BT 512 CCD camera (C4742-98 Hamamatsu Photonics Ltd, UK) controlled with Metamorph software. A series of images were acquired using a 30-min integration time over 80 h. AQM advanced 6 software (Kinetic Imaging, UK) was used for image analysis with background correction. All these experiments were performed at least three times and in each experiment at least 30 cells were recorded and analyzed.

HIF-α Dynamics and Mathematical Modeling

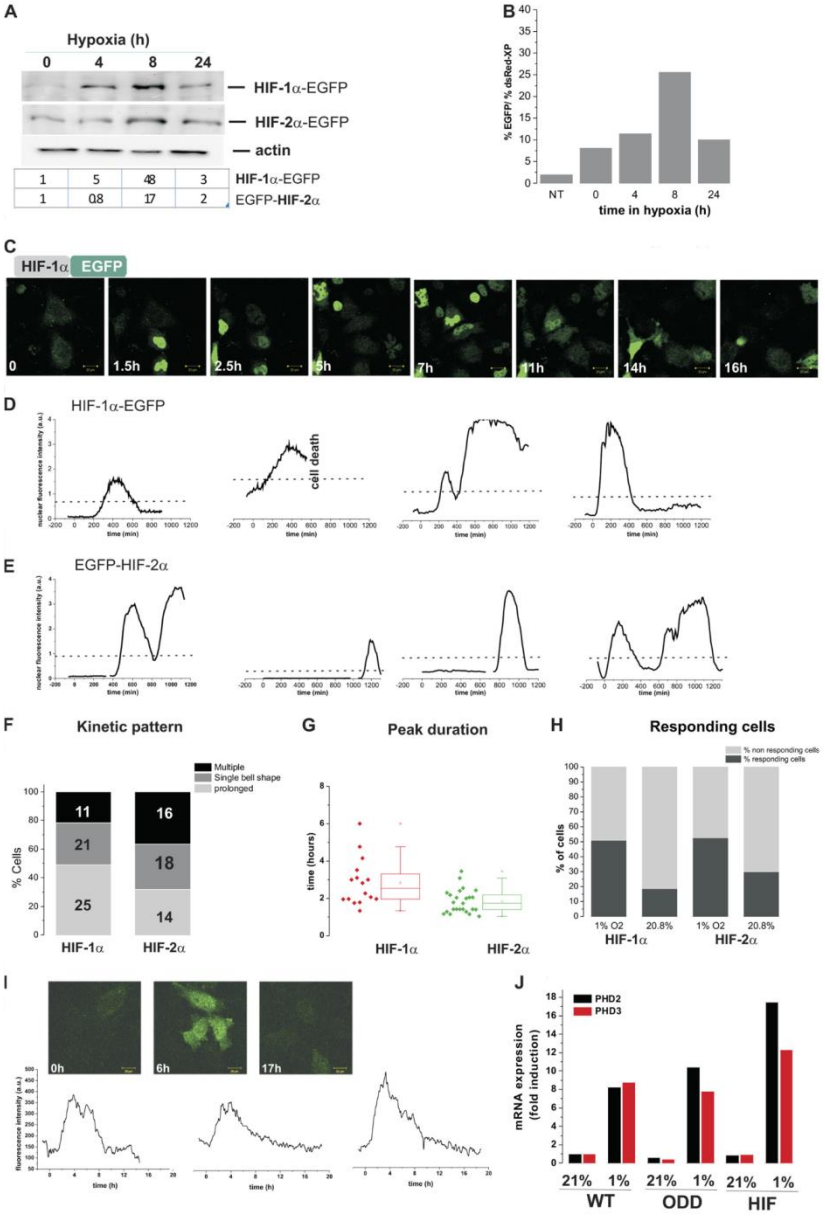

Flow Cytometry

Cells were seeded in 6-cm dishes at a total density of 100,000 cells and co-transfected with HIF1α-EGFP and dsRED-XP, 1 day before hypoxic incubation as indicated. Upon hypoxic incubation, cells were trypsinized and pelleted and then resuspended in 100 μl of PBS. 100 μl of 4% paraformaldehyde was added (final concentration of 2%) and incubated for 15 min at room temperature. Hypoxic samples were fixed in the hypoxic chamber. Analysis was carried out using a Guava EasyCyte Plus Flow Cytometer (Millipore). The percentage of EGFP and dsRed positive cells in each sample was established using GuavaSoft software (Millipore).

Mathematical Modeling

Fig. 3*A* describes the minimal model consisting of two coupled ordinary differential equations: *HIF*-1α (x) is produced through basal synthesis at rate S, induces the transcription of PHD (y) at rate k, and is degraded via PHD-dependent hydroxylation at an oxygen-dependent maximal rate h with saturation threshold, γ. All models were solved in Matlab R2009a using standard ordinary differential equation solvers. Parameters in the two-component model were optimized for each cell time series data by minimizing the sum of squared residuals of the ordinary differential equation solution and the experimental data using the built-in Matlab function *fminsearch*. The ratio of hydroxylation rate in hypoxia to normoxia was taken to be 0.14 based on measured values from the literature for the PHD2 isoform (16). Initially free parameter optimization was performed on bell-shaped single-cell data, and median values were obtained. Parameter optimization was then constrained so that k and d could only vary from the median values by 50%. Parameters S and γ were unconstrained as experimental protocols such as transfection efficiency or laser intensity may result in variability between cells. Fits were classified as good or bad using an error envelope defined by $\mathrm{EXP}(t) \pm 0.35(\max(\mathrm{EXP}(t)) - \min(\mathrm{EXP}(t)))$, where EXP($t$) represents the time series vector of experimental data. Solutions were classified as bad fits if more than 1% of the experimental data points lay outside the error envelope and good fits otherwise.

The two-component model was extended to distinguish PHD1 (y_1), PHD2 (y_2), and PHD3 (y_3).

$$\frac{dx}{dt} = S - \frac{x}{x+y}\sum_{i=1}^{3} h_i y_i \quad \text{(Eq. 1)}$$

$$\frac{dy_1}{dt} = S_1 - d_1 y_1 \quad \text{(Eq. 2)}$$

$$\frac{dy_2}{dt} = S_2 + k_2 x - d_2 y_2 \quad \text{(Eq. 3)}$$

$$\frac{dy_3}{dt} = S_3 + k_3 x - d_3 y_3 \quad \text{(Eq. 4)}$$

PHD2 and PHD3 are HIF inducible with induction rates k_2 and k_3. The PHD basal degradation parameters, d_i (i = 1,2,3) were taken to be the mean values of measured half-lives (Fig. 5*B*). The hydroxylation rate parameters, h_i (i = 1,2,3), were based on measured values from the literature (16). In the extended model, it was necessary to introduce basal synthesis of the PHD proteins, as PHD1 is not produced via HIF induction. To estimate the PHD basal synthesis rates, S_i, the steady state ratio of proteins were taken to be 0.2:0.8:0.1, based on data from Ref. 17. Free parameters were optimized by fitting the 4-component model solution to a median cell generated from the 2-component model optimization of de-oxygenation data.

The HIF-PHD model was coupled to a previous model describing the p53-Mdm2 feedback loop (12). In the original p53-Mdm2 model, HIF binds to p53 reducing the rate at which p53 is degraded when in a complex with Mdm2. In the original model this is represented by a switch in the degradation rate following hypoxic stress. Here the model is extended to allow the degradation rate to be explicitly a function of HIF, $\delta(x) = Ae^{-Bx}$, with constants A and B chosen so that the degradation rate matches the original model when the HIF levels have attained equilibrium steady state values in normoxia (20% oxygen, low HIF) or hypoxia (1% oxygen, high HIF). Model simulations were initially run with HIF switching between equilibrium levels ("steady HIF dependence") to recapitulate the results of Hunziker *et al.* (12). The model was then coupled to the four-component HIF-PHD model ("dynamic HIF dependence").

FIGURE 1. **Single cell dynamics of HIF-α nuclear levels and HIF-dependent transcription.** *A*, HeLa cells were transfected with HIF-1α-EGFP or EGFP-HIF-2α. 24 h after transfection cells were exposed to hypoxia (1% O_2) for the indicated time points. HIF-EGFP fusion protein levels were assessed by Western blot using an anti-GFP antibody and the bands were quantified by densitometry analysis. *B*, HeLa cells were transfected with HIF-1α-EGFP together with dsRED-XP expression plasmid for normalization purposes. % of red and green fluorescent cells were measured by flow cytomtery and plotted as a function of time in hypoxia. Nontransfected controls (*NT*) were used for gating. *C*, selected representative images of HeLa cells transiently co-transfected with HIF-1α-EGFP and an empty dsRED Express control plasmid (not shown on the picture) to monitor the localization and number of transfected cells. Transfection efficiency was ranged from 30 to 40%. Cells were imaged using time lapse confocal microscopy every 5 min in 20.8% O_2 for 1 h and then switched to 1% O_2 for 20 h. See also supplemental Movies S1 and S2. *D* and *E*, nuclear fluorescence levels for HIF-1α (*D*) and HIF-2α (*E*) were plotted as a function of time for 4 representative cells. The *straight line* represents the threshold used for automatic peak detection (see "Experimental Procedures"). All traces for HIF-1α are shown in supplemental Fig. S1*A*. Some traces are shorter than the entire time course due to either cell death or migration out of the imaging field. *F*, classification of the observed HIF-α response kinetics. Transient bell shapes curves and multiple peaks were scored using a threshold (see "Experimental Procedures"). The number of cells scored in each category are indicated on the plot. *G*, duration of the HIF accumulation in transient response. Duration was determined as the time between the point at passing half-maximum fluorescence and returning below this value, the 25th to 75th quintile is indicated on the plot. *H*, percentage of transfected cells showing an increase of green fluorescence levels in hypoxia and normoxia. *I*, a stable HeLa cell line expressing the HIF-1α ODD-dependent ODD from residues (amino acids 529–652) fused to EGFP was generated by lentiviral transduction of a HIV-ODD-EGFP-ires-dTomato vector into HeLa cells. The ODD cell line was imaged in normoxia before a switch to 1% O_2 for 20 h. Fluorescence intensities were quantified and plotted as a function of time. Four representative plots are shown, 50 cells were tracked in total, 82% displayed pulsed dynamics. *J*, HeLa cells were transiently transfected with HIF-1α-EGF, either stably expressing ODD-EGFP or left non-transfected. They were cultured in normoxia or hypoxia (1% O_2) for 8 h prior to cell lysis and mRNA extraction. mRNA levels for PHD2 and -3 were measured by qPCR and normalized to cyclophilin A mRNA.

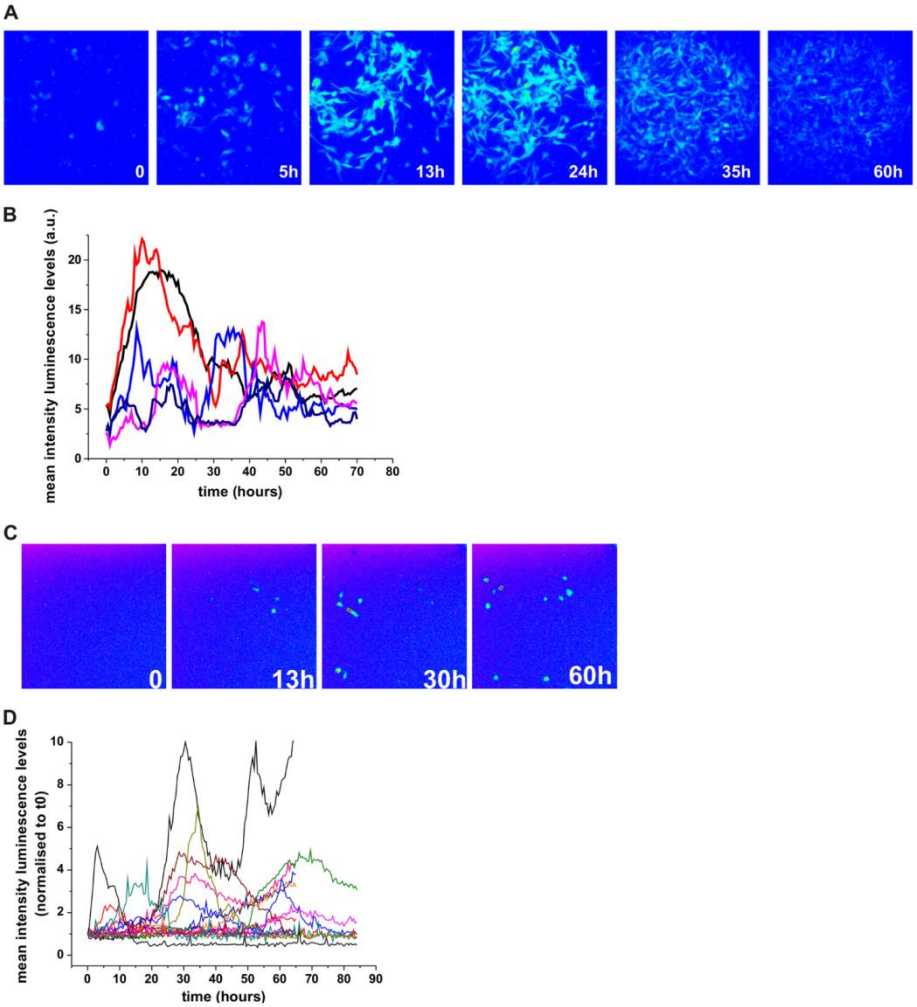

FIGURE 2. *A*, luminescence images of C51 cells stably transfected with HRE-luciferase (PH3SVL cells) in 1% O_2. Luminescence levels were imaged using wide field microcopy in the presence of luciferin in cell culture in 1% O_2 for 80 h. *B*, mean luminescence levels of single cells were plotted as a function of time. Each *color line* is a representative cell. *C*, HeLa cells were transiently transfected with a HRE-luciferase reporter vector. *D*, luminescence levels in hypoxia were acquired and quantified as in *B*.

RESULTS

Single Cell Dynamics of HIF-1α and -2α in Normoxia and Hypoxia—To capture HIF-1α and HIF-2α dynamics, we used time lapse confocal imaging of HIF-EGFP (enhanced green fluorescent protein) fusion proteins in an O_2 controlled environment. HIF-1α-EGFP and EGFP-HIF-2α induction in hypoxia was validated by EGFP detection (Fig. 1*A*). In cells switched from a normoxic to a hypoxic environment, we observed by Western blot (Fig. 1*A*) and flow cytometry (Fig. 1*B*), a HIF-1α-EGFP accumulation at 4–8 h that had decayed by 24 h, which was in agreement with previously published results on endogenous HIF (7, 18, 19). HIF-2α was less inducible by hypoxia, and was already detectable in normoxia. For live-cell imaging, observations were initially taken at 20.8% O_2

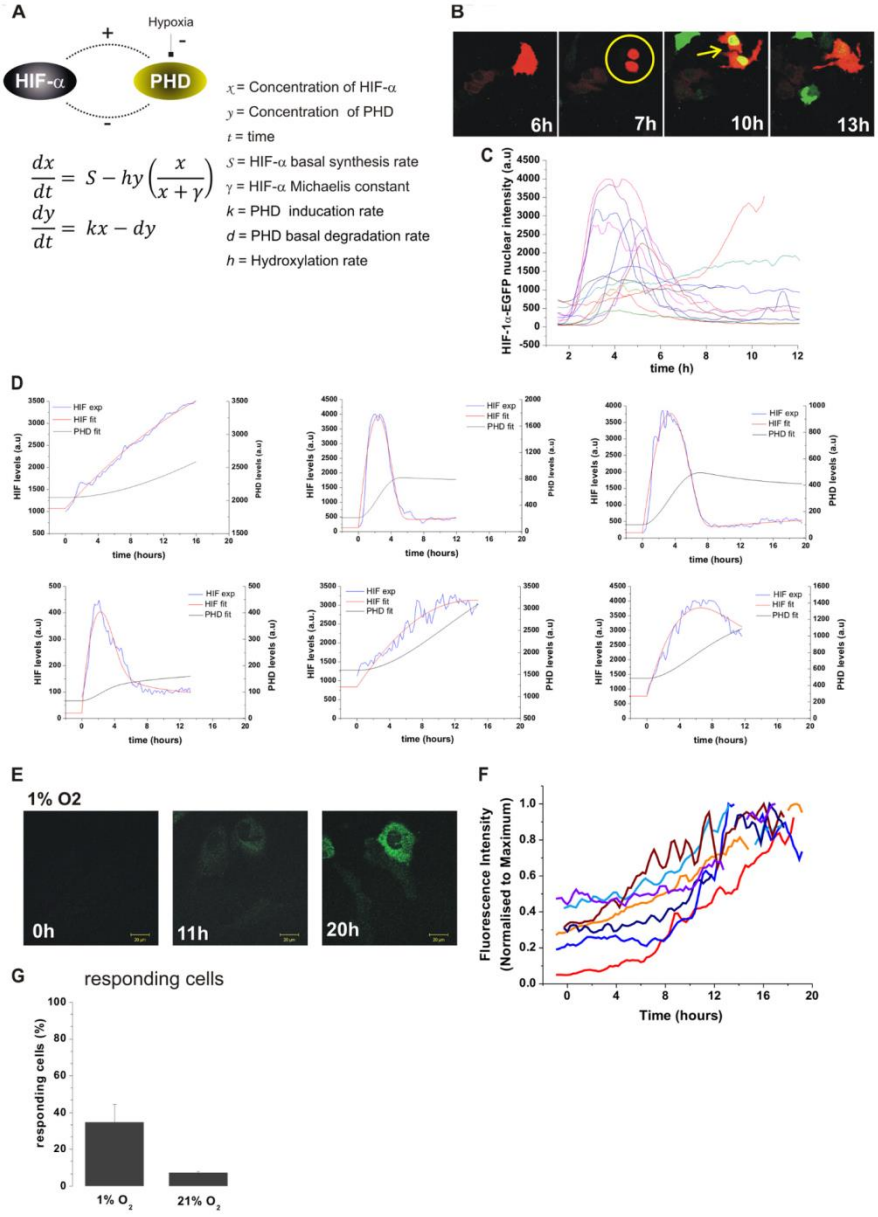

HIF-α Dynamics and Mathematical Modeling

tension as a control for 2 h, then, after a switch from 20.8 to 1% O_2 cells were further imaged for 20 h. Cells subjected to the hypoxic switch showed transient HIF-1α and -2α nuclear accumulation with varied kinetics (Fig. 1, *C–E*, supplemental Fig. S1*A* and Movies S1 and S2). A single transient bell-shaped profile was observed in 30% (21 cells) of the HIF-1α and 32% (18 cells) of HIF-2α responding cells (Fig. 1*F*), which was of similar duration, ~2–4 h; Fig. 1*G*). We observed some spontaneous pulses of HIF-1α nuclear accumulation in normoxic cells (19% of the transfected cells, Fig. 1*H*). These levels were higher for HIF-2α (30% of the transfected cells), consistent with the stabilization observed by Western blots in normoxic conditions. We observed that 22% of HIF-1α (11 cells) and 36% of HIF-2α cells (16 cells) had more than 1 peak of HIF nuclear accumulation. In most cases the subsequent peaks had increased amplitude (Fig. 1, *D–F*). The transient pattern of HIF dynamics was also observed in other cell lines (*e.g.* HEK293T cells, not shown) and also observed in a HeLa cell line stably expressing the oxygen degradation domain (ODD) of HIF-1α fused to EGFP (Fig. 1*H*). Cells visibly expressing ODD-EGFP displayed similar transient dynamics, yet contrary to HIF-1α-EGFP the degradation was slower. This is likely due to the ODD not possessing transcriptional activity and so being unable to further increase the PHD feedback above endogenous regulation, in contrast to full-length HIF exogenous expression (Fig. 1*I*). We also characterized the transient dynamics of HIF activity. The HIF-dependent transcriptional activity in live cells was assessed by imaging the light produced by a hypoxia response element-luciferase reporter gene (*HRE-luc*). We examined C51 cells stably expressing a HRE-luciferase (PH3-SVL C51) (Fig. 2, *A* and *B*) and HeLa cells transiently transfected with HRE-luc (Fig. 2, *C* and *D*). In both conditions, we found a transient luciferase signal, indicating transient transcriptional activity. Some cells displayed 2 or more peaks of luciferase expression, which is consistent with the nuclear accumulation of HIF fluorescent fusion proteins. Interestingly, the stable C51 cells had some basal luminescence signal in normoxia, indicating some degree of spontaneous low amplitude luciferase peaks of transcriptional activity (not shown) in agreement with the observation of spontaneous accumulation of HIF-1α and -2α.

Mathematical Modeling of HIF Nuclear Dynamics during Hypoxia and Re-oxygenation—The known negative feedback from PHD proteins on HIF is a likely candidate for generating the pulses of HIF-1α and -2α (9, 10, 20). To analyze the dynamic behavior of HIF, we developed a simple mathematical model based on the global HIF-PHD negative feedback loop (Fig. 3*A*). We observed heterogeneity in the response time and that HIFα responses occurred after cell division in 50% of dividing cells (see Fig. 3*B* for a typical example). This might have been caused by transient transfection at the time of nuclear breakdown (21). Cells were, therefore, artificially synchronized in the cell cycle (Fig. 3*C*), using the mitosis time as $t = 0$ for mathematical modeling.

We initially fitted the bell-shaped single-cell data (from HIF-1α-EGFP)), which encapsulate more complex dynamics and better mirrors the transiency of accumulation observed by Western blot, by using models previously described for the p53 system (22). A model, which included a saturation coefficient for hydroxylation provided the best fit (Fig. 3*D*, and "Experimental Procedures"). 79% (31/39) of the de-oxygenation single cell data were then successfully fit to the model, subject to the constraint that the parameters k (induced PHD production rate) and d (PHD degradation rate) were similar across all cells (see supplemental Fig. S1A and "Experimental Procedures"). The model predicted a slow gradual increase of PHD. This was in qualitative agreement with the PHD2 dynamics measured in single cells using PHD2-EGFP controlled by the PHD2 proximal promoter (Fig. 3, *E* and *F*); PHD2 up-regulation was observed in 40% (20 cells) of the transfected cells switched to 1% O_2 (Fig. 3*G*).

We further assessed the functionality of the experimental system and the model by fitting re-oxygenation experiments. Therefore, HIF-1α levels were imaged in single cells during re-oxygenation after exposing cells to hypoxia for 6 h. Upon re-oxygenation, HIF-1α-EGFP-transfected cells displayed a rapid loss of fluorescence, presumably due to its degradation (Fig. 4*A*). The kinetics were slower, but consistent with the endogenous HIF-1α degradation observed by Western blot (Fig. 4*B*), supporting the validity of the experimental imaging results. Interestingly, in some cells, the loss of fluorescence was not definitive and these cells had a clear slow return of fluorescence 200 min after re-oxygenation. We fitted all cells obtained from the re-oxygenation experiment with the parameters k and d constrained and good fits were obtained for 74% (31/42) of cells (example of 3 cells shown in Fig. 4*C*, all cells in supplemental Fig. S1*B*).

Role of PHDs in HIF Timing and Transiency—A generic "median cell" based on median parameter values was constructed and used to test the effects of parameter variation (Fig. 4*D*). Varying S (basal synthesis rate of HIF-1α) had a clear effect on the amplitude, but not on the kinetics, of the response. This could explain the difference in amplitude observed in the single cells (visible in Fig. 3*C*), which are likely to have different copy numbers of HIF plasmid due to transfection variability. In con-

FIGURE 3. **Mathematical modeling of the generic HIF-PHD feedback loop.** *A*, description of the model (see "Experimental Procedures"). HIF-α (x) is produced at rate S and removed due to PHD (y) hydroxylation. The maximal hydroxylation rate, h, is oxygen dependent and saturation of hydroxylation is determined by the parameter γ. PHD (y) is produced through induction by HIF-α at rate k and undergoes basal degradation at rate d. *B*, HeLa cells were transiently co-transfected with HIF-1α-EGFP and an empty dsRED-Express control plasmid. Cells were imaged every 5 min after a switch from 20 to 1% O_2 using time lapse confocal microscopy. The pictures show a typical example of HIF-1α nuclear accumulation occurring after cell division. This was observed in 50% of the cells showing a HIF-1α increase. *C*, HIF-1α levels in hypoxia plotted as a function of time, synchronized based on cell cycle. *D*, single cell data of HIF dynamics (*blue line*) were fitted computationally using the model (*red line*). See also supplemental Fig. S1 for more cell fitting. The model PHD profile is in *green*. The model cells are initially at equilibrium in normoxia ($h = 1$) and are de-oxygenated into hypoxia ($h = 0.14$) at $t = 0$. *E*, selected representative images of HeLa cells transiently transfected with the PHD2prom-PHD2-EGFP expression plasmid. Cells were imaged using time lapse confocal microscopy every 5 min in 20.8% O_2 for 1 h and then switched to 1% O_2 for 20 h. *F*, the plots represent the whole cell fluorescence intensity produced from PHD2prom-PHD2-EGFP as a function of time. *G*, the percentage of responsive cells is calculated from the number of transfected cells showing an increase of the green fluorescence level over time from PHD2prom-PHD2-EGFP in hypoxia and in normoxia.

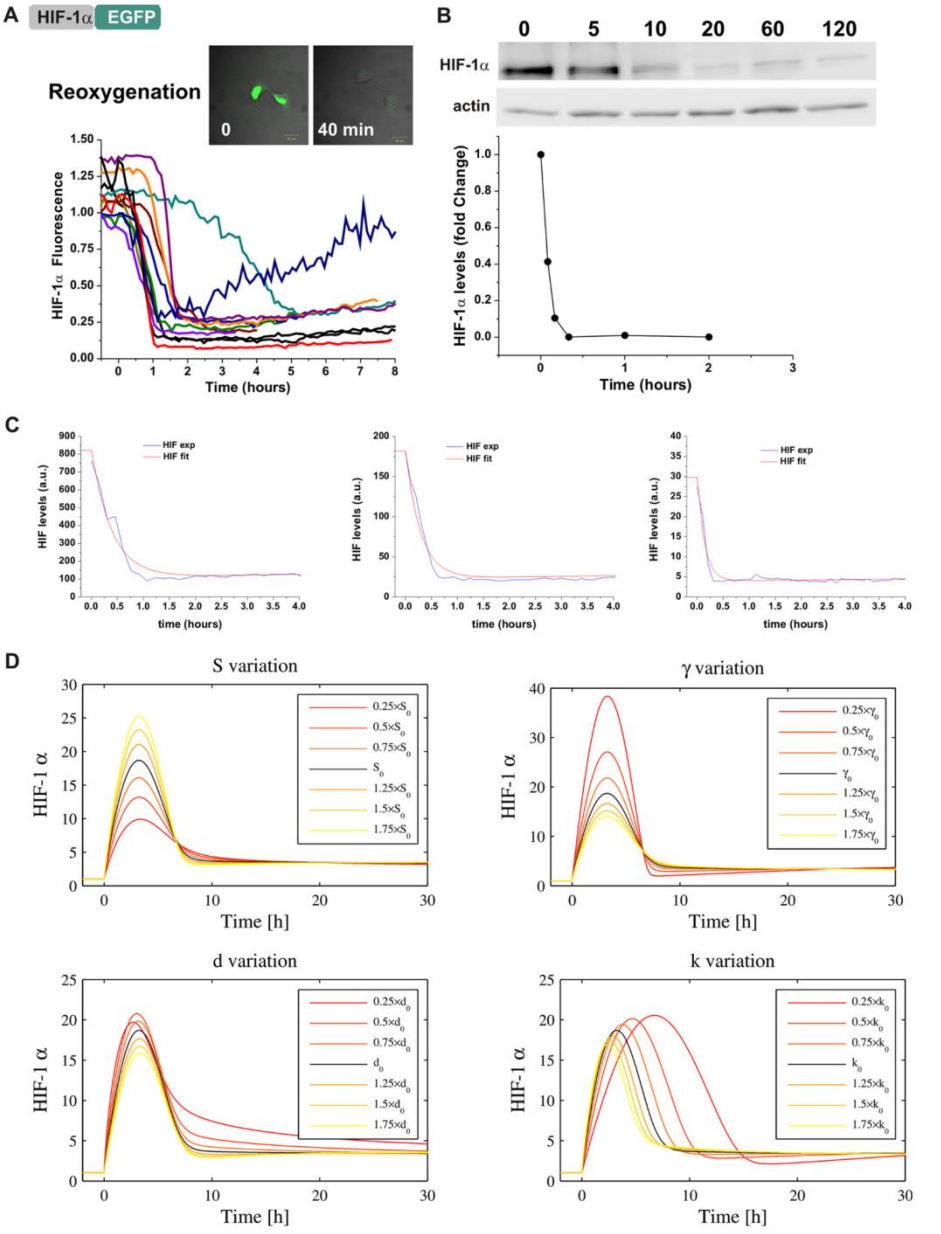

HIF-α Dynamics and Mathematical Modeling

trast, varying k (HIF-dependent PHD induction) affected the duration of HIF accumulation. Therefore, we decided to test computationally the potential redundancy of the PHD feedback in HIF temporal regulation. The model describes a generic PHD, which is in reality a combination of PHD2 and PHD3 (HIF-inducible) and PHD1 (non HIF-inducible). We introduced a new level of complexity, by separating the 3 different PHDs ("Experimental Procedures"), which may have different induction rates and protein stabilities (k and d parameters, respectively). Imaging experiments using cycloheximide to block protein synthesis showed that PHD2 and -1 were stable with a half-life of more than 10 h, whereas PHD3 was less stable with a half-life of 1.7 h (Fig. 5, *A* and *B*). Based on our measurements of mRNA production in hypoxia, we estimated the induction rate (k) of PHD2 and PHD3 to be similar (Fig. 5*C*). The model was run to equilibrium and a switch to hypoxia was applied (Fig. 5, *D* and *E*). In WT cells, the equilibrium value of PHD2 was significantly higher than the other isoforms, because the model was based on the steady state ratio of proteins to be 0.2/0.8/0.1 for isoforms PHD1:PHD2:PHD3 based on (17). Furthermore, PHD2 takes longer than PHD3 to stabilize to an equilibrium level, which can be explained because PHD2 degrades more slowly than PHD3. *In silico* knockdown of PHD1 and PHD3 had little effect on HIF pulse duration. In contrast, removal of PHD2 led to a sustained HIF stabilization (Fig. 6, *A–C*), indicating that this was the most important factor in the control of HIF dynamics. We then tested experimentally the model prediction for PHD2 knock-down, by measuring HIF-1α accumulation in 1% O_2 in HeLa cells lacking PHD2 expression (stable shPHD2). The PHD2 knock-down was validated by Western blot (Fig. 6*D*) and no compensation by PHD3 was observed (Fig. 6*D*). Moreover, no strong overstabilization of HIF-1α was observed in normoxia or hypoxia compared with WT cells (Fig. 6*E*). This disagreed with the model prediction, which showed higher HIF levels in normoxia and hypoxia in the absence of PHD2. However, this could be explained by the differences observed between short-term and long-term knockdown (siPHD2 and shPHD2) previously discussed by Berra *et al.* (23). In hypoxia, HIF-1α dynamics were clearly different from those observed in wild type (WT) HeLa (Western blot Fig. 6*F* and imaging in Fig. 6*G*). We observed in most of the cases an accumulation of HIF-1α, which had either a long duration or did not show any noticeable decrease during the experiment. This was specific to PHD2 knock-down and was not observed in the case of PHD3 knock-down (Fig. 6, *H* and *I*).

Role of HIF Dynamics Controlled by PHD2 on Cell Survival—We observed a very high level of cell death in hypoxic cells up-regulating HIF-1α-EGFP in the shPHD2 cell line (70%) compared with WT HeLa (40%) (Fig. 7, *A* and *B*). Apoptotic cell death was further quantified using Annexin V-PI labeling over a time course of hypoxia in WT and shPHD2/shPHD3 cells. Double labeling of Annexin V and PI was observed in 38% of shPHD2 cells after 24 h exposure to 1% O_2 *versus* 7 and 12% in WT and shPHD3 cells, respectively (Fig. 7, *C* and *D*). Consequently, shPHD2 cells could not be tracked for a very long hypoxic period and the stability of the HIF up-regulation could not be studied. The consequences of the observed altered HIF-1α dynamics were investigated at the transcriptional level on a well defined HIF target gene. VEGF, showed a more sustained expression in shPHD2 cells compared with WT or shPHD3 cells (Fig. 7*E*), confirming a direct functional effect on HIF target genes of the PHD2 silencing. Because HIF has previously been demonstrated to interact with the mdm2 protein and affects p53 activity (11), we further investigated if the changes in HIF dynamics could affect p53 activity and hence explain the observed cell death in hypoxia when PHD2 is silenced. The transcription of two classical p53 target genes involved in pro-apoptotic signaling were measured by qPCR over a time course of hypoxia in WT HeLa cells as wells as in shPHD2 and shPHD3 cells. Interestingly, Noxa and Puma mRNA were both significantly up-regulated in hypoxia in the shPHD2 cells and were only marginally transcribed or even down-regulated in the shPHD3 or WT cells (Fig. 7, *F* and *G*).

To further explain the observed difference in p53 target gene transcription in the context of varying HIF dynamics, a previously described a p53 mathematical model coupled to HIF was used (see "Experimental Procedures"). When a hypoxic switch is represented by an instantaneous switch in HIF levels (Fig. 8*A*), in WT cells, p53 first displays a transitory peak and then establishes oscillatory dynamics as previously observed (12). However, when the dynamic nature of the HIF dynamics is explicitly included, the transitory behavior of p53 is markedly altered; displaying a double peak and delayed onset of oscillatory dynamics (Fig. 8*B*). Furthermore, when PHD2 is silenced, p53 displays sustained high levels (Fig. 8*C*). This is an example of how taking into account real protein dynamics instead of steady states might affect model coupling and could be applied to other systems than the p53 coupling used here. For example, the model coupling HIF with NO homeostasis also used steady state levels (24).

DISCUSSION

Depending on the physiopathological context, cells experiencing hypoxia will be exposed to oxygen levels that vary in amplitude, duration (acute or chronic hypoxia), and possible preconditioning (25). In a situation such as ischemia (acute and strong hypoxia), HIF-1α activity has been associated with cell death (26), whereas in solid tumors it is associated with cell survival and proliferation (27). These diverse contexts and cell fate might be due to specific HIF accumulation profiles and

FIGURE 4. **Single cell dynamics during re-oxygenation and validation of the mathematical model.** *A*, cells were transfected as described in the legend to Fig. 1*B*. 24 h after transfection, cells were exposed to 1% O_2 for 6 h in the microscope stage and then re-oxygenated to 20.8% O_2. Fluorescent levels were measured 1 h prior and during the re-oxygenation period and plotted as a function of time. *B*, HeLa cells were cultured in hypoxia for 6 h and then subjected to re-oxygenation. HIF-1α levels were measured by Western blot at the indicated time points. Densitometry analysis of the bands were plotted as a function of time. *C*, using the model described in the legend to Fig. 2, we fitted the single cell traces obtained experimentally in *A*. The cells are initially at equilibrium in hypoxia (h = 0.14) and are re-oxygenated back into normoxia (h = 1) at $t = 0$. *D*, parameter sensitivity analysis was conducted by varying one parameter at a time, as a perturbation from the artificial cell obtained from the median parameters ($S = 2.38 \times 10^1$ AU min^{-1}, $\gamma = 2.98 \times 10^2$ AU, $k = 4.71 \times 10^{-4}$ min^{-2}, $d = 4.71 \times 10^{-4}$ min^{-1}]). Pre-stimulation (normoxic) equilibria have been normalized to 1 to emphasize the qualitative effects of parameter variation. The *black curve* represents the median cell model output and parameters were individually deviated either way in steps of 25% of the median value varying up to ±75%.

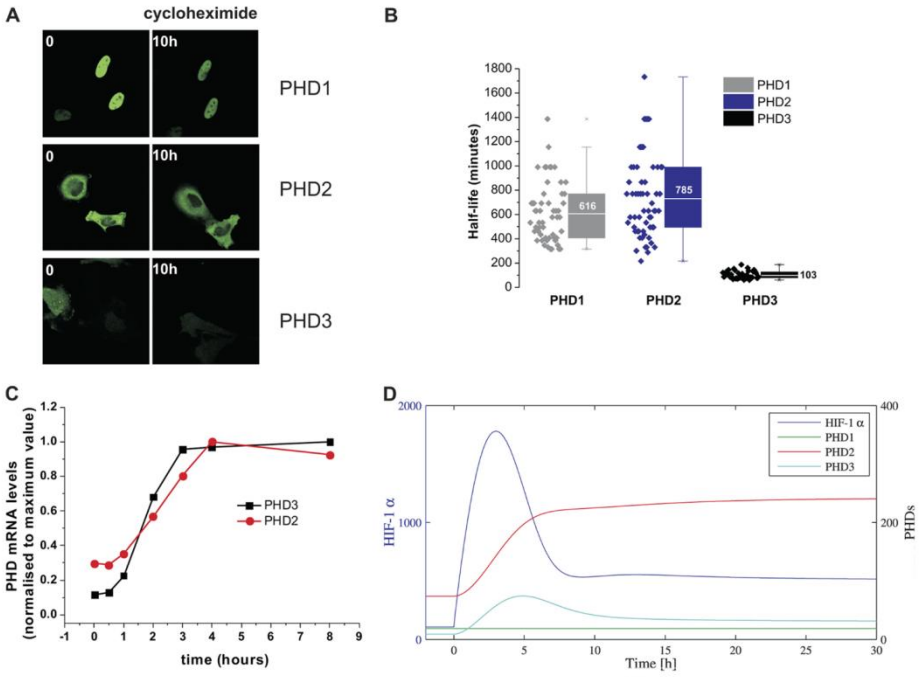

E

Parameters	Value
S	2.38×10^{-1} (fit in 2-component model)
S_1	2.11×10^{-2} (fit in 4-component model)
S_2	2.64×10^{-2} (calculated)
S_3	2.33×10^{-2} (calculated)
d_1	1.13×10^{-3} (measured)
d_2	8.83×10^{-4} (measured)
d_3	6.74×10^{-3} (measured)
k	3.65×10^{-4} (fit in 4-component model)
γ	2.98×10^{2} (fit in 2-component model)
h_1	0.25*Normoxia 0.04*Hypoxia
h_2	1*Normoxia 0.14*Hypoxia
h_3	1.25*Normoxia 0.13*Hypoxia

FIGURE 5. *A*, measurement of the half-life of PHD1, -2, and -3. HeLa cells were transfected with PHD1, -2, -3-EGFP. 24 h after transfection, cells were treated with cycloheximide (10 $\mu g/\mu l$) and the PHDs levels were monitored for up to 24 h by measuring fluorescence intensity. *B*, box and whisker plot of the half-life measured in single cells for PHD1, -2, and -3. *C*, qPCR analysis of PHD2 and PHD3 mRNA induction during a hypoxic time course (1% O_2). Each time point sample was generated in triplicates. The plot is representative of one experiment. The experiment was repeated 4 times. *D*, four component model run. The model cell is initially at equilibrium in normoxia and is then de-oxygenated into hypoxia at $t = 0$. *E*, the parameter sets for the 4-component model are detailed in the table (time units in min).

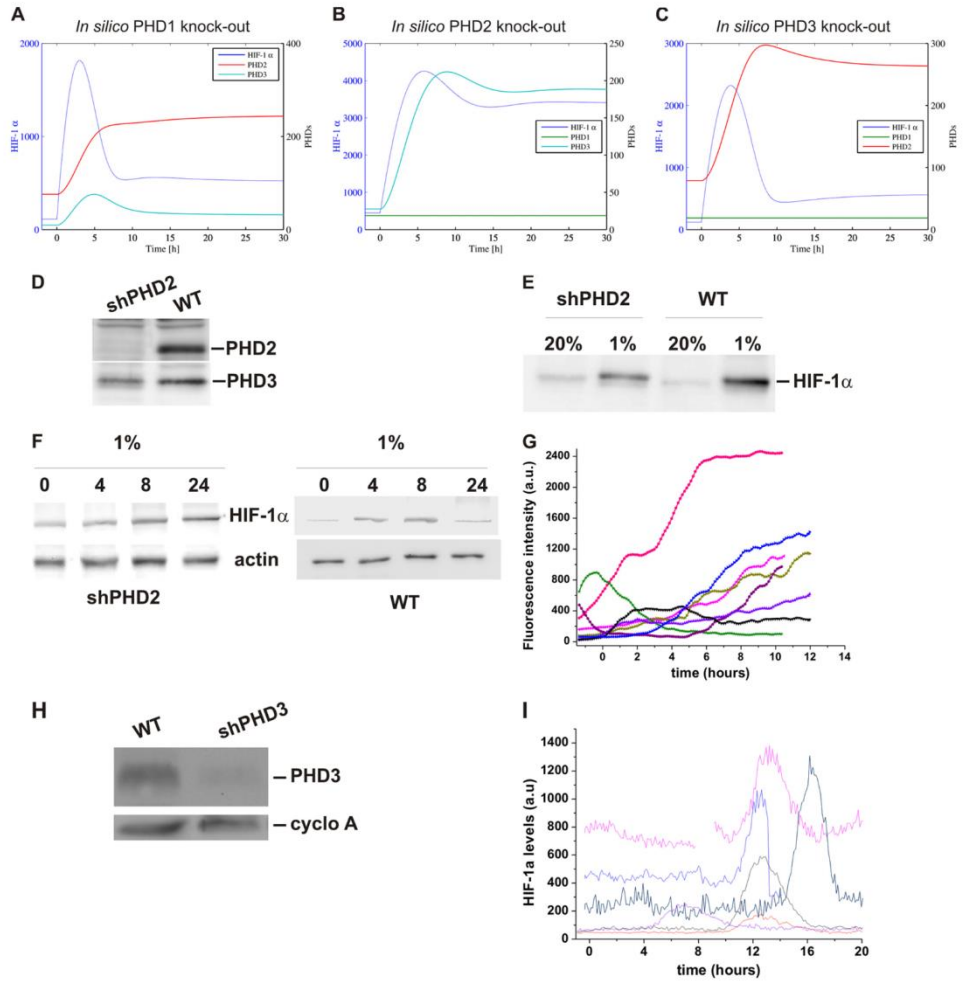

FIGURE 6. **PHD2 knock-down affects HIF temporal profile.** *A–C*, predictions are based on a 4-component model (Fig. 5*A*) with PHD1, -2, or -3 removed representing *in silico* knock-out of PHD1, -2, and -3. The models are initially at equilibrium in normoxia and then de-oxygenated into hypoxia at $t = 0$. *D*, Western blot analysis of PHD2 and PHD3 levels in WT and sh-PHD2 HeLa cells. *E*, Western blot analysis of HIF-1α levels in WT and SH-PHD2 HeLa cells cultured in normoxia submitted to 5 h hypoxia (1% O_2). *F*, Western blot analysis of HIF-1α levels in sh-PHD2 HeLa cells cultured in 1% O_2 for the indicated time points. *G*, single cell analysis of HIF-1α-EGFP levels in sh-PHD2 cells exposed to 1% O_2. *H*, Western blot analysis of PHD3 levels in WT and sh-PHD3 HeLa cells. *I*, single cell analysis of HIF-1α-EGFP levels in sh-PHD3 cells exposed to 1% O_2.

subsequent differential binding to other partners and it is, therefore, important to understand the consequences of the variation of HIF timing to inform future therapeutic strategies aimed at controlling HIF activity. We have shown that in conditions where transient HIF accumulation was lost, there was a high level of cell death, pointing to the importance of elucidating which component of the HIF signaling is the guardian of its timing. Using a mathematical model built on single cell imaging data, we predicted that HIF-1α dynamics will display a range of kinetics depending on the hypoxic situation and that it is PHD2 that is specifically involved in the negative feedback responsible for pulsatile HIF levels.

Single Cell Imaging of HIF: Transiency and Heterogeneity—Using live cell imaging, we observed a range of dynamics of HIF

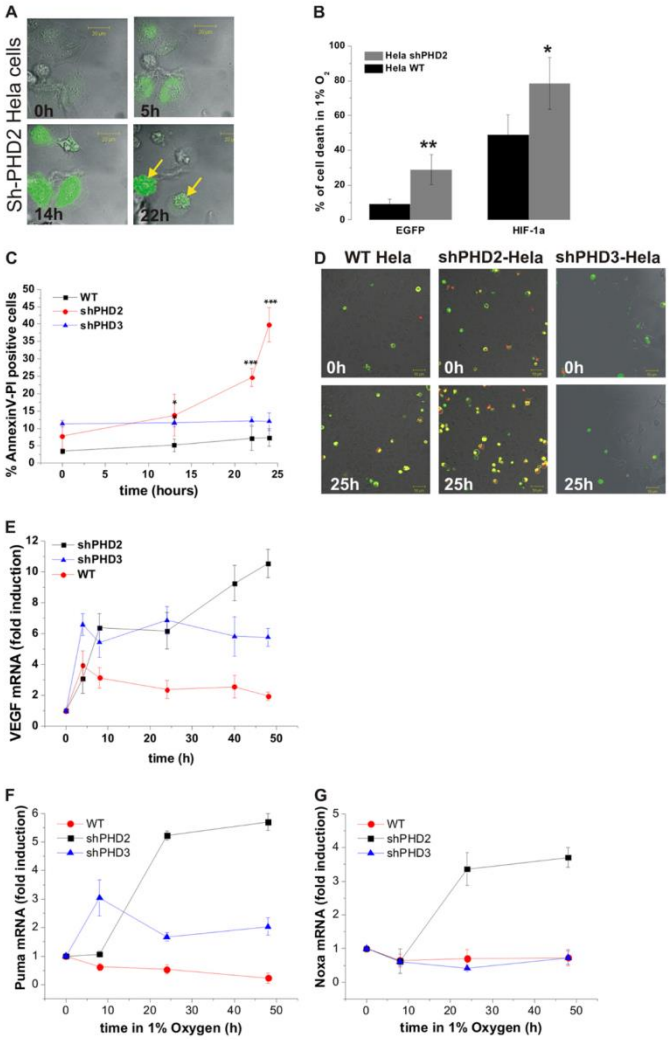

FIGURE 7. *A*, pictures of a representative field of sh-PHD2 cells expressing HIF-1α-EGFP at the indicated times in hypoxia show cell death associated with high and long lasting levels of HIF-1α. *B*, the percentage of transfected sh-PHD2 or WT HeLa cells dying within the 20 h of an imaging experiment was calculated for control cells transfected with either an empty EGFP plasmid or with HIF-1α-EGFP in normoxia and hypoxia ($n = 40$ cells/conditions). *C* and *D*, HeLa cells (WT, shPHD2 or shPHD3 lines) were imaged simultaneously using a 4-compartment glass bottom dish (Greiner). They were labeled with Annexin V-FITC (*green*) and PI (*red*) 10 min before imaging. Cells were imaged for 2 h in normoxia prior to the switch to 1% O_2. Images were recorded every 15 min for 24 h. The number of apoptotic cells (Annexin labeling preceding the PI labeling) was counted out of the total number of cells and plotted (*C*). A typical field of cells at several time points is shown (*D*). *E–G*, WT, HeLa cells, or HeLa cells expressing shPHD2 or shPHD3, were cultured in 1% O_2 for the indicated time points. *E*, VEGF mRNA levels were assessed by qPCR. *F*, PUMA mRNA levels were assessed by qPCR. *G*, Noxa mRNA were assessed by qPCR. *E–G*, the plots represent the average ± S.D. of triplicate samples from a representative experiment. The experiments were performed 4 times. Results are the mean of three independent experiments ± S.E. ***, **, and * indicate statistical difference with $p < 0{,}001$, $p < 0.01$, and $p < 0.05$, respectively.

HIF-α Dynamics and Mathematical Modeling

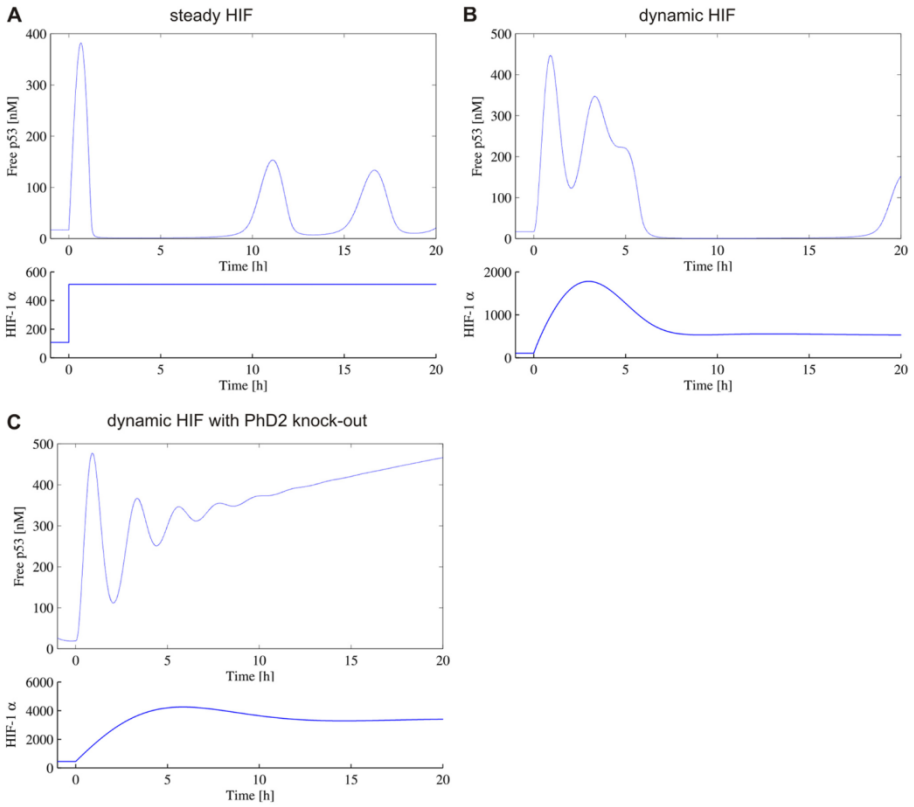

FIGURE 8. **Prediction of p53 dynamics following hypoxic switch.** *A*, the hypoxic switch at $t = 0$ is represented by an instantaneous switch in HIF from a low normoxic equilibrium level to a high hypoxic equilibrium level. The p53 levels are obtained by solving the HIF-dependent p53-MdM2 feedback model. *B* and *C*, the hypoxic switch drives transient HIF dynamics determined by the HIF-PHD model, which is coupled to the p53-MdM2 feedback model. Cells are WT (*B*) or sh-PHD2 (*C*).

nuclear accumulation, including fast and slow kinetics, single and multiple peaks. Although heterogeneity is a common feature of cellular processes (22, 28), this could not be detected using bulk cell analysis approaches and has never been described previously in this system. In the case of the oxygen dependent signaling, inter-cellular heterogeneity may be generated by extrinsic noise such as NO or iron levels, as well as intrinsic noise from transcription (29). We also observed transient HIF accumulation in normoxia (Fig. 1*D*) and spontaneous peaks of transcriptional activity (not shown), which agrees with the previous suggestion of oxygen-independent mechanisms of HIF stabilization (18, 30).

HIF Dynamics: Role of Negative Feedback Loops and Their Mathematical Modeling—Existing HIF models (31–33) have focused on how equilibrium levels of HIF are a function of oxygen levels, in particular probing the possibility of a switch-like behavior in HIF levels in response to hypoxia. Despite being formulated as dynamic models, these previous models have typically focused on the static states of the system. However, the single-cell dynamic data presented here clearly demonstrate that in response to hypoxia, many cells undergo rapid and large amplitude transient dynamics in nuclear HIF, before returning to equilibrium levels, which are comparable with the levels found in normoxic conditions. The model proposed here is highly idealized in that they only consider the dynamics of HIF and the PHD proteins. This simple model might be integrated, in the future, in a recently published model based on HIF transcriptional activity (34). However, even our 2-component model, with the generic PHD, was able to fit a range of the single cell dynamic data and provided a tool to assess the sensitivity of the different model parameters via consideration of a median solution of the system. Furthermore, by expanding the

model to consider separately PHD1, -2 and -3, we were able to test computationally potential specific roles of the PHDs in the control of HIF timing, and demonstrate non-redundancy between PHD1, -2, and -3. We were also able to examine downstream effects by coupling the simple HIF-PHD model to existing biochemical models. Specifically here we coupled HIF to a model of the p53-Mdm2 feedback loop. We were able to demonstrate the importance of capturing not only equilibrium levels of HIF in normoxia and hypoxia, but also the transient dynamics. Specifically we demonstrated that the overshoot HIF levels observed in transient dynamics lead to higher transitory levels of p53, and a delay in the onset of p53 oscillatory behavior. Furthermore, we determined *in silico* the HIF-mediated role that PHD2 has in regulating p53 dynamics, explicitly demonstrating that in shPHD2 cells, p53 displays sustained high levels suggesting apoptotic activity.

Role of the PHD2 Negative Feedback Loop on HIF Timing and Cell Fate—Berra *et al.* (23) addressed the question of the multiplicity of the PHDs relative to HIF-1α and showed, by silencing each PHD isoform individually, that only PHD2 controlled the steady state levels of HIF-1α in HeLa cells and other human cells. By extending a simple mathematical model of the HIF-PHD negative feedback loop it was possible to separate the 3 different PHDs on the basis of their levels, stability, and induction. This pointed to a strong role of PHD2 in the control of HIF nuclear accumulation in hypoxia. It is, however, possible that at other O_2 levels, *e.g.* mild hypoxia or anoxia, the role of the other PHDs will also play an important role and hence contribute to HIF dynamics. The consequences of long lasting HIF-1α levels were observed on VEGF transcription dynamics (Fig. 7*E*), and they are likely to also directly affect HIF-binding proteins such as mdm2 (11), hence altering cell survival in hypoxia. The cell death induced by hypoxia in cells in which PHD2 was silenced (Fig. 7, *A–D*) was in line with the protective role of PHD2 in gliomas against hypoxia-induced tumor cell death (35) and could well represent a new molecular target for cancer drugs. Taken together, our data point to a major role for PHD2 compared with PHD3 in the negative feedback regulation of HIF-1α dynamics, although we cannot rule out the presence of other, non PHD-dependent, mechanisms, as previously suggested (36–39). The potential feedbacks, both oxygen-dependent and -independent, and how they affect HIF-α levels and activity will have to be further investigated.

Cells can experience hypoxia in a wide range of physiological and pathological contexts, where HIF activity is up-regulated and associated with different cell fates. The decision between survival/death, proliferation/cell cycle arrest in hypoxia is likely due to differential gene expression, as well as HIF binding to key proteins involved in these mechanisms (*e.g.* mdm2/p53). In conclusion, we have shown here that one way to trigger hypoxic death is to have uncontrolled high and long lasting HIF levels, and that an important role of PHD2 is to keep HIF on time. Our results show that HIF dynamics have an impact on cell fate through p53 transcriptional activity regulation, and mathematical modeling predictions points to differential p53 dynamics and levels depending on the HIF temporal profile, which will need to be fully investigated in the future.

Acknowledgments—We thank Prof. Melillo for the HRE-luc plasmid, Dr. Stiehl and Dr. Hoogewijs for the shPHD2 cells, shPHD3 lentivirus, and for helpful discussions, and Dr. R. Depping for the PHD2-EGFP plasmid. We thank Bryan Welm for the pHIV-ires-dTomato vector and Didier Trono for pMD2.G and psPAX2 plasmids. We thank Haleh Shahidipour for technical help with qPCR. We also thank Dr. Lehmann and Prof. Wenger for the C51 stable reporter and helpful discussions and the COST action TD0901 for facilitating these interactions. We thank Dr. Paszek for critical reading and Dr. Levy for fruitful discussions.

REFERENCES

1. Maxwell, P. H., Wiesener, M. S., Chang, G. W., Clifford, S. C., Vaux, E. C., Cockman, M. E., Wykoff, C. C., Pugh, C. W., Maher, E. R., and Ratcliffe, P. J. (1999) The tumour suppressor protein VHL targets hypoxia-inducible factors for oxygen-dependent proteolysis. *Nature* **399,** 271–275
2. Sowter, H. M., Ratcliffe, P. J., Watson, P., Greenberg, A. H., and Harris, A. L. (2001) HIF-1-dependent regulation of hypoxic induction of the cell death factors BNIP3 and NIX in human tumors. *Cancer Res.* **61,** 6669–6673
3. Piret, J. P., Mottet, D., Raes, M., and Michiels, C. (2002) Is HIF-1α a pro- or an anti-apoptotic protein? *Biochem. Pharmacol.* **64,** 889–892
4. Blagosklonny, M. V. (2001) Do VHL and HIF-1 mirror p53 and Mdm-2? Degradation-transactivation loops of oncoproteins and tumor suppressors. *Oncogene* **20,** 395–398
5. Lahav, G., Rosenfeld, N., Sigal, A., Geva-Zatorsky, N., Levine, A. J., Elowitz, M. B., and Alon, U. (2004) Dynamics of the p53-Mdm2 feedback loop in individual cells. *Nat. Genet.* **36,** 147–150
6. Purvis, J. E., Karhohs, K. W., Mock, C., Batchelor, E., Loewer, A., and Lahav, G. (2012) p53 dynamics control cell fate. *Science* **336,** 1440–1444
7. Stiehl, D. P., Wirthner, R., Köditz, J., Spielmann, P., Camenisch, G., and Wenger, R. H. (2006) Increased prolyl 4-hydroxylase domain proteins compensate for decreased oxygen levels. Evidence for an autoregulatory oxygen-sensing system. *J. Biol. Chem.* **281,** 23482–23491
8. Berra, E., Ginouvès, A., and Pouysségur, J. (2006) The hypoxia-inducible factor hydroxylases bring fresh air into hypoxia signalling. *EMBO Rep.* **7,** 41–45
9. Metzen, E., Stiehl, D. P., Doege, K., Marxsen, J. H., Hellwig-Bürgel, T., and Jelkmann, W. (2005) Regulation of the prolyl hydroxylase domain protein 2 (*phd2*/*egln-1*) gene. Identification of a functional hypoxia-responsive element. *Biochem. J.* **387,** 711–717
10. Marxsen, J. H., Stengel, P., Doege, K., Heikkinen, P., Jokilehto, T., Wagner, T., Jelkmann, W., Jaakkola, P., and Metzen, E. (2004) Hypoxia-inducible factor-1 (HIF-1) promotes its degradation by induction of HIF-α-prolyl-4-hydroxylases. *Biochem. J.* **381,** 761–767
11. Chen, D., Li, M., Luo, J., and Gu, W. (2003) Direct interactions between HIF-1α and Mdm2 modulate p53 function. *J. Biol. Chem.* **278,** 13595–13598
12. Hunziker, A., Jensen, M. H., and Krishna, S. (2010) Stress-specific response of the p53-Mdm2 feedback loop. *BMC Syst. Biol.* **4,** 94
13. Metzen, E., Berchner-Pfannschmidt, U., Stengel, P., Marxsen, J. H., Stolze, I., Klinger, M., Huang, W. Q., Wotzlaw, C., Hellwig-Bürgel, T., Jelkmann, W., Acker, H., and Fandrey, J. (2003) Intracellular localisation of human HIF-1α hydroxylases. Implications for oxygen sensing. *J. Cell Sci.* **116,** 1319–1326
14. Rabut, G., and Ellenberg, J. (2004) Automatic real-time three-dimensional cell tracking by fluorescence microscopy. *J. Microsc.* **216,** 131–137
15. Shen, H., Nelson, G., Nelson, D. E., Kennedy, S., Spiller, D. G., Griffiths, T., Paton, N., Oliver, S. G., White, M. R., and Kell, D. B. (2006) Automated tracking of gene expression in individual cells and cell compartments. *J. R. Soc. Interface* **3,** 787–794
16. Tuckerman, J. R., Zhao, Y., Hewitson, K. S., Tian, Y. M., Pugh, C. W., Ratcliffe, P. J., and Mole, D. R. (2004) Determination and comparison of specific activity of the HIF-prolyl hydroxylases. *FEBS Lett.* **576,** 145–150
17. Appelhoff, R. J., Tian, Y. M., Raval, R. R., Turley, H., Harris, A. L., Pugh,

C. W., Ratcliffe, P. J., and Gleadle, J. M. (2004) Differential function of the prolyl hydroxylases PHD1, PHD2, and PHD3 in the regulation of hypoxia-inducible factor. *J. Biol. Chem.* **279,** 38458–38465
18. André, H., and Pereira, T. S. (2008) Identification of an alternative mechanism of degradation of the hypoxia-inducible factor-1α. *J. Biol. Chem.* **283,** 29375–29384
19. Moroz, E., Carlin, S., Dyomina, K., Burke, S., Thaler, H. T., Blasberg, R., and Serganova, I. (2009) Real-time imaging of HIF-1α stabilization and degradation. *PLoS One* **4,** e5077
20. Pescador, N., Cuevas, Y., Naranjo, S., Alcaide, M., Villar, D., Landázuri, M. O., and Del Peso, L. (2005) Identification of a functional hypoxia-responsive element that regulates the expression of the egl nine homologue 3 (*egln3*/*phd3*) gene. *Biochem. J.* **390,** 189–197
21. Pellegrin, P., Fernandez, A., Lamb, N. J., and Bennes, R. (2002) Macromolecular uptake is a spontaneous event during mitosis in cultured fibroblasts. Implications for vector-dependent plasmid transfection. *Mol. Biol. Cell* **13,** 570–578
22. Geva-Zatorsky, N., Rosenfeld, N., Itzkovitz, S., Milo, R., Sigal, A., Dekel, E., Yarnitzky, T., Liron, Y., Polak, P., Lahav, G., and Alon, U. (2006) Oscillations and variability in the p53 system. *Mol. Syst. Biol.* **2,** 2006 0033
23. Berra, E., Benizri, E., Ginouvès, A., Volmat, V., Roux, D., and Pouysségur, J. (2003) HIF prolyl-hydroxylase 2 is the key oxygen sensor setting low steady-state levels of HIF-1α in normoxia. *EMBO J.* **22,** 4082–4090
24. Takeda, N., O'Dea, E. L., Doedens, A., Kim, J. W., Weidemann, A., Stockmann, C., Asagiri, M., Simon, M. C., Hoffmann, A., and Johnson, R. S. (2010) Differential activation and antagonistic function of HIF-α isoforms in macrophages are essential for NO homeostasis. *Genes Dev.* **24,** 491–501
25. Grimm, C., Hermann, D. M., Bogdanova, A., Hotop, S., Kilic, U., Wenzel, A., Kilic, E., and Gassmann, M. (2005) Neuroprotection by hypoxic preconditioning. HIF-1 and erythropoietin protect from retinal degeneration. *Semin Cell Dev. Biol.* **16,** 531–538
26. Helton, R., Cui, J., Scheel, J. R., Ellison, J. A., Ames, C., Gibson, C., Blouw, B., Ouyang, L., Dragatsis, I., Zeitlin, S., Johnson, R. S., Lipton, S. A., and Barlow, C. (2005) Brain-specific knock-out of hypoxia-inducible factor-1α reduces rather than increases hypoxic-ischemic damage. *J. Neurosci.* **25,** 4099–4107
27. Brahimi-Horn, M. C., and Pouysségur, J. (2007) Hypoxia in cancer cell metabolism and pH regulation. *Essays Biochem.* **43,** 165–178
28. Feinerman, O., Veiga, J., Dorfman, J. R., Germain, R. N., and Altan-Bonnet, G. (2008) Variability and robustness in T cell activation from regulated heterogeneity in protein levels. *Science* **321,** 1081–1084
29. Swain, P. S., Elowitz, M. B., and Siggia, E. D. (2002) Intrinsic and extrinsic contributions to stochasticity in gene expression. *Proc. Natl. Acad. Sci. U.S.A.* **99,** 12795–12800
30. Mukherjee, T., Kim, W. S., Mandal, L., and Banerjee, U. (2011) Interaction between Notch and Hif-α in development and survival of *Drosophila* blood cells. *Science* **332,** 1210–1213
31. Kohn, K. W., Riss, J., Aprelikova, O., Weinstein, J. N., Pommier, Y., and Barrett, J. C. (2004) Properties of switch-like bioregulatory networks studied by simulation of the hypoxia response control system. *Mol. Biol. Cell* **15,** 3042–3052
32. Dayan, F., Monticelli, M., Pouysségur, J., and Pécou, E. (2009) Gene regulation in response to graded hypoxia. The non-redundant roles of the oxygen sensors PHD and FIH in the HIF pathway. *J. Theor. Biol.* **259,** 304–316
33. Schmierer, B., Novák, B., and Schofield, C. J. (2010) Hypoxia-dependent sequestration of an oxygen sensor by a widespread structural motif can shape the hypoxic response. A predictive kinetic model. *BMC Syst. Biol.* **4,** 139
34. Nguyen, L. K., Cavadas, M. A., Scholz, C. C., Fitzpatrick, S. F., Bruning, U., Cummins, E. P., Tambuwala, M. M., Manresa, M. C., Kholodenko, B. N., Taylor, C. T., and Cheong, A. (2013) A dynamic model of the hypoxia-inducible factor 1α (HIF-1α) network. *J. Cell Sci.* **126,** 1454–1463
35. Henze, A. T., Riedel, J., Diem, T., Wenner, J., Flamme, I., Pouyseggur, J., Plate, K. H., and Acker, T. (2010) Prolyl hydroxylases 2 and 3 act in gliomas as protective negative feedback regulators of hypoxia-inducible factors. *Cancer Res.* **70,** 357–366
36. Demidenko, Z. N., Rapisarda, A., Garayoa, M., Giannakakou, P., Melillo, G., and Blagosklonny, M. V. (2005) Accumulation of hypoxia-inducible factor-1α is limited by transcription-dependent depletion. *Oncogene* **24,** 4829–4838
37. Tan, M., Gu, Q., He, H., Pamarthy, D., Semenza, G. L., and Sun, Y. (2008) *SAG*/*ROC2*/*RBX2* is a HIF-1 target gene that promotes HIF-1α ubiquitination and degradation. *Oncogene* **27,** 1404–1411
38. Horak, P., Crawford, A. R., Vadysirisack, D. D., Nash, Z. M., DeYoung, M. P., Sgroi, D., and Ellisen, L. W. (2010) Negative feedback control of HIF-1 through REDD1-regulated ROS suppresses tumorigenesis. *Proc. Natl. Acad. Sci. U.S.A.* **107,** 4675–4680
39. Bruning, U., Cerone, L., Neufeld, Z., Fitzpatrick, S. F., Cheong, A., Scholz, C. C., Simpson, D. A., Leonard, M. O., Tambuwala, M. M., Cummins, E. P., and Taylor, C. T. (2011) MicroRNA-155 promotes resolution of hypoxia-inducible factor 1α activity during prolonged hypoxia. *Mol. Cell Biol.* **31,** 4087–4096

3.3 Additional work

3.3.1 Improving molecular tools for imaging: HIF-1α-GFP stable cell line

Most of the studies into the dynamics of the HIF-α subunits performed so far have required transient transfection of plasmids encoding HIF-1α / HIF-2α fused with fluorescent proteins such as EGFP or dsRed. Transient transfection has many disadvantages such as heterogeneity in expression levels, the protocol can be unreliable and the reagents can be toxic to the cells. In addition to this, the gene is under the control of a promoter that permits constitutive expression, the CMV promoter, which can lead to high levels of expression that are not necessarily representative of those observed for the endogenous promoter, and expression can vary between cell types (Smith *et al.*, 2000). Therefore, to improve the quality of our HIF dynamic studies, we aimed to create stably transfected cell lines for both HIF-1α and HIF-2α.

The initial plan was to create three stable cell lines via lenti-viral transduction, however creating cell lines stably expressing HIF-1α-EGFP and EGFP-HIF-2α proved difficult and we only had success with the ODD-EGFP construct (mentioned earlier). With this cell line, although similar dynamics to HIF-1α-EGFP (ectopically expressed in WT HeLa) in hypoxia were observed, the degradation appeared to be slower. This is could be explained by the fact that the ODD-EGFP is lacking the DNA binding domain and so is not transcriptionally active, resulting in an increase of substrate (ODD domain) in the system with no additional activation of PHD2 transcription to compensate. In addition to this, the ODD-EGFP only has one prolyl residue for hydroxylation which may result in reduced affinity of pVHL binding, thus less efficient targeting of the ODD-EGFP for proteasomal degradation. Although the ODD-EGFP cell line provides some valuable information, there was a need for a cell line stably expressing fluorescently-labelled full-length HIF-1α and HIF-2α. Given the lack of success with the lenti-virus approach to achieve this, I directed my efforts towards alternative strategies. I tried to generate a cell line stably expressing fluorescently labelled HIF-2α using several methods including zinc finger nucleases (ZFNs), but all were unsuccessful (work not shown) and so all work with HIF-2α-EGFP presented in this thesis was carried out using transient transfection. However, I had the opportunity to use a Bacterial Artificial Chromosome (BAC) for HIF-1α-GFP, thanks to the kind gift from Prof B

van de Water's laboratory (University of Leiden), and was able to create a stable cell line expressing HIF-1α-GFP.

3.3.1.1 HIF-1α-GFP BAC stable cell line

A HIF-1α-EGFP cell line was established via stable transfection of HeLa with a BAC encoding the fusion protein. In comparison to the ODD-EGFP cell line, this gene is under the control of its endogenous promoter and BACs can hold large pieces of mammalian DNA (up to 350 Kb, compared to 15 Kb for plasmids and 7 Kb for lenti-viral vectors) resulting in the inclusion of lengthy flanking regions. Therefore a large proportion of the regulatory elements are incorporated and so utilising a BAC provides a more true reflection of endogenous expression (Adamson *et al.*, 2011;Casali, 2003). Another advantage of the BAC cell line is that it was established from a single cell and is therefore a clonal population and so could provide the opportunity to determine whether the heterogeneity observed in Bagnall *et al.* (2014) is a feature of the HIF signalling system or an artefact of transient transfection.

The HIF-1α-GFP BAC cell line was validated via western blot and imaging. Figure 3.1A shows a strong induction of wild type HIF-1α following treatment with 0.5 mM DMOG (6 h) and a transient induction of endogenous HIF-1α in hypoxia. A second band, approximately 40 kDa higher, follows the same pattern of induction and is presumed to be HIF-1α-GFP. The cells were imaged on a confocal microscope before and after (6 h) treatment with the hypoxia mimic and nuclear accumulation of fluorescent protein was observed (Figure 3.1B). Following these validation experiments, this cell line was utilised to repeat time-lapse experiments that were performed in Bagnall *et al.* (2014).

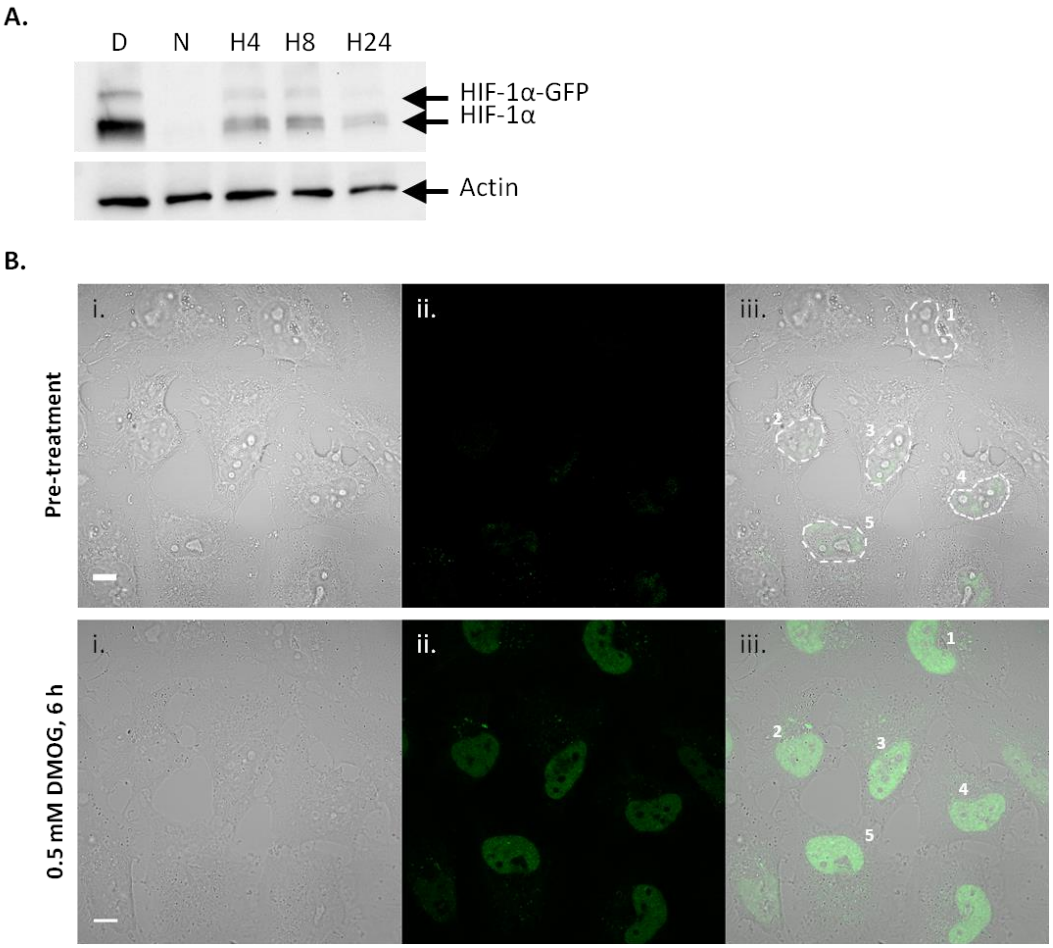

Figure 3.1 | Validation of HIF-1α-GFP stable cell line. *A) Western blot analysis of HIF-1α-GFP HeLa incubated in different conditions (D = 0.5 mM DMOG, 6 h, N = normoxia, H = hypoxia, number indicates number of hours incubated in hypoxia).Immunoblot was probed with anti-HIF-1α (top) and anti-β-actin (bottom) antibodies. B) HIF-1α-GFP HeLa were imaged on a Zeiss LSM780, before and after treatment with 0.5 mM DMOG (i = brightfield, ii = GFP, iii = merge of i and ii). Scale bar = 10 µ. In pre-treatment cells nuclei are outlined in white.*

A.

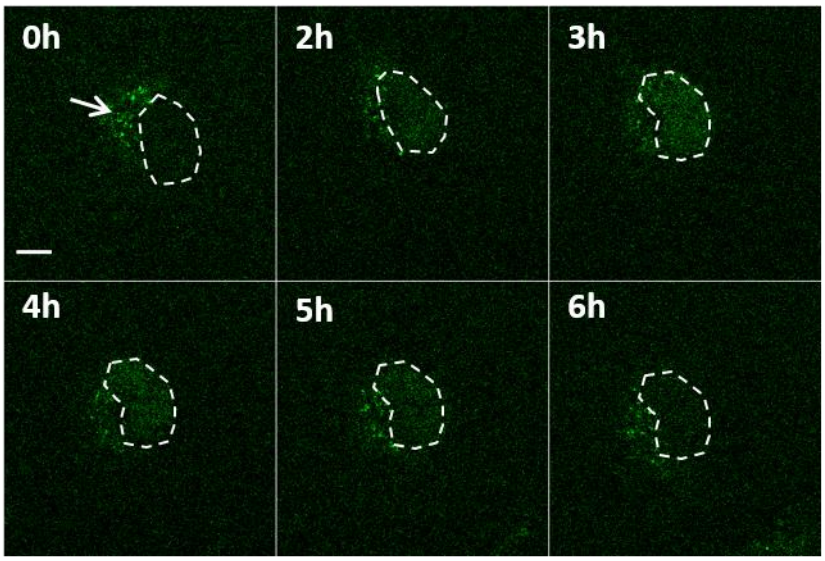

B.

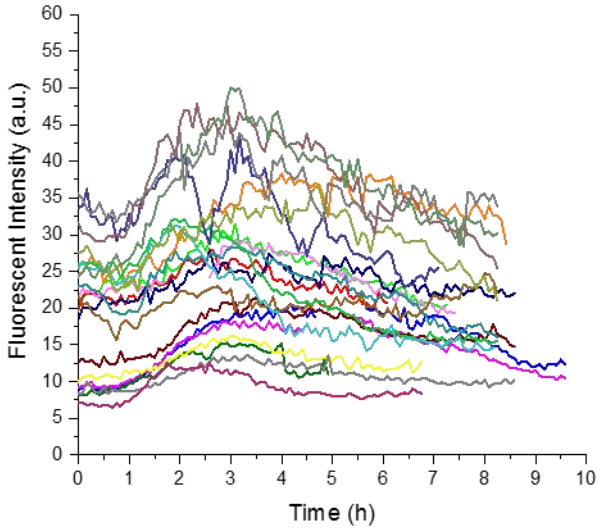

Figure 3.2 | HIF-1α-GFP BAC time-lapse experiments. *A) Confocal images of HIF-1α-GFP BAC cells in 0.5 % O2. Cells were subjected to hypoxic conditions from the second time point onwards. Nuclear boundary highlighted by white dashed line. White arrow indicates perinuclear autofluorescence. B) Quantification of fluorescence signal. Each data series represents the fluorescence measured in the nucleus of a single cell over time.*

Upon incubation in hypoxia, the cells showed a transient induction of HIF-1-GFP. After approximately 1 h the levels of fluorescence started to increase, peaked at 3-3.5 h and then started to decrease, reaching levels similar to those at the start of the time-lapse by 6-8 h (Figure 3.2B, M1 on supplemental CD).

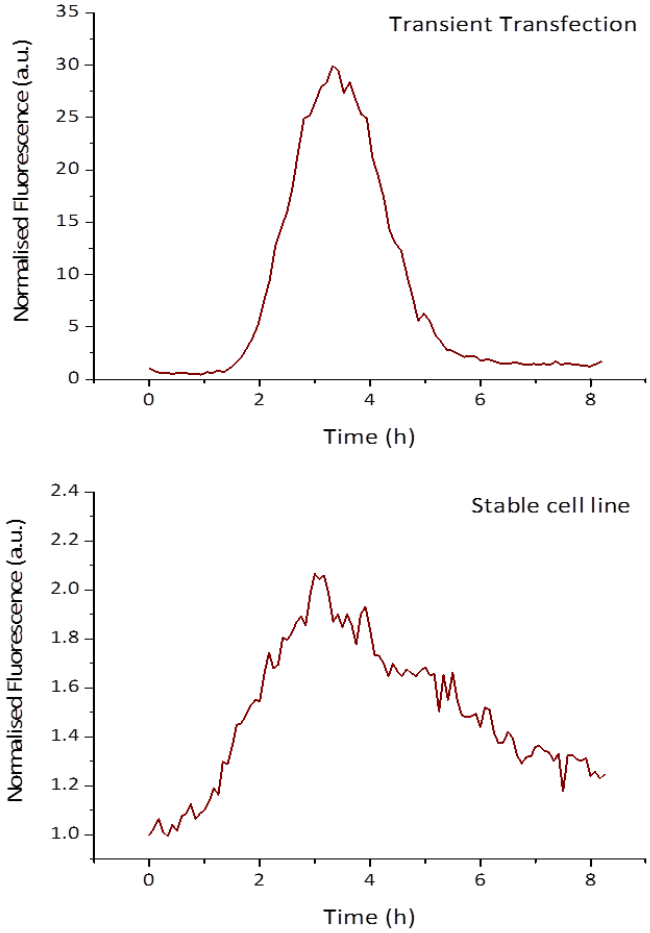

Figure 3.3 | Comparison of HIF-1α dynamics in hypoxia *Example traces from single HeLa cell ectopically expressing CMV-HIF-1α-EGFP (top) and single HIF-1α-GFP BAC cell line (bottom) in hypoxia. Hypoxic incubation starts at 0 h.*

Figure 3.3 compares the typical shape of HIF-1α accumulation in hypoxia in a single cell ectopically expressing CMV-HIF-1α-EGFP (taken from James Bagnall's data set) and one from the HIF-1α-GFP BAC experiments. In both systems the levels of HIF-1α start to increase at around 1-2 hours and peaks around 3-4 hours. Compared to the stable cell line, the cell transiently transfected with HIF-1α-EGFP shows a sharper increase in fluorescence, reaching much higher levels that then decrease more rapidly. The stable cell line exhibits stabilisation of much lower levels and a softer decline in HIF-1α, similar to what was observed with the ODD-EGFP cell line. The difference in the accumulation pattern might be explained by the difference in HIF-1α levels. The very high HIF levels obtained with transient transfection will induce a stronger negative feedback response compared to the 2 fold increase obtained with the BAC cell line.

Although the BAC cell line should be closer to physiological HIF expression at the mRNA levels as the transgene is under the control of the endogenous promoter and other regulatory elements, the dynamic range of HIF-1α-GFP accumulation in hypoxia is poor i.e. the expression of the transgene are much lower than the endogenous protein in the western-blot (Figure 3.1A). Therefore the accumulation pattern observed with this cell line is unlikely to actually represent the reality any more than transient transfection.

3.4 Conclusion

Here we have utilised live single cell imaging to demonstrate that induction of HIF-1α is transient due to an auto-regulatory mechanism. Furthermore we showed that the tight control of HIF-1α dynamics in hypoxia is necessary to prevent cell death. To validate these findings published in Bagnall *et al.* (2014) I repeated time-lapse experiments with cells stably expressing HIF-1α-GFP.

3.4.1 Imaging tools

The difficulties experienced whilst trying to create a cell line stably expressing fluorescently labelled HIF-1/2α via lenti-viral transduction may be due to the final constructs being quite large (pHIV- HIF-1α-EGFP-IRES-dTomato is 10950 bp and pHIV-EGFP-HIF-2α-IRES-dTomato is 11049 bp). It has been shown that constructs containing larger inserts achieve lower viral titres (units / mL) than smaller constructs (Al Yacoub *et al.*, 2007). Also, the size of the construct can result in reduced recovery of the viral particles following the ultracentrifugation step prior to transduction (Al Yacoub *et al.*, 2007).

These stable cell lines that were successfully made are useful tools for studying the temporal and spatial dynamics of HIF-1α at the single cell level. For examples the ODD-EGFP does not have any PAS domains so cannot heterodimerise with HIF-1β and there are no DNA binding domains, therefore there will be no downstream effects of overexpression of the ODD-EGFP as it is not transcriptionally active and therefore any dynamics observed relates purely to the activity of the PHDs. The HIF-1α BAC cell line has other advantages, as the transgene is under the control of the endogenous promoter so any observations take into account regulation at the transcriptional level as well as regulation via protein stability.

Unfortunately, the fluorescent signal in the ODD-EGFP and the HIF-1α BAC cell lines is very dim, which makes quantification of signal difficult and raises issues with acquisition, as higher laser power is required and longer exposure, which can lead to photobleaching and phototoxicity. This poor signal may be due to integration effects. Stable transfection of both lenti-viral vectors and BACs results in the integration of the exogenous reporter gene into the host's genome (Adamson *et al.*, 2011). However, there is little control over where the transgene is inserted and if it occurs within regions of densely packed, inactive heterochromatin then there will be little or no expression (Dillon & Festenstein, 2002;Adamson *et al.*, 2011). Another possibility is that the transgene integrates downstream of silencing elements. One way around this would be to utilise methods that allow targeting integration such a genome editing nucleases (zinc finger nucleases / ZFNs, transcription activator-like effector nuclease / TALENs, clustered regularly interspaced short palindromic repeats / CRISPR).

Such low fluorescence levels have prevented me from performing longer time-lapse experiments, which would have allowed me to investigate whether there are further oscillations in prolonged hypoxia and if there is a link between the HIF dynamics and the cell cycle (as mentioned in the publication).

Chapter 4: Investigating the spatial localisation of HIF-1α and HIF-2α

When investigating the single cell dynamics of HIF-1α and HIF-2α it became apparent that the two alpha subunits exhibit different sub-nuclear localisation.

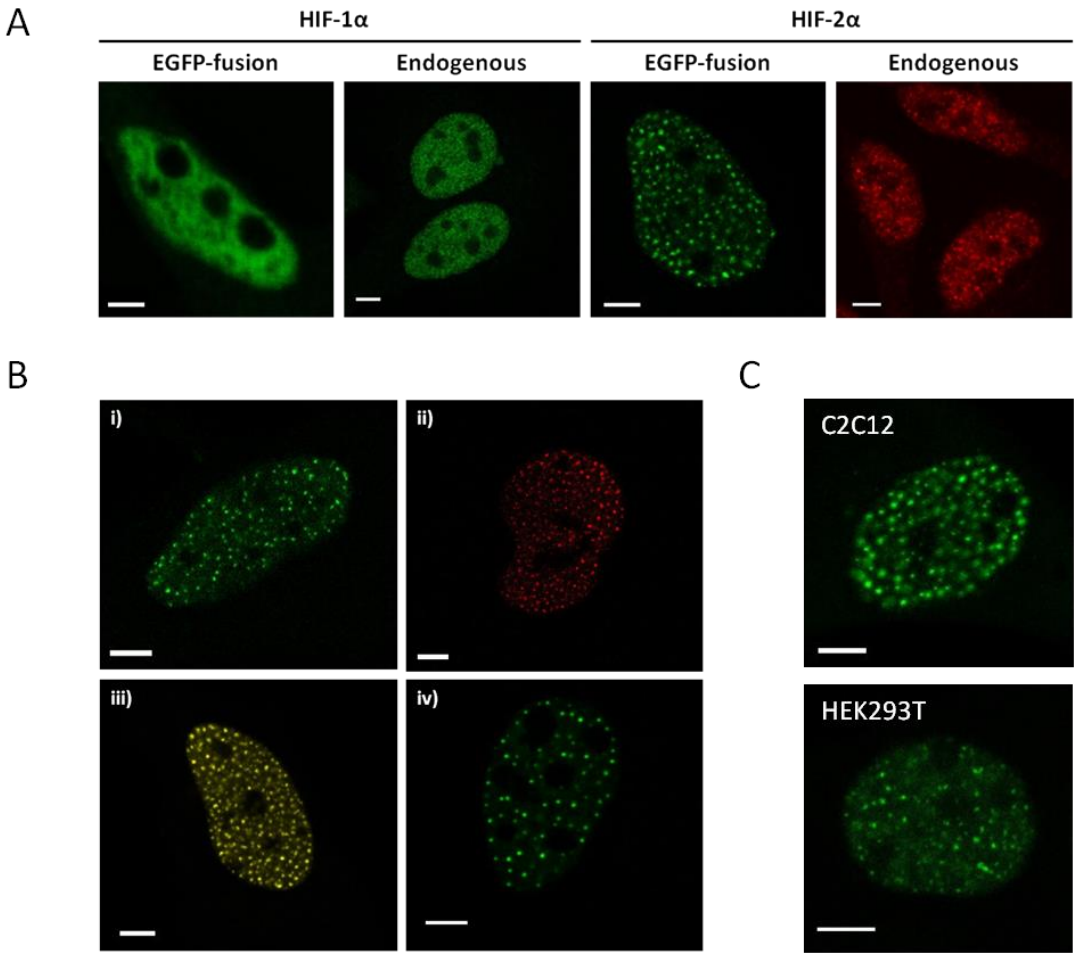

Figure 4.1 | Sub-nuclear localisation of HIF-2α. *A) HeLa cells ectopically expressing HIF-1α and HIF-2α EGFP fusions and endogenous HIF-1α and HIF-2α labelled using the immunofluorescent protocol. Images of HIF-1α-EGFP were taken in the presence of DMOG. Scale bar = 5 µm. B) HeLa cells transiently transfected with plasmids encoding clover-HIF-2α (i), dsRED-HIF-2α (ii), HIF-2α-venus (iii) and Halotag-HIF-2α (iv). The cells expressing Halotag-HIF-2α were labelled with the fluorescent Oregon Green Halotag ligand to visualise the fusion protein. C) Confocal images of C2C12 (mouse myoblast; top) and HEK293T (human embryonic kidney cells; bottom) cells ectopically expressing EGFP-HIF-2α. Scale bar = 5 µm.*

Figure 4.1 shows the localisation of ectopically expressed EGFP fusions of HIF-1α and HIF-2α. HIF-1α accumulates in the nucleus in a homogenous manner upon exposure to hypoxia or following treatment with a hypoxia mimic (DMOG), whereas HIF-2α localises in punctate foci (Figure 4.1A). Immunofluorescent staining of the respective endogenous proteins in HeLa cells shows a similar sub-nuclear localisation, highlighting that this difference is unlikely to be an artefact of overexpression (Figure 4.1A). Figure 4.1B shows that HIF-2α localises heterogeneously regardless of type or orientation (N- or C-terminal of HIF-2α) of

the tag. This non-homogenous protein expression is also observed in human embryonic kidney, mouse myoblast cells (Figure 4.1C), in neuroblastoma (SK-N-AS), medulloblastoma (D283 & Med8) and mouse primary neuronal cell lines (Bagnall, 2011).

These initial findings suggest that the localisation of HIF-2α is not due to artefacts of ectopic expression, the presence of the tag or the model cell line being used. As localisation is often associated with function, the heterogeneous distribution of HIF-2α was investigated further and is the focus of this study.

4.1 Is the non-homogenous nuclear localisation of HIF-2α functionally relevant?

As mentioned previously, spatial organisation within the nucleus is vital for regulating processes and protein function. It has been shown that many nuclear proteins localise in domains or nuclear speckles, which have function as sites of activity, modification or sequestration, for example. Further investigation was carried out to determine the purpose of the localisation of HIF-2α into speckles.

4.1.1 Characterisation of HIF-2α speckles

Analysis of images of the HIF-2α speckles revealed that, in normoxia, there is between 10-200 speckles per nucleus (average 64, n = 25) that are 0.24 (± 0.07) µm in size and take up approximately 3% of the nucleus (Figure 4.2A). The size of the speckles did not change in either hypoxia or DMOG compared to normoxia (Figure 4.2B). However, the average number of speckles did increase significantly following treatment with DMOG (Figure 4.2A).

These results could be explained by the exaggerated effects usually observed following treatment with DMOG i.e. a dramatic increase in HIF protein levels and HIF-dependent transcription, far greater than those observed in hypoxia (unpublished observations from V.Sée group). This drug inhibits all three PHD isoforms (and other hydroxylases) and so the HIF-alpha subunits evade oxygen-dependent degradation. So if there is an increase in stabilised HIF-2α molecules, these must go somewhere and these data suggest that the extra HIF-2α localise in additional speckles, either newly formed or speckles that were already present but were undetectable due to low levels of protein.

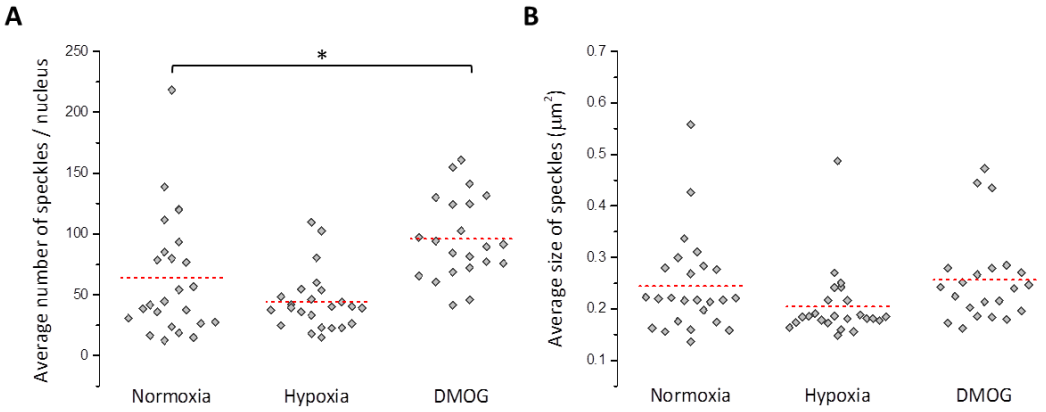

Figure 4.2 | Measurement of HIF-2α speckles. *HeLa cells transiently transfected with EGFP-HIF-2α were imaged on a Zeiss epifluorescent microscope fitted with a very fast and highly sensitive CCD camera (Andor, UK). One thousand frames were acquired per cell in normoxia, hypoxia (1% O2, 16 h) or following treatment with DMOG (0.5 mM, 6 h). The images were analysed using ImageJ. A) The average (±SD) number of speckles per nucleus in each condition was: 64 ± 49 (n=25), 44 ± 24 (n=24) and 96 ± 33 (n=22), respectively. Mean of the sample data represented by the red line. B) The average size of speckles per nucleus over the 1000 frames. The mean values for each condition were: 0.24 ± 0.09 μm (n=25), 0.21 ± 0.07 μm (n=24) and 0.27 ± 0.09 μm (n=22), respectively. The mean values for hypoxia and DMOG were compare to the normoxic values using IBM SPSS statistics software (independent t-test, significance value set at 5%). Mean of the sample data represented by the red line.*

4.1.2 Speckle mobility

On closer inspection of EGFP-HIF-2α in time-lapse movies, the HIF-2α speckles could be seen to move (M2 on attached CD). We therefore decided to characterise and quantify this motion further by tracking the speckles. Briefly, the speckles were identified as features in each frame and then these features were linked frame to frame creating trajectories using ImageJ (Sbalzarini & Koumoutsakos, 2005)(Figure 4.3, supplemental movies M3 and M4). The coordinates of these trajectories were exported to Excel for further analysis. Using a macro (see Appendix 1.3) created by Dr David Mason (Image Analyst, CCI, University of Liverpool), the speed, diffusion coefficient and diffusion mode (denoted by the slope of the moment scaling factor aka SMSS) for each trajectory was calculated.

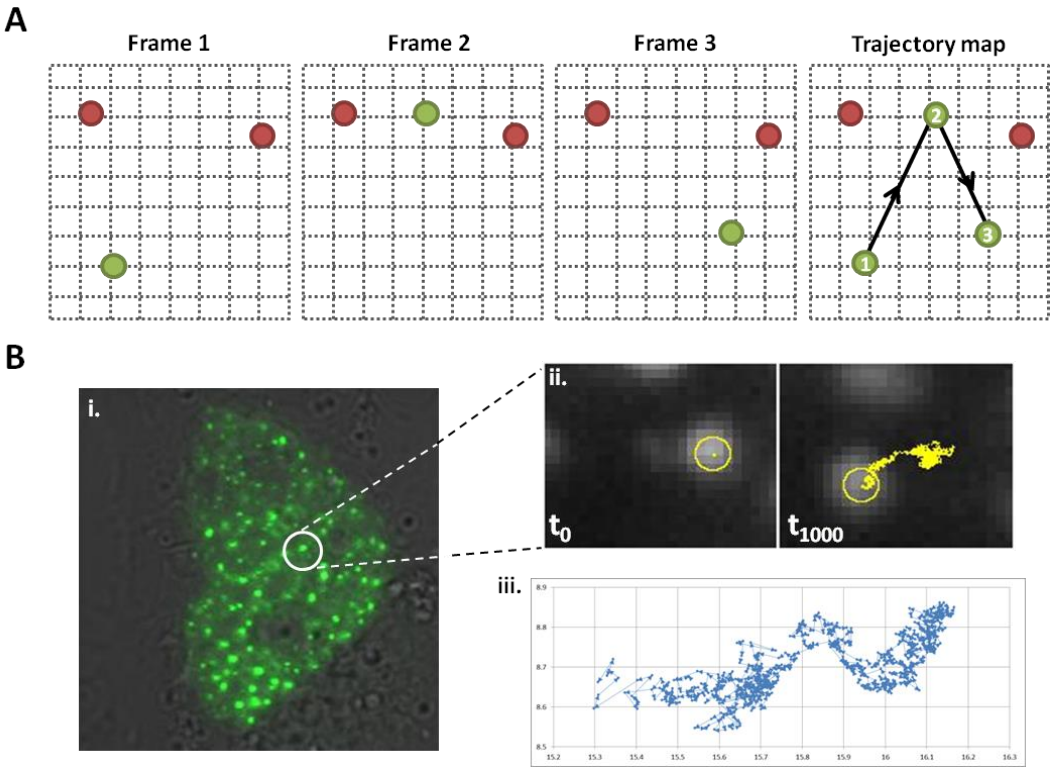

Figure 4.3 | Analysis of the HIF-2α trajectories. *A) Schematic of how speckles were tracked using ImageJ i.e. features were identified in each frame and then linked frame to frame to create a trajectory map. B) EGFP-HIF-2α speckle (i) tracked in ImageJ (ii) showing course of speckles over 1000 frames (yellow). Coordinates of these trajectories exported to excel and plotted (iii).*

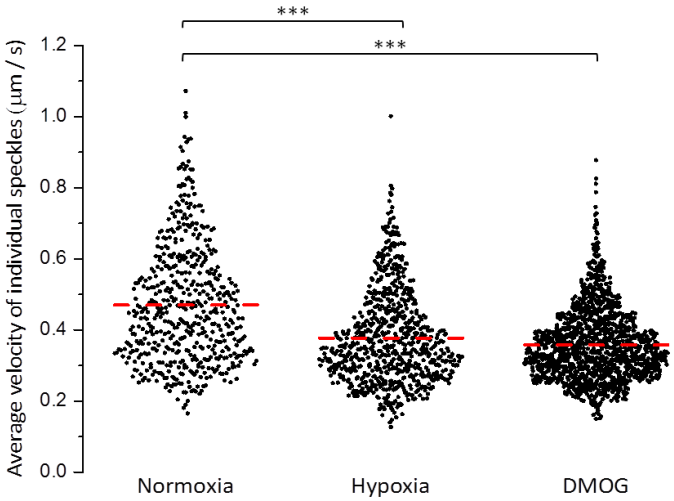

Figure 4.4 | Speed of individual HIF-2α speckles. *Speed at which HIF-2α speckles move. Average (±SD) for normoxia = 0.47 ± 0.17 μm s-1 (N=25, n=522), hypoxia = 0.38 ± 0.13 μm s-1 (N=24, n=760) and DMOG = 0.36 ± 0.10 μm s-1 (N=25, n=1402). Independent t-test, significance level 1%; normoxia compared to hypoxia: t1280=11.238, p<0.001; normoxia compared to DMOG: t1922=17.954, p<0.001.*

The average speed of the speckles was faster in normoxia compared to hypoxia and DMOG, dropping from 0.47 µm s^{-1} to around 0.37 µm s^{-1}. To provide further insight in to the motion of the HIF-2α speckles, the SMSS value was determined for each trajectory (see methods). This value describes the type of movement exhibited by an object (Figure 4.5). For instance a value of 0 indicates that the object is static, 0.5 indicates Brownian diffusion (the movement of molecules in a suspension caused by random collisions with other molecules) and 1 is indicative of ballistic motion (the object moves in a perfectly straight line). The intermediate types of diffusion are "restricted Brownian" (same as Brownian motion, but the objects movement is restricted within an area) and "directed Brownian" (diffusion is random but has overall directionality e.g. molecular motors transporting vesicles or organelles along the cytoskeleton) (Figure 4.5).

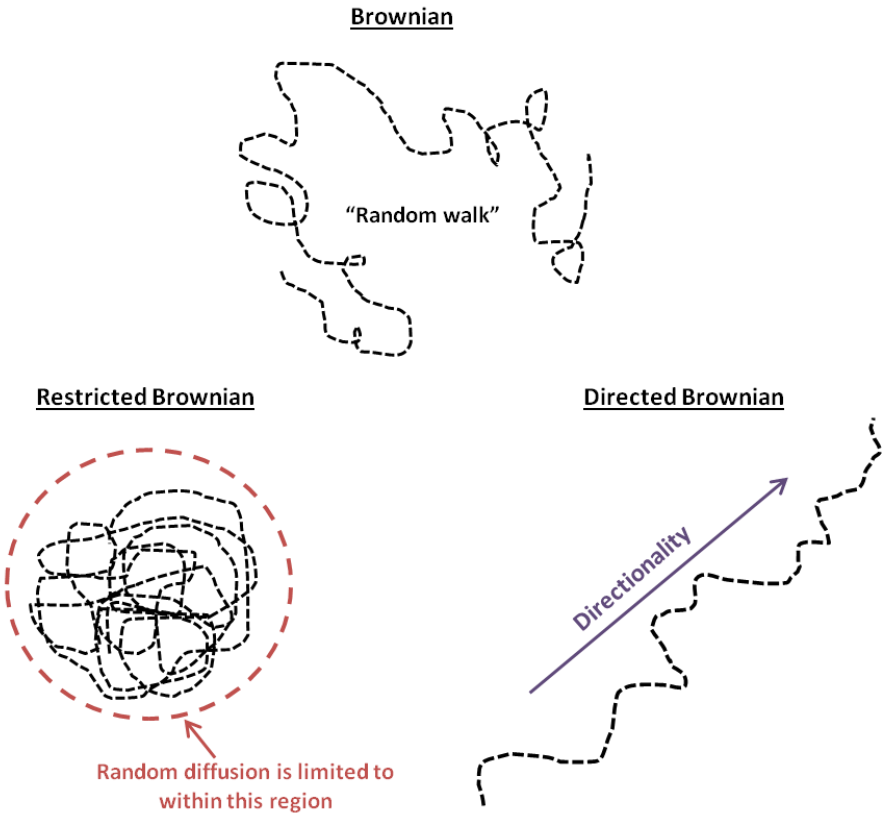

Figure 4.5. Schematic representation of the different types of diffusion. *Brownian diffusion = random movement of an object in solution in any direction (x, y and z). Restricted Brownian = random movement confined to a specific region. Directed Brownian = random diffusion with gradual movement in a certain direction.*

Figure 4.6A shows the SMSS values of individual trajectories of speckles across the three conditions tested. The arbitrary SMSS value ranges attributed to each type of diffusion are depicted on the graph. There was no significant difference between the three conditions, with the average SMSS values being 0.12-0.13. Although the average indicates restricted Brownian motion there are also speckles that do not move. Figure 4.6B highlights that 63% of the speckles fall into the restricted Brownian category, with the remainder being static. The proportion of speckles within each type of diffusion category does not change with oxygen levels or following the inhibition of prolyl hydroxylase enzymes.

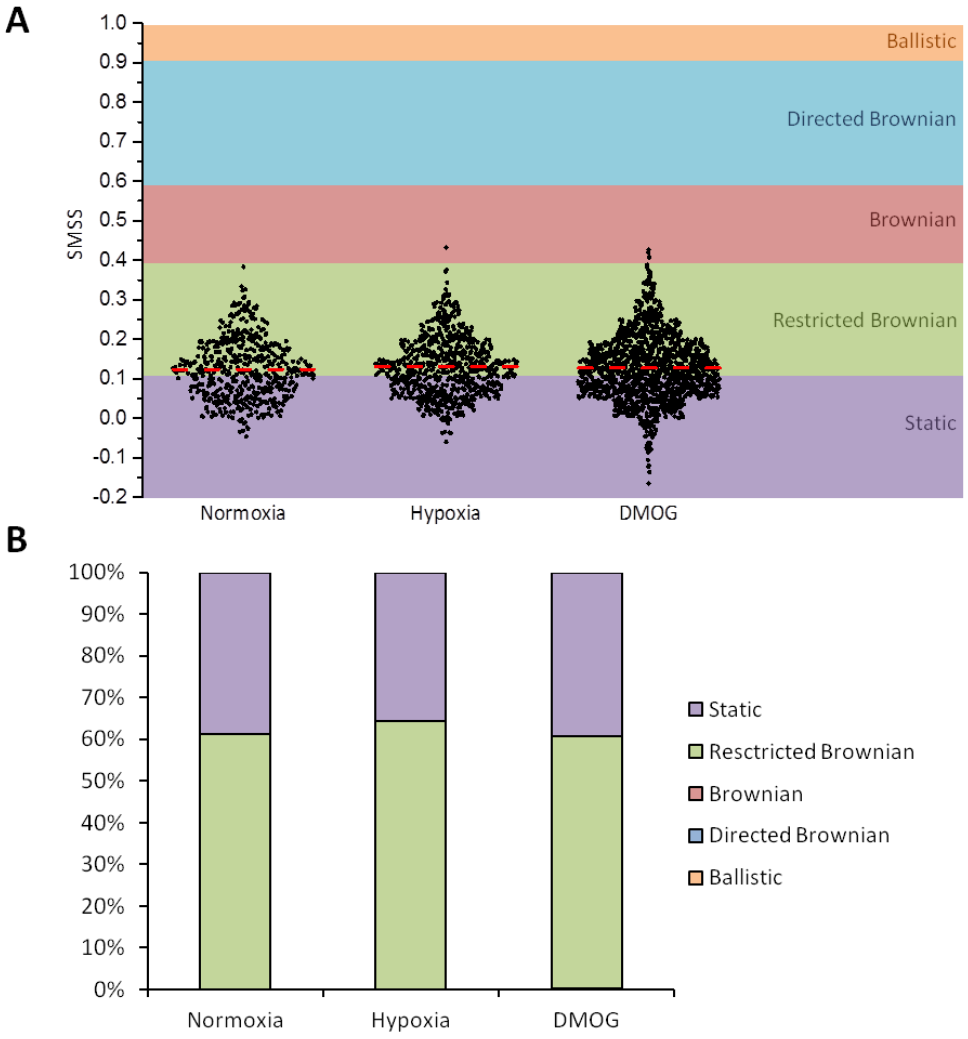

Figure 4.6 | Diffusion mode of the HIF-2α speckles. *A) Schematic representations of the types of diffusion. SMSS values for individual speckles in normoxia, hypoxia and DMOG. Average SMSS (indicated by red line) was 0.12 ± 0.07 (N=25, n=522), 0.13 ± 0.07 (N=24, n=760) and 0.12 ± 0.08 (N=22, n=1402), respectively. B) Percentage of speckles that fall into each category of diffusion. Average: static = 38%, restricted Brownian = 62%.*

These results suggest that these speckles are physically hindered from diffusing out of a localised region. It is likely that they are trapped or, like other nuclear bodies (e.g. Hendzel *et al.* 2001), tethered to a physical structure (such as the nuclear scaffold).

4.1.3 Protein co-localisation

Immunofluorescence imaging and co-localisation analysis were performed to investigate the spatial relationship between HIF-2α and other proteins (Figure 4.7). To provide a benchmark, we measured HIF-2α co-localisation with its known binding partner HIF-1β, in normoxia and upon DMOG treatment. Quantification using a Manders' analysis (Manders *et al.*, 1993) revealed that 33% (standard deviation reported in Figure 4.7B) of HIF-2α co-localises with HIF-1β in normoxia which increases to 47% following treatment with DMOG (Figure 4.7; statistically significant; independent t-test; t_{95}=13.362, p<0.001). As HIF-2α is a transcription factor it was logical to then investigate whether HIF-2α is localising at sites of active transcription. Immunofluorescence was performed using an antibody against phospho(ser5)-RNAPII as a marker for active transcription sites and we found that around 48% of HIF-2α co-localises with the initiating form of RNAPII in normoxia and 54% in hypoxia mimic condition, a marginal yet statistically significant (independent t-test; t_{60}=4.242, p<0.001) increase.

Both of these results make sense given that treatment with DMOG should increase activity of HIF-2α by inhibiting all PHD enzymes and FIH. They indicate that half of the signal from HIF-2α co-localises with its dimerisation partner HIF-1β in hypoxia mimic conditions (DMOG) and that the same level also co-localises with active transcription sites. However, this type of co-localisation analysis is based on whether both red and green signal is present in the same pixel. It could be worth performing object-based co-localisation analysis to determine if the number of speckles that are co-localising changes. It may also be of interest to look at HIF-1β, HIF-2α and RNAPII simultaneously.

A

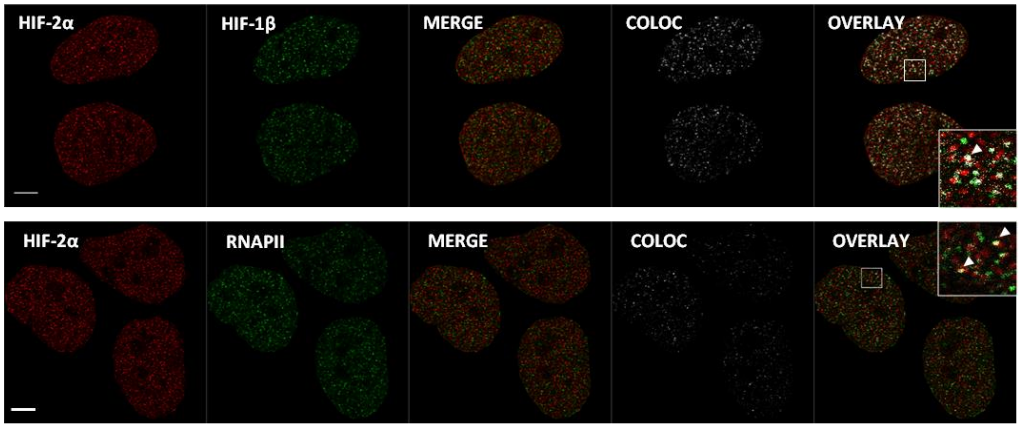

B

Protein B	n	% HIF-2α coloc with protein B		% protein B coloc with HIF-2α	
		Mean	SD	Mean	SD
HIF-1β (normoxia)	52	32.8%	5.8%	44.9%	6.7%
HIF-1β (DMOG)	45	47.3%	4.8%	53.3%	4.4%
RNAPII-pSer5 (normoxia)	26	47.5%	5.0%	52.9%	5.3%
RNAPII-pSer5 (DMOG)	36	54.1%	6.7%	55.5%	4.6%

Figure 4.7 | Co-localisation of HIF-2α.with HIF-1β and RNAPII *A) First image in each panel (far left) is endogenous HIF-2α labelled with Alexa Fluor® 555 (red, psuedocolour). Second image (green, pseudocolour) is a nuclear protein labelled with Alexa Fluor-488®. Merge = HIF-2α (red) image superimposed onto the image (green) of the adjacent nuclear protein. Coloc = co-localisation channel calculated using ImageJ plugin Co-localisation Threshold. White indicates pixels where both red and green signal is found i.e. co-localisation. Overlay = Merge image with coloc image superimposed. Inlay = magnified region (white square). White arrows highlight regions of co-localisation. Scale bar = 5 µm. Abbreviations: RNAPII = RNA Polymerase II phosphor serine 5. B) Immunofluorescent images were analysed using ImageJ plugin Co-localisation Threshold with uses the Coste et al method to automatically create a threshold prior to calculating the Manders coefficient for both proteins i.e. the percentage of protein A (HIF-2α) that co-localised with protein B (HIF-1β or RNAPII) and vice versa.*

4.1.3.1 Other nuclear bodies

We then looked at whether HIF-2α co-localised with other nuclear proteins that are known to localise into nuclear bodies e.g. PML bodies. Previous studies have shown that transcription factors, such as p53 and NRF2, localise into PML bodies leading to the suggestion that one function of this nuclear body is the storage of inactive TFs (Fogal *et al.*,

2000;Ben-Dor *et al.*, 2005). However, immunofluorescent labelling of HIF-2α in HeLa cells stably transfected with PML-YFP show very little co-localisation (Figure 4.8A, top row). In the first instance this is not too surprising as PML bodies have been described as typically 0.5 μm in size and usually 10-30 per cell (Spector, 2001) which does not match the characteristics of the HIF-2α speckles. However, as HIF-2α is mainly inactive in normoxia one would think that more than 18% (Figure 4.8B) would be localised at PML bodies in normoxia, if they are in fact the storage site of inactive transcription factors.

Other well-studied nuclear bodies are SC35 domains also known as splicing factor compartments (SFCs) or interchromatin granule clusters (IGC), which house inactive splicing factors, such as SC35. (Wansink *et al.*, 1993;Phair & Misteli, 2000). It was found that only 13% of HIF-2α co-localised with SC35, but 48% of SC35 co-localised with HIF-2α. The biological relevance of this is unclear. If SFCs store inactive splicing factors that move to the site of transcription when required, it would be logical to assume that, in the interest of efficiency, these sites would be within close proximity to these sites. Therefore if the HIF-2a speckles are also near to transcription sites then there is an increase chance of them occurring in similar locations. Then again, it could be down to the simple fact that there is a vast number of HIF-2α and the SFCs take up a large volume, therefore there is an increased chance of the two entities occurring next to each other.

HDAC5 is a histone deacteylase and localises in to domains that have been termed matrix associated deacetylase bodies (Downes *et al.*, 2000). Images of this protein published in Downes *et al.* (2000) show a sub-nuclear localisation pattern very similar to that of HIF-2α (Figure 4.8A, third row down). We found that 27% of HDAC5-YFP co-localised with HIF-2α and 19% of HIF-2α co-localises with HDAC5-YFP (Figure 4.8B).

Finally, we investigated the localisation of hypoxia associated factor (HAF aka $SART1_{800}$). This protein has been demonstrated to interact with HIF-2α (Koh *et al.*, 2011). However immunofluorescent imaging found that only 16% of endogenous HAF co-localises with HIF-2α and 12.5% of HIF-2α co-localises with HAF (Figure 4.8B).

A

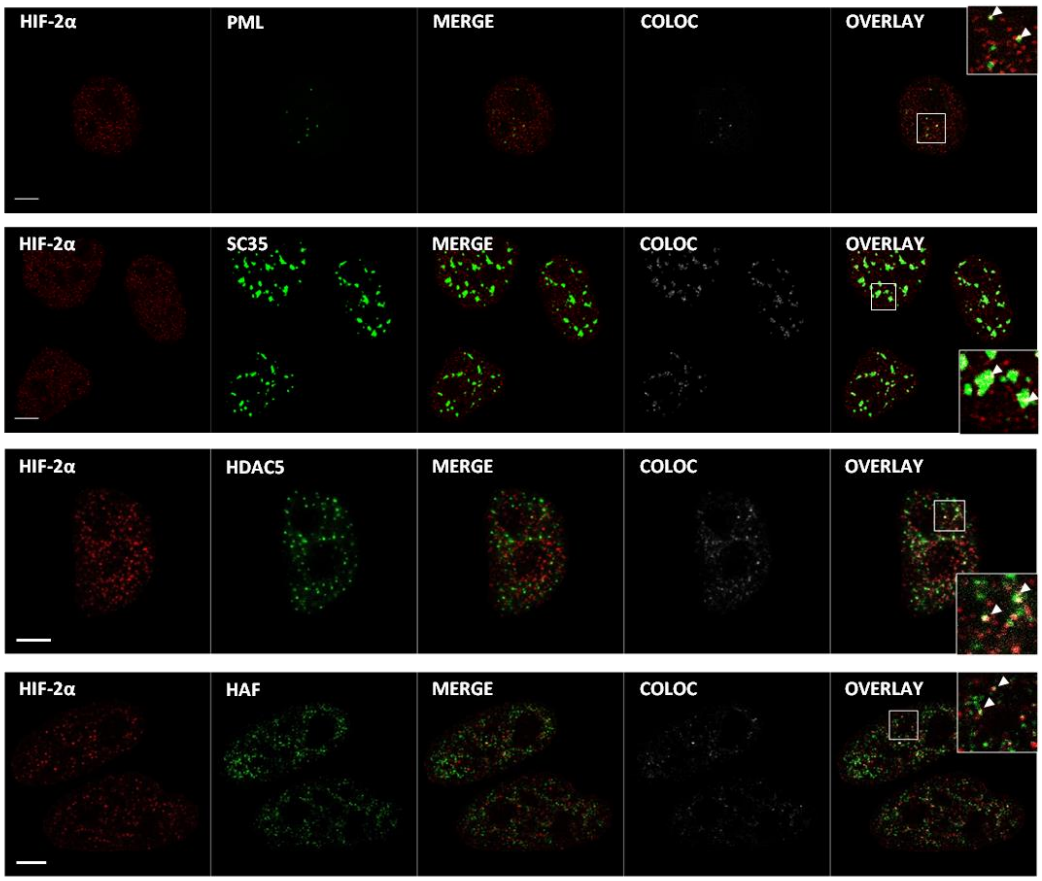

B

Protein B	n	% HIF-2α coloc with protein B		% protein B coloc with HIF-2α	
		Mean	SD	Mean	SD
PML	14	18.99%	3.73%	9.07%	4.54%
SC35	38	13.12%	4.60%	47.67%	10.37%
HDAC5	13	19.42%	5.63%	27.11%	7.48%
HAF	22	12.52%	3.65%	16.22%	3.70%

Figure 4.8 | Co-localisation HIF-2α and other nuclear proteins. *A) Immunolfuorescenct images of HIF-2α and other nuclear proteins that are known to localise into nuclear bodies. First image in each panel (far left) is endogenous HIF-2α labelled with Alexa Fluor® 555 (red, psuedocolour). Second image (green, pseudocolour) is a nuclear protein labelled with Alexa Fluor-488® (SC35, HAF) or YFP (PML and HDAC5). Merge = HIF-2α (red) image superimposed onto the image (green) of the adjacent nuclear protein. Coloc = co-localisation channel calculated using ImageJ plugin Co-localisation Threshold. White indicates pixels where both red and green signal is found i.e. co-localisation. Overlay = Merge image with coloc image superimposed. Inlay = magnified region (white square). White arrows highlight regions of co-localisation. Scale bar = 5 µm. Abbreviations: PML = Promyelocytic leukemia protein, HDAC5 = histone deacetylase 5 , HAF = hypoxia associated factor, YFP = yellow fluorescent protein.B) Immunofluorescent images (Figure 4.7) were analysed using ImageJ plugin Coloc Threshold with uses the Coste et al method to automatically create a threshold prior to calculating the Manders coefficient for both proteins i.e. the percentage of protein A (HIF-2α) that co-localised with protein B (other nuclear protein of interest) and vice versa.*

Overall, the results here indicate that a small proportion of HIF-2α co-localises with each of the nuclear proteins investigated. It is difficult to determine how significant these results are and whether they have any biological relevance. In some instances it is possible that the nuclear bodies are actually separate entities, but diffraction limited microscopy cannot resolve the two so it appears as if they cohabit the same location (such as PML and HIF-2α). Furthermore, we didn't determine what the majority of HIF-2α is co-localising with, if anything. It is possible that the HIF-2α speckles are a novel nuclear domain and / or that they are specific for HIF-2α (although most, if not all, nuclear speckles that have been described in the literature are cohabited by more than one protein).

Admittedly, only a small range of proteins were investigated here. However, randomly picking proteins that happen to localise into nuclear speckles and performing immunofluorescent staining is a costly and somewhat "needle in a haystack" approach, so we moved on to other methods that could provide information on the function of these speckles. For further co-localisation studies, a more targeted approach should be taken such as performing mass spectrometry on a pull down of HIF-2α or EGFP-HIF-2α. From the resulting list of proteins, suitable candidates (e.g. nuclear proteins reported to localise into speckles etc.) could be identified and then investigated using immunofluorescence.

4.1.4 Molecular Mobility

Next, we investigated the mobility of HIF-2α at the single molecule level. Molecular mobility could provide insight into the function of these speckles, for example no movement of molecules between speckles could indicate a storage or sequestration whereas molecule mobility between the speckles and the rest of the nucleus could indicate a release or a change in protein availability / activity such as being released from storage sites.

4.1.4.1 Nuclear proteins and FRAP

FRAP has been key in determining kinetic information (such as chromatin binding time) of over 50 transcription factors (TFs) (Mazza *et al.*, 2012). Interestingly, it has been found that TFs are highly dynamic and bind transiently to target binding sites within genes leading to an overhaul of the longstanding model that TFs form stable complexes (Hemmerich *et al.*, 2011;Mazza *et al.*, 2012).

FRAP has also been used to study the dynamics of RNAPII in the nucleus. Kimura *et al.* (2002) found that 75% is highly mobile and 25% is immobile, additionally they found that these two fraction correlate with inactive and actively transcribing RNAPII, respectively. These data back up the theory that active RNAPII is present at transcription factories (see chapter 1.5.1) whilst the inactive form is freely diffusing through the nucleoplasm.

Photobleaching has also been used to study PML bodies. PML and SP100, which co-localised at PML bodies, show no recovery following bleaching within the nucleoplasm or PML bodies themselves whereas CBP, that also localises to PML bodies under certain conditions, is highly mobile and was shown to move in and out of PML bodies rapidly (Boisvert *et al.*, 2001). Thus supporting the conclusion that PML and SP100 play a structural role in PML bodies but also highlighting that components of the same nuclear body can have different mobility, which can correlate with function.

4.1.4.2 Molecular mobility of HIF-2α

Firstly, FRAP experiments were performed on HeLa cells ectopically expressing EGFP-HIF-2α in normoxia, hypoxia and 6 h after treatment with 0.5 mM DMOG. This was achieved by bleaching half the nucleus and measuring the fluorescence levels in this region over time

(Figure 4.9). The fractional recovery curve of HIF-2α was determined and fitted using a one component exponential equation (see Methods). The mobile fraction (the amount of molecules freely diffusing) and half time (the time taken for the fluorescence in the bleached region to reach half the eventual recovery) of HIF-2α was extrapolated from the fitted curves (see Methods).

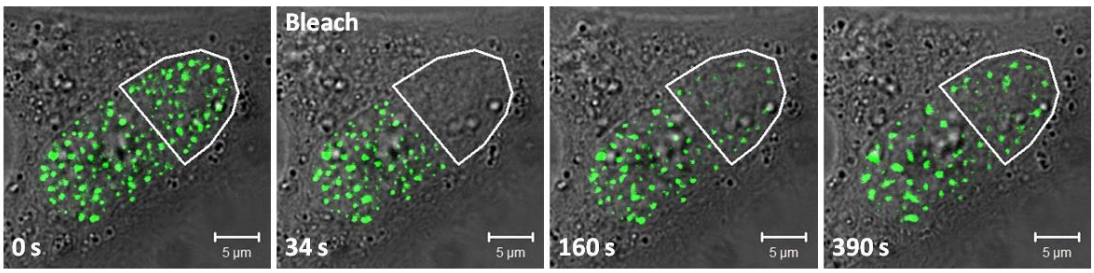

Figure 4.9 | EGFP-HIF-2α FRAP. *A series of confocal images of HeLa cell ectopically expressing EGFP-HIF-2α in the nucleus that has been photobleached. Images at different time points showing gradual recovery of fluorescence into the bleached region (outlined in white).*

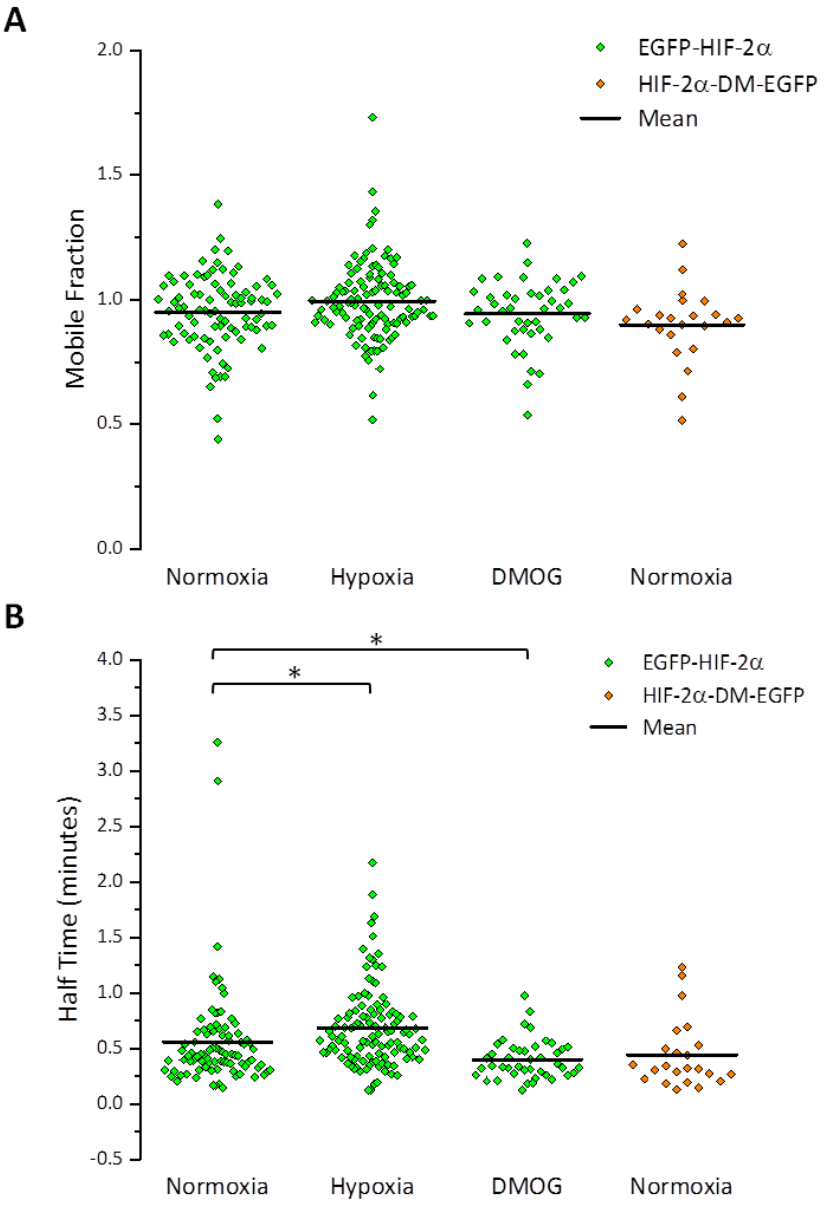

Figure 4.10 | Comparing EGFP-HIF-2α mobility in different conditions. *A) The percentage of mobile EGFP-HIF-2α molecules (mobile fraction) per nucleus. The average (± SD) mobile fraction of EGFP-HIf-2α was 0.95 ± 0.15 (n=89) in normoxia, 0.99 ± 0.16 (n=115) hypoxia and 0.94 ± 0.13 (n=43) following treatment with DMOG. For HIF-2α-DM-EGFP mobile fraction was 0.9 ± 0.15 (n=23). B) The time taken for recovery to reach half the final recovery (half time / t_{HALF}) per nucleus in normoxia, hypoxia and DMOG. The average (± SD) half time was 0.56 ± 0.46 (n=89) minutes, 0.68 ± 0.36 (n=115) minutes and 0.40 ± 0.18 (n=43) minutes, respectively. The half time for HIF-2α-DM-EGFP was 0.44 ± 0.31 (n=23) minutes Independent t-test (α=0.05) was used to compare the mean normoxic half time to those from the hypoxic (t_{202}=2.122, p=0.35) and hypoxia mimic (t_{130}=2.156, p=0.033) conditions. Average represented by black line on graph.*

It was found that the average mobile fraction across the three conditions was 96% (Figure 4.10A) suggesting that a significant amount of HIF-2α molecules are freely diffusing through the nucleus. The average half time was calculated to be 34, 41 and 24 seconds in normoxia, hypoxia and hypoxia mimic, respectively (Figure 4.10B). Although the results from the statistical test suggest that the average half times in hypoxia and DMOG for wild type HIF-2α are significantly higher than that for the normoxic sample, the actual values are only marginally different therefore are unlikely to have a great biological impact.

In line with the observation that hypoxia or DMOG has little effect on HIF-2α mobility, FRAP was performed on a constitutively stable HIF-2α (the two prolyl residues within the ODD domain have been substituted for alanines and so cannot undergo PHD-dependent degradation) and the mobile fraction and half time was found to be very similar to that of wild type HIF-2α treated with DMOG.

To confirm the observations made for wild type HIF-2α, a complimentary photo-perturbation technique, Fluorescence loss in photobleaching (FLIP), was used. In FLIP experiments the GFP positive cells are continually bleached in the same region and the fluorescent signal in the non-bleached region is measured (Figure 4.11A), therefore measuring the signal decay in the non-bleached region. This technique can be used to determine molecular mobility (like FRAP) but also provides information on the movement of molecules around and between cellular compartments (Mueller *et al.*, 2013). In the case of the HIF-2α speckles, continual bleaching in a specific region of the nucleus resulted in loss of fluorescent signal in the non-bleached region in all three conditions within 15 minutes (Figure 4.11B). The fluorescence loss data were plotted in Matlab and fitted using a one component exponential equation. The resulting curve was used to determine the half times of EGFP-HIF-2α (Figure 4.11C). Overall these results show no difference in the molecular mobility of EGFP-HIF-2α between the three conditions. However, it does highlight that HIF-2α must be continually moving in and out of the speckles (and throughout the nucleus) to have complete loss of fluorescent signal.

It is worth noting that, although not significantly different based on statistical testing, the half time values from the FRAP (Figure 4.10C) and FLIP (Figure 4.11B) experiments follow the same pattern across the three conditions. This could be of biological interest however further experiments would be required to confirm whether this is a coincidence.

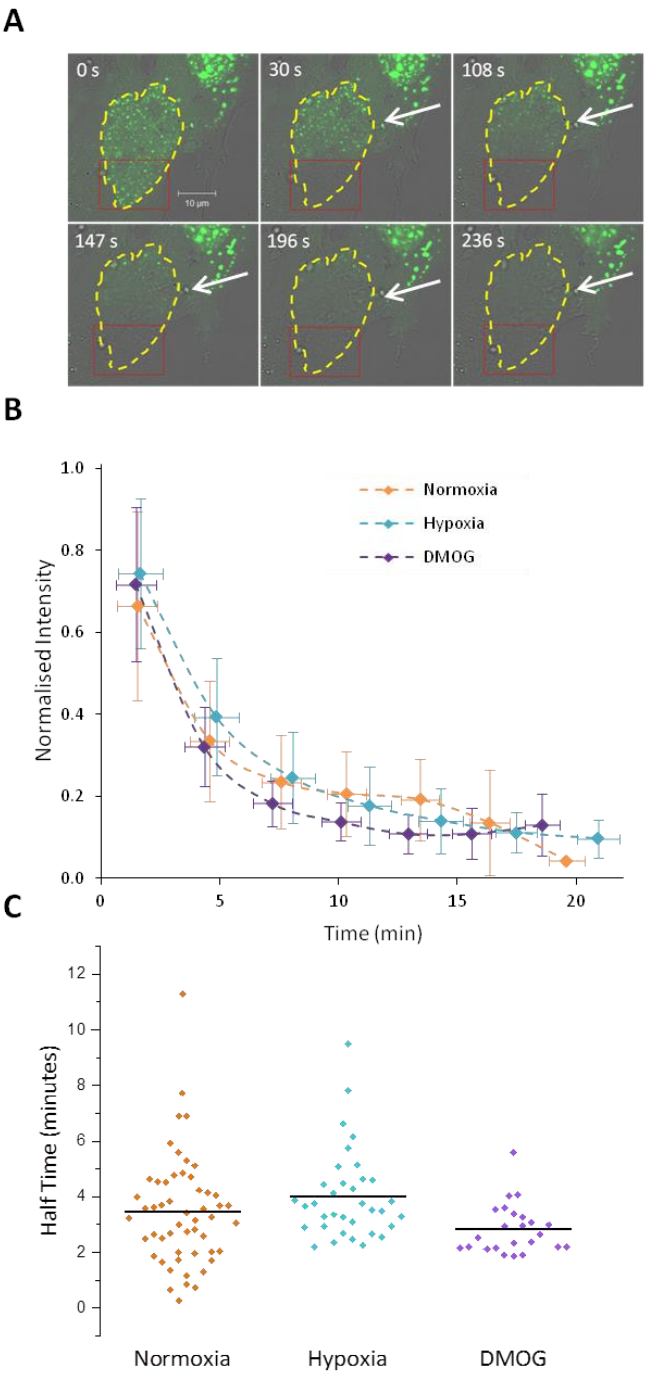

Figure 4.11 | Molecular mobility of HIF-2α measured using FLIP. *A) Confocal images of a HeLa cell ectopically expressing EGFP-HIF-2α that has been continually bleached in one region (red box). Nucleus outlined in yellow. White arrow highlights the loss of fluorescence in the non-bleached region of the nucleus. B) Overview of the average trend of fluorescence loss in normoxia, hypoxia and DMOG. Y-error bars represent standard deviation. The data was grouped ("binned") based on time and the X-error bars represent the standard deviation of these bins. C) Half time values were extrapolated from the curves fitted (as in B) for each cell in the three conditions. Average half time (represented by black line on graph) ± SD: Normoxia = 3.47 ± 1.98 (n=53), Hypoxia = 3.96 ± 1.61 (n = 36), DMOG = 2.88 ± 0.88 (n = 23).*

4.1.4.3 Molecular mobility of HIF-2α compared to HIF-1α

The molecular mobility of HIF-2α was compared to that of HIF-1α. FRAP experiments were only performed on HIF-1α-EGFP in hypoxia or following DMOG treatment, as there is no detectable fluorescent protein in normoxia (Bagnall, 2011).

It was found that the mobile fraction of HIF-1α-EGFP was 92% in both conditions (Figure 4.12A). This mobile fraction is significantly lower than that of EGFP-HIF-2α in hypoxia (99%, Figure 4.10A). This could be due to HIF-1α activating genes as part of the hypoxic response. It has been proposed that HIF-1α is the dominant transcription factor in the acute response to hypoxia whereas HIF-2α is responsible for regulation of genes in chronic hypoxia (>48 h). As FRAP looks at the whole population of molecules, if sufficient HIF-1α is bound at promoters then a global effect on the mobility could be observed. The difference is significant but small (7%).

Conversely, the difference in half time is much greater (Figure 4.12B). These measurements suggest that HIF-1α-EGFP is more than 10-fold and 5-fold faster than EGFP-HIF-2α in hypoxia and hypoxia mimic conditions, respectively. The rapid recovery of HIF-1α is typical of that seen with other transcription factors (Hager *et al.*, 2009). The slower recovery of mobility of HIF-2α is unusual but could simply be explained by the fact that it is in nuclear speckles which physically impedes its mobility whereas HIF-1α-EGFP is dispersed homogenously throughout the nucleus with only obstructions (such as chromatin) and molecular crowding to hinder its movement.

It should also be noted that although tests were performed in our lab to establish that the orientation of the GFP fusion protein (whether at the N- or C-terminus of the protein of interest) had little influence on the transcriptional activity of HIF-1α or HIF-2α (Bagnall, 2011) the mobility results could be affected by the fluorophore orientation; here the fluorophore is attached at different ends of the two proteins of interest. Wotzlaw *et al.* (2011) demonstrated using FRET that the orientation of the fluorescent tag can influence hetero-dimerisation of HIF-1α and HIF-1β, so there is a chance that the orientation of the fusion protein could also impact physical interactions of HIF-2α, which would in turn affect molecular mobility.

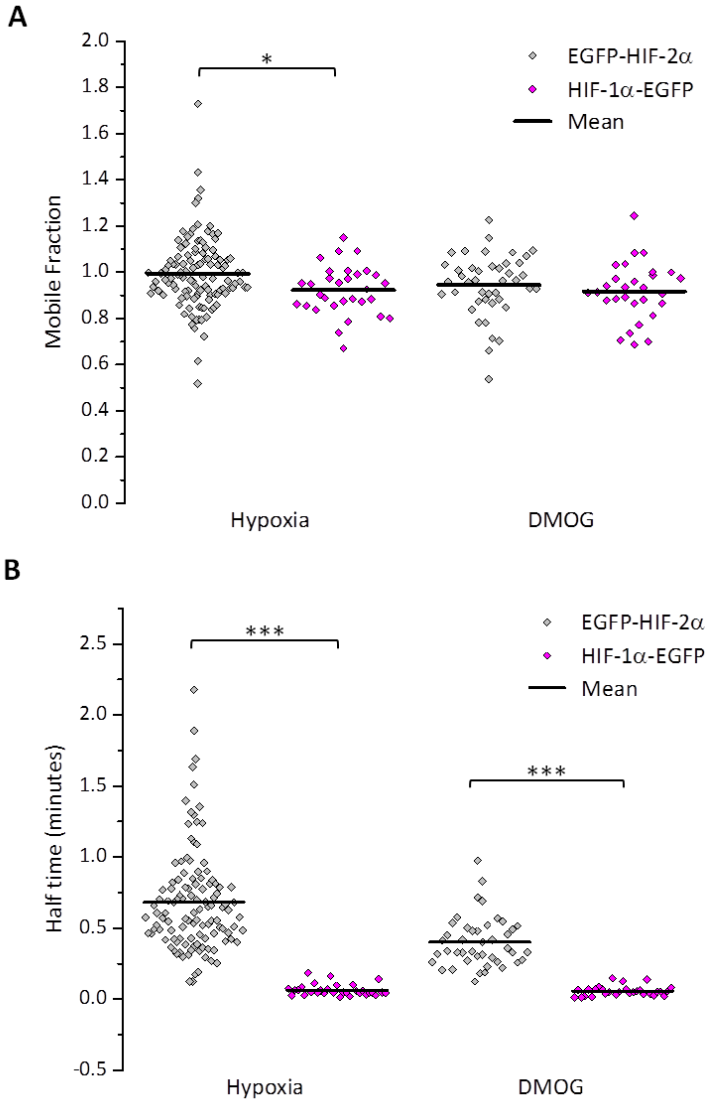

Figure 4.12 | Comparing EGFP-HIF-2α and HIF-1α-EGFP mobility. *The average (± SD) mobile fraction and half time for EGFP-HIF-2α are the same as in figure 4.9. Only hypoxia and DMOG conditions are compared as HIF-1α-EGFP can't be observed in normoxia and so can't be photobleached. A) Mobile fraction of EGFP-HIF-2α compared to HIF-1α-EGFP. The average (±SD) mobile fraction of HIF-1α-EGFP per nucleus was 0.92 ± 0.11 (n=31) hypoxia and 0.92 ± 0.12 (n=29) following treatment with DMOG (0.5 mM, 6 h). Independent t-test (α=0.05) revealed that the mobile fraction of HIF-1α-EGFP in hypoxia is significantly less than EGFP-HIF-2α (t_{144}=2.412, p=0.017). B) The half time of EGFP-HIf-2α compared to that of HIF-1α-EGFP in hypoxia and DMOG. The average (±SD) half time was 0.06 ± 0.04 (n=31) minutes and 0.06 ± 0.03 (n=29) minutes, respectively. In both hypoxic (independent t-test: t_{144}=9.532, p<0.001) and DMOG (independent t-test: t_{70}=10.278, p<0.001) conditions the half time of HIF-1α-EGFP was significantly less than EGFP-HIF-2α. Average values represented by black line on graph.*

For all FRAP experiments, a large variation in the shapes of the recovery curves was observed. This could be due to the inherent heterogeneity of protein expression often seen within a population of transfected cells. A clonal cell line stably expressing a fluorescently tagged HIF-2α or a tuneable expression system where the expression can be increased to desired level using a drug would remove this issue. In addition to this, a major drawback of photobleaching experiments is that only the photo-physical properties are altered via the photobleaching, meaning that the protein of interest is still present and presumed to be functional but can no longer be seen. Therefore, it would be beneficial to utilise photo-convertible proteins such as Dendra2. Here, instead of turning the fluorescent signal off by photobleaching, the signal is changed from green to red using a specific wavelength of light. Using a system such as this would result in the speckles and molecules remaining visible yet distinguishable from the non-converted molecules, therefore providing bi-directional data i.e. one can monitor molecules moving out of the photo bleached region as well as those moving in.

We have performed some spatial analysis on the FRAP experiments by tracking the speckles during bleaching and have observed some cases of recovery in the same place (Supplemental movies M5, M6 and M7), complementing the SMSS data and the possibility that these speckles might be tethered structures in specific locations. However, photo-convertible proteins would allow the switched speckles to remain visible during recovery, thus allow continued monitoring of speckle location and provide more conclusive evidence.

Finally, it would be worth comparing both N- and C-terminally tagged HIF-2α and HIF-1α to make sure that this does not have an influence on the molecular mobility.

4.2 Conclusion

Here we have shown that both endogenous and exogenous HIF-2α display heterogeneous distribution in the nucleus. We observed a small change in the number and movement of these speckles when comparing different conditions. Although statistically significant, the differences are marginal and the biological relevance of these results is difficult to determine. Photobleaching experiments revealed that HIF-2α is freely diffusing in and out of the speckles and throughout the nucleoplasm. Finally, there is some indication that these could be domains that are associated with or 'tethered' to a structure such as the nuclear matrix. ascertain

Hendzel *et al.* (2001) proposed that there are "transcription factor-enriched foci" within the nucleus that act to: concentrate functionally-related proteins in order to streamline assembly of macro-molecular complexes; and, control the concentration of the proteins / complexes in the nucleoplasm. One thought was that the HIF-2α speckles could have a purpose similar to the latter. Stemming from the fact that both endogenous and ectopically expressed HIF-2α is detectable in normoxia (HIF-1α is not), we hypothesised that perhaps HIF-1α is regulated in an oxygen-dependent manner via protein stability (as widely accepted) but HIF-2α is regulated spatially i.e. the alpha subunit accumulates in nuclear speckles and is physically impeded from activating genes in normoxia. However, this has proved somewhat difficult to verify.

In this study, we have shown that EGFP-HIF-2α is continuously moving in and out of speckles, regardless of oxygen levels or PHD enzyme activities. Therefore, it would seem unlikely that these speckles are storage sites, as one would expect a change in the mobile fraction as HIF-2α is released to find and bind to promoters of hypoxia inducible genes. However, it is possible that HIF-2α is localising at a number of sites that have different functions. CREB binding protein (CBP) has been shown to localise with p300 in small foci in the nucleus (Hendzel *et al.*, 2001) but also to transiently localise at PML bodies (Boisvert *et al.*, 2001). So, if one imagines that there are different sub-populations of HIF-2α e.g. some are activating genes, some are forming transcriptional complexes and some are being sequestered, then the results from the co-localisation study become more meaningful.

To probe the function of the HIF-2α speckles further, more advanced techniques such as single molecule tracking (SMT) should be employed which forms the basis of the following chapter.

Chapter 5: Development of tools for single molecule tracking in living cells

We have utilised advanced confocal microscopy techniques, FRAP and FLIP, to investigate the dynamics of HIF-2α and found no considerable changes in the molecular mobility under different conditions. However, these techniques look at the global behaviour of the protein being studied and the 'averaging effects' of these methods may be masking the dynamics of individual molecules. In addition to this we have not established the residence time of HIF-2α molecules in the speckles and whether this changes with oxygen potential. Therefore, the aim was to label HIF-2α with gold nanoparticles and image in the nucleus of living cells, using photothermal heterodyne imaging (PHI). This methodology facilitates the tracking of single gold nanoparticles (and, therefore, single molecules), as demonstrated by Duchesne *et al.* (2012). The single molecule data generated using this technique would provide information on: the movement of HIF-2α between speckles; movement in and out of the nucleus / speckles; and, provide information on velocity and degradation. All of which, could contribute to the elucidation of the function of the HIF-2α nuclear bodies.

As discussed in the introduction (Section 1.7.2.5), SMT can be performed using fluorescently probes such as dyes, proteins or semi-conductor nanocrystals (aka quantum dots), however, this approach has drawbacks. Firstly, probes such as fluorescent dyes and proteins photobleach and only short trajectories of ~10 s can be acquired, even with very careful illumination. Secondly, quantum dots emit a fluctuating and sporadic fluorescent signal. This temporary loss of signal causes issues when tracking molecules (Kuno *et al.*, 2001). Moreover, for optimum results, as much out of focus light as possible must be removed during acquisition, which has led to research groups using more specialist custom-built microscopes, such as those reviewed in Mueller *et al.* (2013) .

Gold nanoparticles are a useful and complementary alternative to fluorescent labels. They have several features that makes them ideal for SMT. Firstly, they are optically stable and do not suffer from the equivalent of photobleaching. Single nanoparticles can be imaged for as long as required (or as long as the stability of the microscope permits) without loss of any signal (Lasne *et al.*, 2006). Secondly, the photothermal signal from gold nanoparticles is continuous. Thirdly, the photothermal signal from gold nanoparticles has little or no background, except for a weak and distinguishable signal from mitochondria (Lasne *et al.*, 2007). Taken together, all these features make gold nanoparticles an ideal probe for single molecule tracking.

Gold nanoparticles also offer imaging versatility as they can also be visualised with an electron microscope, thus providing more information on sub-cellular localisation at molecular scale resolution. More importantly, however they can be specifically and stoichiometrically functionalised, as described in Duchesne *et al*. (2008), Duchesne *et al*. (2012) and Nieves *et al.* (2014). Briefly, gold nanoparticles require passivation *i.e.* the synthesis of a monolayer composed of small ligands (peptides, alkane thiol ethylene glycols with or without peptidols) on their surface that prevents non-specific binding (Lévy *et al.*, 2004;Duchesne *et al.*, 2008). The self-assembled ligand shell can also be functionalised by inserting other biological molecules, such as a nuclear localisation sequence (NLS) that will target the gold nanoparticles to the nucleus. Here the aim was to insert a ligand (Halotag ligand) that will allow the attachment of a protein of interest (POI) via the Halotag protein, facilitating the single molecule dynamics to be monitored by tracking the gold nanoparticles.

Single molecule imaging using gold nanoparticles has previously been successfully utilised in Liverpool to measure how fibroblast growth factor-2 (FGF2) moves through the extracellular matrix via its heparan sulphate binding sites (Duchesne *et al.*, 2012;Nieves *et al.*, 2015). Purified, recombinant HisTag-FGF2 was attached to gold nanoparticles via Tris-Ni^{2+}NTA. Although this method was able to provide useful insight into the single molecule dynamics of FGF2, the Tris-Ni^{2+}NTA on the surface of the gold nanoparticles can be prone to exchange with histadine patches on the surface of endogenous proteins, thereby disrupting the bond between the POI and the probe and so confounding single molecule tracking results. Therefore, the aim here was to utilise the Halotag® as a means to develop a novel method for covalent and stoichiometric (1:1) conjugation of proteins to the surface of a gold nanoparticles.

The Halotag® (Promega) is a modified haloalkane dehalogenase protein that has been designed to bind synthetic ligands that carry a chloroalkane (Los *et al.*, 2008). This reaction is highly specific, as there is no corresponding activity in mammalian cells, and irreversible, since a mutation (His272Phe) in the catalytic centre means that the reaction proceeds no further than the covalent intermediate of substrate-enzyme (Los *et al.*, 2008). The strategy was to incorporate the Halotag ligand (a chloroalkane ligand, see Appendix 1.5) onto the surface of the gold nanoparticle and react this with a Halotag fusion protein. Figure 5.1 gives an outline of the approach.

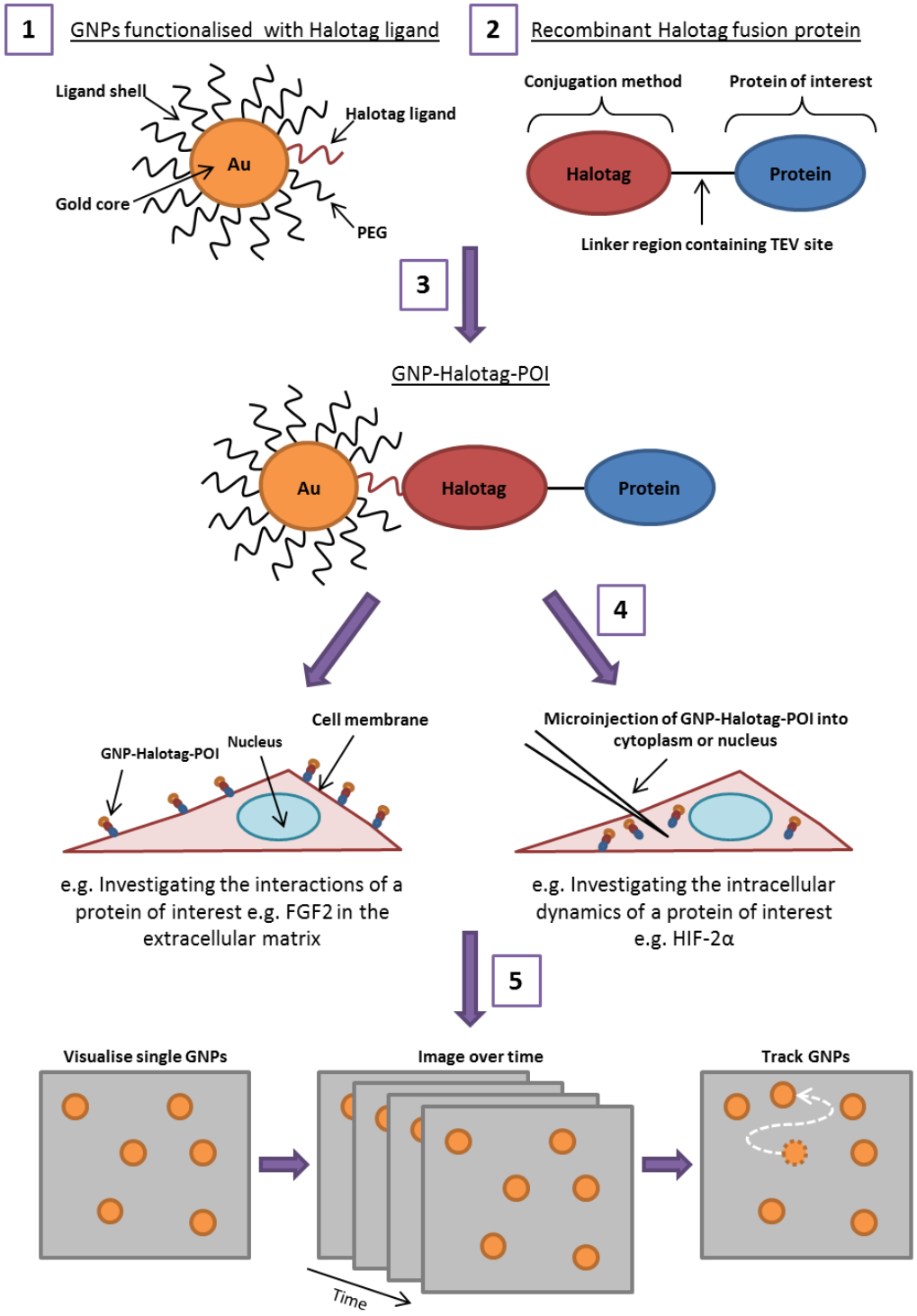

Figure 5.1 | Overview of GNP-Halotag plan. *Flow chart highlighting the key steps to tracking single molecules in living cells. 1) The aim is to incorporate the Halotag ligand into the ligand shell of gold nanoparticles (10 nm gold core) and 2) express and purify recombinant Halotag fusion protein. 3) The GNP-Halotag and Halotag fusion will react to form GNPs carrying the protein of interest (GNP-Halotag-POI). 4) The GNP-Halotag-POI will be delivered to the cells. For extracellular proteins such as FGF-2 (used for proof of principle experiments), the GNP-Halotag-FGF2 are added to the medium and bind to the surface of cells. For intracellular proteins such as HIF-2α, this requires delivery into the cells via microinjection. 5) The single GNPs are visualised and imaged over time using photothermal microscopy. Individual GNPs are tracked allowing the molecular dynamics of the proteins to be determined.*

The initial challenges were:

1) The synthesis of gold nanoparticles carrying the Halotag ligand

2) The conjugation of the gold nanoparticles to a protein of interest

3) The expression and purification of a full length recombinant HIF-2α

The work described in this chapter was a collaborative effort between me and members of both Prof. D. G. Fernig's and Dr R. Lévy's research groups (University of Liverpool, UK). The contributions by each individual were:

- Changye Sun
  - Together we expressed and purified Halotag-FGF2
  - Made the pET14B-Halotag-FGF2 construct
  - Provided advice and guidance on expression of Halotag-HIF-2α and contributed to troubleshooting
  - Contributed reagents
- Dr Umbreen Shaheen
  - Made GNPs carrying Halotag ligand for Halotag-FGF2 work
  - Guided me in making Halotag ligand GNPs for Halotag-HIF-2α work
- Dr Raphaël Lévy
  - Contributed reagents and equipment
  - Provided advice about gold nanoparticle synthesis and conjugation
- Prof Dave Fernig
  - Contributed reagents and equipment
  - Provided advice and guidance regarding protein expression and chromatography
- Dr Daniel Nieves
  - Performed photothermal imaging
  - Provided advice and guidance on protein purification and gold nanoparticle synthesis
- Dr Joanna Wnetrzak (CCI, University of Liverpool)
  - Performed microinjection

5.1 Can the Halotag be used for conjugation of a protein to a gold nanoparticle?

5.1.1 Testing the Halotag approach for labelling a protein of interest with gold nanoparticles

To investigate whether the Halotag can be used to conjugate a protein of interest to a gold nanoparticle, we employed an N-terminal Halotag-fibroblast growth factor 2 (FGF2) fusion protein. We chose to use FGF2 to carry out preliminary experiments, as our collaborator Prof. D. G. Fernig (University of Liverpool) and his research group have substantial experience in expressing and purifying recombinant FGFs (in particular FGF2). Since FGF2 is an extracellular protein that binds to components of the extracellular matrix such as heparan sulfate, obtaining biological validation is easier, as it does not require delivery into the cell. As a proof of principle, we would express and purify Halotag-FGF2, synthesise gold nanoparticles carrying the Halotag ligand and conduct experiments to test whether FGF2 can be labelled with gold-nanoparticles via the Halotag reaction. The work on the production of Halotag-FGF2 has been published (Sun *et al.*, 2015).

5.1.1.1 Expressing recombinant Halotag-FGF2

A bacterial expression vector, pET14B-Halotag-FGF2, encoding the Halotag fused to the N-terminus of full-length FGF2 via a linker region was made by Changye Sun (Prof. D. G. Fernig research group, University of Liverpool). Figure 5.2A illustrates the key characteristics of the Halotag-FGF2 fusion protein.

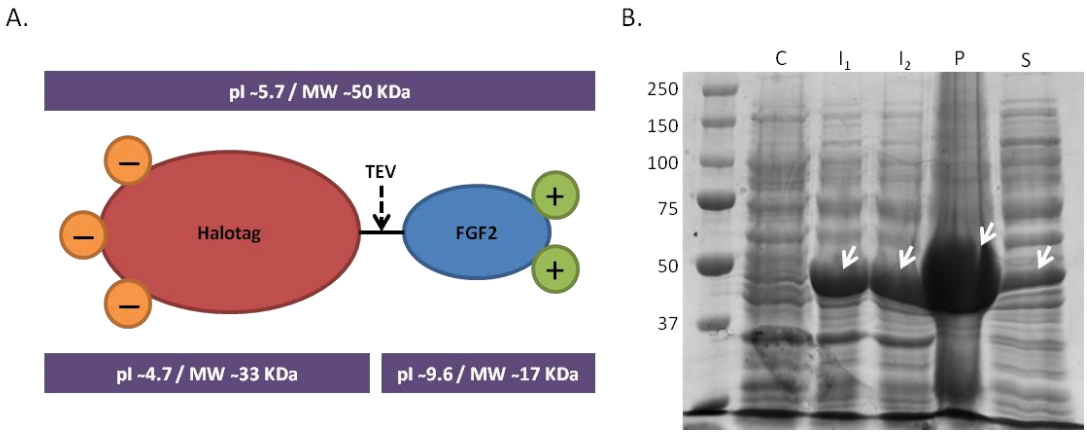

Figure 5.2 | Halotag-FGF2 recombinant protein. *A) Schematic diagram of Halotag-FGF2 recombinant protein expressed from the pET14B-Halotag-FGF2 construct. The Tobacco Etch Virus (TEV) protease cleavage site is highlighted. Calculated molecular weight and isoelectric point values are shown for the whole fusion protein and individual Halotag / FGF2 proteins. B) SDS-PAGE analysis of expression of recombinant Halotag-FGF2 expressed in C41 DE3 E. coli. One mM IPTG was added once cultures reached an OD_{600} of 0.6 and incubated for a further 4h at 37°C. The induced samples (I_1 & I_2) were combined, harvested by centrifugation and the resulting pellet lysed via sonication. To separate the insoluble (P) and soluble (S) proteins the sample was centrifuged at 8000 rpm, 30 min, 4 °C (Sorvall RC6+ Centrifuge; SS34 fixed angle rotor). (C = control, no IPTG added, I = induced protein expression, P = pellet / insoluble protein, S = supernatant / soluble protein). Arrows indicate the band corresponding to the expected size of HT-FGF2. First lane = Molecular weight marker, numbers represent kDa.*

Although Prof Fernig's group have worked with many recombinant FGFs, the addition of the Halotag can affect both the bacterial expression and purification of the recombinant protein. Cultures of C41 DE3 *E. coli,* a strain commonly used for expression of recombinant proteins, transformed with the Halotag-FGF2 construct were incubated for 4 h at 37 °C following the induction of protein expression (via the addition of IPTG) (Xu *et al.*, 2012). Analysis by SDS PAGE and coomassie staining showed a large induced band close to 50 kDa in both samples (Figure 5.2B, lanes labelled I) compared to the control culture (no IPTG added, lane C).

In order to determine the solubility of the expressed Halotag-FGF2, the bacteria (induced sample) were lysed via sonication. Following centrifugation, the soluble (supernatant) and insoluble (pellet) proteins were analysed by SDS PAGE. A band at 50 kDa was observed in both the pellet and supernatant suggesting that both soluble and insoluble Halotag-FGF2 is present (Figure 5.2B, lanes P and S, white arrows). Taking together the fact that the purification of soluble protein is a more straightforward process compared to that of insoluble proteins and that there was good expression of Halotag-FGF2 in the soluble fraction, the fusion protein was purified from the supernatant (Figure 5.2, lane S).

5.1.1.2 Optimisation of Halotag-FGF2 purification protocol

Purification of FGF2 utilises its affinity for heparin, so heparin affinity chromatography was employed for the initial purification of the Halotag-FGF2 fusion protein. Figure 5.3 shows preliminary chromatography of the soluble protein fraction. Analysis via SDS PAGE shows that a protein corresponding to the expected size of Halotag-FGF2 is present in each eluted fraction and that the contaminants are gradually removed resulting in a final eluate that was judged to be reasonably pure Halotag-FGF2 (Figure 5.3B, Blue Box).

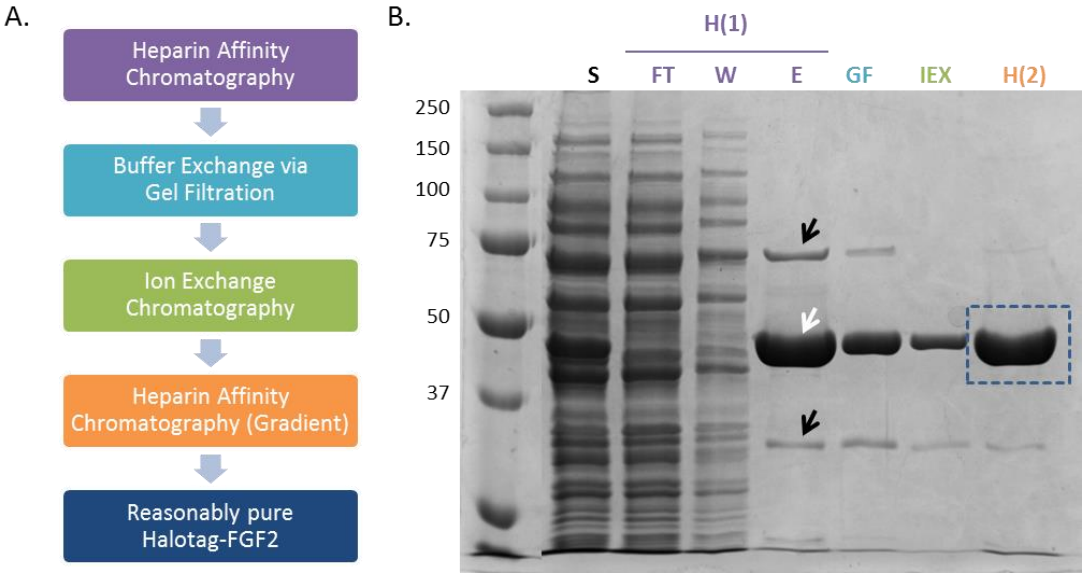

Figure 5.3 | Trial purification of Halotag-FGF2. *A) The steps taken to purify Halotag-FGF2. B) The soluble protein fraction was applied to Heparin Affinity Gel (BioRad, UK). The eluted protein underwent buffer exchange via gel filtration (G25) chromatography and then applied to a CM cation-exchange column (IEX). Finally, the eluate from IEX was applied to a second heparin affinity column and eluted with a gradient of NaCl (using a Biorad Econo pump (EP-1) fitted with UV monitor; set up as follows: 0-70%, 70 minutes. Buffer B = PBS set at 6%, Buffer A = 1.4M NaCl) 29 fractions were collected, fractions 5-29 contained with protein (eluted at approximately 34-68%) and were combined for analysis via SDS PAGE (H(2)). (S = soluble fraction, FT = flow through, W = wash with 0.5 M NaCl, E = fraction eluted with 1.4 M NaCl, GF = Sample following buffer exchange via gel filtration chromatography, IEX = Sample eluted from CM resin column with 0.4 M NaCl, white arrows =Halotag-FGF2, black arrows = contaminants, blue box = reasonably pure Halotag-FGF2)*

To investigate further the binding of Halotag-FGF2 and to determine which additional chromatography steps could be used and the sequence to use them in to further purify the fusion protein, small–scale purification was then performed on the Halotag-FGF2 (Figure 5.3B, blue box). Three chromatography methods: heparin affinity, cation-exchange (CM resin, negatively charged) and anion-exchange (DEAE resin, positively charged), were

tested. Each of these purification methods exploits a different feature of the recombinant protein, namely the binding affinity of FGF2 to heparin, the strong positive charge / very basic pI of FGF2 and, the negative charge / acidic pI of the Halotag. The chromatography was performed with Halotag-FGF2 and TEV-digested Halotag-FGF2.

Analysis via SDS PAGE shows that the Halotag-FGF2 bound to heparin, DEAE and CM resins (Figure 5.4) highlighting that all three methods can be used for purification of the fusion protein. The samples digested with TEV show that these results are due to FGF2 binding to the heparin and CM resin (Figure 5.4A and B, red arrows), and the Halotag binding to the DEAE resin (Figure 5.4C, yellow arrow), as predicted.

Based on these findings the Halotag-FGF2 was purified using all three chromatography steps in the following order: heparin affinity, anion-exchange and cation-exchange chromatography. Details of the final protocol can be found in Sun *et al.* (2015).

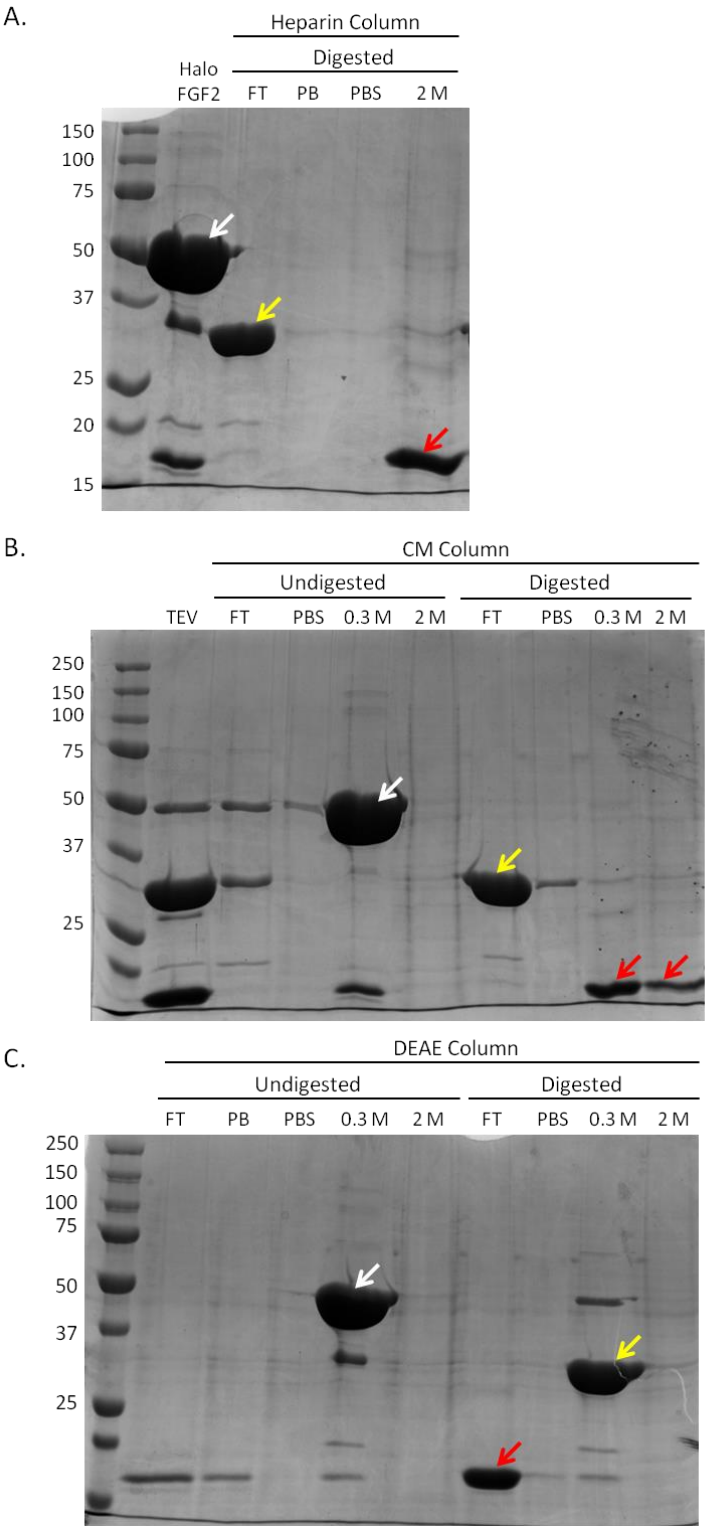

Figure 5.4 | Halotag-FGF2 purification tests. *Halotag-FGF2 was incubated with TEV protease overnight (digested) and applied to a heparin column (A). Digestion results in additional bands of approximately 30 kDa, 27 kDa and 18 kDa, which represent the Halotag, TEV enzyme and FGF2. Samples of undigested and digested Halotag-FGF2 samples were applied to a CM (B) resin column (FT = flow through, W = PBS wash, 0.3 M = 0.3 M NaCl wash, 2 M = 2 M NaCl wash) and DEAE (C) resin column (FT = flow through, W1=PB wash, W2 = PBS wash, 0.3 M = 0.3 M NaCl wash, 2 M = 2 M NaCl wash).*

5.1.1.3 Testing the functionality of purified Halotag-FGF2

Following purification, it was important to determine that both parts of the fusion protein were folded correctly and had retained their function. The fact that the protein bound to heparin and eluted similarly to native FGF2 indicated that the FGF2 possessed an intact primary heparin binding site. Since this is formed from amino acids that are physically adjacent in the tertiary structure, but distant in the protein sequence, it was likely that the FGF2 was correctly folded. Other data demonstrating that the HaloTag-FGF2 protein retains the same activity as the native FGF2 such as stimulating the phosphorylation of p42/44^{MAPK} are described in Sun *et al.* (2015).

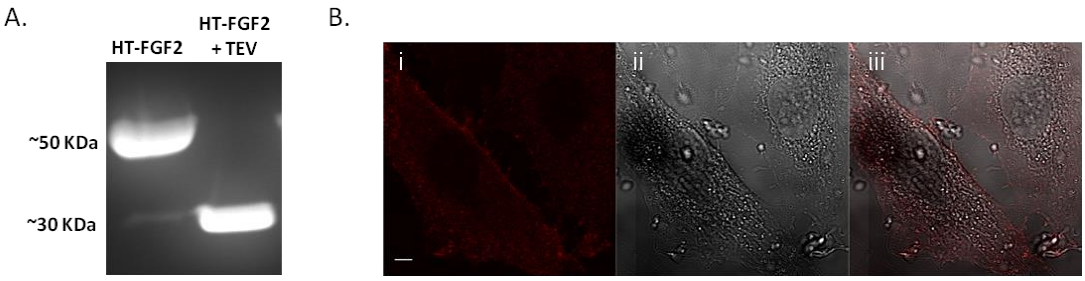

Figure 5.5 | Testing the activity of Halotag-FGF2. *A) Halotag-FGF2 and Halotag-FGF2 digested with TEV protease were labelled with Oregon Green fluorescent Halotag ligand and analysed via SDS PAGE. The fluorescently labelled protein was visualised with an ImageQuant LAS 4000 imager (Sybr green settings). B) 3 µM Halotag-FGF2 was labelled with the red fluorescent (TMR Halotag) ligand (7.5 µM) for 30 minutes at room temperature. The TMR-Halotag-FGF2 was added to Rama 27 fibroblasts (final concentration 2 nM), incubated at room temperature for 1 hour and imaged using a Zeiss LSM 710 confocal microscope. The images here were taken with C-apochromat 63×/1.20 Oil immersion objection, 2.1 zoom. Scale bar represents 10 µm.*

To determine whether the Halotag is functional, the Halotag-FGF2 and Halotag-FGF2 digested by TEV were labelled with a Halotag ligand conjugated to a fluorescent dye (Oregon Green). Figure 5.5A shows a fluorescent band at approximately 50 kDa in the undigested sample and a one at 30 kDa following digestion with TEV, which represent the Halotag-FGF2 and Halotag, respectively. This highlights that the Halotag is functional (*i.e.* can bind its ligand) when it is part of the Halotag-FGF2 fusion protein and after cleavage from FGF2.

As it was determined that both parts of the chimeric protein were functional, the Halotag-FGF2 was reacted with a Halotag ligand carrying a fluorescent dye (TMR) before labelling Rama 27 cells. Figure 5.5B shows that the TMR-Halotag-FGF2 associated with the surface of the cells. The lack of signal in the regions in between the cells highlights that the TMR-

Halotag-FGF2 has specially bound to the cells, likely through the binding of FGF2 to heparan sulfate present in the pericellular matrix.

Following the acquisition of these images, the cells were washed with 2M NaCl to see if the interactions between FGF2 and heparan sulfate could be disrupted. Images were acquired using the same settings and a reduction in TMR-Halotag-FGF2 signal was observed, further contributing to the suggestion that the labelling of the cells observed in Figure 5.5B is due to FGF2 binding heparan sulfate.

5.1.1.4 Labelling Halotag-FGF2 with gold nanoparticles via the Halotag ligand

Since it was shown that TMR-Halotag-FGF2 could bind to the pericellular matrix of cells, the next step was to substitute the fluorescent label with gold nanoparticles. Gold nanoparticles carrying Halotag ligands (chloroalkane, see Appendix) on the surface were prepared by Dr U. Shaheen (Raphaël Lévy group, University of Liverpool). Following conjugation, approximately 5 nM Halotag-FGF2 labelled with gold nanoparticles (GNP-Halotag-FGF2) was added to the medium of Rama 27 cells (Labelling protocol same as for TMR-Halotag-FGF2). Figure 5.6 (right panel) shows the cells clearly labelled with the gold nanoparticles. As a control, Rama 27 cells were also incubated with nanoparticles lacking Halotag-FGF2 and almost no photothermal signal was observed (Figure 5.6, left panel). These results strongly suggest that the Halotag can be utilised as method of conjugating a recombinant protein of interest to gold nanoparticles, thus providing a platform for single molecule imaging.

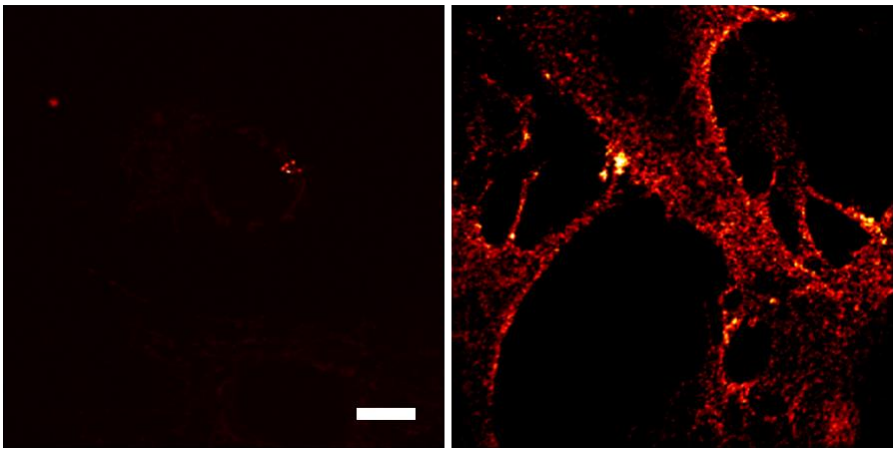

Figure 5.6 | Photothermal images of FGF2-Halotag-nanoparticles. *Photo thermal images of Rama 27 cells labelled with unconjugated nanoparticles (Control; left) or Halotag-FGF2 conjugated gold nanoparticles (GNP-Halotag-FGF2; right). The control GNPs or the Halotag-FGF2-GNPs were added to the medium and after 1 hour the cells were washed and imaged on a photothermal microscope (imaging carried out by Dr D. Nieves, Raphaël Lévy group, University of Liverpool, UK). Scale bar represents 10 µm.*

In this section, it has been shown that: Halotag-FGF2 can be expressed in C41 DE3 *E. coli* and purified using a three step chromatography protocol; both the FGF2 and Halotag parts of the purified protein are functional; and, FGF2 can be labelled via the Halotag with fluorescent dyes and most importantly GNPs. The work described here contributed to a paper entitled: "Halotag is an effective expression and solubilisation fusion partner for a range of fibroblast growth factors" (Sun *et al.*, 2015).

5.2 Expression & purification of Halotag-HIF-2α

The next step was to follow the strategy used for FGF2 with HIF-2α. By expressing and purifying Halotag-HIF-2α from *E.coli* it would then be possible to conjugate it to gold nanoparticles carrying the Halotag ligand.

A DNA vector (pFN21AB4384) containing the Halotag-HIF-2α gene was purchased from Kazusa DNA Research Institute, Japan. In order to check the spatial localisation of the Halotag-HIF-2α in cells, this plasmid was transiently transfected into HeLa cells and labelled with the Oregon-Green Halotag ligand (Promega, WI, USA). Figure 5.7A shows that the Halotag-HIF-2α fusion protein localises into discrete foci in the nucleus, as observed with fluorescent protein fusions and endogenous HIF-2α. Figure 5.7B shows analysis of protein extracts from HeLa cells transiently transfected with CMV-Halotag-HIF-2α via SDS PAGE and

western blot. The samples were labelled with the Oregon Green Halotag ligand prior to separation on SDS PAGE and fluorescent bands were observed at 150 kDa (Figure 5.7B, top panel). Following this, the proteins were transferred onto nitrocellulose membrane and probed with a HIF-2α antibody. Western blot revealed one band at around 100 kDa and another at 150 kDa, representing endogenous HIF-2α and the ectopically expressed Halotag-HIF-2α, respectively (Figure 5.7B, bottom panel). These data show that the Halotag-HIF-2α ectopically expressed in mammalian cells is 150 kDa, can react with the Halotag ligand and exhibits HIF-2α immuno-reactivity. Further to this, confocal microscopy confirmed that fluorescent labelled Halotag-HIF-2α and EGFP-HIF-2α co-localise. All of these results suggest that the Halotag is functional and does not interfere with the spatial localisation of HIF-2α.

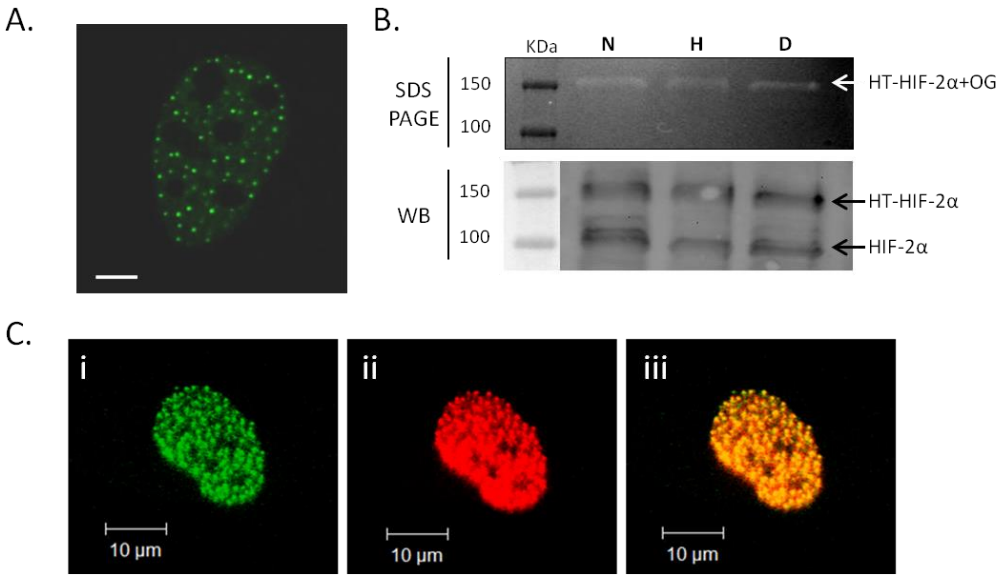

Figure 5.7 | Halotag-HIF-2α recombinant protein in HeLa cells. *A) Live HeLa cell transfected with the Halotag-HIF-2α plasmid and labelled with the fluorescent Oregon Green Halotag Ligand. Fluorescence is localised in nucleus in speckles. Scale bar = 5 µm. B) Protein extracted from HeLa cells transfected with pFN21A-Halotag-HIF-2α. Samples were labelled with the fluorescent Oregon Green Ligand and analysed via SDS PAGE. (N = normoxia, H = hypoxia, D = 0.5 mM DMOG). C) Confocal images of HeLa cells co-transfected with EGFP-HIF-2α and Halotag-HIF-2α and labelled with the TMR conjugated Halotag ligand.*

5.2.1 Expressing Halotag-HIF-2α in bacteria

pETM-11-Halotag-HIF-2α was transformed into three bacterial strains that are commonly used for protein expression: C41 DE3, BL21 DE3 and BL21.pLysS DE3. Figure 5.8 shows gels stained for total protein (left panel) and HIF-2α (western blot, anti-HIF-2α, right panel) for the three strains tested. Different protein expression conditions (variation in temperature and time post induction with IPTG) were trialled. The coomassie staining (Figure 5.8, left) shows no strong induction of protein expression in the cultures treated with 1 mM IPTG compared to the control cultures in all three bacterial strains. Immuno-reactivity was detected in some, but not all, of the induced samples across the three strains. Two bands very close in size are detected at approximately 150 kDa, the expected size for Halotag-HIF-2α, and some additional bands at lower molecular weights (Figure 5.8, right). The 29.8 °C, 16 h sample in the BL21 and BL21.pLysS *E.coli* showed very strong immuno-reactivity, yet this was not correlated with any signal obtained by coomassie staining, suggesting that there is little Halotag-HIF-2α protein present.

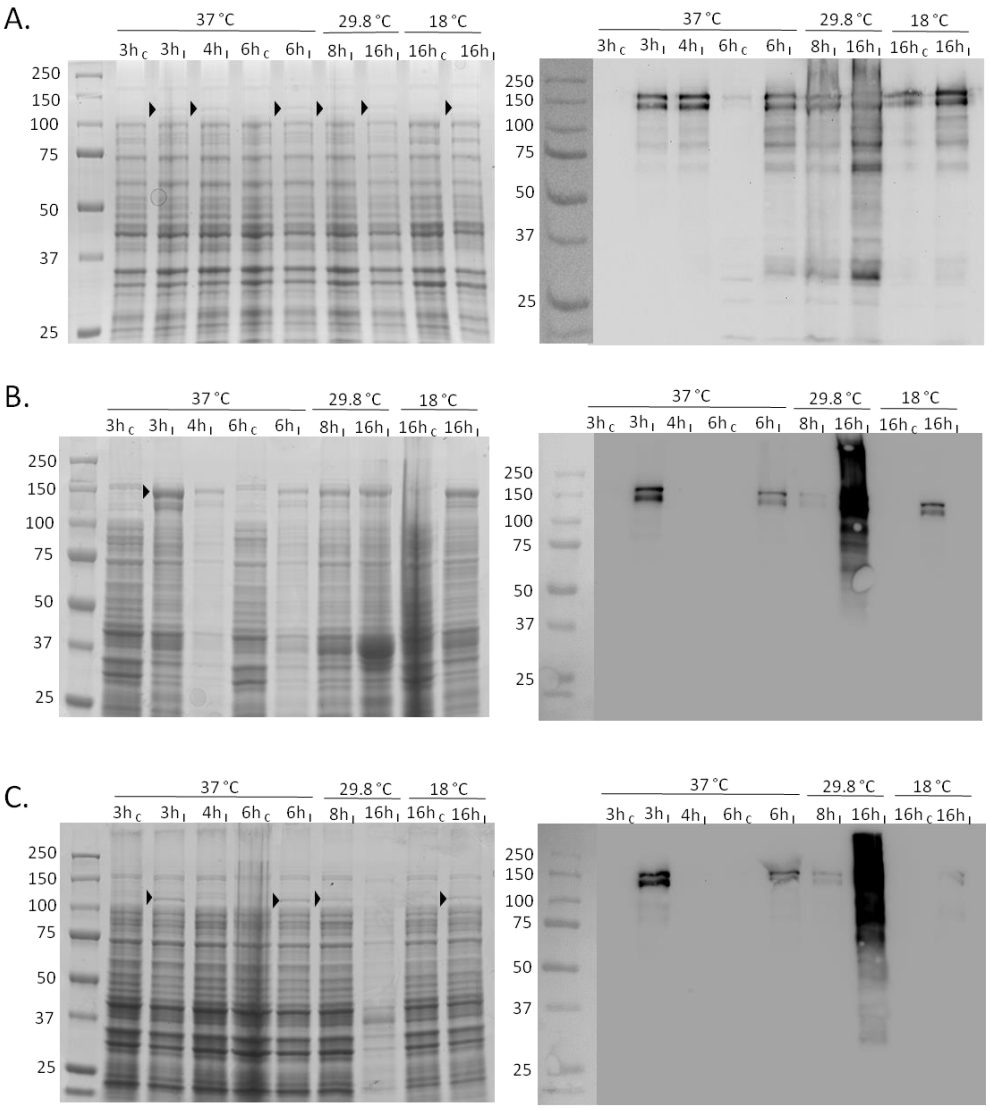

Figure 5.8 | HIS-Halotag-HIF-2α expression in bacteria. *HIS-Halotag-HIF2α recombinant protein expression in C41 DE3 (A), BL21 DE3 (B) and BL21.pLysS DE3 (C) under various conditions. Left coomassie, right western blot (anti-HIF-2α).*

A faint induced band could be seen at around 120 kDa (Figure 5.8, left, black arrows), which is slightly smaller than the expected size of Halotag-HIF-2α. However, analysis of bacteria transformed with different pETM11 constructs shows an induced band at around 120 kDa in all samples treated with IPTG, which suggests that this band corresponds to an endogenous protein (Figure 5.9).

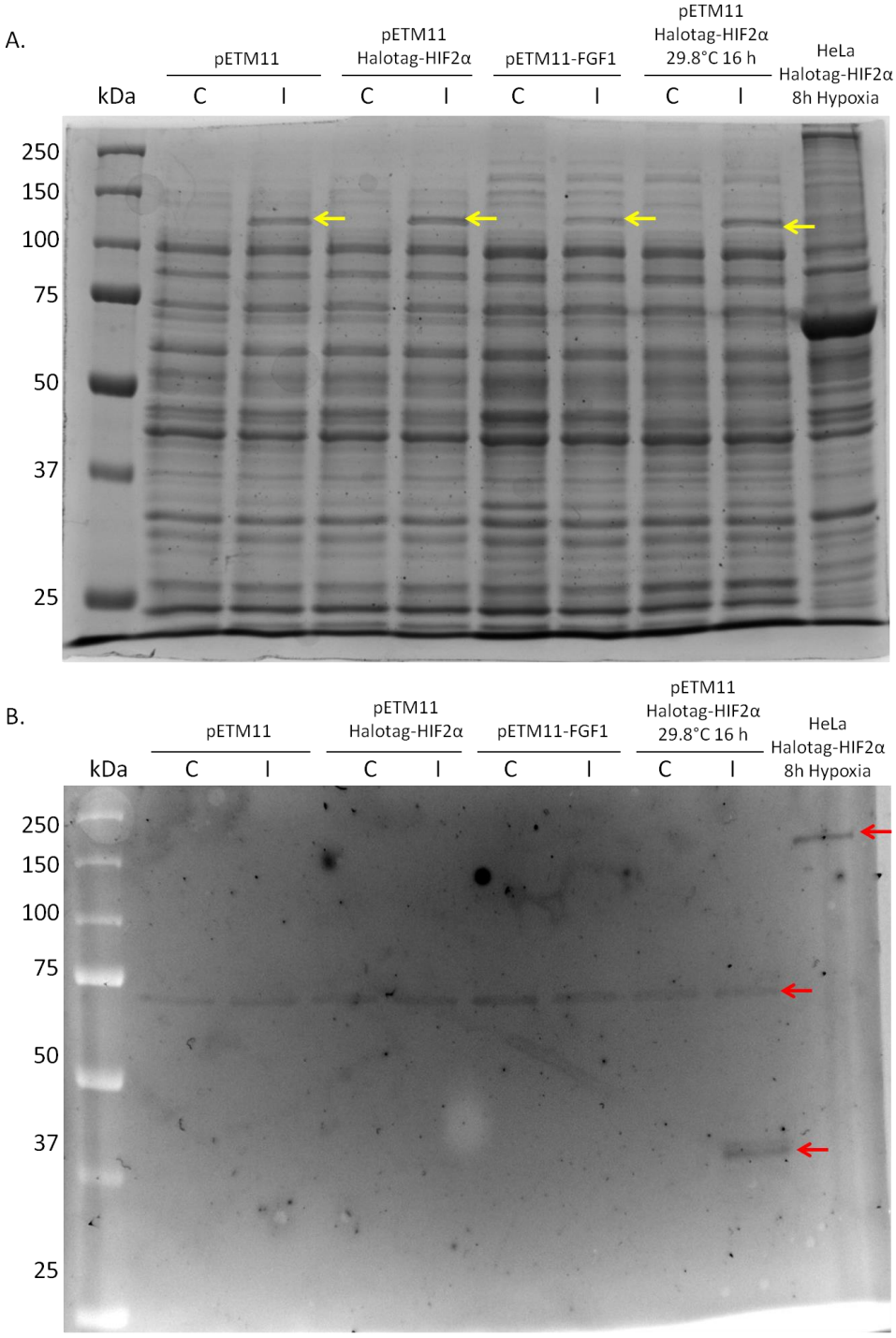

Figure 5.9 | Induction of protein expression from different pETM-11 constructs. *BL21.pLysS DE3 E.coli transformed with an empty pETM-11, pETM-11-Halotag-HIF-2α and pETM-11-FGF1 were incubated for 4 h at 37 °C, post induction of protein expressing via addition of IPTG. An additional condition of 16 h at 29.8 °C was included for Halotag-HIF-2α. A control sample of Hela cells ectopically expressing Halotag-HIF-2α was run alongside the samples. A) Coomassie Yellow arrows = induced protein. B) Fluorescent Oregon Green Halotag ligand. Image inverted to aid visualisation of the bands. Red arrows = proteins labelled with Halotag ligand.*

Although a band corresponding to recombinant Halotag-HIF-2α cannot be seen with coomassie staining, analysis via western blot with an anti-HIF-2α antibody highlights that there is potentially some Halotag-HIF-2α present, albeit in small amounts (Figure 5.10A & B). Samples from the soluble (supernatant) and insoluble (pellet) fractions of BL21.pLysS (37 °C, 4 h) were labelled with the fluorescent Oregon Green Halotag ligand and analysed by SDS PAGE (Figure 5.10C). The fluorescent bands on the gel suggest that there is protein present that reacts with the Halotag ligand, but none of these are the expected size of 150 kDa (Figure 5.10C). There is a strong band at around 40 kDa which is likely to be the Halotag (Figure 5.10C, Lane S, black arrow). In the insoluble fraction (lane P) there are multiple bands (Figure 5.10C, white arrowheads), suggesting either the expression of proteins of different sizes or protein degradation or incomplete transcription/translation. Either way, these results indicate that the Halotag is being expressed, but the HIF-2α part of the fusion protein is not complete.

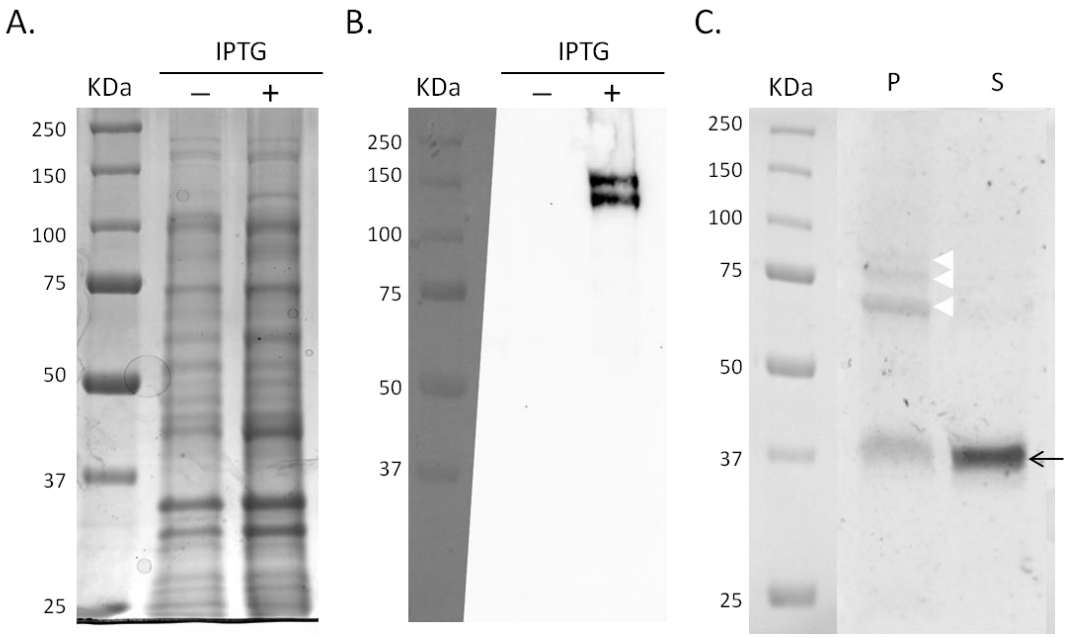

Figure 5.10 | BL21.pLysS DE3 E.coli expression and solubility test. *BL21.pLysS DE3 E.coli incubated at 37 °C for 3 h post IPTG addition (+). Control sample (-) = no IPTG added but incubated in the same conditions. A) Coomassie stained SDS Page. B) Protein was transferred to nitrocellulose membrane and probed with anti-HIF-2α antibody. C) The induced BL21.pLysS culture was sonicated and the soluble (supernatant) and insoluble (pellet) proteins were separated by centrifugation. Samples from the pellet (P) and the supernatant (S) were labelled with Oregon Green Halotag ligand and analysed via SDS PAGE. Black arrow = fluorescent bands likely to correspond to the Halotag. Image inverted to aid visualisation of the bands. White arrowheads = fluorescent bands likely to correspond to several truncated versions of Halotag-HIF-2α.*

In the three bacterial expression systems used here it appears that several things could be happening. Firstly, full length recombinant HT-HIF-2α is expressed at such low quantities that it can only be seen via western blot and although small amounts of protein could potentially be purified, for the envisaged application it would not be sufficient. Secondly, it is being degraded due to endogenous proteases. Or, truncated forms are being translated, possibly due to the high number of codons rarely used by *E. coli* in the coding region of HIF-2α.

5.2.1.1 Bacterial Expression System: Troubleshooting

To address some of the potential causes of the poor Halotag-HIF-2α protein expression discussed above we tried several other strains of *E. coli*.

E. coli have different preferences for codons compared to mammals (Zhang *et al.*, 1991). Many codons found in mammalian genes are rarely found in bacterial genomes hence the term 'rare codons'. Rosetta™ DE3, a strain of BL21 *E. coli* engineered for the expression of eukaryotic proteins containing a high proportion of rare codons (Merck Millipore, Germany), was tried. Figure 5.9A shows the total protein for induced (I) versus non-induced (C) for each condition, with an induced band at approximately 150 kDa. The sample grown at 37 °C following induction was further analysed. The bacteria were lysed, centrifuged and the proteins present in the pellet and supernatant separated via SDS PAGE. A band at around 150 kDa is present in both fractions, suggesting that there is both insoluble and soluble protein (Figure 5.11A, Lane P & S).

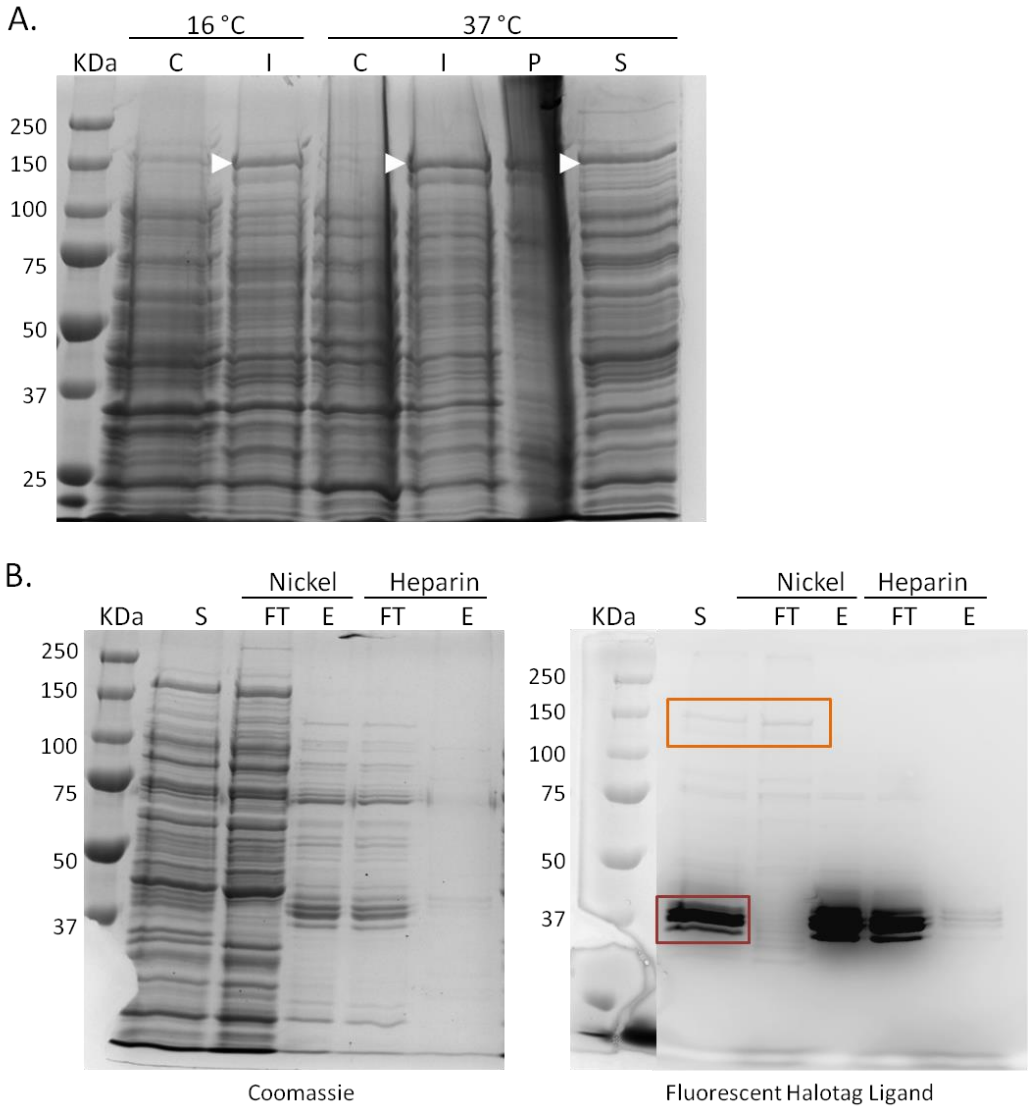

Figure 5.11 | HIS-Halotag-HIF-2α expression in Rosetta DE3 *E.coli.* *5 mL cultures of Rosetta DE3 transformed with the pETM-11-Halotag-HIF-2α vector were incubated for 18 h at 16 ℃ or 4 h at 37 ℃. A) Coomassie stained SDS PAGE. (C = control, I = induced protein expression with 1 mM IPTG, P = pellet / insoluble proteins, S = supernatent / soluble proteins). White arrowheads highlight induced protein observed at around 150 kDa. B) Trial purification was performed on a sample of the supernatant (S). A column was prepared with 0.6 mL ProBond™ nickel-chelating resin (Invitrogen, CA, USA), the resin was washed with 300 mM imidazole and sonication buffer prior to adding the sample. 3 mL of filtered supernatant was applied to the column and the flow through (FT) collected, any additional unbound protein was removed from the column with PBS washes and the bound fraction (E) eluted with 300 mM Imidazole. The eluted protein (E) was then applied to a column of heparin agarose (as described for Halotag-FGF2). Samples (20 µL) were labelled with 4 µL Oregon Green Halotag ligand (50 µM) and analysed by SDS PAGE. Left = coomassie, right = fluorescence SDS PAGE. Orange box = faint fluorescent band at around 150 kDa. Red box = several strong fluorescent bands around 40 kDa.*

Trial purification of the protein from lane S (Figure 5.11A) was performed. The bacterial expression plasmid, into which the Halotag-HIF-2α gene was cloned, resulted in the addition of a poly-histidine tag to the N-terminal end of the recombinant protein, allowing

it to bind to a nickel chelation resin. The supernatant was filtered and applied to a nickel chelation column. The eluted fraction (presumed to contain Halotag-HIF-2α) was then applied to a heparin column, due to the presence of a DNA binding domain HIF-2α should bind to this sulfated polysaccharide. The flow through (FT) and eluted (E) fractions were labelled with the fluorescent halotag ligands and analysis by SDS PAGE from which two observations can be made. Firstly, a 150 kDa protein (presumed to be Halotag-HIF-2α) was present in the supernatant and the flow through of the nickel column (Figure 5.11B, Orange box) indicating that this protein did not bind to the nickel resin, suggesting that either the Halotag-HIF-2α is missing the poly histidine tag or the tag is not exposed. Secondly, several fluorescently labelled proteins of varying sizes between 35 – 40 kDa (Figure 5.11B, red box) were observed in the supernatant. These bands were also present in the fraction eluted from the nickel column, but were in the flow through from the heparin column, indicating that these proteins were able to bind the Halotag ligand and to the nickel resin but not heparin, suggesting that these are truncated or partly degraded forms of the His-Halotag-HIF-2α protein where the His-tag and Halotag portion has remained intact and functional.

Even though there appears to be some protein that is of the predicted size that binds the Halotag-ligand, the amount of protein is very low. This is a problem, as during protein purification the yield of protein tends to diminish with increasing chromatography steps, therefore, it is best to start with a large amount of target protein. In this case, it is likely that the protein yield after protein purification would be far too low for the experiments planned.

Other bacterial strains, such as Lemo21, useful for difficult (e.g. toxic, membrane, insoluble) proteins and SoluBL21(DE3), were used. However, the yield of full-length Halotag-HIF-2α could not be improved.

5.2.1.2 Expression of Halotag-HIF-2α in *E.coli*: Conclusion

To conclude, the expression of recombinant Halotag-HIF-2α in bacteria did not yield sufficient protein for further purification and analysis. Possible reasons for this could be due to degradation by endogenous bacterial proteolytic enzymes. For instance, the full length recombinant protein could be expressed, but the protein is being degraded from the HIF-2α end, leaving the Halotag intact. However, this contradicts the fact that the bacteria used for protein expression tend to be engineered to have fewer endogenous proteases to prevent

this from happening. Another, (possibly more likely) scenario is that the bacteria are expressing truncated forms of the recombinant protein, i.e. the translation starts at the poly-histidine / Halotag end and proceeds unperturbed until the ribosome reaches the HIF-2α region where translation is stalled. Furthermore, it is likely that the induced band observed at around 120 kDa is a bacterial protein involved in transcription or translation, as this band is only present in cultures that have been induced with IPTG and is present regardless of the recombinant protein being expressed.

In the interest of time and due to exhausting a substantial number of routes for bacterial protein expression, it was decided to express Halotag-HIF-2α by other means.

5.2.2 Cell-free protein expression

A second approach for the expression of recombinant proteins was tested, the PureExpress *in vitro* system (NEB), was tested. This kit contains all the components (as purified recombinant his-tagged proteins) from bacteria that are required for protein expression, thus removing any chance of proteolysis. Although this system gives a lower yield than bacteria, it may produce sufficient amounts of full-length Halotag-HIF-2α for the present purpose.

Figure 5.12(1) shows a western blot of the products of the *in vitro* translation. There was immuno-reactivity to the HIF-2α antibody at around 150 kDa. However, the fluorescent Oregon Green Halotag ligand signal was detected at a range of sizes. To test whether this was non-specific binding due to using a high concentration of Halotag ligand, the reaction was re-run and samples were labelled with various concentrations of ligand ranging from 2 μM to 8 μM. All concentrations showed a similar band pattern (data not shown). These results suggest that the protein is being translated, but some products are truncated*, i.e*. the Halotag part is being translated and then the ribosome is stopping or falling off before reaching the end of the coding part of the mRNA, so full length HIF-2a is not produced. This could result in many truncated proteins that react with the Halotag ligand, but only a few that will exhibit immuno-reactivity against the HIF-2α antibody. This method of protein production was, therefore, also abandoned.

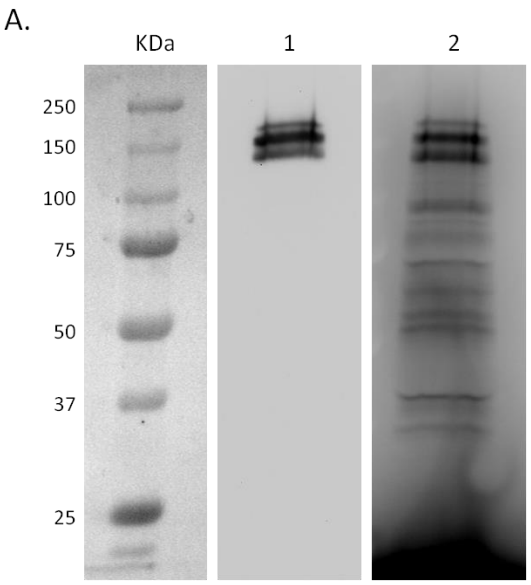

Figure 5.12 | PureExpress *in vitro* Protein Expression System (NEB). *in vitro expression analysed via western blot (1) and fluorescent SDS PAGE (2). The sample was labelled with 10 µM Oregon Green ligand.*

5.2.3 Mammalian expression system

As previously shown, the Halotag-HIF-2α can be expressed in mammalian cells (Figure 5.7). However, using mammalian cells for recombinant protein expression has drawbacks, such as it is more expensive, the yield of protein is much lower and purification is difficult due to the vast number of endogenous proteins present. Therefore, we chose to take a slightly different approach that does not involve purification of the protein via chromatography, which I have termed *in vitro* and *in vivo* conjugation (Figure 5.13). Briefly: the HL-GNPs would be added to the cell lysate of HEK293t ectopically expressing Halotag-HIF-2α (*in vitro* conjugation), following incubation to allow conjugation to occur the lysate would be centrifuged to "pull down" the GNP-labelled protein, which would then be microinjected into cells for imaging. Alternatively, live HeLa cells expressing Halotag-HIF-2α would be microinjected with HL-GNPs and imaged (*in vivo* conjugation).

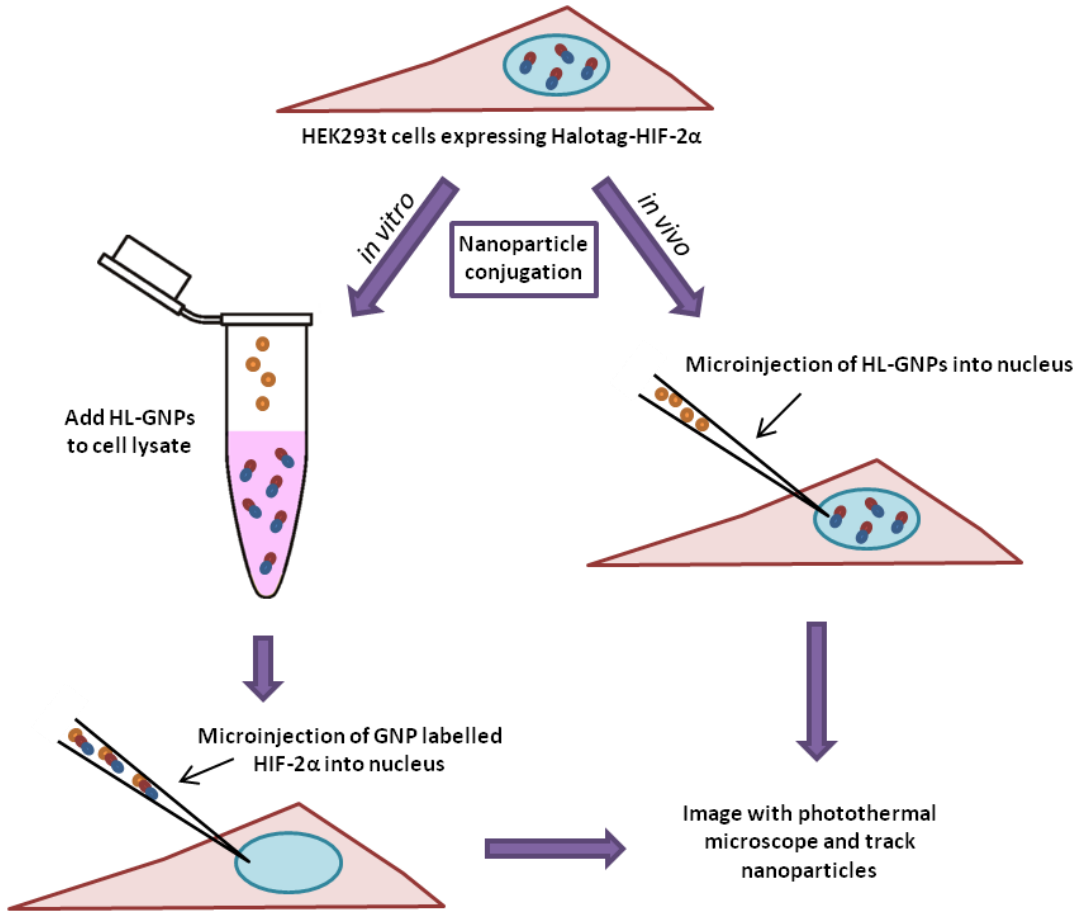

Figure 5.13 | Plan for conjugation of mammalian expressed Halotag-HIF-2α. *An overview of two strategies for conjugating Halotag-HIF-2α to HL-GNPs. in vitro conjugation: labelling of Halotag-HIF-2α before injection into cells for imaging i.e.HEK293t cells ectopically expressing Halotag-HIF-2α are lysed and HL-GNPs added, unbound protein is removed and the nanoparticles are injected into cells. in vivo conjugation: labelling of Halotag-HIF-2α occurs inside the cells that are to be imaged i.e. cells ectopically expressing Halotag-HIF-2α are injected with the HL-GNPs and the cells are imaged directly.*

5.2.3.1 *in vivo* conjugation

The protocol for *in vivo* conjugation has several drawbacks such as once injected it relies on the nanoparticles finding and reacting with the Halotag-HIF-2α in the cells. Also, there is no way to control non-specific interactions. However, the primary issue was identifying cells for microinjection, as the pFN21A-Halotag-HIF-2α construct does not have a fluorescent marker. To overcome this, a fragment of DNA encoding an internal ribosome entry site preceding the fluorophore dTomato (IRES-dTomato) was inserted at the C-terminus of Halotag-HIF-2α to create a construct that expresses the Halotag-HIF-2α and dTomato separately (Figure 5.14). Thus providing a way to identify cells to be microinjected with HL-GNPs and bypass the need for co-transfection.

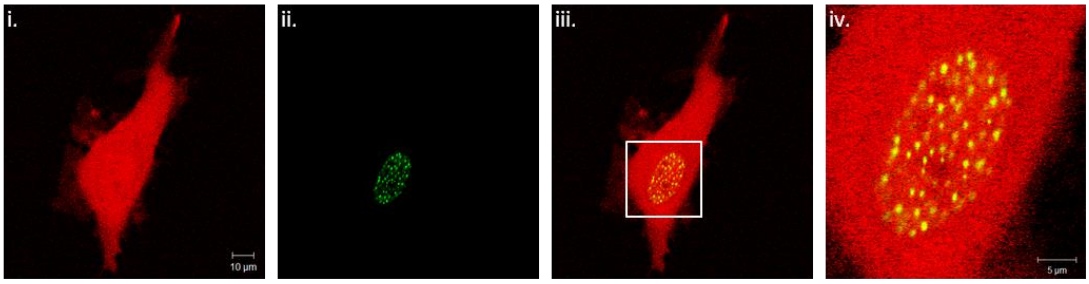

Figure 5.14 | Halotag-HIF-2α-IRES-dTomato. *HeLa cell ectopically expressing Halotag-HIF-2α-IRES-dTomato labelled with 5 µM Fluorescent Halotag Ligand (Oregon Green). i) Halotag-HIF-2α-IRES-dTomato, ii) Oregon Green, iii) Merge, iv Magnification of highlighted region (white square).*

5.2.3.2 *in vitro* conjugation

Figure 5.15 shows a protein sample taken from HEK293T cells transiently transfected with pFN21A-Halotag-HIF-2α that has been analysed by SDS-PAGE, western blot and fluorescence. A strong band of the expected size (150 kDa) that exhibits immuno-reactivity against the anti-HIF-2α and anti-Halotag antibody was observed. The lysate was incubated with the fluorescent (Oregon Green) Halotag ligand prior to denaturation and analysis by SDS PAGE. The fluorescent band in lane 1 (Figure 5.15) indicates that a functional Halotag makes up part of this the 150 kDa.

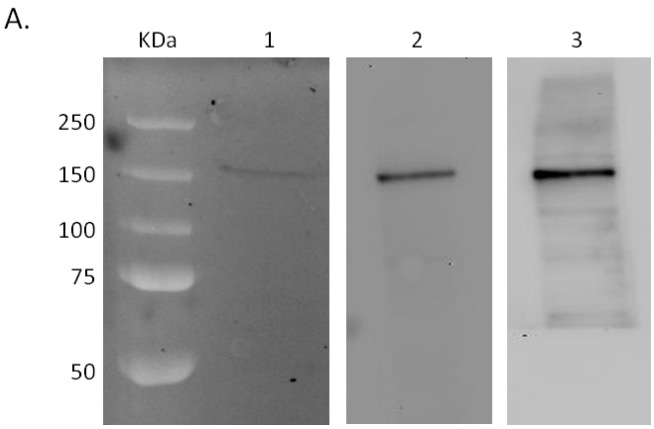

Figure 5.15 | Halotag-HIF-2α expressed in HEK293T cells. *pFN21A-Halotag-HIF-2α was transfected into HEK293T cells. Protein extraction was carried out and samples taken for analysis. Oregon Green Halotag ligand (1), Halotag antibody (2) and HIF-2α antibody (3).*

Gold nanoparticles carrying the Halotag ligand were incubated with the lysate of HEK293T cells that were transfected with Halotag-HIF-2α (transfected lysate). As a control HL-GNPs were also incubated with the lysate of non-transfected cells (control lysate) or with just PBS (- Lysate). Samples from each condition were spotted onto nitrocellulose membrane and

probed for HIF-2α. Alongside these experiments, gold nanoparticles with a ligand shell consisting of only polyethylene glycol (PEG-GNPs) were tested as negative controls. The dot blots in figure 5.16 show that there is HIF-2α non-specifically bound to HL-GNPs and PEG-GNPs in the transfected and control lysate pre-wash. However, following a wash step to remove weakly bound proteins, a faint signal is only seen for the sample from the HL-GNPs incubated with the transfected lysate, suggesting that HIF-2α has specifically bound to the surface of the gold nanoparticles via the Halotag ligand (Figure 5.16C, red circle).

To confirm the size of the protein attached to the surface of the nanoparticles, the ligand shell was stripped from the gold core with DTT (Chen *et al.*, 2012) and analysed via western blot. Following several washes, to remove aspecifically bound proteins, the nanoparticles were treated with 50 mM DTT for 36 h. Figure 5.16D shows that upon stripping, a strong HIF-2α immunoreactivity at 150 kDa was observed (Lane labelled DTT), suggesting a clear conjugation of HIF-2α to gold nanoparticles (last lane). As a control, samples of from the transfected cells (size control for HT-HIF-2α) and from the wash steps were separated on the same gel. HIF-2α was detected only in the first wash, suggesting any non-specifically bound HIF-2α was removed by subsequent washes. Altogether, these results suggest that Halotag-HIF-2α is covalently bound to the gold nanoparticles via the Halotag ligand that is incorporated into the ligand shell.

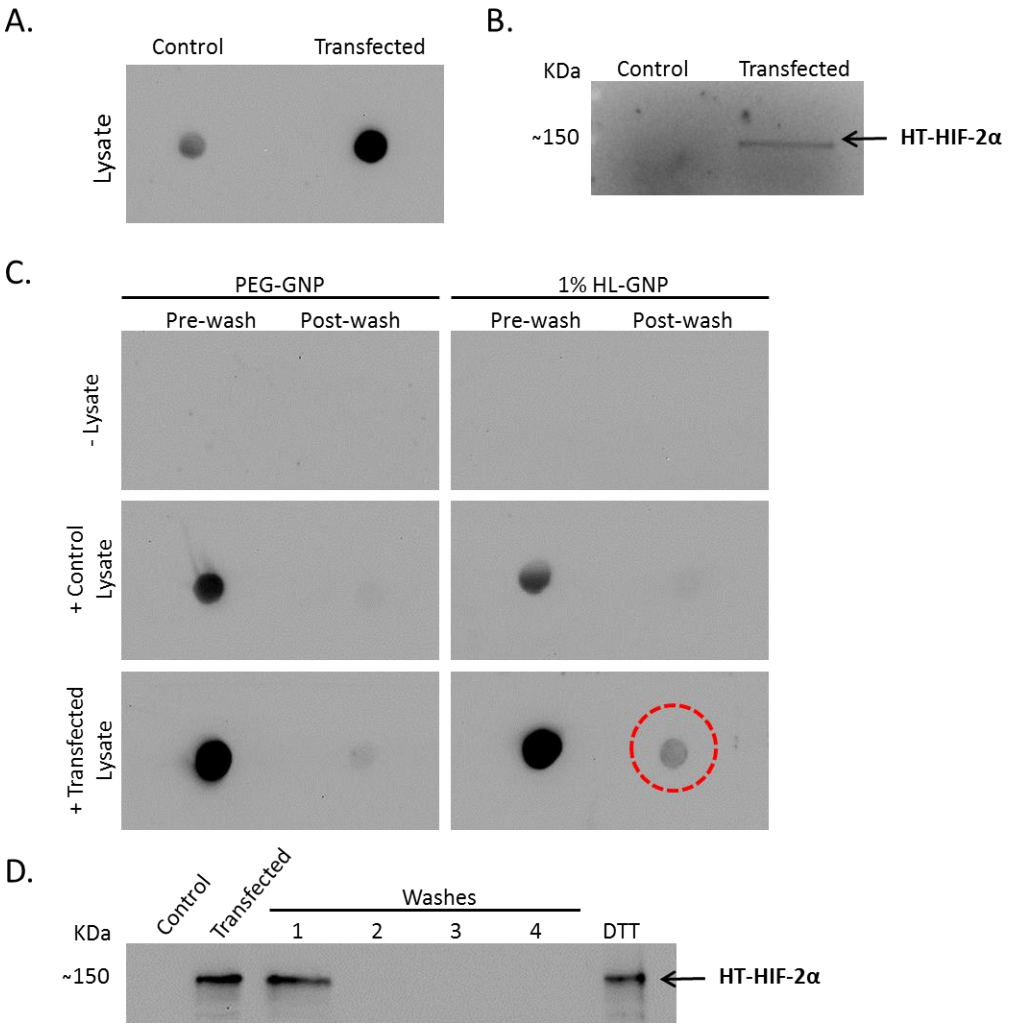

Figure 5.16 | Conjugation of HL-GNPs to Halotag-HIF-2α from mammalian cell lysate. *A) Lysates from HEK293T cells not expressing (control) and expressing Halotag-HIF-2α were spotted onto a nitrocellulose membrane and probed with a HIF2α antibody (Abcam, UK). B) Fluorescence image of 200 µg of lysates from (A) labelled with 10 µM of HaloTag Oregon Green ligand resolved via SDS PAGE. C) Nanoparticles after overnight incubation with lysates from (A) or without lysate were spotted onto nitrocellulose membrane and probed with anti-HIF2α (Abcam, UK). Dot blot shows before (pre) and after (post) four washes with PBST to remove unbound / weakly bound protein. D) To determine the size of the protein attached to the gold nanoparticles the ligand shell and, therefore, anything bound, was stripped from the gold core and analysed via western blot. HL-GNPs were incubated with HT-HIF-2α lysate. The nanoparticles were washed four times in PBST to removed weakly bound proteins. After washing, the nanoparticles were incubated with 50 mM DTT for 36 h. The ligand shell was separated from the gold via centrifugation and the presence of HT-HIF-2α was determined immunoblotting (anti-HIF-2α).*

Although this result was very promising, we observed variability in success rates of conjugation between different batches of HL-GNPs and experienced difficulties in consistently reproducing the results observed in figure 5.16. Taking this into consideration, along with the development of new approaches for nanoparticle conjugation to proteins

(Leduc *et al.*, 2013), we decided to pursue a different strategy for coupling HIF-2α to gold nanoparticles.

5.2.3.3 Anti-GFP Nanobodies: A compromise?

Nanobody is a term that refers to a single variable domain (V_HH) derived from heavy chain only antibodies (IgG) found in camelid species such as alpaca (Hamerscasterman *et al.*, 1993;Muyldermans *et al.*, 1994;Muyldermans & Lauwereys, 1999). These nanobodies are a fraction of the size of conventional antibodies (full length 160 kDa), with a molecular weight of around 15 kDa (Doshi *et al.*, 2014). Their small size, 2.5 x 4.2 nm, gives them certain advantages over antibodies (Revets *et al.*, 2005;Muyldermans *et al.*, 2009), such as a much smaller minimal linkage distance between the tag and the target, which is of particular value for super-resolution imaging and single molecule tracking (Ries *et al.*, 2012;Leduc *et al.*, 2013)

Leduc *et al.* (2013) have already shown that nanobodies to GFP can be used as a means for labelling proteins of interest with gold nanoparticles (Leduc *et al.*, 2013). This method requires an EGFP fusion of the protein of interest, which we already had available for HIF-2α and was, therefore, appealing to enable the study of HIF-2α at the single molecule level.

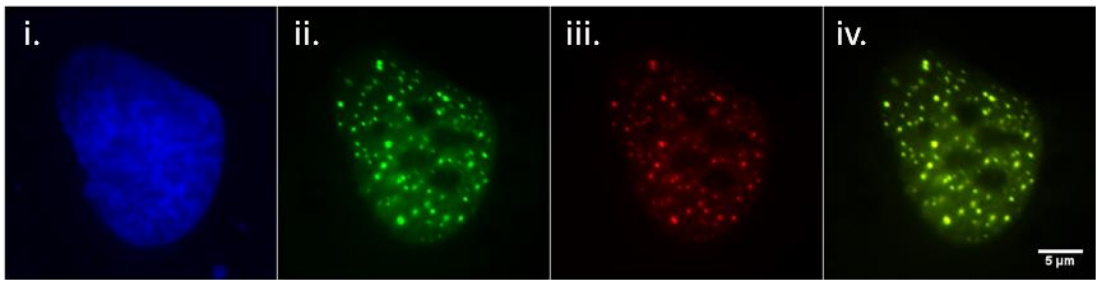

Figure 5.17 | Labelling cells expressing EGFP-HIF-2α with anti-GFP nanobodies. *HeLa cells transiently transfected with EGFP-HIF-2α were fixed, permeabilised and labelled with anti-GFP nanobodies. i) nuclear stain (Hoechst), ii) EGFP-HIF-2α, iii) ATTO594 conjugated anti-GFP nanobodies, iv) merge of ii & iii. Yellow indicates colocalisation.*

Preliminary experiments show that highly specific labelling of EGFP-HIF-2α with GFP nanobodies (conjugated with fluorescent dye ATTO594) can be achieved using standard immuno-fluorescent protocols (Figure 5.15). Figure 5.16 shows an example of a HeLa cells ectopically expressing EGFP-HIF-2α that has been microinjected with the anti-GFP-ATTO594 nanobodies. Nuclear colocalisation between the green and red channels can be observed (Figure 5.16iv.). These promising results suggest that ectopically expressed EGFP-HIF-2α

could potentially be labelled with GNPs via anti-GFP nanobodies in live cells using microinjection as the delivery method.

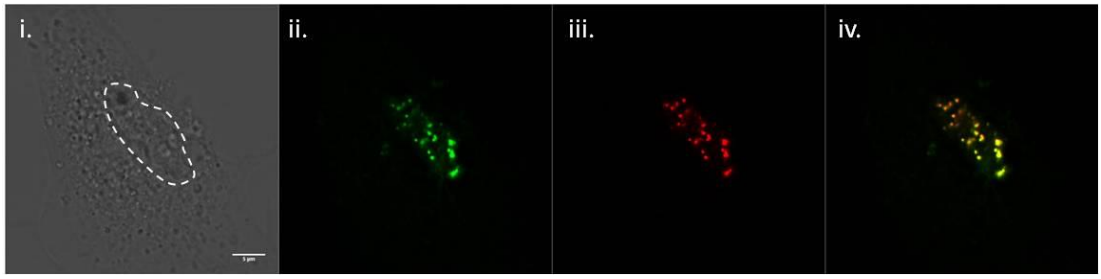

Figure 5.18 | Microinjection of anti-GFP nanobodies into cells ectopically expressing EGFP-HIF-2α. *Live HeLa cells transiently transfected with EGFP-HIF-2α were injected with anti-GFP nanobodies.i) Brightfield, ii) EGFP-HIF-2α, iii) anti-GFP ATTO594 nanobodies, iv) merge of ii & iii.*

Incorporation of the anti-GFP nanobodies onto the surface of the gold nanoparticles requires a different protocol to that of the Halotag-ligand which would need optimisation. As I was approaching the end of my time in the laboratory, and the size and scope of this work was unknown, the GFP-nanobody project was passed onto another member of the laboratory and is currently under development.

5.3 Conclusion

The aim of the work described in this chapter was to develop a method of labelling single molecules of HIF-2α with gold nanoparticles to facilitate their tracking in live cells. The initial plan was to use the Halotag, an enzyme that specifically and irreversibly binds to chloroalkanes. In collaboration with Promega, a Halotag ligand was specifically designed so that it could be incorporated into the ligand shell of a gold nanoparticle but protrude far enough so that it could react with a Halotag fusion protein.

Preliminary 'proof of principle' experiments were conducted with fibroblast growth factor-2 (FGF2). Recombinant Halotag-FGF2 was expressed in bacteria and purified using a three-step chromatography protocol. We showed that FGF2 could be coupled to gold nanoparticles via the Halotag technology.

However, when we moved on to the protein of interest, HIF-2α, several issues were encountered. Despite work published in Sun, C. *et al* (2015) suggesting that having the Halotag at the N-terminal of the fusion protein can aid bacterial expression of recalcitrant

protein and although many different bacterial strains and variations of protocols were trialled, expression of full-length recombinant Halotag-HIF-2α in useful amounts was not achieved. The poor expression observed could be due to the large size of the protein or the large proportion of rare codons in the coding sequence HIF-2α. The latter interpretation is supported by the marginal improvement in expression observed in the Rosetta strain. At present there are no crystal structures of full length HIF-2α available, only structures of the HIF-2α PAS-B domain (Erbel *et al.*, 2003;Card *et al.*, 2005;Scheuermann *et al.*, 2009;Key *et al.*, 2009;Scheuermann *et al.*, 2013;Rogers *et al.*, 2013;Guo *et al.*, 2015), suggesting that others may have also struggled to express full-length recombinant HIF-2α.

Secondly, we encountered problems with reproducibility with regards to nanoparticle production / conjugation. Although it was shown that FGF2 could be conjugated to gold nanoparticles via the Halotag, we were unable to consistently conjugate HIF-2α to HL-GNPs. One possible reason for this is that the Halotag-FGF2 / nanoparticle conjugation reaction occurred in more favourable conditions (*in vitro*) *i.e.* as we are able to express & purify recombinant Halotag-FGF2, the reaction occurred in excess of Halotag-FGF2 and with no interference from other proteins. In the case of Halotag-HIF-2α, we seemingly could on express full-length Halotag-HIF-2α in mammalian cell. However, any protein expressed was only visible via western blot (an amplification technique) and not on an SDS PAGE stained with coomassie blue. It is difficult to calculate the concentration of fusion protein that is present in the lysate, but we can be sure that it is far less than that of the purified Halotag-FGF2. In addition to this, there is competition from other endogenous proteins that may non-specifically interact with the surface of the nanoparticle, blocking Halotag-HIF-2a from reacting with the Halotag-ligand. Both of these factors would reduce the chances of successful conjugation.

Another explanation for this could be that the Halotag ligand is inaccessible to the Halotag protein. The Halotag ligand was designed to protrude far enough out of the ligand shell so that it can react with the Halotag protein, however, there are hydrophobic regions along the ligand (for ligand structure see Appendix 1.5) and it is possible that this causes the Halotag ligand to reorient itself so that these regions are immersed in the ligand shell, thus resulting in the Halotag protein being unable to react with the chloroalkane part of the ligand.

Despite lack of reproducibility, the results presented here suggest that it is possible to conjugate HIF-2α to gold nanoparticles via the Halotag protein. With improvements to the design of the Halotag ligand and optimisation of a robust protocol for making Halotag ligand gold nanoparticles, this would be an invaluable technique for labelling proteins of interest for single molecule tracking.

Nanobodies are another promising and versatile method for labelling a protein of interest with gold nanoparticles. The anti-GFP nanobodies can be used with any GFP (and GFP derivative)-fusion proteins. They have been shown to have uses in numerous microscopy techniques, not only for single molecule tracking but also for super-resolution microscopy (Leduc *et al.*, 2013;Ries *et al.*, 2012)

Chapter 6: Discussion

In this thesis, we have demonstrated that the HIF-1α subunits transiently stabilise in hypoxia and that this dynamic accumulation is the result of a negative feedback mechanism that ensures a controlled HIF response and is specifically controlled by PHD2. We have further demonstrated that HIF-1α and HIF-2α exhibit different sub-nuclear distributions, with HIF-2α being localised in nuclear foci. I have shown that HIF-2α freely diffuses in and out of the nuclear speckles and through the inter-speckle space. We initially hypothesised that HIF-2α might be regulated by molecular availability, as opposed to protein stability, yet my results show no clear difference in HIF-2α molecular availability or diffusion rate in normoxia and hypoxia. However, the diffusion of HIF-2α molecules is much slower than HIF-1α irrespective of oxygen tension. All these results were obtained using live cell imaging and for this project, I have generated several useful tools for imaging from the nano-scale to the cellular scale. I have developed a method for conjugating gold nanoparticles to a protein of interest for single molecule tracking and I have also created several lentiviral plasmids and stable cell lines for quantitative imaging of HIF-1α/ 2α.

6.1 Utilising fluorescent confocal microscopy to investigate protein dynamics in living cells: Reflection and future prospects

6.1.1 Stable cell lines

We have utilised fluorescent fusion proteins to monitor and quantify a protein of interest. This method however has drawback, for example: delivery of the construct encoding the fusion protein which can be variable and lacks control; the fusion protein is under the control of an exogenous promoter such as the CMV promoter which can provide heterogeneous levels of expression between experiments and cell types (Smith *et al.*, 2000); and, it is not the endogenous protein that is being observed.

To overcome some of these problems we have endeavoured to make cell lines stably expressing fluorescent fusions of HIF-1α and HIF-2α. Although some success was had via the use of a BAC for HIF-1α, the resulting cell lines were still less than ideal as the signal was very weak. Many of the drawbacks of BACs were discussed in chapter 3, one of which is the lack of control over where the transgene integrates into the genome. One way around this is to utilise genome editing nucleases such as zinc finger nucleases (ZFNs), Transcription

activator-like effector nucleases (TALENs) or clustered regularly interspaced short palindromic repeats (CRISPr). These technologies facilitate directed integration of the transgene into the host's genome. There are two options: (1) insert an exogenous fusion of the protein of interest (e.g. HIF-1α-EGFP) at a predetermined site (e.g. AAVS1 locus) or (2) insert an exogenous tag (e.g. EGFP or Halotag) downstream of the gene of interest. The latter option means that the endogenous protein is transcribed with the tag attached under the control of endogenous promoter; it also means that any other regulatory elements are also still having an effect and therefore any observations made are more physiologically relevant.

6.1.2 Data analysis

One difficulty with microscope experiments, particularly time-lapse experiments, is turning the qualitative information in to quantitative data that can be analysed and interpreted. A particular problem with analysing live cells is that they can move and / or change shape over the course of the experiment. So in order to measure the fluorescent signal from the nucleus of one cell, one has to track the nucleus through the time course. If the protein of interest is not visible for the entirety of the experiment (such as HIF-1α), then automated detection and tracking is difficult as the loss of signal means software (such as Imaris, Bitplane) loses the object during these periods. This can be overcome by using a nuclear marker, however with regards to the HIF-1α-GFP BAC cell line, finding a spectrally suitable, non-toxic nuclear marker that will last the duration of the experiment (>24 h) proved difficult. This meant that for these experiments there was no way to automatically track the region of interest, resulting in the tedious task of manually drawing the boundaries of each cell nuclei and moving through each frame of the time-lapse checking for cell movement and adjusting the boundaries accordingly. To make the analysis of future experiments less laborious, I would create a construct encoding either lamin or histone-2b (H2B) fused with a red fluorescent protein such as dTomato or mCherry.

6.1.3 Investigating molecular dynamics

Although work continues with investigating methods (e.g. nanobodies) of labelling HIF-2α *in vivo* with gold nanoparticles, it would be worth considering other methods of SMT. I believe a useful tool for investigating the molecular dynamics of the HIF-α subunits would be a fusion of HIF-1α or HIF-2α with a photo-switchable / convertible protein. This could provide

more comprehensive information for FRAP such as bi-directional diffusion and can be utilised for super-resolution techniques such as fPALM and single molecule tracking.

Continually, the Halotag can be specifically and irreversibly labelled with a cell-permeable Halotag ligand carrying a synthetic dye (e.g. TMR) and has been utilised by several groups for SMT (Abrahamsson *et al.*, 2013;Mazza *et al.*, 2012). So we could utilise the Halotag-HIF-2α construct and the TMR ligand for SMT in living cells. This work would also benefit from the opportunity to use the equipment at the Advanced Imaging Centre (AIC) at Janelia Farm, USA. This facility has many custom-built state of the art pieces of equipment designed for super-resolution single molecule tracking and throughout the year they run a call for proposals where external researchers can bring their own samples to the facility for imaging.

6.2 HIF-1α versus HIF-2α

6.2.1 Normoxic stabilisation of HIF-2α

The literature suggests that both HIF alpha subunits are regulated in an oxygen-dependent manner whereby they are hydroxylated by the PHD enzymes, which results in association with VHL and subsequently degradation via the proteasome. However, in contradiction with this model, we observe normoxic stabilisation of both endogenous and ectopically expressed HIF-2α in a variety of cells line (HeLa, HEK, SK-N-AS cells) via different methods (live cell imaging, immunofluorescence and western blot) and so are confident that is that this is not an artefact.

One possibility is that the cell lines used have reduced activity of the components involved in the oxygen-dependent hydroxylation and VHL-dependent degradation, such as the co-factors required for hydroxylation of the prolyl residues located within the ODD domain (Figure 6.1). However, as we do not observe normoxic stabilisation of HIF-1α this is unlikely to be the case. This also suggests that it is something specific to HIF-2α.

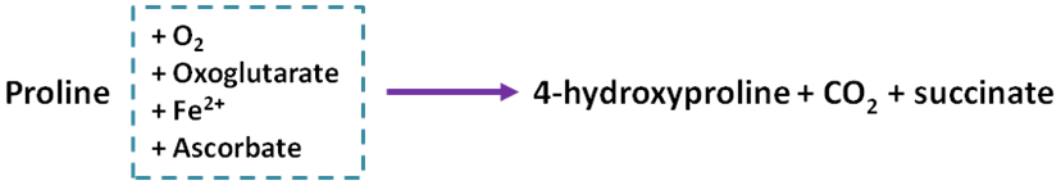

Figure 6.1 | PHD enzymatic reaction. *The reaction that takes place when the PHD proteins hydroxylate the prolyl residues located within the ODD domain. Essential co-substrates and co-factors are highlight in the blue box.*

There is evidence that there are deubiquitinases (DUBs) that modify HIF-1α (e.g. ubiquitin specific peptidase 29 / USP29) and positively influence its stability (Edurne Berra,CIC bioGUNE, Spain; unpublished; communication at the Hypoxia: From Basic Mechanisms to Therapeutics (E3) Keystone meeting 2015). If there are also DUBs that specifically modify HIF-2α, then this would result in evasion of proteasomal degradation and give rise to normoxic stabilisation (Figure 6.2). It could also be possible that there is an enzyme that reverses the actions of the PHD enzymes, which would prevent association of pVHL with the alpha subunit and the subsequent targeting to the proteasome. Lastly, there could be a protein similar to a chaperone protein that protects HIF-2α from degradation by physically preventing PHDs or pVHL interacting with and modifying the subunit.

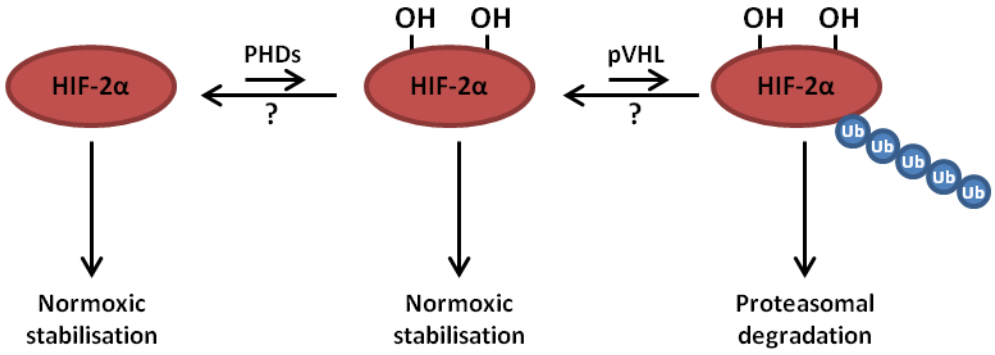

Figure 6.2 | Theory of normoxic stabilisation of HIF-2α.

6.2.2 Not just a backup system

For a long time HIF-2α has been considered the "under-study" of HIF-1α. However, interest in HIF-2α is growing as there is more and more evidence that this isoform is not just HIF-1α's fall back, but that it has specific roles and unique target genes. However, one of the main conundrums is how does gene specificity arise. David Mole and colleagues have performed genome wide analysis of HIF (HIF-1α/HIF-1β or HIF-2α/HIF-1β) and found that

when comparing HIF-1 (HIF-1α + HIF-1β) and HIF-2 (HIF-2α + HIF-1β) specific binding sites there is no obvious difference in the consensus sequence and proximal sequences, therefore the specificity does not lie within the sequence that the two isoforms bind to (Schödel *et al.*, 2011). Peter Ratcliffe and colleagues have found that when HIF-1α and HIF-2α are both present, then certain genes will be preferentially bound by HIF-1α, but when HIF-1α is knocked down then HIF-2α is found to bind these genes. This highlights that both isoforms can bind to the "HIF-1α-specific gene" but there is competition for binding (Peter Ratcliffe, University of Oxford, unpublished, communication at the Hypoxia: From Basic Mechanisms to Therapeutics (E3) Keystone meeting 2015), suggesting that gene specificity arises due to HIF-1α having a stronger affinity for these genes or due to mobility i.e. HIF-1α diffuses more quickly than HIF-2α so arrives at the gene first, which would fit with our FRAP results.

6.3 Final remarks

The hypoxia signalling pathway is a vital oxygen deprivation survival mechanism that plays a role in many normal physiological and developmental processes. It has also been implicated in various diseases and there is a large focus on HIF as a potential therapeutic target in cancer, stroke and transplant rejection (for example). Therefore, it is important to gain a full understanding of how these two transcription factors and their activity is regulated and so further investigation is a needed into what causes the discrepancies, such as gene specificity, protein stabilisation and spatial localisation, between HIF-1α and HIF-2α.

References

Abbe, E. (1873). Beiträge zur Theorie des Mikroskops und der mikroskopischen Wahrnehmung. *Archiv für mikroskopische Anatomie* **9**, 413-418.

Abrahamsson, S., Chen, J., Hajj, B., Stallinga, S., Katsov, A. Y., Wisniewski, J., Mizuguchi, G., Soule, P., Mueller, F., Darzacq, C. D., Darzacq, X., Wu, C., Bargmann, C. I., Agard, D. A., Dahan, M. & Gustafsson, M. G. L. (2013). Fast multicolor 3D imaging using aberration-corrected multifocus microscopy. *Nature Methods* **10**, 60-U80.

Adamson, A. D., Jackson, D. & Davis, J. R. E. (2011). Novel approaches to in vitro transgenesis. *Journal of Endocrinology* **208**, 193-206.

Al Yacoub, N., Romanowska, M., Haritonova, N. & Foerster, J. (2007). Optimized production and concentration of lentiviral vectors containing large inserts. *Journal of Gene Medicine* **9**, 579-584.

Almeida, F., Saffrich, R., Ansorge, W. & Carmo-Fonseca, M. (1998). Microinjection of Anti-coilin Antibodies Affects the Structure of Coiled Bodies. *J Cell Biol* **142**, 899-912.

Appelhoff, R. J., Tian, Y. M., Raval, R. R., Turley, H., Harris, A. L., Pugh, C. W., Ratcliffe, P. J. & Gleadle, J. M. (2004). Differential function of the prolyl hydroxylases PHD1, PHD2, and PHD3 in the regulation of hypoxia-inducible factor. *J Biol Chem* **279**, 38458-38465.

Ascoli, C. A. & Maul, G. G. (1991). Identification of a novel nuclear domain. *Journal of Cell Biology* **112**, 785-795.

Ashall, L., Horton, C. A., Nelson, D. E., Paszek, P., Harper, C. V., Sillitoe, K., Ryan, S., Spiller, D. G., Unitt, J. F., Broomhead, D. S., Kell, D. B., Rand, D. A., See, V. & White, M. R. (2009). Pulsatile stimulation determines timing and specificity of NF-kappaB-dependent transcription. *Science* **324**, 242-246.

Axelrod, D. (1981). Cell-substrate contacts illuminated by total internal-reflection fluorescence. *Biophysical Journal* **33**, A200-A200.

Bacskai, B. J., Hochner, B., Mahautsmith, M., Adams, S. R., Kaang, B. K., Kandel, E. R. & Tsien, R. Y. (1993). Spatially resolved dynamics of camp and protein kinase-a subunits in aplysia sensory neurons. *Science* **260**, 222-226.

Bagnall, J., Leedale, J., Taylor, S. E., Spiller, D. G., White, M. R. H., Sharkey, K. J., Bearon, R. N. & See, V. (2014). Tight control of hypoxia-inducible factor-alpha transient dynamics is essential for cell survival in hypoxia. *J Biol Chem* **289**, 5549-5564.

Bagnall, J. S. (2011). *Single-cell imaging and mathematical modelling of the hypoxia-inducible factor signalling network*. Eds.), pp. Thesis Ph.D., Liverpool.

Bangoura, G., Liu, Z.-S., Qian, Q., Jiang, C.-Q., Yang, G.-F. & Jing, S. (2007). Prognostic significance of HIF-2 alpha/EPAS1 expression in hepatocellular carcinoma. *World Journal of Gastroenterology* **13**, 3176-3182.

Ben-Dor, A., Steiner, M., Gheber, L., Danilenko, M., Dubi, N., Linnewiel, K., Zick, A., Sharoni, Y. & Levy, J. (2005). Carotenoids activate the antioxidant response element transcription system. *Mol Cancer Ther* **4**, 177-186.

Berezney, R. & Coffey, D. S. (1977). Nuclear matrix - Isolation and characterization of a framework structure from rat-liver nuclei. *Journal of Cell Biology* **73**, 616-637.

Berta, M. A., Mazure, N., Hattab, M., Pouyssegur, J. & Brahimi-Horn, M. C. (2007). SUMOylation of hypoxia-inducible factor-l alpha reduces its transcriptional activity. *Biochem Biophys Res Commun* **360**, 646-652.

Betzig, E., Patterson, G. H., Sougrat, R., Lindwasser, O. W., Olenych, S., Bonifacino, J. S., Davidson, M. W., Lippincott-Schwartz, J. & Hess, H. F. (2006). Imaging Intracellular Fluorescent Proteins at Nanometer Resolution. *Science* **313**, 1642-1645.

Blouin, C. C., Page, E. L., Soucy, G. M. & Richard, D. E. (2004). Hypoxic gene activation by lipopolysaccharide in macrophages: Implication of hypoxia-inducible factor 1 alpha. *Blood* **103**, 1124-1130.

Boisvert, F. M., Kruhlak, M. J., Box, A. K., Hendzel, M. J. & Bazett-Jones, D. P. (2001). The transcription coactivator CBP is a dynamic component of the promyelocytic leukemia nuclear body. *Journal of Cell Biology* **152**, 1099-1106.

Boudonck, K., Dolan, L. & Shaw, P. J. (1999). The Movement of Coiled Bodies Visualized in Living Plant Cells by the Green Fluorescent Protein. *Mol Biol Cell* **10**, 2297-2307.

Bracken, C. P., Fedele, A. O., Linke, S., Balrak, W., Lisy, K., Whitelaw, M. L. & Peet, D. J. (2006). Cell-specific regulation of hypoxia-inducible factor (HIF)-1alpha and HIF-2alpha stabilization and transactivation in a graded oxygen environment. *J. Biol. Chem.* **281**, 22575-22585.

Brahimi-Horn, M. C. & Pouyssegur, J. (2009). HIF at a glance. *J Cell Sci* **122**, 1055-1057.

Brameshuber, M. & Schuetz, G. J. (2008). How the sum of its parts gets greater than the whole. *Nat Methods* **5**, 133-134.

Brand, K. A. & Hermfisse, U. (1997). Aerobic glycolysis by proliferating cells: A protective strategy against reactive oxygen species. *FASEB Journal* **11**, 388-395.

Brasch, K. & Ochs, R. L. (1992). Nuclear bodies (NBs): a newly "rediscovered" organelle. *Exp Cell Res* **202**, 211-223.

Bruick, R. K. & McKnight, S. L. (2001). A conserved family of prolyl-4-hydroxylases that modify HIF. *Science* **294**, 1337-1340.

Busch, H. & Smetana, K. (1970). *The Nucleolus*. Eds.), pp. Acad. Press, New York,

Cam, H., Easton, J. B., High, A. & Houghton, P. J. (2010). mTORC1 Signaling under Hypoxic Conditions Is Controlled by ATM-Dependent Phosphorylation of HIF-1 alpha. *Molecular Cell* **40**, 509-520.

Card, P. B., Erbel, P. J. A. & Gardner, K. H. (2005). Structural basis of ARNT PAS-B dimerization: Use of a common beta-sheet interface for hetero- and homodimerization. *J Mol Biol* **353**, 664-677.

Carmo-Fonseca, M., Mendes-Soares, L. & Campos, I. (2000). To be or not to be in the nucleolus. *Nat Cell Biol* **2**, E107-E112.

Carreau, A., El Hafny-Rahbi, B., Matejuk, A., Grillon, C. & Kieda, C. (2011). Why is the partial oxygen pressure of human tissues a crucial parameter?: Small molecules and hypoxia. *J. Cell Mol. Med.* 1239-1253.

Casali, N. (2003). E.coli Plasmid Vectors: Methods and Applications. **235**, 316.

Chalfie, M., Tu, Y., Euskirchen, G., Ward, W. W. & Prasher, D. C. (1994). Green fluorescent protein as a marker for gene-expression. *Science* **263**, 802-805.

Chen, C. H., Pore, N., Behrooz, A., Ismail-Beigi, F. & Maity, A. (2001). Regulation of glut1 mRNA by hypoxia-inducible factor-1 - Interaction between H-ras and hypoxia. *Journal of Biological Chemistry* **276**, 9519-9525.

Chen, J., Zhang, Z., Li, L., Chen, B.-C., Revyakin, A., Hajj, B., Legant, W., Dahan, M., Lionnet, T., Betzig, E., Tjian, R. & Liu, Z. (2014). Single-Molecule Dynamics of Enhanceosome Assembly in Embryonic Stem Cells. *Cell* **156**, 1274-1285.

Chen, X., Qoutah, W. W., Free, P., Hobley, J., Fernig, D. G. & Paramelle, D. (2012). Features of Thiolated Ligands Promoting Resistance to Ligand Exchange in Self-Assembled Monolayers on Gold Nanoparticles. *Australian Journal of Chemistry* **65**, 266-274.

Chestukhin, A., Litovchick, L., Rudich, K. & DeCaprio, J. A. (2002). Nucleocytoplasmic shuttling of p130/RBL2: Novel regulatory mechanism. *Mol Cell Biol* **22**, 453-468.

Chin, M. T., Maemura, K., Fukumoto, S., Jain, M. K., Layne, M. D., Watanabe, M., Hsieh, C. M. & Lee, M. E. (2000). Cardiovascular basic helix loop helix factor 1, a novel transcriptional repressor expressed preferentially in the developing and adult cardiovascular system. *Journal of Biological Chemistry* **275**, 6381-6387.

Cleven, A. H. G., Wouters, B. G., Schutte, B., Spiertz, A. J. G., van Engeland, M. & de Bruine, A. P. (2008). Poorer outcome in stromal HIF-2 alpha- and CA9-positive

colorectal adenocarcinomas is associated with wild-type TP53 but not with BNIP3 promoter hypermethylation or apoptosis. *British Journal of Cancer* **99**, 727-733.

Cmarko, D., Smigova, J., Minichova, L. & Popov, A. (2008). Nucleolus: The ribosome factory. *Histology and Histopathology* **23**, 1291-1298.

Cockman, M. E., Masson, N., Mole, D. R., Jaakkola, P., Chang, G. W., Clifford, S. C., Maher, E. R., Pugh, C. W., Ratcliffe, P. J. & Maxwell, P. H. (2000). Hypoxia inducible factor-alpha binding and ubiquitylation by the von Hippel-Lindau tumor suppressor protein. *Journal of Biological Chemistry* **275**, 25733-25741.

Coons, A. H., Creech, H. J. & Jones, R. N. (1941). Immunological properties of an antibody containing a fluorescent group. *Proceedings of the Society for Experimental Biology and Medicine* **47**, 200-202.

Coons, A. H., Creech, H. J., Jones, R. N. & Berliner, E. (1942). The demonstration of pneumococcal antigen in tissues by the use of fluorescent antibody. *Journal of Immunology* **45**, 159-170.

Covello, K. L., Kehler, J., Yu, H., Gordan, J. D., Arsham, A. M., Hu, C. J., Labosky, P. A., Simon, M. C. & Keith, B. (2006). HIF-2alpha regulates Oct-4: effects of hypoxia on stem cell function, embryonic development, and tumor growth. *Genes Dev* **20**, 557-570.

Criscimanna, A., Duan, L.-J., Rhodes, J. A., Fendrich, V., Wickline, E., Hartman, D. J., Monga, S. P. S., Lotze, M. T., Gittes, G. K., Fong, G.-H. & Esni, F. (2013). PanIN-Specific Regulation of Wnt Signaling by HIF2 alpha during Early Pancreatic Tumorigenesis. *Cancer Res* **73**, 4781-4790.

Depping, R., Steinhoff, A., Schindler, S. G., Friedrich, B., Fagerlund, R., Metzen, E., Hartmann, E. & Kohler, M. (2008). Nuclear translocation of hypoxia-inducible factors (HIFs): Involvement of the classical α/β pathway. *Biochim Biophys Acta* **1783**, 394-404.

Dillon, N. & Festenstein, R. (2002). Unravelling heterochromatin: competition between positive and negative factors regulates accessibility. *Trends in Genetics* **18**, 252-258.

Dioum, E. M., Chen, R., Alexander, M. S., Zhang, Q., Hogg, R. T., Gerard, R. D. & Garcia, J. A. (2009). Regulation of hypoxia-inducible factor 2alpha signaling by the stress-responsive deacetylase sirtuin 1. *Science* **324**, 1289-1293.

Doshi, R., Chen, B. R., Vibat, C. R. T., Huang, N., Lee, C.-W. & Chang, G. (2014). In vitro nanobody discovery for integral membrane protein targets. *Scientific Reports* **4**,

Downes, M., Ordentlich, P., Kao, H. Y., Alvarez, J. G. A. & Evans, R. M. (2000). Identification of a nuclear domain with deacetylase activity. *Proc Natl Acad Sci USA* **97**, 10330-10335.

Drutel, G., Kathmann, M., Heron, A., Schwartz, J. C. & Arrang, J. M. (1996). Cloning and selective expression in brain and kidney of ARNT2 homologous to the Ah receptor nuclear translocator (ARNT). *Biochem Biophys Res Commun* **225**, 333-339.

Duchesne, L., Gentili, D., Comes-Franchini, M. & Fernig, D. G. (2008). Robust Ligand Shells for Biological Applications of Gold Nanoparticles. *Langmuir* **24**, 13572-13580.

Duchesne, L., Octeau, V., Bearon, R. N., Beckett, A., Prior, I. A., Lounis, B. & Fernig, D. G. (2012). Transport of fibroblast growth factor 2 in the pericellular matrix is controlled by the spatial distribution of its binding sites in heparan sulfate. *Plos Biology* **10**, e1001361-e1001361.

Dungwa, J. V., Hunt, L. P. & Ramani, P. (2012). HIF-1 alpha up-regulation is associated with adverse clinicopathological and biological factors in neuroblastomas. *Histopathology* **61**, 417-427.

Dunwoodie, S. L. (2009). The Role of Hypoxia in Development of the Mammalian Embryo. *Dev Cell* **17**, 755-773.

Eisinger-Mathason, T. S. K., Zhang, M. S., Qiu, Q., Skuli, N., Nakazawa, M. S., Karakasheva, T., Mucaj, V., Shay, J. E. S., Stangenberg, L., Sadri, N., Pure, E., Yoon, S. S., Kirsch, D. G. & Simon, M. C. (2013). Hypoxia-Dependent Modification of Collagen Networks Promotes Sarcoma Metastasis. *Cancer Discovery* **3**, 1190-1205.

Ellinger, P. & Hirt, A. (1929). Mikroskopische Beobachtungen an lebenden Organen mit Demonstrationen (Intravitalmikroskopie). *Naunyn-Schmiedebergs Archiv für experimentelle Pathologie und Pharmakologie* **147**, 63-63.

Ema, M., Hirota, K., Mimura, J., Abe, H., Yodoi, J., Sogawa, K., Poellinger, L. & Fujii-Kuriyama, Y. (1999). Molecular mechanisms of transcription activation by HLF and HIF1 alpha in response to hypoxia: their stabilization and redox signal-induced interaction with CBP/p300. *Embo Journal* **18**, 1905-1914.

Ema, M., Taya, S., Yokotani, N., Sogawa, K., Matsuda, Y. & Fujii-Kuriyama, Y. (1997). A novel bHLH-PAS factor with close sequence similarity to hypoxia-inducible factor 1alpha regulates the VEGF expression and is potentially involved in lung and vascular development. *Proc Natl Acad Sci U S A* **94**, 4273-4278.

Emmanouilidou, E., Teschemacher, A. G., Pouli, A. E., Nicholls, L. I., Seward, E. P. & Rutter, G. A. (1999). Imaging Ca2+ concentration changes at the secretory vesicle surface with a recombinant targeted cameleon. *Current Biology* **9**, 915-918.

Epstein, A. C., Gleadle, J. M., McNeill, L. A., Hewitson, K. S., O'Rourke, J., Mole, D. R., Mukherji, M., Metzen, E., Wilson, M. I., Dhanda, A., Tian, Y. M., Masson, N.,

Hamilton, D. L., Jaakkola, P., Barstead, R., Hodgkin, J., Maxwell, P. H., Pugh, C. W., Schofield, C. J. & Ratcliffe, P. J. (2001). C. elegans EGL-9 and mammalian homologs define a family of dioxygenases that regulate HIF by prolyl hydroxylation. *Cell* **107**, 43-54.

Erbel, P. J. A., Card, P. B., Karakuzu, O., Bruick, R. K. & Gardner, K. H. (2003). Structural basis for PAS domain heterodimerization in the basic helix-loop-helix-PAS transcription factor hypoxia-inducible factor. *Proc Natl Acad Sci U S A* **100**, 15504-15509.

Erni, R., Rossell, M. D., Kisielowski, C. & Dahmen, U. (2009). Atomic-Resolution Imaging with a Sub-50-pm Electron Probe. *Physical Review Letters* **102**, 096101.

Ewers, H., Smith, A. E., Sbalzarini, I. F., Lilie, H., Koumoutsakos, P. & Helenius, A. (2005). Single-particle tracking of murine polyoma virus-like particles on live cells and artificial membranes. *Proc Natl Acad Sci U S A* **102**, 15110-15115.

Fedele, A. O., Whitelaw, M. L. & Peet, D. J. (2002). Regulation of gene expression by the hypoxia-inducible factors. *Molecular interventions* **2**, 229-243.

Florczyk, U., Czauderna, S., Stachurska, A., Tertil, M., Nowak, W., Kozakowska, M., Poellinger, L., Jozkowicz, A., Loboda, A. & Dulak, J. (2011). Opposite effects of HIF-1 alpha and HIF-2 alpha on the regulation of IL-8 expression in endothelial cells. *Free Radical Biology and Medicine* **51**, 1882-1892.

Fogal, V., Gostissa, M., Sandy, P., Zacchi, P., Sternsdorf, T., Jensen, K., Pandolfi, P. P., Will, H., Schneider, C. & Del Sal, G. (2000). Regulation of p53 activity in nuclear bodies by a specific PML isoform. *Embo J* **19**, 6185-6195.

Fong, G. H. & Takeda, K. (2008). Role and regulation of prolyl hydroxylase domain proteins. *Cell Death Differ* **15**, 635-641.

Forristal, C. E., Wright, K. L., Hanley, N. A., Oreffo, R. O. C. & Houghton, F. D. (2010). Hypoxia inducible factors regulate pluripotency and proliferation in human embryonic stem cells cultured at reduced oxygen tensions. *Reproduction* **139**, 85-97.

Förster, T. (1946). Energiewanderung und fluoreszenz. *Naturwissenschaften* **33**, 166-175.

Forsythe, J. A., Jiang, B. H., Iyer, N. V., Agani, F., Leung, S. W., Koos, R. D. & Semenza, G. L. (1996). Activation of vascular endothelial growth factor gene transcription by hypoxia-inducible factor 1. *Mol Cell Biol* **16**, 4604-4613.

Franovic, A., Holterman, C. E., Payette, J. & Lee, S. (2009). Human cancers converge at the HIF-2 alpha oncogenic axis. *Proc Natl Acad Sci U S A* **106**, 21306-21311.

Gadella, T. W. J. & Jovin, T. M. (1995). Oligomerization of epidermal growth-factor receptors on A431 cells studied by time-resolved fluorescence imaging microscopy - A stereochemical model for tyrosine kinase receptor activation. *Journal of Cell Biology* **129**, 1543-1558.

Gall, J. G. (2000). Cajal bodies: The first 100 years. *Annual Review of Cell and Developmental Biology* **16**, 273-300.

Gilkes, D. M. & Semenza, G. L. (2013). Role of hypoxia-inducible factors in breast cancer metastasis. *Future Oncology* **9**, 1623-1636.

Gordan, J. D., Bertout, J. A., Hu, C. J., Diehl, J. A. & Simon, M. C. (2007). HIF-2alpha promotes hypoxic cell proliferation by enhancing c-myc transcriptional activity. *Cancer Cell* **11**, 335-347.

Gruber, M. (2007). Acute postnatal ablation of Hif-2α results in anemia. *Proc. Natl Acad. Sci. USA* **104**, 2301-2306.

Gu, Y. Z., Moran, S. M., Hogenesch, J. B., Wartman, L. & Bradfield, C. A. (1998). Molecular characterization and chromosomal localization of a third alpha-class hypoxia inducible factor subunit, HIF3 alpha. *Gene Expression* **7**, 205-213.

Gunaratnam, L. (2003). Hypoxia inducible factor activates the transforming growth factor-α/epidermal growth factor receptor growth stimulatory pathway in VHL−/− renal cell carcinoma cells. *J. Biol. Chem.* **278**, 44966-44974.

Guo, Y., Scheuermann, T. H., Partch, C. L., Tomchick, D. R. & Gardner, K. H. (2015). Coiled-coil Coactivators Play a Structural Role Mediating Interactions in Hypoxia-inducible Factor Heterodimerization. *Journal of Biological Chemistry* **290**, 7707-7721.

Gustafsson, M. G. L. (2000). Surpassing the lateral resolution limit by a factor of two using structured illumination microscopy. *Journal of Microscopy-Oxford* **198**, 82-87.

Haase, V. H. (2013). Regulation of erythropoiesis by hypoxia-inducible factors. *Blood Reviews* **27**, 41-53.

Hager, G. L., McNally, J. G. & Misteli, T. (2009). Transcription Dynamics. *Molecular Cell* **35**, 741-753.

Hamerscasterman, C., Atarhouch, T., Muyldermans, S., Robinson, G., Hamers, C., Songa, E. B., Bendahman, N. & Hamers, R. (1993). Naturally-Occurring Antibodies Devoid of Light-Chains. *Nature* **363**, 446-448.

Hara, S., Hamada, J., Kobayashi, C., Kondo, Y. & Imura, N. (2001). Expression and characterization of hypoxia-inducible factor (HIF)-3 alpha in human kidney: Suppression of HIF-mediated gene expression by HIF-3 alpha. *Biochem Biophys Res Commun* **287**, 808-813.

Hara, S., Kobayashi, C. & Imura, N. (1999). Nuclear localization of hypoxia-inducible factor-2alpha in bovine arterial endothelial cells. *Mol. Cell. Biol. Res. Commun.* **2**, 119-123.

Hay, N. & Sonenberg, N. (2004). Upstream and downstream of mTOR. *Genes Dev* **18**, 1926-1945.

Heim, R. & Tsien, R. Y. (1996). Engineering green fluorescent protein for improved brightness, longer wavelengths and fluorescence resonance energy transfer. *Current Biology* **6**, 178-182.

Heimstadt, O. (1911). Das Fluoreszenzmikroskop. *Z. Wiss. Mikrosk.* **28**, 330-337.

Hell, S. W. & Wichmann, J. (1994). Breaking the diffraction resolution limit by stimulated-emission-depletion fluorescence microscopy. *Optics Letters* **19**, 780-782.

Hemmerich, P., Schmiedeberg, L. & Diekmann, S. (2011). Dynamic as well as stable protein interactions contribute to genome function and maintenance. *Chromosome Research* **19**, 131-151.

Hendzel, M. J., Kruhlak, M. J., MacLean, N. A. B., Boisvert, F. M., Lever, M. A. & Bazett-Jones, D. P. (2001). Compartmentalization of regulatory proteins in the cell nucleus. *The Journal of Steroid Biochemistry and Molecular Biology* **76**, 9-21.

Hess, S. T., Girirajan, T. P. K. & Mason, M. D. (2006). Ultra-high resolution imaging by fluorescence photoactivation localization microscopy. *Biophysical Journal* **91**, 4258-4272.

Hirose, K., Morita, M., Ema, M., Mimura, J., Hamada, H., Fujii, H., Saijo, Y., Gotoh, O., Sogawa, K. & Fujii-Kuriyama, Y. (1996). cDNA cloning and tissue-specific expression of a novel basic helix-loop-helix/PAS factor (Arnt2) with close sequence similarity to the aryl hydrocarbon receptor nuclear translocator (Arnt). *Mol Cell Biol* **16**, 1706-1713.

Hoffman, E. C., Reyes, H., Chu, F. F., Sander, F., Conley, L. H., Brooks, B. A. & Hankinson, O. (1991). Cloning of a factor required for activity of the ah (dioxin) receptor. *Science* **252**, 954-958.

Hogenesch, J. B., Chan, W. K., Jackiw, V. H., Brown, R. C., Gu, Y. Z., PrayGrant, M., Perdew, G. H. & Bradfield, C. A. (1997). Characterization of a subset of the basic-helix-loop-helix-PAS superfamily that interacts with components of the dioxin signaling pathway. *Journal of Biological Chemistry* **272**, 8581-8593.

Holmquist-Mengelbier, L., Fredlund, E., Lofstedt, T., Noguera, R., Navarro, S., Nilsson, H., Pietras, A., Vallon-Christersson, J., Borg, A., Gradin, K., Poellinger, L. & Pahlman, S. (2006). Recruitment of HIF-1alpha and HIF-2alpha to common target genes is differentially regulated in neuroblastoma: HIF-2alpha promotes an aggressive phenotype. *Cancer Cell* **10**, 413-423.

Hu, C. J., Wang, L. Y., Chodosh, L. A., Keith, B. & Simon, M. C. (2003). Differential roles of hypoxia-inducible factor 1 alpha (HIF-1 alpha) and HIF-2 alpha in hypoxic gene regulation. *Mol Cell Biol* **23**, 9361-9374.

Huang, B., Wang, W., Bates, M. & Zhuang, X. (2008). Three-Dimensional Super-Resolution Imaging by Stochastic Optical Reconstruction Microscopy. *Science* **319**, 810-813.

Huang, L. E., Arany, Z., Livingston, D. M. & Bunn, H. F. (1996). Activation of hypoxia-inducible transcription factor depends primarily upon redox-sensitive stabilization of its alpha subunit. *Journal of Biological Chemistry* **271**, 32253-32259.

Huang, L. E., Gu, J., Schau, M. & Bunn, H. F. (1998). Regulation of hypoxia-inducible factor 1 alpha is mediated by an O-2-dependent degradation domain via the ubiquitin-proteasome pathway. *Proc Natl Acad Sci U S A* **95**, 7987-7992.

Hudson, C. C., Liu, M., Chiang, G. G., Otterness, D. M., Loomis, D. C., Kaper, F., Giaccia, A. J. & Abraham, R. T. (2002). Regulation of hypoxia-inducible factor 1 alpha expression and function by the mammalian target of rapamycin. *Mol Cell Biol* **22**, 7004-7014.

Hui, E. P., Chan, A. T. C., Pezzella, F., Turley, H., To, K. F., Poon, T. C. W., Zee, B., Mo, F., Teo, P. M. L., Huang, D. P., Gatter, K. C., Johnson, P. J. & Harris, A. L. (2002). Coexpression of hypoxia-inducible factors 1 alpha and 2 alpha, carbonic anhydrase IX, and vascular endothelial growth factor in nasopharyngeal carcinoma and relationship to survival. *Clinical Cancer Research* **8**, 2595-2604.

Iborra, F. J., Jackson, D. A. & Cook, P. R. (2001). Coupled Transcription and Translation Within Nuclei of Mammalian Cells. *Science* **293**, 1139-1142.

Iborra, F. J., Pombo, A., Jackson, D. A. & Cook, P. R. (1996). Active RNA polymerases are localized within discrete transcription 'factories' in human nuclei. *J Cell Sci* **109**, 1427-1436.

Imamura, T., Kikuchi, H., Herraiz, M. T., Park, D. Y., Mizukami, Y., Mino-Kenduson, M., Lynch, M. P., Rueda, B. R., Benita, Y., Xavier, R. J. & Chung, D. C. (2009). HIF-1alpha and HIF-2alpha have divergent roles in colon cancer. *Int J Cancer* **124**, 763-771.

Isaacs, J. S., Jung, Y. J., Mimnaugh, E. G., Martinez, A., Cuttitta, F. & Neckers, L. M. (2002). Hsp90 regulates a von Hippel Lindau-independent hypoxia-inducible factor-1 alpha-degradative pathway. *Journal of Biological Chemistry* **277**, 29936-29944.

Ivan, M., Kondo, K., Yang, H. F., Kim, W., Valiando, J., Ohh, M., Salic, A., Asara, J. M., Lane, W. S. & Kaelin, W. G. (2001). HIF alpha targeted for VHL-mediated destruction by proline hydroxylation: Implications for O_2 sensing. *Science* **292**, 464-468.

Iyer, N. V., Kotch, L. E., Agani, F., Leung, S. W., Laughner, E., Wenger, R. H., Gassmann, M., Gearhart, J. D., Lawler, A. M., Yu, A. Y. & Semenza, G. L. (1998). Cellular and developmental control of O2 homeostasis by hypoxia-inducible factor 1 alpha. *Genes Dev* **12**, 149-162.

Jackson, D. A., Hassan, A. B., Errington, R. J. & Cook, P. R. (1993). Visualization of focal sites of transcription within human nuclei. *Embo Journal* **12**, 1059-1065.

Jackson, D. A., Iborra, F. J., Manders, E. M. M. & Cook, P. R. (1998). Numbers and organization of RNA polymerases, nascent transcripts, and transcription units in HeLa nuclei. *Mol Biol Cell* **9**, 1523-1536.

Jeong, J. W., Bae, M. K., Ahn, M. Y., Kim, S. H., Sohn, T. K., Bae, M. H., Yoo, M. A., Song, E. J., Lee, K. J. & Kim, K. W. (2002). Regulation and destabilization of HIF-1 alpha by ARD1-mediated acetylation. *Cell* **111**, 709-720.

Jiang, B., Rue, E., Wang, G. L., Roe, R. & Semenza, G. (1996). Dimerization, DNA binding and transactivation properties of hypoxia-inducible factor 1. *J Biol Chem* **271**, 17771–17778.

Jiang, B. H., Agani, F., Passaniti, A. & Semenza, G. L. (1997). V-SRC induces expression of hypoxia-inducible factor 1 (HIF-1) and transcription of genes encoding vascular endothelial growth factor and enolase 1: Involvement of HIF-1 in tumor progression. *Cancer Res* **57**, 5328-5335.

K, H., R, F., S, T., S, K.-k., T, A., K, F. & G, S. (2004). Induction of hypoxia-inducible factor-1 activity by muscarinic acetylcholine receptor signalling. *J Biol Chem* **279**, 41521-41528.

Kallio, P. J., Okamoto, K., O'Brien, S., Carrero, P., Makino, Y., Tanaka, H. & Poellinger, L. (1998). Signal transduction in hypoxic cells: Inducible nuclear translocation and recuitment of CBP/p300 coactivator by the hypoxia-inducible factor-1α. *EMBO J.* **17**, 6573-6586.

Kallio, P. J., Wilson, W. J., O'Brien, S., Makino, Y. & Poellinger, L. (1999). Regulation of the hypoxia-inducible transcription factor 1 alpha by the ubiquitin-proteasome pathway. *Journal of Biological Chemistry* **274**, 6519-6525.

Kalousi, A., Mylonis, I., Politou, A. S., Chachami, G., Paraskeva, E. & Simos, G. (2010). Casein kinase 1 regulates human hypoxia-inducible factor HIF-1. *J Cell Sci* **123**, 2976-2986.

Kamura, T., Sato, S., Iwai, K., Czyzyk-Krzeska, M., Conaway, R. C. & Conaway, J. W. (2000). Activation of HIF1 alpha ubiquitination by a reconstituted von Hippel-Lindau (VHL) tumor suppressor complex. *Proc Natl Acad Sci U S A* **97**, 10430-10435.

Kapitsinou, P. P. (2010). Hepatic HIF-2 regulates erythropoietic responses to hypoxia in renal anemia. *Blood* **116**, 3039-3048.

Keith, B., Johnson, R. S. & Simon, M. C. (2012). HIF1 alpha and HIF2 alpha: sibling rivalry in hypoxic tumour growth and progression. *Nature Reviews Cancer* **12**, 9-22.

Kenworthy, A. K. & Edidin, M. (1998). Distribution of a glycosylphosphatidylinositol-anchored protein at the apical surface of MDCK cells examined at a resolution of < 100 angstrom using imaging fluorescence resonance energy transfer (vol 142, pg 69, 1998). *Journal of Cell Biology* **142**, 883-883.

Key, J., Scheuermann, T. H., Anderson, P. C., Daggett, V. & Gardner, K. H. (2009). Principles of Ligand Binding within a Completely Buried Cavity in HIF2 alpha PAS-B. *J Am Chem Soc* **131**, 17647-17654.

Kimura, H., Sugaya, K. & Cook, P. R. (2002). The transcription cycle of RNA polymerase II in living cells. *Journal of Cell Biology* **159**, 777-782.

Koh, M. Y., Darnay, B. G. & Powis, G. (2008). Hypoxia-associated factor, a novel E3-ubiquitin ligase, binds and ubiquitinates hypoxia-inducible factor 1alpha, leading to its oxygen-independent degradation. *Mol Cell Biol* **28**, 7081-7095.

Koh, M. Y., Lemos Jr, R., Liu, X. P. & Powis, G. (2011). The Hypoxia-Associated Factor Switches Cells from HIF-1 alpha to HIF-2 alpha-Dependent Signaling Promoting Stem Cell Characteristics, Aggressive Tumor Growth and Invasion. *Cancer Res* **71**, 4015-4027.

Koshiji, M., Kageyama, Y., Pete, E. A., Horikawa, I., Barrett, J. C. & Huang, L. E. (2004). HIF-1 alpha induces cell cycle arrest by functionally counteracting Myc. *Embo Journal* **23**, 1949-1956.

Koshiji, M., To, K. K. W., Hammer, S., Kumamoto, K., Harris, A. L., Modrich, P. & Huang, L. E. (2005). HIF-1 alpha induces genetic instability by transcriptionally downregulating MutS alpha expression. *Molecular Cell* **17**, 793-803.

Koukourakis, M. I., Giatromanolaki, A., Polychronidis, A., Simopoulos, C., Gatter, K. C., Harris, A. L. & Sivridis, E. (2006). Endogenous markers of hypoxia/anaerobic metabolism and anemia in primary colorectal cancer. *Cancer Sci* **97**, 582-588.

Kuno, M., Fromm, D. P., Hamann, H. F., Gallagher, A. & Nesbitt, D. J. (2001). “On”/“off” fluorescence intermittency of single semiconductor quantum dots. *The Journal of Chemical Physics* **115**, 1028-1040.

Kutner, R. H., Zhang, X. Y. & Reiser, J. (2009). Production, concentration and titration of pseudotyped HIV-1-based lentiviral vectors. *Nature Protocols* **4**, 495-505.

Lahav, G., Rosenfeld, N., Sigal, A., Geva-Zatorsky, N., Levine, A. J., Elowitz, M. B. & Alon, U. (2004). Dynamics of the p53-Mdm2 feedback loop in individual cells. *Nat Genet* **36**, 147-150.

Lai, H. K. & Borden, K. L. B. (2000). The promyelocytic leukemia (PML) protein suppresses cyclin D1 protein production by altering the nuclear cytoplasmic distribution of cyclin D1 mRNA. *Oncogene* **19**, 1623-1634.

Lamond, A. I. & Earnshaw, W. C. (1998). Structure and Function in the Nucleus. *Science* **280**, 547-553.

LaMorte, V. J., Dyck, J. A., Ochs, R. L. & Evans, R. M. (1998). Localization of nascent RNA and CREB binding protein with the PML-containing nuclear body. *Proc Natl Acad Sci U S A* **95**, 4991-4996.

Lando, D., Peet, D. J., Whelan, D. A., Gorman, J. J. & Whitelaw, M. L. (2002). Asparagine hydroxylation of the HIF transactivation domain a hypoxic switch. *Science* **295**, 858-861.

Lasne, D., Blab, G. A., Berciaud, S., Heine, M., Groc, L., Choquet, D., Cognet, L. & Lounis, B. (2006). Single nanoparticle photothermal tracking (SNaPT) of 5-nm gold beads in live cells. *Biophysical Journal* **91**, 4598-4604.

Lasne, D., Blab, G. A., De Giorgi, F., Ichas, F., Lounis, B. & Cognet, L. (2007). Label-free optical imaging of mitochondria in live cells. *Opt Express* **15**, 14184-14193.

Laughner, E., Taghavi, P., Chiles, K., Mahon, P. C. & Semenza, G. L. (2001). HER2 (neu) signaling increases the rate of hypoxia-inducible factor 1 alpha (HIF-1 alpha) synthesis: Novel mechanism for HIF-1-mediated vascular endothelial growth factor expression. *Mol Cell Biol* **21**, 3995-4004.

Leduc, C., Si, S., Gautier, J., Soto-Ribeiro, M., Wehrle-Haller, B., Gautreau, A., Giannone, G., Cognet, L. & Lounis, B. (2013). A Highly Specific Gold Nanoprobe for Live-Cell Single-Molecule Imaging. *Nano Letters* **13**, 1489-1494.

Lee, J. W., Bae, S. H., Jeong, J. W., Kim, S. H. & Kim, K. W. (2004). Hypoxia-inducible factor (HIF-1)alpha: its protein stability and biological functions. *Exp Mol Med* **36**, 1-12.

Lévy, R., Thanh, N. T. K., Doty, R. C., Hussain, I., Nichols, R. J., Schiffrin, D. J., Brust, M. & Fernig, D. G. (2004). Rational and Combinatorial Design of Peptide Capping Ligands for Gold Nanoparticles. *J Am Chem Soc* **126**, 10076-10084.

Li, Z., Bao, S., Wu, Q., Wang, H., Eyler, C., Sathornsumetee, S., Shi, Q., Cao, Y., Lathia, J., McLendon, R. E., Hjelmeland, A. B. & Rich, J. N. (2009). Hypoxia-Inducible Factors Regulate Tumorigenic Capacity of Glioma Stem Cells. *Cancer Cell* **15**, 501-513.

Li, Z., Wang, D., Messing, E. M. & Wu, G. (2005). VHL protein-interacting deubiquitinating enzyme 2 deubiquitinates and stabilizes HIF-1α. *EMBO Reports* **6**, 373-378.

Lim, J.-H., Lee, Y.-M., Chun, Y.-S., Chen, J., Kim, J.-E. & Park, J.-W. (2010). Sirtuin 1 Modulates Cellular Responses to Hypoxia by Deacetylating Hypoxia-Inducible Factor 1 alpha. *Molecular Cell* **38**, 864-878.

Liu, L., Ning, X., Sun, L., Zhang, H., Shi, Y., Guo, C., Han, S., Liu, J., Sun, S., Han, Z., Wu, K. & Fan, D. (2008). Hypoxia-inducible factor-1 alpha contributes to hypoxia-induced chemoresistance in gastric cancer. *Cancer Sci* **99**, 121-128.

Liu, Y. V., Baek, J. H., Zhang, H., Diez, R., Cole, R. N. & Semenza, G. L. (2007). RACK1 competes with HSP90 for binding to HIF-1alpha and is required for O(2)-independent and HSP90 inhibitor-induced degradation of HIF-1alpha. *Mol Cell* **25**, 207-217.

Loboda, A., Jozkowicz, A. & Dulak, J. (2010). HIF-1 and HIF-2 transcription factors--similar but not identical. *Mol Cells* **29**, 435-442.

Lok, C. N. & Ponka, P. (1999). Identification of a hypoxia response element in the transferrin receptor gene. *Journal of Biological Chemistry* **274**, 24147-24152.

Los, G. V., Encell, L. P., McDougall, M. G., Hartzell, D. D., Karassina, N., Zimprich, C., Wood, M. G., Learish, R., Ohane, R. F., Urh, M., Simpson, D., Mendez, J., Zimmerman, K., Otto, P., Vidugiris, G., Zhu, J., Darzins, A., Klaubert, D. H., Bulleit, R. F. & Wood, K. V. (2008). HatoTag: A novel protein labeling technology for cell imaging and protein analysis. *ACS Chem Biol* **3**, 373-382.

Luo, J. C. & Shibuya, M. (2001). A variant of nuclear localisation signal of bipartite-type is required for the nuclear translocation of hypoxia inducible factors (1α, 2α and 3α). *Oncogene* **20**, 1435-1444.

Luo, W., Zhong, J., Chang, R., Hu, H., Pandey, A. & Semenza, G. L. (2010). Hsp70 and CHIP Selectively Mediate Ubiquitination and Degradation of Hypoxia-inducible Factor (HIF)-1 alpha but Not HIF-2 alpha. *Journal of Biological Chemistry* **285**, 3651-3663.

Lyon, C. E., Bohmann, K., Sleeman, J. & Lamond, A. I. (1997). Inhibition of protein dephosphorylation results in the accumulation of splicing snRNPs and coiled bodies within the nucleolus. *Exp Cell Res* **230**, 84-93.

Maltepe, E., Keith, B., Arsham, A. M., Brorson, J. R. & Simon, M. C. (2000). The role of ARNT2 in tumor angiogenesis and the neural response to hypoxia. *Biochem Biophys Res Commun* **273**, 231-238.

Manders, E. M. M., Verbeek, F. J. & Aten, J. A. (1993). Measurement of colocalization of objects in dual-color confocal images. *Journal of Microscopy-Oxford* **169**, 375-382.

Matera, A. G. (1999). Nuclear bodies: multifaceted subdomains of the interchromatin space. *Trends Cell Biol* **9**, 302-309.

Matz, M. V., Fradkov, A. F., Labas, Y. A., Savitsky, A. P., Zaraisky, A. G., Markelov, M. L. & Lukyanov, S. A. (1999). Fluorescent proteins from nonbioluminescent Anthozoa species. *Nat Biotech* **17**, 969-973.

Maul, G. G. (1998). Nuclear domain 10, the site of DNA virus transcription and replication. *Bioessays* **20**, 660-667.

Maxwell, P. H., Wiesener, M. S., Chang, G. W., Clifford, S. C., Vaux, E. C., Cockman, M. E., Wykoff, C. C., Pugh, C. W., Maher, E. R. & Ratcliffe, P. J. (1999). The tumour suppressor protein VHL targets hypoxia-inducible factors for oxygen-dependent proteolysis. *Nature* **399**, 271-275.

Maynard, M. A., Evans, A. J., Hosomi, T., Hara, S., Jewett, M. A. S. & Ohh, M. (2005). Human HIF-3 alpha 4 is a dominant-negative regulator of HIF-1 and is down-regulated in renal cell carcinoma. *Faseb J* **19**, 1396-1406.

Maynard, M. A., Qi, H., Chung, J., Lee, E. H. L., Kondo, Y., Hara, S., Conaway, R. C., Conaway, J. W. & Ohh, M. (2003). Multiple splice variants of the human HIF-3 alpha locus are targets of the von Hippel-Lindau E3 uhiquitin ligase complex. *J Biol Chem* **278**, 11032-11040.

Mazumdar, J. (2010). HIF-2α deletion promotes Kras-driven lung tumor development. *Proc. Natl Acad. Sci. USA* **107**, 14182-14187.

Mazumdar, J., Hickey, M. M., Pant, D. K., Durham, A. C., Sweet-Cordero, A., Vachani, A., Jacks, T., Chodosh, L. A., Kissil, J. L., Simon, M. C. & Keith, B. (2010). HIF-2 alpha deletion promotes Kras-driven lung tumor development. *Proc Natl Acad Sci U S A* **107**, 14182-14187.

Mazza, D., Abernathy, A., Golob, N., Morisaki, T. & McNally, J. G. (2012). A benchmark for chromatin binding measurements in live cells. *Nucleic Acids Res* **40**,

Mekhail, K., Gunaratnam, L., Bonicalzi, M.-E. & Lee, S. (2004). HIF activation by pH-dependent nucleolar sequestration of VHL. *Nat Cell Biol* **6**, 642-647.

Menrad, H., Werno, C., Schmid, T., Copanaki, E., Deller, T., Dehne, N. & Bruene, B. (2010). Roles of Hypoxia-Inducible Factor-1 alpha (HIF-1 alpha) Versus HIF-2 alpha in the Survival of Hepatocellular Tumor Spheroids. *Hepatology* **51**, 2183-2192.

Minsky, M. (1961). Microscopy Apparatus.

Misteli, T. (2001). The concept of self-organization in cellular architecture. *Journal of Cell Biology* **155**, 181-185.

Mitchell, J. A. & Fraser, P. (2008). Transcription factories are nuclear subcompartments that remain in the absence of transcription. *Genes Dev* **22**, 20-25.

Miyawaki, A., Llopis, J., Heim, R., McCaffery, J. M., Adams, J. A., Ikura, M. & Tsien, R. Y. (1997). Fluorescent indicators for Ca2+ based on green fluorescent proteins and calmodulin. *Nature* **388**, 882-887.

Mole, D. R., Blancher, C., Copley, R. R., Pollard, P. J., Gleadle, J. M., Ragoussis, J. & Ratcliffe, P. J. (2009). Genome-wide association of hypoxia-inducible factor (HIF)-1alpha and HIF-2alpha DNA binding with expression profiling of hypoxia-inducible transcripts. *J Biol Chem* **284**, 16767-16775.

Mueller, F., Stasevich, T. J., Mazza, D. & McNally, J. G. (2013). Quantifying transcription factor kinetics: At work or at play? *Crit Rev Biochem Mol Biol* **48**, 492-514.

Mukhopadhyay, C. K., Mazumder, B. & Fox, P. L. (2000). Role of hypoxia-inducible factor-1 in transcriptional activation of ceruloplasmin by iron deficiency. *Journal of Biological Chemistry* **275**, 21048-21054.

Muyldermans, S., Atarhouch, T., Saldanha, J., Barbosa, J. & Hamers, R. (1994). Sequence and Structure of V-H Domain From Naturally-Occurring Camel Heavy-Chain Immunoglobulins Lacking Light-Chains. *Protein Engineering* **7**, 1129-1135.

Muyldermans, S., Baral, T. N., Retarnozzo, V. C., De Baetselier, P., De Genst, E., Kinne, J., Leonhardt, H., Magez, S., Nguyen, V. K., Revets, H., Rothbauer, U., Stijemans, B., Tillib, S., Wernery, U., Wyns, L., Hassanzadeh-Ghassabeh, G. & Saerens, D. (2009). Camelid immunoglobulins and nanobody technology. *Veterinary Immunology and Immunopathology* **128**, 178-183.

Muyldermans, S. & Lauwereys, M. (1999). Unique single-domain antigen binding fragments derived from naturally occurring camel heavy-chain antibodies. *Journal of Molecular Recognition* **12**, 131-140.

Mylonis, I., Chachami, G., Samiotaki, M., Panayotou, G., Paraskeva, E., Kalousi, A., Georgatsou, E., Bonanou, S. & Simos, G. (2006). Identification of MAPK phosphorylation sites and their role in the localization and activity of hypoxia-inducible factor-1alpha. *J Biol Chem* **281**, 33095-33106.

Nardinocchi, L., Puca, R., Sacchi, A. & D'Orazi, G. (2009). Inhibition of HIF-1alpha activity by homeodomain-interacting protein kinase-2 correlates with sensitization of chemoresistant cells to undergo apoptosis. *Mol Cancer* **8**, 1.

Nelson, D. E., Ihekwaba, A. E., Elliott, M., Johnson, J. R., Gibney, C. A., Foreman, B. E., Nelson, G., See, V., Horton, C. A., Spiller, D. G., Edwards, S. W., McDowell, H. P., Unitt, J. F., Sullivan, E., Grimley, R., Benson, N., Broomhead, D., Kell, D. B. & White, M. R. (2004). Oscillations in NF-kappaB signaling control the dynamics of gene expression. *Science* **306**, 704-708.

Nieves, D. J., Azmi, N. S., Xu, R., Levy, R., Yates, E. A. & Fernig, D. G. (2014). Monovalent maleimide functionalization of gold nanoparticles via copper-free click chemistry. *Chemical Communications* **50**, 13157-13160.

Nieves, D. J., Li, Y., Fernig, D. G. & Lévy, R. (2015). *Photothermal raster image correlation spectroscopy of gold nanoparticles in solution and on live cells*. Eds.), pp.

Nilsson, H., Jogi, A., Beckman, S., Harris, A. L., Poellinger, L. & Pahlman, S. (2005). HIF-2 alpha expression in human fetal paraganglia and neuroblastoma: relation to sympathetic differentiation, glucose deficiency, and hypoxia. *Exp Cell Res* **303**, 447-456.

O'Rourke, J. F., Tian, Y.-M., Ratcliffe, P. J. & Pugh, C. W. (1999). Oxygen-regulated and transactivating domains in endothelial PAS protein 1: Comparison with hypoxia-inducible factor-1alpha. *Journal of Biological Chemistry* **274**, 2060-2071.

Ohh, M., Park, C. W., Ivan, N., Hoffman, M. A., Kim, T. Y., Huang, L. E., Pavletich, N., Chau, V. & Kaelin, W. G. (2000). Ubiquitination of hypoxia-inducible factor requires direct binding to the beta-domain of the von Hippel-Lindau protein. *Nat Cell Biol* **2**, 423-427.

Osborne, C. S., Chakalova, L., Brown, K. E., Carter, D., Horton, A., Debrand, E., Goyenechea, B., Mitchell, J. A., Lopes, S., Reik, W. & Fraser, P. (2004). Active genes dynamically colocalize to shared sites of ongoing transcription. *Nat Genet* **36**, 1065-1071.

Pederson, T. (1998). The plurifunctional nucleolus. *Nucleic Acids Res* **26**, 3871-3876.

Peng, J., Zhang, L. Y., Drysdale, L. & Fong, G. H. (2000). The transcription factor EPAS-1/hypoxia-inducible factor 2 alpha plays an important role in vascular remodeling. *Proc Natl Acad Sci U S A* **97**, 8386-8391.

Peters, R., Peters, J., Tews, K. H. & Bahr, W. (1974). Microfluorimetric study of translational diffusion in erythrocyte-membranes. *Biochim Biophys Acta* **367**, 282-294.

Phair, R. D. & Misteli, T. (2000). High mobility of proteins in the mammalian cell nucleus. *Nature* **404**, 604-609.

Platani, M., Goldberg, I., Lamond, A. I. & Swedlow, J. R. (2002). Cajal body dynamics and association with chromatin are ATP-dependent. *Nat Cell Biol* **4**, 502-508.

Platani, M., Goldberg, I., Swedlow, J. R. & Lamond, A. I. (2000). In vivo analysis of Cajal body movement, separation, and joining in live human cells. *J Cell Biol* **151**, 1561-1574.

Ploem, J. S. (1967). *The use of a vertical illuminator with interchangeable dichroic mirrors for fluorescence microscopy with incident light*. Eds.), pp.

Pombo, A., Jackson, D. A., Hollinshead, M., Wang, Z., Roeder, R. G. & Cook, P. R. (1999). *Regional specialization in human nuclei: visualization of discrete sites of transcription by RNA polymerase III*. Eds.), pp. 2241-2253.

Qing, G. & Simon, M. C. (2009). Hypoxia inducible factor-2 alpha: a critical mediator of aggressive tumor phenotypes. *Curr Opin Genet Dev* **19**, 60-66.

Rankin, E. B., Biju, M. P., Liu, Q., Unger, T. L., Rha, J., Johnson, J. R., Simon, M. C., Keith, B. & Haase, V. H. (2007). Hypoxia-inducible factor-2 (HIF-2) regulates hepatic erythropoietin in vivo. *J. Clin. Invest.* **117**, 1068-1077.

Raval, R. R. (2005). Contrasting properties of hypoxia-inducible factor 1 (HIF-1) and HIF-2 in von Hippel-Lindau-associated renal cell carcinoma. *Mol. Cell. Biol.* **25**, 5675-5686.

Revets, H., De Baetselier, P. & Muyldermans, S. (2005). Nanobodies as novel agents for cancer therapy. *Expert Opinion on Biological Therapy* **5**, 111-124.

Reyes, H., Reiszporszasz, S. & Hankinson, O. (1992). Identification of the Ah receptor nuclear translocator protein (ARNT) as a component of the DNA-binding form of the Ah receptor. *Science* **256**, 1193-1195.

Ries, J., Kaplan, C., Platonova, E., Eghlidi, H. & Ewers, H. (2012). A simple, versatile method for GFP-based super-resolution microscopy via nanobodies. *Nat Methods* **9**, 582-584.

Rigler, R. & Widengren, J. (1990). Ultrasensitive detection of single molecules by fluorescence correlation spectroscopy. *BioScience* **3**, 180-183.

Rogers, J. L., Bayeh, L., Scheuermann, T. H., Longgood, J., Key, J., Naidoo, J., Melito, L., Shokri, C., Frantz, D. E., Bruick, R. K., Gardner, K. H., MacMillan, J. B. & Tambar, U. K. (2013). Development of Inhibitors of the PAS-B Domain of the HIF-2 alpha Transcription Factor. *Journal of Medicinal Chemistry* **56**, 1739-1747.

Rolfs, A., Kvietikova, I., Gassmann, M. & Wenger, R. H. (1997). Oxygen-regulated transferrin expression is mediated by hypoxia-inducible factor-1. *J Biol Chem* **272**, 20055-20062.

Romoser, V. A., Hinkle, P. M. & Persechini, A. (1997). Detection in living cells of Ca2+-dependent changes in the fluorescence emission of an indicator composed of two green fluorescent protein variants linked by a calmodulin-binding sequence - A new class of fluorescent indicators. *Journal of Biological Chemistry* **272**, 13270-13274.

Ruska, E. (1987). The development of the electron-microscope and of electron-microscopy. *Bioscience Reports* **7**, 607-629.

Rust, M. J., Bates, M. & Zhuang, X. (2006). Sub-diffraction-limit imaging by stochastic optical reconstruction microscopy (STORM). *Nat Methods* **3**, 793-795.

Ryan, H. E., Lo, J. & Johnson, R. S. (1998). HIF-1 alpha is required for solid tumor formation and embryonic vascularization. *Embo Journal* **17**, 3005-3015.

Sanchez, M., Galy, B., Muckenthaler, M. U. & Hentze, M. W. (2007). Iron-regulatory proteins limit hypoxia-inducible factor-2 alpha expression in iron deficiency. *Nat Struct Mol Biol* **14**, 420-426.

Sbalzarini, I. F. & Koumoutsakos, P. (2005). Feature point tracking and trajectory analysis for video imaging in cell biology. *Journal of Structural Biology* **151**, 182-195.

Schermelleh, L., Carlton, P. M., Haase, S., Shao, L., Winoto, L., Kner, P., Burke, B., Cardoso, M. C., Agard, D. A., Gustafsson, M. G. L., Leonhardt, H. & Sedat, J. W. (2008). Subdiffraction Multicolor Imaging of the Nuclear Periphery with 3D Structured Illumination Microscopy. *Science* **320**, 1332-1336.

Scheuermann, T. H., Li, Q., Ma, H.-W., Key, J., Zhang, L., Chen, R., Garcia, J. A., Naidoo, J., Longgood, J., Frantz, D. E., Tambar, U. K., Gardner, K. H. & Bruick, R. K. (2013). Allosteric inhibition of hypoxia inducible factor-2 with small molecules. *Nat Chem Biol* **9**, 271-276.

Scheuermann, T. H., Tomchick, D. R., Machius, M., Guo, Y., Bruick, R. K. & Gardner, K. H. (2009). Artificial ligand binding within the HIF2 alpha PAS-B domain of the HIF2 transcription factor. *P Natl Acad Sci USA* **106**, 450-455.

Schindelin, J., Arganda-Carreras, I., Frise, E., Kaynig, V., Longair, M., Pietzsch, T., Preibisch, S., Rueden, C., Saalfeld, S., Schmid, B., Tinevez, J. Y., White, D. J., Hartenstein, V., Eliceiri, K., Tomancak, P. & Cardona, A. (2012). Fiji: an open-source platform for biological-image analysis. *Nat Methods* **9**, 676-682.

Schneider, C. A., Rasband, W. S. & Eliceiri, K. W. (2012). NIH Image to ImageJ: 25 years of image analysis. *Nat Meth* **9**, 671-675.

Schödel, J., Oikonomopoulos, S., Ragoussis, J., Pugh, C. W., Ratcliffe, P. J. & Mole, D. R. (2011). High-resolution genome-wide mapping of HIF-binding sites by ChIP-seq. *Blood* **117**, e207-e217.

Schoenenberger, M. J., Krek, W. & Kovacs, W. J. (2015). EPAS1/HIF-2 alpha is a driver of mammalian pexophagy. *Autophagy* **11**, 967-969.

Schweizer, J. C. (2007). Practical Course: Single-Particle-Tracking.

Schwille, P., Meyer-Almes, F. J. & Rigler, R. (1997). Dual-color fluorescence cross-correlation spectroscopy for multicomponent diffusional analysis in solution. *Biophysical Journal* **72**, 1878-1886.

Scortegagna, M., Ding, K., Oktay, Y., Gaur, A., Thurmond, F., Yan, L. J., Marck, B. T., Matsumoto, A. M., Shelton, J. M., Richardson, J. A., Bennett, M. J. & Garcia, J. A. (2003). Multiple organ pathology, metabolic abnormalities and impaired homeostasis of reactive oxygen species in Epas1(-/-) mice. *Nature Genetics* **35**, 331-340.

Seagroves, T. N., Ryan, H. E., Lu, H., Wouters, B. G., Knapp, M., Thibault, P., Laderoute, K. & Johnson, R. S. (2001). Transcription factor HIF-1 is a necessary mediator of the pasteur effect in mammalian cells. *Mol Cell Biol* **21**, 3436-3444.

Semenza, G. L. & Wang, G. L. (1992). A nuclear factor induced by hypoxia via de novo protein synthesis binds to the human erythropoietin gene enhancer at a site required for transcriptional activation. *Mol Cell Biol* **12**, 5447-5454.

Shen, H., Nelson, G., Nelson, D. E., Kennedy, S., Spiller, D. G., Griffiths, T., Paton, N., Oliver, S. G., White, M. R. & Kell, D. B. (2006). Automated tracking of gene expression in individual cells and cell compartments. *J. R. Soc. Interface* **3**, 787-794.

Shroff, H., Galbraith, C. G., Galbraith, J. A. & Betzig, E. (2008). Live-cell photoactivated localization microscopy of nanoscale adhesion dynamics. *Nat Meth* **5**, 417-423.

Skuli, N. (2009). Endothelial deletion of hypoxia-inducible factor-2α (HIF-2α) alters vascular function and tumor angiogenesis. *Blood* **114**, 469-477.

Smith, R. L., Traul, D. L., Schaack, J., Clayton, G. H., Staley, K. J. & Wilcox, C. L. (2000). Characterization of promoter function and cell-type-specific expression from viral vectors in the nervous system. *J Virol* **74**, 11254-11261.

Spector, D. L. (2001). Nuclear domains. *J Cell Sci* **114**, 2891-2893.

Spiller, D. G., Wood, C. D., Rand, D. A. & White, M. R. H. (2010). Measurement of single-cell dynamics. *Nature* **465**, 736-745.

Steinhoff, A., Pientka, F. K., Mockel, S., Kettelhake, A., Hartmann, E., Kohler, M. & Depping, R. (2009). Cellular oxygen sensing: Importins and exportins are mediators of intracellular localisation of prolyl-4-hydroxylases PHD1 and PHD2. *Biochem Biophys Res Commun* **387**, 705-711.

Sternsdorf, T., Jensen, K., Reich, B. & Will, H. (1999). The nuclear dot protein Sp100, characterization of domains necessary for dimerization, subcellular localization, and modification by small ubiquitin-like modifiers. *Journal of Biological Chemistry* **274**, 12555-12566.

Stiehl, D. P., Wirthner, R., Köditz, J., Spielmann, P., Camenisch, G. & Wenger, R. H. (2006). Increased Prolyl 4-Hydroxylase Domain Proteins Compensate for Decreased Oxygen Levels: Evidence for an autoregulatory oxygen-sensing system. *Journal of Biological Chemistry* **281**, 23482-23491.

Stryer, L. & Haugland, R. P. (1967). Energy transfer - a spectroscopic ruler. *Proc Natl Acad Sci U S A* **58**, 719-&.

Stuurman, N., Degraaf, A., Floore, A., Josso, A., Humbel, B., Dejong, L. & Vandriel, R. (1992). A monoclonal-antibody recognizing nuclear matrix-associated nuclear-bodies. *J Cell Sci* **101**, 773-784.

Stuurman, N., Meijne, A. M. L., Vanderpol, A. J., Dejong, L., Vandriel, R. & Vanrenswoude, J. (1990). The nuclear matrix from cells of different origin - Evidence for a common set of matrix proteins. *Journal of Biological Chemistry* **265**, 5460-5465.

Sun, C., Li, Y., Taylor, S. E., Mao, X., Wilkinson, M. C. & Fernig, D. G. (2015). HaloTag is an effective expression and solubilisation fusion partner for a range of fibroblast growth factors. *PeerJ* **3**, e1060.

Sun, H.-X., Xu, Y., Yang, X.-R., Wang, W.-M., Bai, H., Shi, R.-Y., Nayar, S. K., Devbhandari, R. P., He, Y.-z., Zhu, Q.-F., Sun, Y.-F., Hu, B., Khan, M., Anders, R. A. & Fan, J. (2013). Hypoxia inducible factor 2 alpha inhibits hepatocellular carcinoma growth through the transcription factor dimerization partner 3/E2F transcription factor 1-dependent apoptotic pathway. *Hepatology* **57**, 1088-1097.

Tacchini, L., Bianchi, L., Bernelli-Zazzera, A. & Cairo, G. (1999). Transferrin receptor induction by hypoxia - HIF-1-mediated transcriptional activation and cell-specific post-transcriptional regulation. *Journal of Biological Chemistry* **274**, 24142-24146.

Takahashi, R., Kobayashi, C., Kondo, Y., Nakatani, Y., Kudo, I., Kunimoto, M., Imura, N. & Hara, S. (2004). Subcellular localization and regulation of hypoxia-inducible factor-2 alpha in vascular endothelial cells. *Biochem Biophys Res Commun* **317**, 84-91.

Takeda, N., O'Dea, E. L., Doedens, A., Kim, J. W., Weidemann, A., Stockmann, C., Asagiri, M., Simon, M. C., Hoffmann, A. & Johnson, R. S. (2010). Differential activation and antagonistic function of HIF-alpha isoforms in macrophages are essential for NO homeostasis. *Genes Dev* **24**, 491-501.

Takemura, M., Ohoka, F., Perpelescu, M., Ogawa, M., Matsushita, H., Takaba, T., Akiyama, T., Umekawa, H., Furuichi, Y., Cook, P. R. & Yoshida, S. (2002). Phosphorylation-dependent migration of retinoblastoma protein into the nucleolus triggered by binding to nucleophosmin/B23. *Exp Cell Res* **276**, 233-241.

Talks, K. L., Turley, H., Gatter, K. C., Maxwell, P. H., Pugh, C. W., Ratcliffe, P. J. & Harris, A. L. (2000). The expression and distribution of the hypoxia-inducible factors HIF-1 alpha and HIF-2 alpha in normal human tissues, cancers, and tumor-associated macrophages. *American Journal of Pathology* **157**, 411-421.

Tanimoto, K., Makino, Y., Pereira, T. & Poellinger, L. (2000). Mechanism of regulation of the hypoxia-inducible factor-l alpha by the von Hippel-Lindau tumor suppressor protein. *Embo Journal* **19**, 4298-4309.

Tian, H., Hammer, R. E., Matsumoto, A. M., Russell, D. W. & McKnight, S. L. (1998). The hypoxia-responsive transcription factor EPAS1 is essential for catecholamine homeostasis and protection against heart failure during embryonic development. *Genes Dev* **12**, 3320-3324.

Tian, H., McKnight, S. L. & Russell, D. W. (1997). Endothelial PAS domain protein 1 (EPAS1), a transcription factor selectively expressed in endothelial cells. *Genes Dev* **11**, 72-82.

Toschi, A., Lee, E., Gadir, N., Ohh, M. & Foster, D. A. (2008). Differential Dependence of Hypoxia-inducible Factors 1 alpha and 2 alpha on mTORC1 and mTORC2. *Journal of Biological Chemistry* **283**, 34495-34499.

Uchida, T., Rossignol, F., Matthay, M. A., Mounier, R., Couette, S., Clottes, E. & Clerici, C. (2004). Prolonged hypoxia differentially regulates hypoxia-inducible factor (HIF)-1alpha and HIF-2alpha expression in lung epithelial cells: implication of natural antisense HIF-1alpha. *J Biol Chem* **279**, 14871-14878.

van Hagen, M., Overmeer, R. M., Abolvardi, S. S. & Vertegaal, A. C. (2010). RNF4 and VHL regulate the proteasomal degradation of SUMO-conjugated Hypoxia-Inducible Factor-2alpha. *Nucleic Acids Res* **38**, 1922-1931.

Van Meer, G., Stelzer, E. H. K., Wijnaendts-Van Resandt, R. W. & Simons, K. (1987). Sorting of sphingolipids in epithelial madin-darby canine kidney cells. *Journal of Cell Biology* **105**, 1623-1636.

Vanderklish, P. W., Krushel, L. A., Holst, B. H., Gally, J. A., Crossin, K. L. & Edelman, G. M. (2000). Marking synaptic activity in dendritic spines with a calpain substrate exhibiting fluorescence resonance energy transfer. *Proc Natl Acad Sci U S A* **97**, 2253-2258.

Varma, R. & Mayor, S. (1998). GPI-anchored proteins are organized in submicron domains at the cell surface. *Nature* **394**, 798-801.

Visintin, R. & Amon, A. (2000). The nucleolus: the magician's hat for cell cycle tricks (vol 12, pg 372, 2000). *Curr Opin Cell Biol* **12**, 752-752.

Wang, G. L., Jiang, B. H., Rue, E. A. & Semenza, G. L. (1995). Hypoxia-inducible factor 1 is a basic-helix-loop-helix-PAS heterodimer regulated by cellular O2 tension. *Proc Natl Acad Sci USA* **92**, 5510-5514.

Wang, G. L. & Semenza, G. L. (1993). Characterization of Hypoxia-Inducible Factor-I and Regulation of DNA-Binding Activity by Hypoxia. *J Biol Chem* **268**, 21513-21518.

Wang, G. L. & Semenza, G. L. (1995). Purification and Characterization of Hypoxia-Inducible Factor-1. *J Biol Chem* **270**, 1230-1237.

Wang, Y., Li, Z., Zhang, H., Jin, H., Sun, L., Dong, H., Xu, M., Zhao, P., Zhang, B., Wang, J., Pan, Y. & Liu, L. (2010). HIF-1 alpha and HIF-2 alpha correlate with migration and invasion in gastric cancer. *Cancer Biology & Therapy* **10**, 376-382.

Wansink, D., Schul, W., van der Kraan, I., van Steensel, B., van Driel, R. & de Jong, L. (1993). Fluorescent labeling of nascent RNA reveals transcription by RNA polymerase II in domains scattered throughout the nucleus. *J Cell Biol* **122**, 283-293.

Wenger, R. H. & Gassmann, M. (1997). Oxygen(es) and the hypoxia-inducible factor-1. *Biol Chem* **378**, 609-616.

White, J. G., Amos, W. B. & Fordham, M. (1987). An evaluation of confocal versus conventional imaging of biological structures by fluorescence light-microscopy. *Journal of Cell Biology* **105**, 41-48.

Wiener, L., Feola, M., Templeton, J. Y., 3rd, Hamarman, H. M. & Venkataswamy, A. R. (1976). Monitoring tissue oxygenation of the heart after myocardial revascularization. *Am. J. Cardiol.* **38**, 38-45.

Wiesener, M. S., Jurgensen, J. S., Rosenberger, C., Scholze, C. K., Horstrup, J. H., Warnecke, C., Mandriota, S., Bechmann, I., Frei, U. A., Pugh, C. W., Ratcliffe, P. J., Bachmann, S., Maxwell, P. H. & Eckardt, K. U. (2003). Widespread hypoxia-inducible expression of HIF-2alpha in distinct cell populations of different organs. *Faseb J* **17**, 271-273.

Wolfe, B. B. & Voelkel, N. F. (1983). Effects of Hypoxia on Atrial Muscarinic Cholinergic Receptors and Cardiac Parasympathetic Responsiveness. *Biochem Pharmacol* **32**, 1999-2002.

Wotzlaw, C., Otto, T., Berchner-Pfannschmidt, U., Metzen, E., Acker, H. & Fandrey, J. (2007). Optical analysis of the HIF-1 complex in living cells by FRET and FRAP. *Faseb J* **21**, 700-707.

Xu, R., Ori, A., Rudd, T. R., Uniewicz, K. A., Ahmed, Y. A., Guimond, S. E., Skidmore, M. A., Siligardi, G., Yates, E. A. & Fernig, D. G. (2012). Diversification of the structural determinants of fibroblast growth factor-heparin interactions; implications for binding specificity. *Journal of Biological Chemistry*

Xu, X., Gerard, A. L. V., Huang, B. C. B., Anderson, D. C., Payan, D. G. & Luo, Y. (1998). Detection of programmed cell death using fluorescence energy transfer. *Nucleic Acids Res* **26**, 2034-2035.

Yang, S.-L., Liu, L.-P., Jiang, J.-X., Xiong, Z.-F., He, Q.-J. & Wu, C. (2014). The Correlation of Expression Levels of HIF-1 and HIF-2 in Hepatocellular Carcinoma

with Capsular Invasion, Portal Vein Tumor Thrombi and Patients Clinical Outcome. *Japanese Journal of Clinical Oncology* **44**, 159-167.

Yoo, Y. G., Kong, G. & Lee, M. O. (2006). Metastasis-associated protein 1 enhances stability of hypoxia-inducible factor-1 alpha protein by recruiting histone deacetylase 1. *Embo Journal* **25**, 1231-1241.

Yoon, H. (2014). Differential roles of Sirt1 in HIF-1a and HIF-2a mediated hypoxic responses. *FASEB Journal* **28**,

Zaccolo, M., De Giorgi, F., Cho, C. Y., Feng, L. X., Knapp, T., Negulescu, P. A., Taylor, S. S., Tsien, R. Y. & Pozzan, T. (2000). A genetically encoded, fluorescent indicator for cyclic AMP in living cells. *Nat Cell Biol* **2**, 25-29.

Zhang, N., Fu, Z., Linke, S., Chicher, J., Gorman, J., Visk, D., Haddad, G., Poellinger, L., Peet, D., Powell, F. & Johnson, R. (2010). The asparaginyl hydroxylase factor inhibiting HIF-1 alpha is an essential regulator of metabolism. *Cell Metab* **11**, 364-378

Zhang, S. P., Zubay, G. & Goldman, E. (1991). Low-usage Codons in Escherichia-Eoli, Yeast, Fruit-fly and Primates. *Gene* **105**, 61-72.

Zhao, D., Zhai, B., He, C., Tan, G., Jiang, X., Pan, S., Dong, X., Wei, Z., Ma, L., Qiao, H., Jiang, H. & Sun, X. (2014). Upregulation of HIF-2 alpha induced by sorafenib contributes to the resistance by activating the TGF-alpha/EGFR pathway in hepatocellular carcinoma cells. *Cell Signal* **26**, 1030-1039.

Zhou, Z., Sim, J., Griffith, J. & Reed, R. (2002). Purification and electron microscopic visualization of functional human spliceosomes. *Proc Natl Acad Sci U S A* **99**, 12203-12207.

Appendix

1.1 Amino acid sequences of each domain for HIF-1α and HIF-2α

>bHLH_HIF1a
RRKEKSRDAARSRRSKESEVFYELAHQLPLPHNVSSHLDKASVMRLTISYLRVR

>bHLH_HIF2a
RRKEKSRDAARCRRSKETEVFYELAHELPLPHSVSSHLDKASIMRLAISFLRTH

>PAS-A_HIF1a
KAQMNCFYLKALDGFVMVLTDDGDMIYISDNVNKYMGLTQFELTGHSVFDFTHPCDHEEMREMLTHRNGLVKK
G

>PAS-A_HIF2a
DQQMDNLYLKALEGFIAVVTQDGDMIFLSENISKFMGLTQVELTGHSIFDFTHPCDHEEIRENLSLKNGSG

>PAS-B_HIF1a
PHPSNIEIPLDSKTFLSRHSLDMKFSYCDERITELMGYEPEELLGRSIYEYYHALDSDHLTKTHHDMFTKG

>PAS-B_HIF2a
QHPSHMDIPLDSKTFLSRHSMDMKFTYCDDRITELIGYHPEELLGRSAYEFYHALDSENMTKSHQNLCTKG

>NTAD_HIF1a
FKLELVEKLFAEDTEAKNPFSTQDTDLDLEMLAPYIPMDDDFQLR

>NTAD_HIF2a
LKIEVIEKLFAMDTEAKDQCSTQTDFNELDLETLAPYIPMDGEDFQL

>CTAD_HIF1a
SMDESGLPQLTSYDCEVNAPIQGSRNLLQGEELLRALDQVN

>CTAD_HIF2a
SFESYLLPELTRYDCEVNVPVLGSSTLLQGGDLLRALDQAT

>NLS_HIF1a(711-730)
LALQNAQRKRKMEHDGSLFQ

>NLS_HIF2a(731-750)
STSHLMWKRMKNLRGGSCPL

>ODD_HIF1a
APAAGDTIISLDFGSNDTETDDQQLEEVPLYNDVMLPSPNEKLQNINLAMSPLPTAETPKPLRSSADPALNQEVALK
LEPNPESLELSFTMPQIQDQTPSPSDGSTRQSSPEPNSPSEYCFYVDSDMVNEFKLELVEKLFAEDTEAKNPFSTQDT
DLDLEMLAPYIPMDDDFQLRSFDQLSPLESSSASPESASPQSTVTVFQ

>ODD_HIF2a
TQTDFNELDLETLAPYIPMDGEDFQLSPICPEERLLAENPQSTPQHCFSAMTNIFQPLAPVAPHSPFLLDKFQQQLES
KKTEPEHRPMSSIFFDAGSKASLPPCCGQASTPLSSMGGRSNTQWPPDPPLHFGPTKWAVGDQRTEFLGAAPLGP
PVSPPHVSTFKTR

1.2 Alignment of HIF-1α and HIF-2α ODD domain protein sequence

Sequence alignment of ODD domains using BlastP:

Range 1: 7 to 26 Graphics ▼ Next Match ▲ Previous Match

Score	Expect	Method	Identities	Positives	Gaps
33.9 bits(76)	5e-07	Compositional matrix adjust.	16/20(80%)	18/20(90%)	1/20(5%)

```
Query  156  DLDLEMLAPYIPMD-DDFQL  174
            +LDLE LAPYIPMD +DFQL
Sbjct  7    ELDLETLAPYIPMDGEDFQL  26
```

Range 2: 129 to 144 Graphics ▼ Next Match ▲ Previous Match ▲ First Match

Score	Expect	Method	Identities	Positives	Gaps
16.5 bits(31)	0.23	Compositional matrix adjust.	6/16(38%)	7/16(43%)	0/16(0%)

```
Query  11   LDFGSNDTETDDQQLE  26
            L FG      DQ+ E
Sbjct  129  LHFGPTKWAVGDQRTE  144
```

Range 3: 40 to 56 Graphics ▼ Next Match ▲ Previous Match ▲ First Match

Score	Expect	Method	Identities	Positives	Gaps
16.5 bits(31)	0.27	Compositional matrix adjust.	8/20(40%)	11/20(55%)	3/20(15%)

```
Query  113  PNSPSEYCFYVDSDMVNEFK  132
            P S  ++CF   S M N F+
Sbjct  40   PQSTPQHCF---SAMTNIFQ  56
```

Sequence alignment of ODD domains using MUSCLE:

```
ODD_HIF1a   APAAGDTIISLDFGSNDTETDDQQLEEVPLYNDVMLPSPNEKL 43
ODD_HIF2a   ---------------TQTDFNELDLETLAPY----IPMDGEDF 24

ODD_HIF1a   QNINLAMSPLPTAETPKPLRSSADPALNQEVALKLEPNPESLE 86
ODD_HIF2a   QLSPICPEERLLAENPQ---STPQHCFSAMTNIFQPLAPVAPH 64

ODD_HIF1a   LSFTMPQIQDQTPSPSDGSTRQSSPEPNSPSEYCFYVDSDMVN 129
ODD_HIF2a   SPFLLDKFQQQLES------KKTEPE-HRPMSSIFFDAGSKAS 100

ODD_HIF1a   EFKLELVEKLFAEDTEAKNPFSTQDTDLDLEMLAPYIPMD-DD 171
ODD_HIF2a   ---------LPPCCGQASTPLSSMGGRSNTQ-WPPDPFLHFGP 133

ODD_HIF1a   FQLRSFDQLSP-LESSSASPESASPQSTVTVFQ           203
ODD_HIF2a   TKWAVGDQRTEFLGAAPLGPPVSPPHVSTFKTR           166
```

1.3 Explanation of macro used for tracking HIF-2α speckles

Tracking macro (step-by-step)

1) User Input

- Get user input.
    - calibration in x & y [xyCalib]
    - z [zCalib]
    - temporal interval [tCalib]
    - minimum track length [intMinTrackLen]

2) Pre-processing

- Find number of trajectories (from last trajectory number in Column B) [intTotalTracks]
- For each trajectory
    - Check if trajectory is shorter than intMinTrackLen. If so, move onto next.
    - If longer, Copy Trajectory out to a new sheet named [tXX] where XX is trajectory number

3) Analysis of Trajectory for tau=1

- If absent add a summary sheet
- Spatially calibrate the data (x,y,z)
- For each timepoint:
    - Calculate the euclidean distance (displacement) between the coordinates of t (x,y,z) and t+1 (x_1, y_1, z_1).

$$d = \sqrt{(x - x_1)^2 + (y - y_1)^2 + (z - z_1)^2}$$

    - Record a running sum of displacements for d^x where x=1 to 6
- Record the trajectory length [trajectoryLength]
- Calculate the whole trajectory displacement (using equation above with start and finish coordinates)
- Calculate the instantaneous velocity for a given window [intWindow] as the sum of step distances divided by the calibrated time.

4) Calculate Displacements for tau>1

- For each time window (tau) from 2 to trajectoryLength-1, calculate the displacements and (as above) record the running sum of displacements for d^x where x=1 to 6
- Divide the running sums by the number of frames to get the moments of the mean displacements (*i.e.* mean displacement, mean squared displacements, mean cube displacements ...)
- Make a note of the MSD with the calibrated time.

5) The Moment Scaling Spectrum

- Plot a double log graph of Tau vs Moment for moments 1-6
- Calculate the Scaling Coefficients from the slopes of the double log plots and plot (below) and calculate the slope of the moment scaling spectrum (sMSS) by fitting a trendline.

Note: Variables used in macro given in brackets

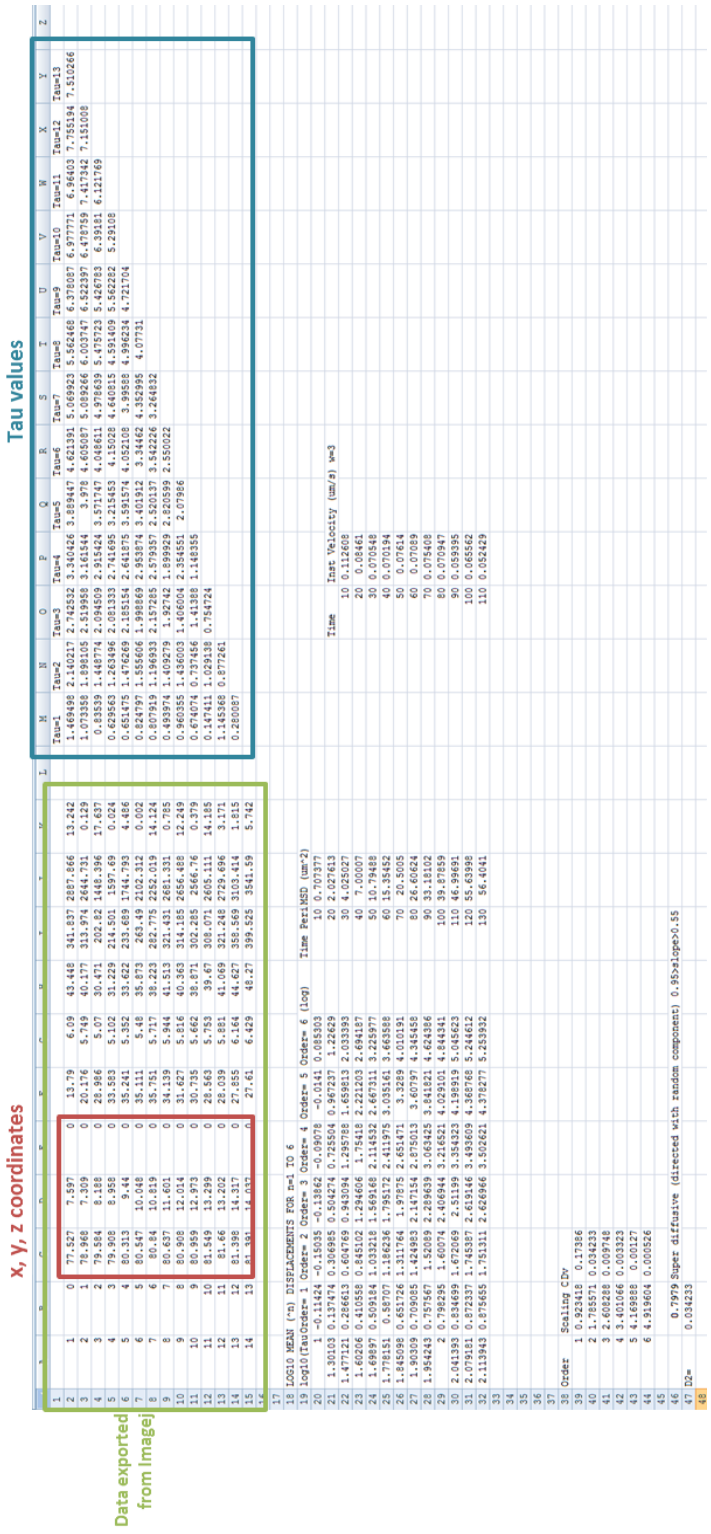

Figure 1. Analysis of individual trajectory. Screenshot of the output generated by the macro for a single trajectory.

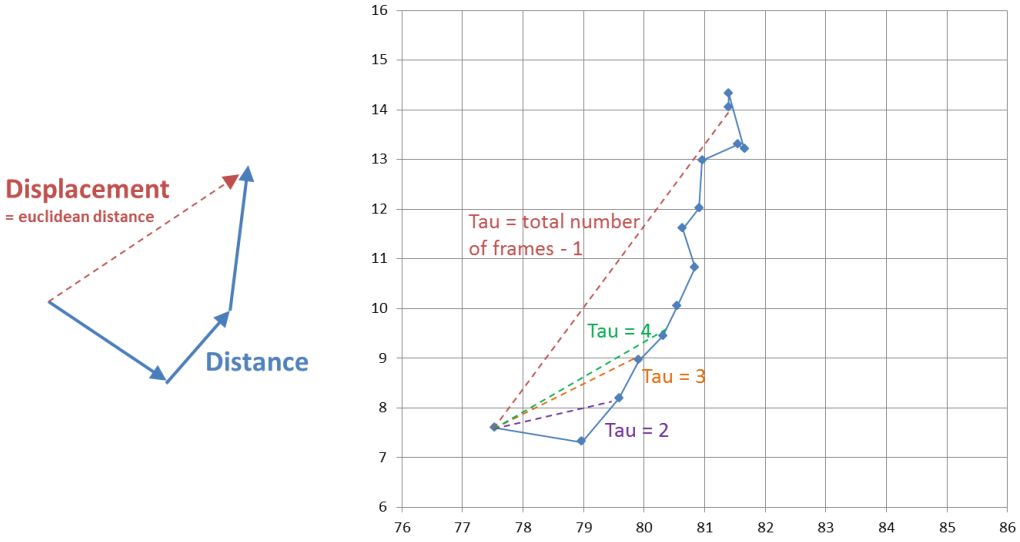

Figure 2. Depiction of the difference between distance and displacement (left) and what "Tau = x" represents.

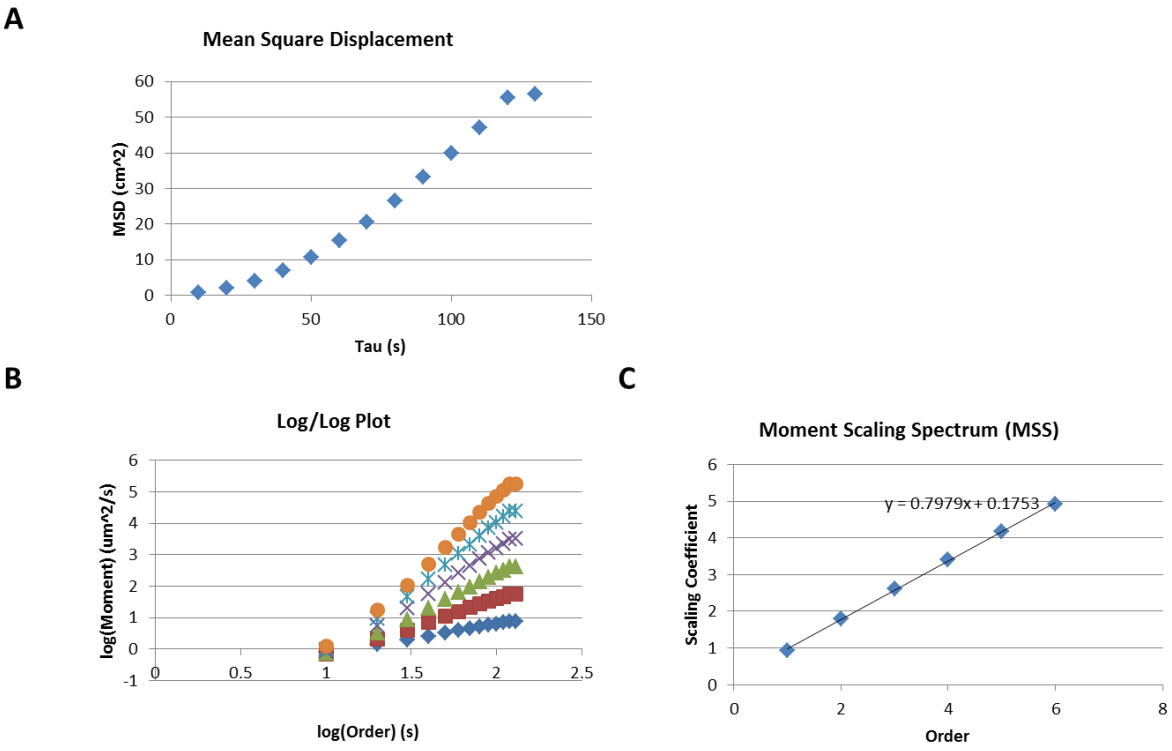

Figure 3. Graphs calculated by macro. A) Mean squared displacement. B) Log/log plot. C) Moment scaling spectrum.

1.4 Matlab code for FRAP analysis

```
%%FRAP ANALYSIS

% For analysis of FRAP data in excel spreadsheet format or CSV
format with
% Time, Bleached Regoin,Non-bleached Region and Background.
% By using the code, the end product
% will be the value of Y at time infinity, the rate of the
% and goodness of fit of the curve.

%--                                                  Written By Si Seet
Chan, March 2015
%--                                                    v5+ Revisions by
Dave Mason [dnmason@liv.ac.uk]

%-- VERSION HISTORY
%
% v3: Added ability to read in csv, xls, xlsx, txt files
% v4: Final version for SiSeet's project. Can process multiple
sheets at once.
% v5: Added option for a master log of results
% v6: v5 breaks with multisheet excel files - reads xls and xlsx
with "xlsread" and others (csv, txt) with
%       importdata as v5. Also changed figure background to white on
initialisation. Altered title to include filename
%       (without extension) and cancel Latex Interpretation.
% v7: Reduced bleach threshold to 30%
% v7.1: Error messages changed to start with 'Dave says'
% Clear the workspace and command history
clear all
close all
clc

%-- Ask if there's a master file
useMaster=questdlg('Do you have a master file? Select No to make a
new one or Cancel not to bother','Master');
if strcmp(useMaster,'Yes')
    [mastFile,mastPath]=uigetfile('*','Select Master File');
    %-- Load in existing data
    [~, ~, mastData]=xlsread([mastPath mastFile]);
elseif strcmp(useMaster,'No')
    mastPath=uigetdir('Select a folder in which to make a new Master
File');
    mastFile='masterFRAP.xls';
    %-- No file, so store a new header
    mastData={'Timestamp','Path','Filename','Plateau','Rate','R
squared'};
end
%-- catch empty master path here if useMaster is no or cancel
#######


% To get data from the workspace
% In the form of Time, Bleach (ROI1), Control (ROI2) and Background
(ROI3)
% Find data in different format
```

```
[inFile,
inPath]=uigetfile({'*.*';'*.xls';'*.txt';'*.csv';'*.xlsx'},'select
file(s)','multiselect','on');
if inPath<0;
    disp('DAVE SAYS - Error in finding file')
    return
end

% For multiselection of files to occur, need code to see whether is
it
% multiple files or single files. Multiple files = char, single file
= cell
if iscell(inFile)
    for n=1:length(inFile)


%-- Get extension then test. If Excel, only import first sheet
[tempPath tempFile tempExt]=fileparts([inPath inFile{n}]);
if strfind(tempExt,'xls')>0
    D=xlsread(fullfile([inPath inFile{n}]),1);
    Data=D(:,1:4);
else
    D=importdata(fullfile([inPath inFile{n}]));
    Data=D.data;
end

    Time=Data(:,1);
    ROI1=Data(:,2);
    ROI2=Data(:,3);
    ROI3=Data(:,4);

% csv, old xls and txt format is 3, xlsx format is 4 (the code count
the
% number to delete to replace the format
        h=length(inFile{n})-strfind(inFile{n},'.');
% Set Variables
% Number of PREBLEACH values
for i=1:size(ROI1,1)-1
    NUM_PREBLEACH=i;
   if (ROI1(i)-ROI1(i+1))/ROI1(i)>0.3
       break
   end
       if NUM_PREBLEACH>round((0.5*(size(ROI1))))
           disp('DAVE SAYS - Error in finding prebleach value')
            return
       end
end

% NUM_PREBLEACH=input('How many pre-bleach values?');

%Find the mean of Background
        Mean_ROI3=mean(ROI3);

% Background Substraction for ROI1 and ROI2
        BGSUB_ROI1=ROI1-Mean_ROI3;
        BGSUB_ROI2=ROI2-Mean_ROI3;

% Pre-bleach values for both ROI1 and ROI2
```

```
        Pre_ROI1=ROI1(1:NUM_PREBLEACH);
        Pre_ROI2=ROI2(1:NUM_PREBLEACH);

% Mean of Pre-bleach value for both ROI1 and ROI2
        Mean_PreROI1=mean(Pre_ROI1);
        Mean_PreROI2=mean(Pre_ROI2);

%Divide BG substraction for ROI1 and ROI2 with mean of Pre-bleach
value
        Norm_ROI1=BGSUB_ROI1/Mean_PreROI1;
        Norm_ROI2=BGSUB_ROI2/Mean_PreROI2;

% Correct for non-specfic bleachng (Rt)
        Rt=Norm_ROI1./Norm_ROI2;

% First Post Bleach Value (Rp)
        Rp=Rt(NUM_PREBLEACH+1);

% Correct for Bleach Function
        Bleach_Fraction=(Rt-Rp)/(1-Rp);

% Correct time for value after bleaching
        Norm_Time=Time(NUM_PREBLEACH+1:end)-Time(NUM_PREBLEACH+1);

% Get the Norm recovery data from first post bleach value till end
        Norm_Recovery=Bleach_Fraction(NUM_PREBLEACH+1:end);

% Curve Fitting
        Equation='(a-b)*exp(-c*x)+b';
% where a= Value of Y where line cross Y axis
% b= Value of Y a infinity
% c= rate constant for graph

% Plotting of graph and set the starting point for the equation to
fit the
% graph for normalised recovery

[fit1,fit1_gof,fit1_alg]=fit(Norm_Time,Norm_Recovery,Equation,'Start
Point',[1 1 0.01]);

% Flagged low Rsqaure value (less than 0.7 percent)
% plot residuals here against NormTime - don't forget to label axes
and
% give the graph a title - use Figure to make a new figure
fit1_alg.residuals
        if fit1_gof.rsquare<0.7
             figure('Color',[1 1 1]);
            plot(Norm_Time,fit1_alg.residuals);
            xlabel('Time (min)');
            ylabel('Residuals');
            title(['Residuals     -     '     inFile{n}(1:end-(h+1))],
'Interpreter','none');
            legend('Residuals','location','northeast')
            axis('square')
            disp('DAVE SAYS - Low Rsquare value for graph')
            F=getframe(gcf);
            imwrite(F.cdata,[inPath           inFile{n}(1:end-(h+1))
'_residuals.png'],'png');
```

```
       end
% Flagged negative Rsquare value
        if fit1_alg.exitflag<0
            disp('DAVE SAYS - Fail to fit equation')
            return
        end

% Plotting of graphs (Raw Data and Normalised Recovery)
% Put both graphs into one plot
         figure('Color',[1 1 1]);
        % Set the figure position and size of the figure
set(gcf,'position',[100 100 960 430])
movegui(gcf,'center') %-- Do this to make sure that the figure isn't
cut off (or including other windows) when exporting

% Plotting Raw Data - plot(Time,ROI1,Time,ROI2,Time,ROI3)
% Labeling of graph and axis, graphs are in square format so that it
is
% easier to look at datapoints
        subplot(1,2,1);
        plot(Time,ROI1,Time,ROI2,Time,ROI3);
        title(['FRAP    Data    -    '    inFile{n}(1:end-(h+1))],
'Interpreter','none');
        xlabel('Time (min)');
        ylabel('Fluorescence Intensity (a.u.)');
        legend
('Bleach','Control','Background','location','northeast')
        xlim('auto')
        ylim('auto')
        axis('square')

%       Plotting       Normalised       Recovery       graph       -
plot(fit1,Norm_Time,Norm_Recovery)
% Labeling of graph, axis and setting limits to y axis
% Putting the graphs in square format so that it is easier to look
at the
% datapoint
        subplot(1,2,2);
        plot(fit1,Norm_Time,Norm_Recovery);
        title(['Normalised  Recovery  Graph  -  '  inFile{n}(1:end-
(h+1))], 'Interpreter','none');
        xlabel('Time (min)');
        ylabel('Fractional Recovery');
        legend('Normalised                          Recovery','Curve
Fitting','location','southeast')
        xlim('auto')
        ylim([0 1.2])
        axis('square')

% Save figure in png format
        F=getframe(gcf);
        imwrite(F.cdata,[inPath inFile{n}(1:end-h),'png']);

% Save workspace in mat format
        save([inPath inFile{n}(1:end-h),'mat']);

%-- If selected, write out data to master
```

```
if strcmp(useMaster,'Yes') || strcmp(useMaster,'No')
    c=fix(clock);
    c=strcat(int2str(c(1)),'-',sprintf('%02d',c(2)),'-
',sprintf('%02d',c(3)),'-
',sprintf('%02d',c(4)),sprintf('%02d',c(5)));
    %-- Append new data
    mastData=vertcat(mastData,{c  inPath  inFile{n}  num2str(fit1.b)
num2str(fit1.c) num2str(fit1_gof.rsquare)});
    %-- Write out master
    xlswrite([mastPath '\' mastFile],mastData);
    %-- Running batch to a master file, you probably don't want the
images to stay open so...
    close all
end

% Report data needed for analysis
        disp(['----- ' inFile{n} ' -----'])
        disp(['Y value at time infinity = ' num2str(fit1.b)])
        disp(['Rate Constant =' num2str(fit1.c)])
        disp(['R  Square  value  for  fitness  of  the  equation='
num2str(fit1_gof.rsquare)])
    end


%-- Single file selected
else
%-- Get extention then test. If Excel, only import first sheet
[tempPath tempFile tempExt]=fileparts([inPath inFile]);
if strfind(tempExt,'xls')>0
    D=xlsread(fullfile([inPath inFile]),1);
    Data=D(:,1:4);
else
    D=importdata(fullfile([inPath inFile]));
%     Data=D.data;
end

    Time=Data(:,1);
    ROI1=Data(:,2);
    ROI2=Data(:,3);
    ROI3=Data(:,4);

% csv, old xls and txt format is 3, xlsx format is 4 (make it into a
% variable so that the code could find out whether is it csv,xls,txt
or
% xlsx format
h=length(inFile)-strfind(inFile,'.');

% Set Variables
% Number of PREBLEACH values
for i=1:size(ROI1,1)-1
    NUM_PREBLEACH=i;
   if (ROI1(i)-ROI1(i+1))/ROI1(i)>0.3
       break
   end
       if NUM_PREBLEACH>(0.5*(size(ROI1)))
           disp('DAVE SAYS - Error in finding good prebleach value')
            return
       end
end
```

```
% NUM_PREBLEACH=input('How many pre-bleach values?');

%Find the mean of Background
Mean_ROI3=mean(ROI3);

% Background Substraction for ROI1 and ROI2
BGSUB_ROI1=ROI1-Mean_ROI3;
BGSUB_ROI2=ROI2-Mean_ROI3;

% Pre-bleach values for both ROI1 and ROI2
Pre_ROI1=ROI1(1:NUM_PREBLEACH);
Pre_ROI2=ROI2(1:NUM_PREBLEACH);

% Mean of Pre-bleach value for both ROI1 and ROI2
Mean_PreROI1=mean(Pre_ROI1);
Mean_PreROI2=mean(Pre_ROI2);

%Divide BG substraction for ROI1 and ROI2 with mean of Pre-bleach
value
Norm_ROI1=BGSUB_ROI1/Mean_PreROI1;
Norm_ROI2=BGSUB_ROI2/Mean_PreROI2;

% Correct for non-specfic bleachng (Rt)
Rt=Norm_ROI1./Norm_ROI2;

% First Post Bleach Value (Rp)
Rp=Rt(NUM_PREBLEACH+1);

% Correct for Bleach Function
Bleach_Fraction=(Rt-Rp)/(1-Rp);

% Correct time for value after bleaching
Norm_Time=Time(NUM_PREBLEACH+1:end)-Time(NUM_PREBLEACH+1);

% Get the Norm recovery data from first post bleach value till end
Norm_Recovery=Bleach_Fraction(NUM_PREBLEACH+1:end);

% Curve Fitting
Equation='(a-b)*exp(-c*x)+b';
% where a= Value of Y where line cross Y axis
% b= Value of Y a infinity
% c= rate constant for graph

% Plotting of graph and set the starting point for the equation to
fit the
% graph for normalised recovery
[fit1,fit1_gof,fit1_alg]=fit(Norm_Time,Norm_Recovery,Equation,'Start
Point',[1 1 0.01]);

% Flagged low Rsqaure value (less than 0.7 percent)
% plot residuals here against NormTime - don't forget to label axes
and
% give the graph a title - use Figure to make a new figure
fit1_alg.residuals
if fit1_gof.rsquare<0.7
     figure('Color',[1 1 1]);
```

```
    plot(Norm_Time,fit1_alg.residuals);
    xlabel('Time (min)');
    ylabel('Residuals');
    title(['Residuals - ' inFile{n}(1:end-(h+1))],
'Interpreter','none');
    legend('Residuals','location','northeast')
    axis('square')
    set(gcf,'position',[100 100 450 450])
movegui(gcf,'center') %-- Do this to make sure that the figure isn't
cut off (or including other windows) when exporting
    disp('DAVE SAYS - Low Rsquare value for graph')
    F=getframe(gcf);
    imwrite(F.cdata,[inPath inFile(1:end-(h+1))
'_residuals.png'],'png');
end
% Flagged negative Rsquare value
if fit1_alg.exitflag<0
    disp('DAVE SAYS - Fail to fit equation')
    return
end

% Plotting of graphs (Raw Data and Normalised Recovery)
% Put both graphs into one plot
 figure('Color',[1 1 1]);
% Set the figure position and size of the figure
set(gcf,'position',[100 100 960 430])
movegui(gcf,'center') %-- Do this to make sure that the figure isn't
cut off (or including other windows) when exporting

% Plotting Raw Data - plot(Time,ROI1,Time,ROI2,Time,ROI3)
% Labeling of graph and axis, graphs are in square format so that it
is
% easier to look at datapoints
subplot(1,2,1);
plot(Time,ROI1,Time,ROI2,Time,ROI3);
%title('FRAP Data ');
title(['FRAP Data - ' inFile(1:end-(h+1))], 'Interpreter','none');
xlabel('Time (min)');
ylabel('Fluorescence Intensity (a.u.)');
legend ('Bleach','Control','Background','location','northeast')
xlim('auto')
ylim('auto')
axis('square')

% Plotting Normalised Recovery graph -
plot(fit1,Norm_Time,Norm_Recovery)
% Labeling of graph, axis and setting limits to y axis
% Putting the graphs in square format so that it is easier to look
at the
% datapoint
subplot(1,2,2);
plot(fit1,Norm_Time,Norm_Recovery);
%title('Normalised Recovery Graph');
title(['Normalised Recovery Graph - ' inFile(1:end-(h+1))],
'Interpreter','none');
xlabel('Time (min)');
ylabel('Fractional Recovery');
legend('Normalised Recovery','Curve Fitting','location','southeast')
xlim('auto')
```

```
ylim([0 1.2])
axis('square')

% Save figure in png format
F=getframe(gcf);
imwrite(F.cdata,[inPath inFile(1:end-h),'png']);

% Save workspace in mat format
save([inPath inFile(1:end-h),'mat']);

%-- If selected, write out data to master
if strcmp(useMaster,'Yes') || strcmp(useMaster,'No')
    c=fix(clock);
    c=strcat(int2str(c(1)),'-',sprintf('%02d',c(2)),'-
',sprintf('%02d',c(3)),'-
',sprintf('%02d',c(4)),sprintf('%02d',c(5)));
    %-- Append new data
    mastData=vertcat(mastData,{c   inPath   inFile   num2str(fit1.b)
num2str(fit1.c) num2str(fit1_gof.rsquare)});
    %-- Write out master
    xlswrite([mastPath '\' mastFile],mastData);
end

% Report data needed for analysis
disp(['----- ' inFile ' -----'])
disp(['Y value at time infinity = ' num2str(fit1.b)])
disp(['Rate Constant =' num2str(fit1.c)])
disp(['R   Square   value   for   fitness   of   the   equation='
num2str(fit1_gof.rsquare)])
end
%-- Clear the variable used to write out
clear mastData
```

1.5 Structure of Halotag ligand

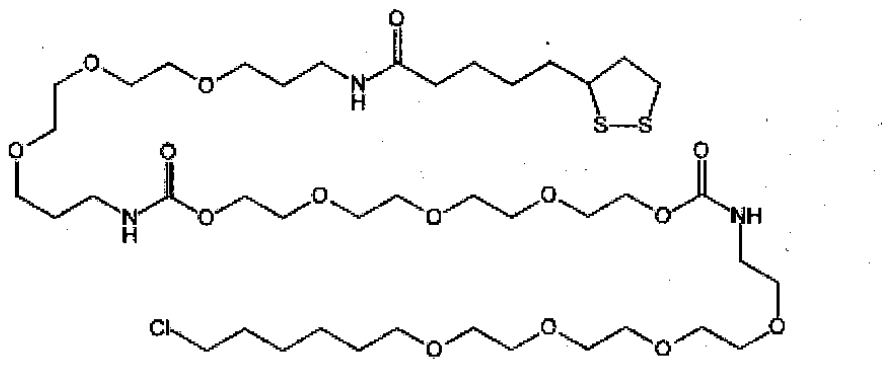

1.6 Legends for supplementary movies

M1: Timelapse of HIF-1α-GFP BAC cells in hypoxia. HIF-1α-GFP BAC HeLa cells were plated in a 35 mm glass-bottom dish and incubated on the microscope stage in 1 % O_2. Images were taken every 5 min. Total length of movie is 17 h. Frame rate = 8 frames / s.

M2: Timelapse of EGFP-HIF-2α speckles. HeLa cells were transiently transfected with EGFP-HIF-2α and plated in a 35 mm glass-bottom dish 24h prior to imaging. Cells were placed on the microscope stage in normoxic conditions. Timelapse shows the movement of the HIF-2α speckles.

M3: Example of EGFP-HIF-2α speckle trajectories (1). EGFP-HIF-2α speckle (highlighted by white circle) tracked using ImageJ and the trajectory recorded (white line). Highlights a speckle exhibiting more restricted / confined movement.

M4: Example of EGFP-HIF-2α speckle trajectories (2). EGFP-HIF-2α speckle (highlighted by yellow circle) tracked using ImageJ and the trajectory recorded (yellow line). Highlights a speckles exhibiting less restricted movement.

M5: Example of tracking locations of EGFP-HIF-2α speckles during photobleaching experiment. Location of EGFP-HIF-2α speckles during FRAP experiment was analysed using ImageJ. Speckles were identified prior to bleaching and tracked during experiment to determine if recovery of fluorescence occurs in the same location.

M6 and M7: Example of individual speckles tracked during photobleaching experiments. Two examples that suggest that EGFP-HIF-2α recovers into pre-existing speckles (speckles that were present prior to bleaching).